



HELMHOLTZ
CENTRE FOR
ENVIRONMENTAL
RESEARCH – UFZ

PhD Dissertation 11/2010

**Distributed Hydrologic Model Parameterization:
Application in a Mesoscale River Basin**

Rohini Kumar

ISSN 1860-0387

Distributed Hydrologic Model
Parameterization: Application in a
Mesoscale River Basin

Dissertation

zur Erlangung des akademischen Grades doctor rerum naturalium
(Dr. rer. nat.)

vorgelegt dem Rat der Chemisch-Geowissenschaftlichen Fakultät der
Friedrich-Schiller-Universität Jena

von

Rohini Kumar

geboren am 20.12.1982 in Darbhanga, India

Supervisor: Prof. Dr. Sabine Attinger
Co-supervisor: Dr. Luis E. Samaniego

Diese Dissertation ist während meiner Beschäftigung als wissenschaftlicher Mitarbeiter am Department für Hydrosystemmodellierung innerhalb des Helmholtz-Zentrums für Umweltforschung - UFZ in Leipzig entstanden.

Promotionskommission:

Prof. Dr. Sabine Attinger	Friedrich-Schiller-Universität Jena
Prof. Dr. Karsten Schulz	Ludwig-Maximilians-Universität München
Prof. Dr. Kai-Uwe Totsche	Friedrich-Schiller-Universität Jena
Prof. Dr. Ralf Seppelt	Martin-Luther-Universität Halle-Wittenberg
Prof. Dr.-Ing. Olaf Kolditz	Technische-Universität Dresden
PD Dr. habil. Michael Pirrung	Friedrich-Schiller-Universität Jena

Die Dissertationsverteidigung fand am 19th May 2010 in Jena statt.

ISSN 1860-0387

Copyright © 2010 by Rohini Kumar

All rights reserved. No part of the material protected by this copyright notice may be reproduced or utilised in any form or by any means, electronic or mechanical, including photocopying, recording or by any information storage and retrieval system, without the prior permission of the author.

Author email: rohini.kumar@ufz.de

*"Water is the earth's eye, looking into which the beholder measures
the depth of his own nature"*

Henry D. Thoreau

Contents

List of Figures	V
List of Tables	XI
Acronyms and Abbreviations	XIII
Acknowledgement	XV
Zusammenfassung	XVII
1 Introduction	1
1.1 Background	1
1.2 Hydrological Modeling at Catchment Scale	3
1.3 Research Objectives	11
2 Development of a Mesoscale Hydrologic Model (mHM)	13
2.1 Introduction	13
2.2 Hierarchy of Spatial Scales	14
2.3 The Grid-based mHM Model	15
2.3.1 Model Formulation	15
2.3.2 Canopy Interception	18
2.3.3 Snow Accumulation and Melting	18
2.3.4 Soil Moisture Dynamics	20
2.3.5 Infiltration and Surface Runoff	23
2.3.6 Evapotranspiration	24
2.3.7 Subsurface Storage and Discharge Generation	25
2.3.8 Baseflow	26
2.3.9 Discharge Attenuation and Flood Routing	26
2.4 mHM Model Parameters	29

3	Distributed Model Parameterization	33
3.1	Problem Description	33
3.2	Regionalization of Hydrologic Model Parameters	35
3.3	Multiscale Parameter Regionalization (MPR)	39
3.3.1	Parameter Regionalization	41
3.3.2	Estimation of Effective Parameter	42
3.3.3	Implementation of MPR in mHM	43
3.3.4	Remarks on the MPR Technique	49
4	Applications of mHM in a Mesoscale River Basin	53
4.1	Introduction	53
4.2	General Description of the Study Area	54
4.3	Data Availability and Processing	56
4.3.1	Physiographical Characteristics	56
4.3.2	Land Cover Characteristics	59
4.3.3	Meteorological Variables	62
4.3.4	Discharge Data	70
4.4	Global Parameter Identification	71
4.5	Evaluation Criteria	76
4.6	Application of mHM in the Upper Neckar River Basin	76
4.6.1	Streamflow Prediction	78
4.6.2	Prediction of Spatial Patterns of Soil Moisture and Snow Cover	87
4.6.2.1	Soil Moisture Simulation	88
4.6.2.2	Snow Cover Simulation	91
4.6.3	Effects of Frozen Soil on Streamflow Predictions	91
4.6.4	Effects of Canopy Interception on Streamflow Predictions	94
4.6.5	Comparison of mHM with the HBV model	95
4.6.6	Model Time Complexity and Coding	99
5	Comparison of Regionalization Methods	101
5.1	Introduction	101
5.2	Numerical Experiments and Evaluation Criteria	102
5.2.1	Effect of the Sub-grid Variability	102
5.2.2	Transferability of Global Parameters across Modeling Scales	103
5.2.3	Preservation of Spatial Patterns	105

5.3	Implementation of MPR and SR within mHM	105
5.4	Analysis of Numerical Experiments	109
5.4.1	Sensitivity of Model Efficiency to the Sub-grid Variability	109
5.4.2	Sensitivity of Streamflow Simulations to Global Parameters	111
5.4.3	Effects of the Sub-grid Variability on Model Parameters	116
5.4.4	Sensitivity of the Mass Balance to Global Parameters Calibrated at Various Modeling Scales	116
5.4.5	Preservation of Spatial Patterns	122
5.4.6	Transferability of Global Parameters to Ungauged Loca- tions	122
6	Predictions of Streamflow Characteristics: High and Low flows	127
6.1	Introduction	127
6.2	Implementation of mHM in Upper Neckar River Basin	128
6.2.1	HRU Parameterization	129
6.3	Parameter Identification	131
6.3.1	Formulation of Calibration Objective Function	132
6.3.2	Parametric Uncertainty Analysis	134
6.4	Seasonal High and Low Flow Characteristics	135
6.5	Results and Discussion	138
6.5.1	Daily Discharge Simulations	138
6.5.2	Prediction of the Seasonal High and Low Flow Charac- teristics	145
6.5.2.1	High Flow Characteristics	147
6.5.2.2	Low Flow Characteristics	148
7	Summary and Outlook	155
7.1	Summary	155
7.2	Outlook	161
	Bibliography	163
	Selbständigkeitserklärung	179
	Curriculum Vitae	180

List of Figures

1	Vergleich der Oberflächen-Bodenfeuchteverteilung im Jahr 2000, Tag 255...	XXIII
2	Linkes Bild: Leistungen von MPR und SR bezüglich der...Rechts Bild: Diskrepanz zwischen den Flüssen simuliert auf zwei...	XXV
2.1	General mHM model structure for a cell i at time point t ...	14
2.2	Hierarchy of data and modeling levels in mHM.	15
2.3	Schematic representation of different components accounted in mHM...	19
2.4	Schematic derivation of a drainage network at the level-1 based on level-0...	28
3.1	Schematic comparison between MPR, SR and HRU parameterization methods...	40
3.2	Estimation of effective regionalized parameters β^1 at level-1 based on regionalized model parameters β^0 at level-0...	41
3.3	Nonlinear evolution of a variable x^0 from sub-grid scale (level-0) to x^1 at modeling scale (level-1)...	44
4.1	Overview of the upper Neckar river basin located within the state of Baden-Württemberg, Germany.	55
4.2	Physiographical characteristics map for the study area...	58
4.3	Variation in soil textural properties within the study area...	59
4.4	Variation in geological formation within the study area...	59
4.5	Land cover maps for the study area classified for the year 1975, 1984, 1993...	61
4.6	Long term yearly distribution of LAI for three land cover classes: Forest, impervious cover and permeable areas...	62

4.7	Location of precipitation and temperature stations in and around the study area. Source: DWD.	63
4.8	Experimental and fitted theoretical spherical variogram for the daily total precipitation and the daily average air temperature... .	65
4.9	Spatial distribution of the long term mean of daily total precipitation and daily average, maximum...	66
4.10	Spatial distribution of the long term mean of daily total potential evapotranspiration...	68
4.11	Box plots with the yearly fluctuations of the daytime/nighttime air temperature...	69
4.12	Long-term diurnal cycle of the PET for January and July... . .	70
4.13	Location of the interior gauging stations within the Upper Neckar river basin.	72
4.14	Upscaling of river network on modeling scale at 2000 m from 100 m flow direction and flow accumulation...	78
4.15	Variability of a subset of transfer function parameters or global parameters γ	80
4.16	Comparison of the observed and the ensemble values for the streamflow at Plochingen...	81
4.17	Comparison of the observed and the ensemble values for the streamflow at Plochingen...	82
4.18	Yearly evolution of the NSE obtained between observed and simulated discharge as well as between for their logarithmic transformation...	84
4.19	Monthly discharge and seasonal total drought duration in the evaluation period at Plochingen.	84
4.20	Comparison of the observed and the ensemble values for the streamflow at an interior Horb...	86
4.21	Plausibility test of soil moisture patterns for five summer days in year 2000...	89
4.22	Ensemble model simulation of soil moisture patterns compared with MODIS derived LST...	90
4.23	Daily discharge simulations at Plochingen during the plausibility test of soil moisture patterns...	90

4.24	Plausibility test for the mHM simulated snow cover with the MODIS derived snow cover data...	92
4.25	Effect of the frozen soil algorithm on the daily discharge hydrograph of the Eschach river at Horgen-Kläranlage gauging station.	93
4.26	Spatial variation of the fraction of semi-impervious area due to frozen soil conditions in the Eschach river basin.	94
4.27	Spatio-temporal variability of daily mean maximum canopy interception storage during three months...	96
4.28	Evolution of annual NSEs between observed and models (i.e. mHM and HBV) simulated daily discharge at the Horb gauging station during the modeling period.	97
4.29	Comparison between HBV and mHM during selected winter and summer seasons...	98
4.30	Comparison of the top-layer soil moisture distribution for the year 2000...	99
5.1	Evaluation scheme for the evaluation of the continuity principle between two modeling scales...	104
5.2	Mean and $P_{95} - P_5$ quantile range of the spatial correlation (\bar{r}) between 2 km resolution of (a) daily total precipitation, (b) daily average temperature, and (c) daily total potential evapotranspiration...	107
5.3	Spatial distribution of precipitation on day 21-09-2000 at the spatial resolutions of (a) 2 km, (b) 4 km, (c) 8 km, (d) 16 km, and (e) 32 km.	108
5.4	Mean and $P_{95} - P_5$ quantile range of the spatial correlation (\bar{r}) of (a) daily soil moisture, (b) daily total evapotranspiration, and (c) runoff between simulations obtained with a fixed modeling scale...	110
5.5	Mean and range of NSE obtained between observed and simulated daily streamflow simulations using MPR and SR...	113
5.6	Sensitivity of the monthly water balance obtained by shifting global parameters from the calibration to the simulation scales for both regionalization schemes...	115

5.7	Spatial variability of the porosity (mm mm^{-1} of the top-soil layer (i.e. $\beta_6^{(1)}$) estimated at three different modeling scales, $\ell_1 = (2, 4, 8)$ km, and for both regionalization techniques...	117
5.8	Evaluation of the conservation of mass for actual evapotranspiration at various control scales based on MPR and SR parameterizations...	119
5.9	Evaluation of the conservation of mass for total discharge at various control scales based on MPR and SR...	120
5.10	Evaluation of the conservation of mass top thin root zone soil moisture at various control scales based on MPR and SR...	121
5.11	Discrepancy between fluxes simulated at two different modeling scales (the control scale $\ell_1 = 4$ km and the finer scale $\ell'_1 = 2$ km) during the modeling period...	123
5.12	Land Surface Temperature ($^{\circ}\text{C}$) from MODIS and simulated volumetric water content (mm mm^{-1}) in the top-soil layer estimated with SR and MPR...	124
5.13	Location of interior locations within the Upper Neckar river basin. The basin's outlet corresponds to gauge Nr. 10. at Plochingen	125
5.14	Performance of MPR and SR for daily discharge simulations at internal locations within the study area...	126
6.1	Location of modeling cells at level-1 ($\ell_1 = 4$ km) within a particular HRU for the study area.	130
6.2	Schematic representation of high flow characteristics...	136
6.3	Schematic representation of low flow characteristics...	136
6.4	Performance of the lumped and the distributed models for daily discharge simulations at Plochingen...	140
6.5	Ensemble of daily streamflow simulations at Plochingen during the evaluation water year...	143
6.6	Ensemble of daily streamflow simulations at Horb gauging station (internal) during the water year 1988 using the HRU (a) and the MPR (b)...	145
6.7	Sensitivity of the lumped and the distributed models performance for the prediction of seasonal specific volume of high flows (a) and cumulative specific deficit...	146

6.8	Performance of the lumped (a) and the distributed model with the HRU (b) and the MPR (b) parameterization methods...	149
6.9	Performance of the lumped (a) and the distributed model with the HRU (b) and MPR (b) parameterization methods...	151
6.10	Performance of the HRU (a) and the MPR (b) parameterization methods employed in the distributed model...	153

List of Tables

2.1	Main differences between mHM and other distributed hydrologic models.	30
2.2	List of mHM model parameters.	31
3.1	Description of basin predictors used in MPR.	45
3.2	Predictors used in the regionalization functions...	46
3.3	Types of upscaling operators to derive an effective parameter at level-1 based on regionalized parameters at level-0...	47
3.4	Regionalization (or transfer) functions and upscaling operators used in the mHM...	47
4.1	Range and a priori guess of transfer function parameters (γ) for the Upper Neckar river basin.	75
4.2	Statistics of the good sets of transfer function parameters.	79
4.3	Ensemble mean value and 5% and 95% percentile ranges obtained for six estimators for daily discharge simulations at Plochingen...	83
4.4	Ensemble mean value and 5% and 95% percentile ranges obtained for six estimators for daily discharge simulations at an interior Horb gauging station...	85
5.1	Effect of the sub-grid variability $\ell_0 = (100, 500, 1000, 2000)$ m on three model efficiency statistics (RMSE, NSE, and r) obtained for the daily discharge simulation...	109
5.2	RMSE and NSE obtained with both the multiscale (MPR) and the standard (SR) parameter regionalization techniques at various modeling scales obtained with daily streamflow values.	112

5.3	Mean annual water balance over the whole basin obtained at different scales using global parameters transferred from a given modeling scale ($\ell_1 = 4$ km)...	114
5.4	Performance of MPR and SR for the daily streamflow predictions at the interior locations during the evaluation period (1989-2001)...	126
6.1	Physiographical characteristics used for the delineation of HRUs in the study area.	130
6.2	Range of mHM model parameters for the HRU parameterization method during the calibration process...	132
6.3	Mathematical formulation of seasonal high and low flow characteristics.	137
6.4	Ensemble median statistics of daily discharge simulations at Plochingen (outlet) during calibration and validation periods for lumped and distributed versions...	139
6.5	Ensemble median statistics of daily discharge simulations at Horb during modeling period (1980-2001)...	144
6.6	Ensemble median statistics between observed and simulated seasonal high flow characteristics at Plochingen...	147
6.7	Ensemble median statistics between observed and simulated seasonal high flow characteristics at Horb...	150
6.8	Ensemble median statistics between observed and simulated seasonal low flow characteristics at Plochingen...	152
6.9	Ensemble median statistics between observed and simulated seasonal low flow characteristics at Horb...	153

Acronyms and Abbreviations

ARNO	A hydrologic model name based on the Arno river, Italy
ATI	Antecedent Temperature Index
DDS	Dynamically Dimensioned Search
DDS-UA	DDS-Approximation of Uncertainty
DEM	Digital Elevation Model
DMIP-I	Distributed Model Intercomparison Project, Phase 1
DOF	Degree Of Freedom
DWD	Deutscher Wetterdienst
EDK	External Drift Krigging
GCM	Global Circulation Model
GIS	Geographical Information Systems
HBV	Hydrologiska Byråns Vattenbalansavdelning Model
HRU	Hydrologic Response Units
IWS	Institut für Wasserbau
mHM	Mesoscale Hydrologic Model
MIKE-SHE	Name of a physically based hydrologic model emerged from System Hydrologique European
MODIS	Moderate Resolution Imaging Spectroradiometer
MPR	Multiscale Parameter Regionalization
LAI	Leaf Area Index
LST	Land Surface Temperature
LUBW	Landesanstalt für Umwelt, Messungen und Naturschutz
NASA	National Aeronautics and Space Administration
NDVI	Normalized Difference Vegetation Index
NSE	Nash Sutcliffe Efficiency
ODE	Ordinary Differential Equation
PDE	Partial Differential Equation
PGI	Acronym used by the Portland Group for Fortran compiler
POT	Peak-Over-Threshold
PTF	Pedotransfer function
PUB	Predictions in Ungauged Basins
RCM	Regional Climate Model

RMSE	Root Mean Square Error
SA	Simulated Annealing
SAC-SMA	Sacramento Soil Moisture Accounting Model
SCE-UA	Shuffled Complex Evolution - University of Arizona
SR	Standard Regionalization
TM	Thematic Mapper
TOPMODEL	TOPography-based hydrological MODEL
TRMM	Tropical Rainfall Measuring Mission
TUH	Triangular Unit Hydrograph
VIC	Variable Infiltration Capacity model
WASIM-ETH	Water Flow and Balance Simulation Model
	Eidgenössische Technische Hochschule, Zürich

Acknowledgement

One day God came on Earth and ask a man – “If I and your Teachers would be standing together to whom will you pray first ?”. After thinking for a while the man replied – “Hey Lord ! First I will pray to my Teachers, who taught me about your existence.”

Proverb from Sanskrit literature

Before I start acknowledging those, who contributed to the preparation of this dissertation, let me first express my sincere gratitude to all my teachers starting from my primary education to all along the way here, who made me capable of what I am today. This work is dedicated to them: **My Teachers.**

Research does not exist in a vacuum, every thesis involves a huge amount of efforts, ideas, support and guidance of many people. Mine was no exception. During the last three years of my research, I've had the pleasure of talking and working with many helpful minds. I express my sincere gratitude and appreciation to all those who contributed to the long and arduous journey towards the preparation of this dissertation. I still owe my deepest thanks to those individuals who I could not mention here by name.

First and foremost, I would like to thank my supervisors, Prof. Dr. Sabine Attinger and Dr. Luis E. Samaniego, for their direction and vision. Without their help, supervision and continuous encouragement it would have not been possible for me to get the opportunity to work in such a nice and conducive environment for research. Indeed, it is mainly their support and guidance which has made this thesis possible.

In particular, I would like to thank Dr. Luis E. Samaniego for his outstanding guidance as a role of advisor, friend and mentor. He has taught me what research is, how it is performed, and how it is communicated. His incisive comments and accent on rigor and clarity made an enormous difference to the quality of work. Whether it had been a problem on programming language or statistical analysis or theoretical understanding of the subject, his suggestions had always led me to find an appropriate solution. I would like to also thank Prof. Dr. Sabine Attinger for her faith on me to perform research freely. Thanks are also due to her for allowing me to visit international conferences.

In summary, it has been a privilege and honor to have worked with both of them.

I am also grateful to all members of the department of Computational Hydro Systems with whom I overlapped with and learned from: Anke, Jan, Guido, Matthias, Radu, Saadia, Christoph, Abdullah, Falk, Juliane, Jude, Sven, Maren, Tino, Mehmet, Hu Yao, Sindy, Thomas, Christine. Thank you for providing me a wonderful time.

Anything I write about my parents and my brother is woefully inadequate for their influence on me in providing the secure background on which I stand. Words are not enough to describe their efforts. I am deeply indebted to them for their love, patience, continuous support, and understanding.

Finally, let me express my special thanks to my friend Leonie and her parents, who provided much needed reminders that there is more to life than computer programming. It is their moral support and family atmosphere which seldom let me feel that I am thousand miles away from my homeland. Thank you for being with me.

Zusammenfassung

Wasser ist sowohl für alle Lebewesen, als auch für die sozioökonomische Entwicklung einer Region sowie für das Bestehen jeglicher natürlicher Ökosysteme von essentieller Bedeutung. Wachsende Probleme hinsichtlich der Qualität und Quantität von Wasserressourcen sorgen für große Besorgnis unter Wissenschaftlern, Fachleuten im Bereich des Wasserressourcen-Managements und politischen Entscheidungsträgern: Der Klimawandel, entweder durch natürliche und/oder anthropogene Aktivitäten verursacht, wird den hydrologischen Zyklus intensivieren, beschleunigen oder verbessern. Dies verändert wiederum die Wahrscheinlichkeit des Auftretens extremer hydrologischer Ereignisse wie Überschwemmungen und Dürren. Beide Extremereignisse stellen eine erhebliche Bedrohung für das Leben dar und bringen sozioökonomische und ökologische Konsequenzen mit sich. Aufrufe, sowohl von wissenschaftlicher als auch von politischer Seite, sollen nicht nur zu einem besseren Verständnis der den hydrologischen Systemen zugrunde liegenden Prozessen unter sich verändernden Umweltbedingungen führen, sondern auch ein brauchbares Werkzeug zu deren Messung bereitstellen. Hydrologische Modelle, welche die Bewegung und Lagerung von Wasser im hydrologischen System beschreiben, sind Werkzeuge, die primär zur Vorhersage solcher Ereignisse verwendet werden.

Jüngste Fortschritte von Fernerkundungstechniken und geographischen Informationssystemen haben die Entwicklung von verteilten Modellen, d.h. Modellen mit räumlich expliziten Parametern, voran getrieben. Diese stellen einen erfolgversprechenden Ansatz für Simulationen und Vorhersagen dar. Die Anforderungen an hydrologische Modelle, wie die Berücksichtigung der Auswirkung von Bodenbedeckung auf natürliche hydrologische Prozesse, eine Verbesserung der Echtzeit-Fließgeschwindigkeits-Prognose sowie eine angemessene Einschätzung der räumlichen und zeitlichen Dynamik von Bodenfeuchte und Schneebedeckung sowie weitere wichtige variable Größen, sind ein Grund für die fortschreitende Entwicklung hydrologischer Modelle.

Verteilte hydrologische Modelle auf der Mesoskala zeigen verschiedene Probleme auf. Dies betrifft insbesondere die oftmals zu große und unübersichtliche Anzahl an Parametern, das Fehlen einer wirksamen Technik, mit deren Hilfe die räumliche Heterogenität physiographischer Merkmale integriert werden kann, die Tatsache, dass Parameter auf andere Skalen und Standorte nicht

übertragbar sind sowie die erhebliche Dauer, die zur Ausführung der numerischen Simulationen benötigt wird. Ziel dieser Arbeit ist die simultane Untersuchung dieser Probleme. Vornehmlich präsentiert diese Arbeit die Ergebnisse einer wissenschaftlichen Arbeit, die den folgenden zwei verschiedenen, jedoch miteinander verwandten Fragestellungen unterliegt:

1. *Wie kann ein robustes und rechnerisch effizientes verteiltes hydrologisches Modell für ein mesoskaliges Flussgebiet entwickelt werden, welches zugleich die Abflussganglinie an jedem willkürlich gewählten Punkt innerhalb des Gebiets reproduziert als auch räumlich und zeitlich dynamische Komponenten von Bodenfeuchte, Schnee(bedeckung) und weiteren wichtigen variablen Komponenten bereitstellt?*
2. *Wie können räumliche Verteilungen der Modellparameter ermittelt werden, die robust genug sind, um die hohe Anzahl an Parametern zu reduzieren, aber dennoch ausreichen um die Heterogenität von in Raster geteilten Gebieten bei gleichzeitiger Gewährleistung der Übertragbarkeit von Modellparametern auf andere Skalen und Orte zu berücksichtigen?*

Die Motivation hinter der ersten Frage liegt in der Tatsache, dass die aktuelle Entwicklung, insbesondere von den sogenannten physikalisch basierten hydrologischen Modellen nur eingeschränkte Verwendungsmöglichkeiten für mesoskalige Einzugsgebiete aufweist. In den meisten praktischen Fällen ist dies hauptsächlich auf die Annahmen in den Formulierungen zurückzuführen, welche a) das Fortbestehen aller räumlichen und zeitlichen Charakteristiken und b) die vollständige Skalierbarkeit der relevanten physikalischen Gleichungen (z. B. Richards Gleichung) von der Punktskala zur Mesoskala betreffen. In der Realität werden beide Aspekte selten gleichermaßen erfüllt. Konzeptuelle hydrologische Modelle, die sich an die allgemeinen physikalischen Mechanismen annähern, konzentrieren sich hingegen hauptsächlich auf die Fließgeschwindigkeit und ihre unsichere Vorhersagbarkeit. Sie richten nur wenig Aufmerksamkeit auf wichtige Aspekte wie die räumliche und zeitliche Verteilung von Eingangswerten, Zustandsvariablen und Wasserflussgrößen, die für eine sicherere Vorhersagbarkeit des Zeitpunkts und Ausmaßes von Fließbewegungen relevant sind. Außerdem stellen sie Schlüsselfaktoren für die Beschäftigung mit neuen gesellschaftlich verursachten Problemen hinsichtlich der Wasserressourcen dar. Die Motivation aus welcher heraus sich die zweite Frage ergibt, beruht auf der

Tatsache, dass verteilte Modelle generell eine sehr hohe Anzahl an Parametern benötigen, die auf der Mesoskala wichtige Einheiten darstellen und durch Kalibrierung geschätzt werden. Ein Modell mit einer signifikanten Menge an freien Parametern für jede einzelne Modelleinheit zu kalibrieren, würde zu einer zu großen Parameteranzahl führen. Ein aktueller Lösungsansatz für dieses Problem ist die Zusammenlegung einzelner Modelleinheiten (Rasterzellen) zu mehr oder weniger homogenen Einheiten, die in der Regel als Hydrological Response Unit (HRU) bezeichnet werden. Diese Modelle enthalten demnach weniger Parameter, da die Parameter durch Kalibrierung einer HRU zugewiesen werden. Dies bringt jedoch wiederum den Nachteil mit sich, dass es sich um statische Größen handelt und die geographische Lage der HRU nicht unbedingt explizit ist. Ein weiterer Ansatz ist die Nutzung von Regionalisierungs-Techniken, um Modellparameter mit physikalischen Eigenschaften der Einzugsgebiete zu verbinden, was zu einer signifikanten Reduktion des Kalibrierungsproblems führt. Dies insbesondere indem nur wenige funktionelle Parameter regionaler Beziehungen geschätzt werden, statt Modellparameter (für jedes Raster) selbst. Da des Weiteren eine dynamische Verknüpfung zwischen Modellparametern und den entsprechenden Merkmalen der Gebiete (wie Bodenbedeckung) erreicht wird, können die Auswirkungen solcher Veränderungen effektiver bestimmt werden. Weder die HRU-Methode noch der Regionalisierungsansatz tragen der Variabilität der einzelnen sich unterscheidenden Merkmale der Unterraster eines Messgebietes Rechnung und sind somit auf der gleichen Größenordnung wie die Modelleinheiten definiert. Folglich gehen dabei in der Regel wertvolle Informationen hinsichtlich der Heterogenität ihrer Unterraster verloren, welche eng mit verschiedenen kleinskaligen hydrologischen Prozessen verbunden sind (einschließlich des Abflussprozesses an Hängen).

Auf der Grundlage dieser Voraussetzungen und unter Berücksichtigung des aktuellen Standes der Wissenschaft, konzentriert sich diese Arbeit auf die Entwicklung eines räumlich verteilten Modelles mit einer Parameterisierungstechnik, die sowohl für wissenschaftliche Zwecke als auch für den praktischen Betrieb in mesoskaligen Einzugsgebieten geeignet ist.

Das im Rahmen dieser Arbeit entwickelte mesoskalige hydrologische Modell (mHM) ist ein voll-verteiltes, prozess-basiertes konzeptionelles Wasserausgleichs-Modell, welches Rasterzellen als primäre hydrologische Einheiten benutzt und die folgenden hydrologischen Prozess simuliert: Überwachung der Bodende-

ckung, Anhäufung und Schmelzen von Schnee, Dynamik der Bodenfeuchte, Infiltration und Oberflächenabfluss, Verdunstung, ober- und unterirdische Lagerung und Wasserfluss, tiefe Versickerung und Basisabfluss sowie Abflussschwächung und Hochwasserabflussberechnung. mHM basiert auf numerischen Annäherungen vorherrschender hydrologischer Prozesse, welche in dem bekannten HBV-Modell (Bergström, 1995) getestet wurden. mHM enthält des Weiteren eine Reihe von neuen Funktionen, welche Prozesse wie das Einfrieren und Auftauen des Bodens, der oberflächennahen Bodenfeuchte, Abdeckungsveränderungen und die Flusslenkung von Zelle zu Zelle überwachen. Es enthält außerdem ein Modul zum automatischen Upscaling und zur Abgrenzung des Flow-Routing-Netzwerks, sowie einer neuen Parameterisierungstechnik, die im Folgenden beschrieben wird. Diese neuen Module wurden integriert, um die Vorhersagefähigkeit des Modells zu verbessern. Angesichts der Tatsache, dass mHM Rasterzellen verwendet, HVB im Gegensatz dazu vordefinierte Teileinzugsgebiete, kann es effektiv genutzt werden, um Abflusshydrographen an jedem Punkt des Fluss-Netzwerkes eines Einzugsgebiets zu schätzen.

Eines der wichtigsten Merkmale des mHM ist, dass es drei Ebenen räumlicher Diskretisierung verwendet, um die räumliche Variabilität der hydrologischen Prozesse und Input-Daten besser zu integrieren. Diese Ebenen sind, nach ihrer zunehmenden räumlichen Auflösung, folgende: Die obere Ebene (Level-2) für das Führen meteorologischer Variablen (z. B. Niederschlag, Temperatur), die mittlere Ebene (Level-1) für die Beschreibung der vorherrschenden hydrologischen Prozesse und die untere Ebene (Level-0), welche die gerasterten Informationen über statischen und dynamischen Einzugsgebiete, physikalische Eigenschaften wie Bodenhöhe und -textur, geologische Formationen, Bodenbedeckung und weitere Informationen enthält. mHM besteht aus 28 Parametern, von denen 26 für jede Modell-Rasterzelle benötigt werden. Die verbleibenden zwei Parameter sind mit dem Flusslenkungs-Prozess verbunden.

Eine multiskalige Parameter-Regionalisierungstechnik (MPR) wird, zur Bestimmung der räumlichen Bereiche der Modellparameter in dieser Arbeit vorgeschlagen, mit dem Ziel die Parameteranzahl zu verringern und gleichzeitig die Variabilität der Unterraster zu berücksichtigen. Um dies zu erzielen, folgt MPR dem zweistufigen Verfahren. Im ersten Schritt wird die Regionalisierung auf der feineren Skala (Level-0) mit linearen oder nichtlinearen Transfer-Funktionen, die auf dem Verständnis von Prozessen und/oder empirischen Grundlagen

(z. B. Peto-Transfer -Funktionen) beruhen, durchgeführt. Diese Funktionen sollen eine quasi-kontinuierliche dynamische Verknüpfung zwischen Modellparametern und Einzugsgebietsprädiktoren mit Hilfe von Transfer-Funktions-Parametern festlegen. Anschließend, in einem zweiten Schritt, werden die räumlichen Bereiche effektiver Parameter in einen größeren Modellierungsmaßstab (Level-1) mit den entsprechenden Parametern der feineren Auflösung verbunden. Dies geschieht durch einen Upscaling-Operator, wie beispielsweise einfacher Mittelwert, harmonischer Mittelwert, oder andere. Das Zwei-Stufen-Verfahren der MPR stellt sicher, dass der Kalibrierungsalgorithmus gute Lösungen für die Transfer-Funktionen-Parameter ($s = 62$) findet, statt der Modellparameter ($P = 28$) für jede Rasterzelle. Dies wiederum impliziert eine starke Reduktion der Komplexität, da $P \times N \gg s$, wobei N die Gesamtzahl der Zellen eines gegebenen Modells bezeichnet. Damit senkt MPR deutlich die Parameterzahl des Modells und berücksichtigt zugleich implizit die Heterogenität der Unterraster eines Regionalisierungsrahmens. Einer der wesentlichen Vorteile dieser Methode ist, dass die Informationen auf dem Level-0 Parameter-Feld (aus Schritt 1) immer verfügbar sind und effizient genutzt werden können, um Parameter Felder des Level-1 auf jeder Ebene der Skala zu errechnen (nur mit Hilfe des Upscaling-Operators ohne neue Kalibrierung).

mHM wurde mit der MPR Parametrierungs-Technik auf das Ober-Neckar-Einzugsgebiet, in der Nähe von Stuttgart in Deutschland, angewandt. Das Untersuchungsgebiet ist durch die Messstation Plochingen erfasst, die ein Einzugsgebiet von einer ca. 4000 km^2 großen Fläche umfasst. Die Untersuchung wurde in den Jahren von 1980 bis 2001 durchgeführt. Die benötigten Eingabedaten für die Umsetzung des Modells wurden von verschiedenen staatlichen Stellen erhalten und beinhalten Folgendes: Geländehöhe, digitalisierte Bodenkarte und geologische Karte von LUBW und Landbedeckungs-Daten von Landsat TM5 Scene, die in drei Hauptgruppen eingestuft wurden: Wald, versiegelte Flächen und durchlässige Bodenbedeckung. Punktuelle täglich gemessene meteorologische Variablen (Niederschlag und Temperatur) von mehreren Klimastationen im Untersuchungsgebiet und dessen Umgebung wurden von DWD erhalten und anschließend auf die gewünschten Modellraster mit einer externen Drift-Krigging-Methode interpoliert. Andere Satellitendaten beinhalten einen wöchentlichen Blattflächenindex, Oberflächentemperatur und Daten zur Schneebedeckung. Durchschnittliche tägliche Flussmessungen für den Ab-

fluss des Einzugsgebiets sowie zehn Innenräumen wurden von LUBW erhalten. Das Modell wurde hinsichtlich seiner Leistung in verschiedenen räumlichen Aufteilung von Level-1 (Level-2 = Level-1) Stufen von 1 km auf 32 km sowie Level-0 Leistung von 100 m auf 2000 m getestet. Die gesamte Modellperiode wurde in zwei Teile gegliedert: 1980-1988 als Kalibrierungsphase, um den geeigneten Einsatz von Transfer-Funktions-Parametern, welche lediglich die Daten einer Ventilstation berücksichtigen, herauszufinden, sowie der folgende Teil 1989-2001 als Evaluationsphase.

Die vorgeschlagene MPR Technik im mHM verringert nicht nur die Komplexität des Modells, sondern führt auch zu einem schnellen und robusten hydrologischen Modell, welches in der Lage ist, gute Abflusshydrographen nicht nur an der Austrittsstelle des Einzugsgebiets sondern auch im Innern zu reproduzieren. Darüber hinaus ist eine Plausibilitätsprüfung durchgeführt worden, um die räumlich-zeitlichen Muster der Schneebedeckung und Bodenfeuchte mit direkten Satellitendaten und Proxies von MODIS (zu Schneebedeckung und Oberflächentemperatur LST) zu vergleichen. Das Ergebnis zeigte, dass diese gut miteinander übereinstimmen. Insbesondere die räumlichen Muster zwischen den nahe der Oberflächen-Bodenfeuchte simulierten Modellergebnissen und der von MODIS abgeleiteten LST-Daten zeigten starke negative Abhängigkeiten, was zu erwarten war. Die Einbeziehung sowohl der Abdeckungsüberwachung als auch der Boden-Frost-Prozesse des mHM-Modells zeigte eine deutliche Verbesserungen in Simulationen zum Tagesabfluss. Die Einbeziehung dieser Prozesse wurde noch deutlicher im Vergleich von mHM mit dem dezentralen HBV-Modell. mHM zeigte eine klare Überlegenheit gegenüber HBV hinsichtlich der Simulationen des Tagesabflusses sowohl in der Sommer als auch im Winter. Darüber hinaus zeigte ein Vergleich mit den von MODIS-LST gewonnenen Daten, dass das räumliche Muster der Bodenfeuchte, simuliert durch mHM mit der MPR Parametrierungs-Methode deutlich realistischer ist, als jenes räumliche Muster, welches durch HBV mit der HRU Parametrierungs-Methode simuliert wurde (Abb. 1).

Um die vorgeschlagene MPR-Methode vor dem Hintergrund des aktuellen wissenschaftlichen Stands zu evaluieren, wurden verschiedene numerische Experimente entwickelt, die im Folgenden als Standard-Regionalisierungs-Methode (SR) bezeichnet werden. Beide Regionalisierungsmethoden wurden in mHM mit den gleichen Transfer-Funktionen implementiert. Ergebnisse der Ausführung

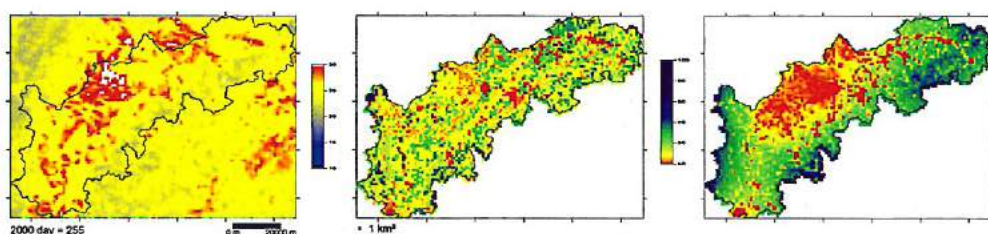


Abbildung 1: Vergleich der Oberflächen-Bodenfeuchteverteilung im Jahr 2000, Tag 255. Von links nach rechts: LST (MODIS), Bodenfeuchte ermittelt jeweils durch HBV-HRU und mHM-MPR.

des Modells mit beiden Methoden auf mehreren räumlichen Auflösungsebenen (von 2 km bis 32 km) zeigten auf, dass beide Methoden, solange sie für eine bestimmte Modellskala kalibriert und evaluiert wurden, sich nur in geringem Maße hinsichtlich der Güte der Tagesabfluss-Simulationen unterscheiden. Dass dennoch erhebliche Unterschiede bestehen, wurde deutlich, als die Übertragungs-Funktionsparameter auf den Modellierungsskalen verschoben wurden. In diesen Fällen, zeigte MPR eine deutliche Überlegenheit in Bezug auf SR (Abb.2.2). Dieses experimentelle Ergebnis zeigt deutlich die Signifikanz der Unterraster-Varirabilität und die Tendenz, die sich aus der Aggregation von Input-Daten in Regionalisierungsverfahren ergeben kann. Das Ergebnis einer solchen Aggregation konnte auch im räumlichen Muster effektiver Modellparameter auf verschiedenen Skalen von Level-1 beobachtet werden, da sie für beide Methoden deutliche Unterschiede aufzeigten. Ein Vergleich der Unterraster-Verteilung des gesättigten Feuchtegehalts des Bodens auf Level-0, mit den entsprechenden effektiven Parameterwerten auf der Modellskala (Level-1), jeweils durch MPR und SR erhalten, zeigte, dass die MPR-Methode das räumliche Muster deutlich besser darstellt, als die SR Methode.

Das numerische Experiment zur Erhaltung des Mengengleichgewichts wurde für zwei wichtige Wasserflüsse (effektive Evapotranspiration und Gesamtabfluss) sowie eine feststehende Variable (Bodenfeuchte der obersten Bodenschicht) bei einer gegebenen Kontrollgrösse durchgeführt. Für beide Methoden wurden, die auf einem feineren Skalenniveau erreichten Modellsimulationen, zu der größeren Kontrollskala aggregiert und mit den Simulationen verglichen, die auf größeren Skalenniveau erhalten wurden. Auf größeren Skalenniveau wurden die Simulationen mit zwei Funktionsparametersätzen ausgeführt: Erstens

durch Kalibrierung auf ihrer eigenen Skala, um diese Simulationen als Baseline wert beizubehalten, damit die Leistungsmessung z. B. NSE geschätzt werden kann, sowie Zweitens bezüglich der Parametersätze, welche von der Kalibrierung auf kleinem Skalenniveau erhalten wurden, um die Übertragungsfähigkeit dieser Parameter zu einer größeren Skala hin zu prüfen. Beide Regionalisierungsmethoden zeigten, dass die Bodenfeuchte der obersten Bodenschicht den stärksten Einfluss auf die Übertragbarkeit der globalen Parameter für gröbere räumliche Auflösung aufwies, während die eigentliche Evapotranspiration die am wenigsten wichtigste Variable darstellte. Allerdings variiert der Einfluss je nach Regionalisierungsmethode; ein systematischer Mangel in SR wurde im Vergleich zu MRP für die Erhaltung des Mengengleichgewichts (d.h. in jeder Kontrollmodellierungszelle) sowohl der Bodenfeuchte als auch des Gesamtabflusses festgestellt (Abb. 2; rechtes Bild). Diese Ergebnisse zeigten, dass die mit SR erhaltenen Parameter, im Vergleich zu MPR, skalenspezifischer und damit nicht übertragbar sind. Außerdem zeigte der ausgeführte Plausibilitätstest für die Erhaltung räumlicher Muster durch den Vergleich von modellsimulierter dünner Oberflächenfeuchte mit MODIS-LST Daten eine stärkere negative Korrelation für MPR als diejenigen durch SR-Methode erhalten wurden.

Die Tagesabfluss-Simulationen in Binnenlagen, erhalten durch MPR, waren durchschnittlich besser als die durch SR erhaltenen. Obwohl beide Methoden eine Verschlechterung der Simulationen an Binnenlagen im Gegensatz zu Simulationen der Außenlagen des Einzugsgebiets aufzeigten, kann festgestellt werden, dass die Verschlechterung von MPR wesentlich geringer war (im Durchschnitt 50% in NSE Werten) als die der SR-Methode (Abb. 2; linkes Bild). Diese Ergebnisse beziehen sich auf die Durchführungen, in denen Parameter von anderen Skalen als der in der Simulation an Binnenlagen verwendeten, transformiert wurden, was wiederum die Stabilität der MPR Methode gegenüber der SR-Methode unter Beweis stellt.

Schließlich wurde eine Fallstudie durchgeführt, um die Modellfähigkeit, das Abflussverhalten unter extremen saisonalen Gegebenheiten (Winter und Sommer) darzustellen, zu prüfen. Dies beinhaltet Folgendes: spezifisches Volumen, Gesamtdauer, Häufigkeit des Schnellflusses und spezifische Defizite, Gesamtdauer von Dürre und die maximale Dürreintensität für Niederwasserabfluss. Insbesondere war Ziel dieser Studie die Auswirkungen der räumlichen Diskretisierung, Modell-Parametrisierung und die Auswirkungen der Kalibrierung sowohl

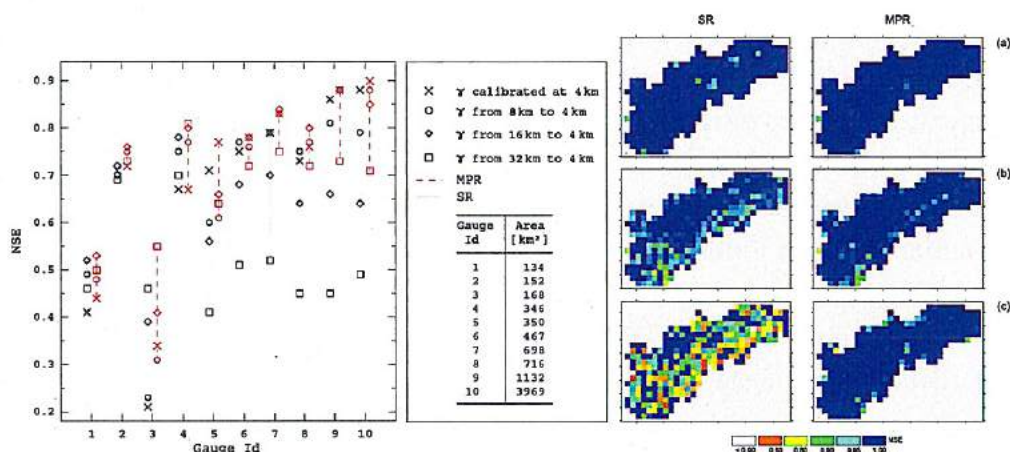


Abbildung 2: Linkes Bild: Leistungen von MPR und SR bezüglich der Tagesabflusssimulationen an verschiedenen Stellen im Einzugsgebiet des Oberen Neckars. Simulationen, unter Nutzung von verschiedenen Transfer-Funktions-Parametern (γ) für beide Methoden wurden an der Modellierungsskala (Level-1 = 4 km) durchgeführt, welche von verschiedenen Skalen erhalten wurde (Level-1 = (4, 8, 16, 32) km). Gauge-Id 10 gehört zum Einzugsgebietsabgang. Rechtes Bild: Diskrepanz zwischen den Flüssen simuliert auf zwei verschiedenen Modellierungsskalen. [Die Kontrollskala (4 km) und die feinere Skala (2 km)] während der Modellierungsperiode. Das NSE wurde als Korrespondenzmaß zwischen den simulierten Flüssen auf der Kontrollskala als Baseline erachtet und die räumliche Aggregation von Flüssen genutzt. Die räumliche Verteilung des NSE für die tägliche Evapotranspiration, den vollständigen Abfluss und die Oberflächenbodenfeuchte ist in den jeweiligen Feldern (a), (b), und (c) dargestellt.

hinsichtlich der Tagesabflusssimulation als auch der jahreszeitlichen Abflusseigenschaften zu untersuchen. Zu diesem Zweck wurde mHM in dem Untersuchungsgebiet mit zwei räumlichen Auflösungen angewendet: aggregiert und räumlich verteilt. In dieser Fallstudie wurde das verteilte Modell mit der MPR und der HRU Methode parametrisiert. Die Kalibrierung der freien Parameter wurde für drei Varianten der Zielfunktion durchgeführt, die separat Schnellfluss, Niederwasserfluss und eine Kombination dieser beiden betonen.

Die Ergebnisse zeigen, dass das Modell bei den Tagesabfluss-Simulationen sowie beim saisonalen Abflussverhalten empfindlich auf die Zielfunktion reagierte, wobei die stärkste Empfindlichkeit beim aggregierten Modell, die geringste beim verteilten Modell mit der MPR Parameterisierung auftrat. Die Zielfunktion, die Schnellfluss und Niederwasserfluss gemeinsam berücksichtigt, erzielte durchweg bessere Leistungen. Die Leistung des verteilten Modells, ungeachtet des Parametrisierungsschemas und der Zielfunktion der Kalibrierung, war bei der Simulation von Tages-Beobachtungs Hydrographen besonders bei Hoch-

wasserrückgangs und Niederwasserfluss Perioden durchweg besser als die des aggregierten Modells. Die relativ schwache Leistung des aggregierten Modells unterstreicht, wie wichtig es ist, physikalische Eigenschaften von Einzugsgebieten zu berücksichtigen, da Niedrigwasserfluss, bei dem große Divergenzen beobachtet werden konnten, hauptsächlich von eben diesen Charakteristiken des Einzugsgebiet bestimmt wird. Allerdings bleibt zu erwähnen, dass die Leistungsfähigkeit des verteilten Modells stark von der angewendeten Parameterisierungsmethode abhängt. Die MPR-Methode konnte im Vergleich zur HRU-Methode nicht nur die Komplexität des verteilten Modells reduzieren sondern auch bessere Ergebnisse für die Simulation vom Tagesfluss im Ablauf und im Inneren des Einzugsgebiets vorweisen.

Hinsichtlich der saisonalen Schnellwasser-Flusseigenschaften konnten keine signifikanten Unterschiede in der Leistungsfähigkeit zwischen dem aggregierten Model und dem verteilten Modell gefunden werden. Im Gegensatz dazu, waren verteiltes Modell mit beiden Parametrisierungsmethoden in Simulationen von Niedrigwasser-Flusseigenschaften dahingegen leistungsfähiger als aggregierte Modelle. Dieses Ergebnis zeigt die Wirkung räumlicher Diskretisierung, wobei gleichzeitig die räumliche Heterogenität physikalischer Eigenschaften von Einzugsgebieten, die eine signifikante Rolle auf die Prognose saisonaler Niedrigwasser-Flusseigenschaften gespielt haben, berücksichtigt werden. Die Leistungsfähigkeit des verteilten Modells, insbesondere der Eigenschaften des Niedrigwasser-Flusses, hingen stark von der Parameterisierungsmethode ab, die angewendet wurde, um räumliche Felder der Modellparameter zu erhalten. MPR lieferte im Vergleich zu HRU, die Simulationen betreffend, nicht nur durchweg bessere Ergebnisse, sondern bewies auch größere Stabilität und Verlässlichkeit bei der Prognose an Binnenlagen dieser Charakteristika. Abschließend, kann angemerkt werden, dass im Vergleich zu Schnellwasser-Flüssen die Leistungsfähigkeit aller Modelle für Niedrigwasser-Flüsse relativ schwach ist. Um die Modelle für Niedrigwasser-Flüsse zu verbessern, sind weitere wissenschaftliche Untersuchungen notwendig.

Zusammenfassend ist anzumerken, dass die vorliegende Arbeit ein effizientes räumlich-verteiltes hydrologisches Modell (mHM) mit einer widerstandsfähigen multiskaligen Parameter-Regionalisierungs-Technik (MPR) aufzeigt, welches für verschiedene Zwecke einschließlich Wasserlaufvorhersage überall entlang eines Kanalsystems innerhalb eines Stromgebiets sowie für die Lieferung ge-

eigneter räumlicher und zeitlicher Dynamik der Bodenfeuchte, Schneebedeckung, etc. anwendbar ist. Die zweiphasige MPR-Parametrisierungs-Methode grenzte nicht nur die Komplexität des Modells hinsichtlich der Anzahl offener, durch die Kalibrierung grob eingeschätzter Parameter ein, sondern zeigte auch einen Weg, die Unterversorgungssystem-Heterogenität der physischen Einflussgebietscharakteristika zu vereinigen, welche die Transfermöglichkeit von globalen Parametern über weitere, nicht für die Modell-Kalibrierung genutzte Skalen und Positionen erleichtert. Die MPR-Methode ist in verschiedener Hinsicht widerstandsfähiger und zuverlässiger, als die momentan verwendete SR-Methode und üblicherweise verwendete HRU-Methode. Diese Dissertation verdeutlicht des Weiteren die Vorteile des räumlich verteilten Modells gegenüber einem aggregierten Modell. Zu letzt gilt es zu erwähnen, dass das im Rahmen dieser Arbeit entwickelte Modell und die Parameterisierungsmethode generell anwendbar sind, insofern die benötigten Informationen verfügbar sind. Die in dieser Studie vorgestellten Ergebnisse betreffen dennoch ausschließlich das Einzugsgebiet des Oberen Neckars. Der Verfasser dieser Arbeit testet das Modell zur Zeit in anderen mesoskaligen Einzugsgebieten in und außerhalb Deutschlands.

Chapter 1

Introduction

"Water is the most critical resource of our lifetime and our children's lifetime. The health of our waters is the principal measure of how we live on the land"

Luna B. Leopold

1.1 Background

Water is essential to human life, functioning of natural ecosystems and for the sustainable socio-economic development of a region. For most of their activities, human beings are strongly dependent on the availability of clean and sufficient water resources. Such activities involve water for drinking purpose, growing food, fibers and woods, generating power and running industries. Over the years, for satisfying most of their needs, humans have shaped their natural environment either by building dams, reservoirs and diversions, to have the most efficient use of the available water, or by cutting down forests to expand agricultural lands or urban areas. The impact associated with such human activities on both water quantity and quality was either insignificant or unnoticed at the beginning of the "Anthropocene"¹ Era. This, however, has changed. During the industrial age, human interactions (e.g. urbanization, deforestation, burning of fossil fuels) with natural environmental processes have increased in intensity. The effects of which are now perceivable at regional and continental scale, as for e.g. changes in the frequency and magnitude of

¹The term "anthropocene" was first introduced by the atmospheric scientist Paul Crutzen in the mid-1970s.

floods and droughts, degradation of water quality (Parry et al., 2007). Main drivers of this growing impact are population and economic growth, which lead to rapidly rising demand of water for food production as well as for industrial water usage.

As we continue through a new millennium the increasing stress on freshwater resources, brought about by growing demand and profligate use, remains to occupy a great area of concern for scientists, water resource professionals and policy makers. A sound planning and management of water resources is needed to satisfy present and future environmental and societal water demands as well as to meet one of the main objectives of the Millennium Development Goals (UNDP, 2003) i.e. sustainable development of water resources.

Along with water management, concerns regarding adverse impact of anthropogenic activities on the natural course of hydrological processes have received a considerable attention both from the scientific and the political sides. There is a general consensus among scientists that global warming induced either due to natural activities (e.g. volcanic eruptions) and/or anthropogenic activities (e.g. deforestation) will intensify, accelerate or enhance the hydrological cycle [e.g. see Parry et al. (2007)]. This enhancement will modify the likelihood of the occurrence of extreme hydrological events such as floods and droughts. Evidently, both extreme events pose a significant threat to human life and entail substantial socioeconomic and environmental consequences such as reduction in water availability for agriculture, industry and domestic use, decrease in hydropower generation, damages to the basic infrastructure, increasing hazard of forest fires and landslides, as well as famines and people's migration.

Not only, but especially because of the consequences associated with the expected changes, it is of crucial importance to improve our understanding of the underlying processes in the hydrological system² and to quantify them. For these purposes, hydrological modeling studies have been pursued. Such modeling exercises generally involve hydrologic models. These models attempt to translate our scientific understanding regarding the movement and storage of water in a complex natural or anthropogenic hydrological system in simplified mathematical formulations. As a result, these models which are mainly driven

²"A hydrologic system is defined as a structure or volume in space, surrounded by a boundary, that accepts water and other inputs, operates on them internally, and produces an outputs. Examples for such system can be a small plot or hillslope, a catchment, a large river basin" (Chow, 1964).

by meteorological inputs (e.g. precipitation and temperature), can reproduce some – but not all – hydrological responses (e.g. streamflow, soil moisture, evapotranspiration).

A brief overview on complexities and challenges involved in such modeling exercises at catchment scale are provided in the following section. Based on the overview, research objectives formulated for this study are presented in the last section of this chapter.

1.2 Hydrological Modeling at Catchment Scale

Although modeling of hydrological processes can be performed from a small plot or hillslope over a catchment to a large river basin, the present research focus on hydrological modeling of a catchment scale or mesoscale because *“catchments are widely recognized as being the most fundamental landscape unit for the cycling of water, which integrates all aspects of the hydrological cycle within a clearly defined area in a way that can be studied, quantified, and acted upon”* (Wagener et al., 2004; Sivapalan, 2005). Additionally, a mesoscale river basin, whose drainage area is within the range of $(10^2, 10^4)$ km² (Dooge, 1986), is generally considered as an appropriate scale to support regional water resources planning and management decisions to address several societal water demands including flood estimation and drought mitigation (Uhlenbrook et al., 2004).

Modeling of hydrological processes at a catchment scale poses, however, a significant challenges mainly because *“catchments are open, highly heterogenous and dynamic complex systems with evolving entities such as vegetation, soil structure, morphology, as well as human beings and living organisms”* (Sivapalan, 2005). As a result, hydrological processes arising due to the interactions between climate inputs and heterogenous landscape properties within a catchment are highly complex and exhibit tremendous variability over a wide range of space and time scales (Dooge, 1986; Blöschl and Sivapalan, 1995). Most of these processes – if not all – are tightly coupled to each other and exhibit intrinsic nonlinear relationships with delayed responses and feedback loops (Beven, 2001b; Porporato and Ridolfi, 2003). Furthermore, as catchments are not only the complex systems but they are also *poorly defined systems*. There often exists a discrepancy between the scale at which models operate (tens of meters up

to several kilometers) and the scale at which routine observations (most often at a point scale) are made (Sivapalan, 2005; Kirchner, 2006). Both practical and financial constraints limit the sampling of required information with fine resolution in a mesoscale control volume. Moreover, many hydrological processes occurring within a catchment take place underground, which in many cases can not be easily measured or observed at every locations. Examples of such processes are: infiltration, sub-surface flow, groundwater flow.

In spite of these complexities and restrictions, a remarkable progress in analyzing and modeling of hydrological process has been achieved during the past decades. During this period, a range of hydrologic models with various levels of conceptualization and parameterization have been developed to support water resources management decisions as well as for the scientific investigation purposes (Russo et al., 1994; Singh, 1995; Vieux, 2001; Singh and Frevert, 2002, 2006). Hydrologic model can be classified into lumped and spatially distributed, depending on the spatial scale at which they model different processes.

A lumped hydrologic model assumes a homogeneous distribution of the catchment characteristics and meteorological inputs and thus represents a catchment as a single modeling entity to simulate the temporal dynamics of streamflow at a given location. Examples of lumped model are: the Stanford model (Crawford and Linsley, 1966), the HBV model (Bergström, 1976), the Xinanjiang model (Zhao et al., 1980), and the SAC-SMA model (Burnash, 1995). However, their applications are limited because these types of models are not suitable to evaluate the effects of spatially distributed environmental changes such as land cover (Bronstert, 2004).

Spatially distributed hydrologic models, on the other hand, account for most of the basin physical characteristics and the spatial variability of the meteorological inputs by discretizing the modeling domain into small individual homogenous units – usually referred as grid cells. These models can simulate the spatial distribution of hydrological processes over the whole modeling domain as well as they have the ability to provide estimates of discharge volume along the entire length of the channel network. Examples of distributed model are: the MIKE-SHE model (Refsgaard and Storm, 1995), the WASIM-ETH model (Schulla and Jasper, 2007), the TOPMODEL (Beven et al., 1995), the ARNO model (Todini, 1996), the distributed HBV model (Lindström et al.,

1997), the VIC model (Liang et al., 1994). During the last decades, there have been a mounting interest towards the development of such models due to their wide range of application. Their applications include, for instance, streamflow forecasts, impact assessment studies such as land cover change on basin response (Hundecha and Bárdossy, 2004), streamflow predictions at interior locations within a basin (Reed et al., 2004) or in ungauged basins (Samaniego et al., 2010a), for the investigation of operational usages of meteorological data sets obtained from satellites and radar networks (Reed et al., 2004), exploratory analysis for integrated water resources management (Samaniego and Bárdossy, 2007). Moreover, the recent advances in remote sensing acquisition techniques, geographical information systems (GIS) and computational powers, have also significantly contributed to this development process.

However, this development process at a mesoscale has not always contributed to find the “right” answers to the main problems of the contemporary hydrology. These problems according to Beven (2001a) are *nonlinearity, scale, uniqueness, equifinality, uncertainty, overparameterization, considerably large execution time*.

Recent developments, especially from the so-called “physically based” hydrologic models, based on the blueprint proposed by Freeze and Harlan (1969), have not properly addressed these problems, in most practical cases, mainly due to the following reasons. Firstly, media properties (both vegetation and soil) are essentially unknown or at least poorly known (Blöschl et al., 2008), this implies that any system’s characteristic will always exhibit some spatial variability regardless of the grid cell resolution chosen for modeling purposes. Hence, trying to use point scale physics (e.g. Richard’s equation) at the basin scale implies that both the media and the boundary conditions should be known specially at the scale of the equations. This, in turn, requires prohibitive amounts of input data, which in most cases goes far beyond practical limitations even for small experimental plots (Zehe et al., 2006). And even if it is possible to gather such information (in near future), the representativeness at the grid scale of point measures would be a matter of concern (Beven, 2001a). Secondly, since the required information seldom exists, modelers are forced to find “effective parameters” via calibration³. As a result, these types

³“Calibration is a process in which model parameters are adjusted so as to match as closely as possible the dynamic behavior of the model to the observed behavior of the catchment such as streamflow” (Gupta et al., 2002)

of models are transmuted into “overparameterized conceptual models” (Beven, 2001a; Kirchner, 2006).

In contrast, “conceptual models” approximate the general physical mechanisms governing the hydrological process on the basis that the assumptions stated above are usually not fulfilled. In particular regarding the assumption of using point scale physics (e.g. Richard’s equation) to a mesoscale level, since the nonlinearity of the governing equations hinders its upscaling from smaller to larger scales through simple averaging (Beven, 2001a; Hopmans et al., 2002; Zhu and Mohanty, 2002). The dominant governing processes in conceptual models, on the contrary, are mainly based on the process understanding and are consequently formulated as a system of location specific ordinary differential equations (Blöschl et al., 2008) as opposed to the partial differential equations which are commonly used in a physically based hydrologic model. As a result, conceptual models are more computationally efficient than physically based models, and therefore they have been commonly used in operational hydrology (e.g. real time flood forecasting). Conceptual models have been mainly focused on the integrated behavior of the hydrologic system, in particular, streamflow hydrograph and its predictive uncertainty. While streamflow is important for characterizing the hydrologic regime of a basin, new problems imposed by society and changing environmental conditions cannot be satisfied without considering the reliable predictions of other interior water fluxes and state variables, such as soil moisture, evapotranspiration, amongst others. Spatio-temporal dynamics of near surface soil moisture and snow cover, as well as spatial heterogeneities of basin physical characteristics (e.g. topography, land cover, vegetation dynamics) are the key factors to improve our ability to better predict the timing and magnitude of streamflow events. Moreover the dynamics of near surface soil moisture, and evapotranspiration, as well as, the spatio-temporal of near surface frozen soil are of fundamental for coupling a hydrologic model with regional climate models (Seneviratne and Stöckli, 2008) and vegetation growth models.

While incorporating the spatial variability of basin physical characteristics and meteorological variables in a distributed hydrologic model should, in theory, improve the overall hydrologic response of a basin (e.g. streamflow simulations), as compared to the simulated responses of its lumped counterpart. However, there are controversies regarding the use of distributed models over lumped

ones (Beven and Binley; 1992; Grayson et al., 1992). For instance, Reed et al. (2004), based on the findings of a comprehensive inter-comparison test between several physically based and conceptual distributed models and lumped models in a phase one of Distributed Model Intercomparison Project (DMIP-I) for the streamflow simulations concluded that “... *lumped model outperformed distributed models in more cases than distributed models outperformed the lumped model* ...”. Similarly, others have also found no significant improvement in daily streamflow simulations using a spatially distributed model [e.g. see Refsgaard and Knudsen (1996); Booij (2005); Das et al. (2008); Pokhrel and Gupta (2009)]. Given these conclusions and the magnitude of research efforts expended during the last decades to realize the benefits of distributed models, it is not yet clear how well these models will help to improve the predictions of hydrologic response of a basin. And therefore whether they can be used for the operational forecasting purpose.

One of the major obstacles in the implementation of a spatially distributed model at mesoscale is its spatial complexity and its parameterization (Refsgaard, 1997; Yilmaz et al., 2008). A spatially distributed model requires a spatial field of model parameters to characterize the spatio-temporal variability of different hydrological processes. Model parameter at a mesoscale are by definition “effective quantities” which can not be inferred from measurement data but need to be estimated through a calibration process. When implementing a spatially distributed models over a large spatial domain the number of unknown model parameters grows quickly as the modeling resolution goes finer and finer. This would eventually lead to a model overparameterization problem. For example, if a distributed model would require 10 parameters per grid cell, in a simplest case, and would be applied in a basin covering an area of 1000 km² with a spatial resolution of 1 km², then the dimension of the calibration problem would be $10 \times 1000 = 10\,000$, a daunting computational task! This high dimensionality of optimization problem not only result in an ill posed and a numerically intractable calibration problem (Doherty, 2003), but also would impose severe restrictions on use of the state-of-the-art optimization algorithms for model calibration (Pokhrel et al., 2008). Model overparameterization could further complicates the parameter identification process due to the equifinality⁴ of feasible parameter sets (Beven, 2001a). This would seriously

⁴Equifinality is the principle that in open systems a given end state can be reached by many

compromise for the predictive validity of model outputs (Seibert, 2003).

Concerns have been also raised regarding the transferability of model parameters from one spatial scale to another scale. Implementing a distributed model in a mesoscale river basin at a coarser spatial scale (e.g. 8 km, 16 km) offers several advantages as compared to applying it at a finer scale (e.g. 1 km, 2 km). These advantages include for instance, a considerable reduction in running time, coupling its hydrological components with a regional climate model, to incorporate an extensive coarser resolution remotely sensed data sets, amongst others. However, the prediction of spatially distributed water fluxes is still required at the finer resolution, for instance, for improving our understanding of underlying processes and thereby for making better predictions. Recent hydrologic studies have reported that model parameters estimated through calibration are not generally transferable to different scales other than that used during calibration [e.g. see Haddeland et al. (2002); Liang et al. (2004); Troy et al. (2008); Samaniego et al. (2010b)].

It is worthwhile mentioning here that the problem of the non-transferability of model parameter across scales is directly or indirectly related to the parameterization process of a distributed hydrologic model. The practical implementation of a distributed model in a mesoscale river basins would be limited without addressing the solution to this problem.

The most common approach for the distributed model parameterization scheme mainly relies on reducing the spatial variability by grouping modeling cells — the smallest modeling spatial unit — into somehow homogeneous regions called “Hydrologic Response Units (HRU)”⁵ (Leavesley et al., 1983; Flügel, 1995). This approach has been commonly used in distributed model parameterization [e.g. Leavesley et al. (1983); Flügel (1995); Donigian et al. (1995); Beldring et al. (2003); Arnold and Fohrer (2005); Das et al. (2008); Blöschl et al. (2008); Viviroli et al. (2009), amongst many others]. The basic assumption behind this approach is that the set of model parameter which control the spatial dynamics of hydrological processes within a particular HRU shares a common value regardless of their location in modeling domain. In this way the HRU method reduces the spatial complexity and thus the model complexity

potential means. The word “*equifinality*” was first used by L. von Bertalanffy in year 1968 in his book named of “General Systems Theory” which was further adopted and popularized in the context of environmental modelling by K. J. Beven and coworkers.

⁵HRU is a “distributed, heterogeneously structured entities having a common pedo-topo-geological characteristics controlling their hydrological dynamics” (Flügel, 1995)

as an unique set of model parameters is assigned to each HRU through a calibration process. Its disadvantages, however, become apparent when a model based on this concept is applied to particular situations. For example, to assess the impacts of a changing input variable such as the land cover, or to estimate reasonable spatio-temporal distribution of state variables or water fluxes such as the soil moisture. In both situations the application of the HRU concept is completely inappropriate mainly because it is based on the static categorical classification and also its geographic location is not necessarily explicit, it does not necessarily preserve an existing local relationship between model parameters and catchment characteristics (Beighley et al., 2005; Viviroli et al., 2009). Furthermore, there is no universally accepted guidelines available regarding how many and which basin predictors can be used for identifying HRUs. As a result, if a model based on this parameterization technique is applied to capture sufficient variability of hydrological processes there is always a danger of a model overparameterization. For example, if a distributed model with 10 parameters is applied in a basin whose drainage area is 1000 km², it would require at least 20 to 30 (or even more) HRUs to capture the spatial variability of hydrological processes [e.g. see Das (2006)]. This imply an optimization problem with at least 200 degree of freedoms. As a result the HRU method could still leads to a highly parameterized model.

An another parameterization scheme which is increasingly used in distributed models and is gaining popularity in recent years is based on the concept of regionalization – *the method to transfer the information (i.e. the set of model parameters) from one location to other* (Blöschl and Sivapalan, 1995). The basic assumption behind this approach is the fact that model parameters are not independent entities that can take any arbitrary values, but rather their values are somehow linked to the basin physical characteristics (Grayson and Blöschl, 2000; Pokhrel et al., 2008). The traditional approach for implementing a regionalization procedure in model parameterization relies on two-step procedure. The first step consists of estimating a set of model parameters in several catchments through a calibrating process. In the next step, a regional relationship is established between the respective basin physical characteristics and the optimum parameter set found in first step (Abdulla and Lettenmaier, 1997; Seibert, 1999; Merz and Blöschl, 2004; Wagener and Wheeler, 2006). This approach is quite simple to implement but disadvantageous because it

does not account for the equifinality of feasible parameter sets or the parametric uncertainty in the regionalization procedure. It uses a unique set of model parameters to establish a regional relationship. As a result such regional relationship may – most likely – provide an inconsistent result for other equally good parameter set and therefore the so-established regional relationships are likely to be weak or inconsistent (Fernandez et al., 2000; Hundecha and Bárdossy, 2004).

The improved approach for the parameter regionalization scheme that take care of the problem of the previous approach relies in treating the both steps of the previous approach concurrently so to simultaneously strengthen the regional relationships and estimating the model parameters (Fernandez et al., 2000). This approach is currently used in parameterizations of various distributed models (Hundecha and Bárdossy, 2004; Götzinger and Bárdossy, 2007; Pokhrel et al., 2008; Samaniego et al., 2010b). The model parameterization based on this approach is also more appealing than the HRU method because it not only reduces considerably the feasible space for the parameter search process in calibration by estimating only few functional parameters instead of model parameters for each cell (Pokhrel et al., 2008; Samaniego et al., 2010b), but also because it attempts to establish a quasi continuous link between basin physical characteristics and model parameters which could be effectively used, for instance, to study the impact of changes in the catchment characteristics, like land cover, on the response of catchment (Hundecha and Bárdossy, 2004). This technique is also being effectively used for transferring the set of model parameters from gauged to ungauged locations or for the predictions in ungauged basins (Abdulla and Lettenmaier, 1997; Seibert, 1999; Merz and Blöschl, 2004; Young, 2006; Wagener and Wheeler, 2006; Samaniego et al., 2010a).

One of the main shortcomings of the both parameterization schemes (i.e. based on the HRU and the regionalization methods) described above are that they do not explicitly account for the sub-grid heterogeneity of basin physical characteristics. These physical characteristics are commonly estimated through pre-defined aggregation techniques such as averaging, majority, amongst others. They remain fixed at the same scale as that of the modeling units (i.e. the grid cells). As a result, both parameterization techniques lose the valuable information regarding the sub-grid heterogeneity which are intimately related to several sub-grid hydrological processes, such as runoff generation at hills-

lope (Barling et al., 1994; Becker and McDonnell, 1998; Grayson and Blöschl, 2000; McDonnell et al., 2001; Zehe and Blöschl, 2004). Moreover in the case of parameter regionalization, the aggregation of catchment physical characteristics from a sub-grid scale to a coarser modeling grid scale could induce a significant noise that can diminish a functional relationship between basin physical characteristics and model parameters, even when a theoretically strong relationship exist (Kling and Gupta, 2009).

1.3 Research Objectives

This thesis presents the results of a course of research designed to address two different but related questions that emerged from the above presented discussions on the practical implementation of a spatially distributed hydrologic model in a mesoscale river basin.

1. *How to formulate a robust and computationally efficient spatially distributed hydrologic model for a mesoscale river basin, which can not only reproduce the discharge hydrograph at any point within a basin but also able to provide a reasonable estimate of the spatio-temporal dynamics of soil moisture, snow cover, amongst other state variables?*
2. *How to obtain spatial fields of model parameters robust enough to reduce the overparameterization problem but still adequate enough to incorporate the sub-grid basin heterogeneity, while ensuring the transferability of model parameters to scales other than that used during model calibration?*

To address these questions, the following research objectives were considered in this study:

- To develop a grid based distributed hydrologic model suitable for both scientific and operation purposes at a mesoscale river basin;
- To formulate and evaluate a robust parameterization method for a spatially distributed hydrologic model;
- To evaluate the efficiency of proposed parameterization method over other existing methods for their performance to preserve the spatial patterns of water fluxes as well as for the conservation the mass balance

of water fluxes at a given control volume, when model parameters are shifted across scales, and

- Finally, to realize the potential benefits of a spatially distributed model over a lumped one for their capability to represent extreme runoff characteristics such as magnitude and frequency of high and low flows.

The structure of this thesis is as follows. Chapter 2 provides a detail description of the formulation of a spatially distributed hydrologic model. In Chapter 3, a review on the state-of-the art regionalization methods is presented. Following to that a method for obtaining the spatial fields of model parameters and its implementation within a proposed distributed model are described in detail. In Chapters 4, 5, and 6, extensive evaluations of a proposed model and a parameterization scheme in a mesoscale river basin are presented. Finally, a summary on the findings of the present study along with a short outline on the future perspectives of this work is presented in Chapter 7.

Chapter 2

Development of a Mesoscale Hydrologic Model (mHM)¹

"The aim of a model is, of course, precisely not to reproduce reality in all its complexity. It is rather to capture in a vivid, often formal, way what is essential to understanding some aspect of its structure or behavior.... We select, for inclusion in our model, those features of reality that we consider to be essential to our purpose... the ultimate criteria, being based on intentions and purposes as they must be, are finally determined by the individual, that is, human, modeler."

Joseph Weizenbaum

2.1 Introduction

In this Chapter, the development of a process based spatially distributed hydrologic model (mHM) suitable for both operational and research purposes at a mesoscale river basin is described. mHM is a continuous water balance model which is based on numerical approximations of dominant hydrological processes that have been tested in well known HBV model (Bergström, 1995; Hundecha and Bárdossy, 2004). mHM also includes a number of new features which are described in the next section(s). In general, mHM uses a *grid cell* as a primary hydrological unit and simulates the following dominant hydrological processes

¹This chapter is a modified version of the manuscript: Samaniego, L., Kumar, R., and S. Attinger. A parsimonious spatially distributed hydrologic model for water resources management at the mesoscale.(Manuscript to be submitted).

(Fig. 2.1): canopy interception, snow accumulation and melting, soil moisture dynamics, infiltration and surface runoff, evapotranspiration, surface and sub-surface storage and discharge generation, deep percolation and baseflow, and discharge attenuation and flood routing.

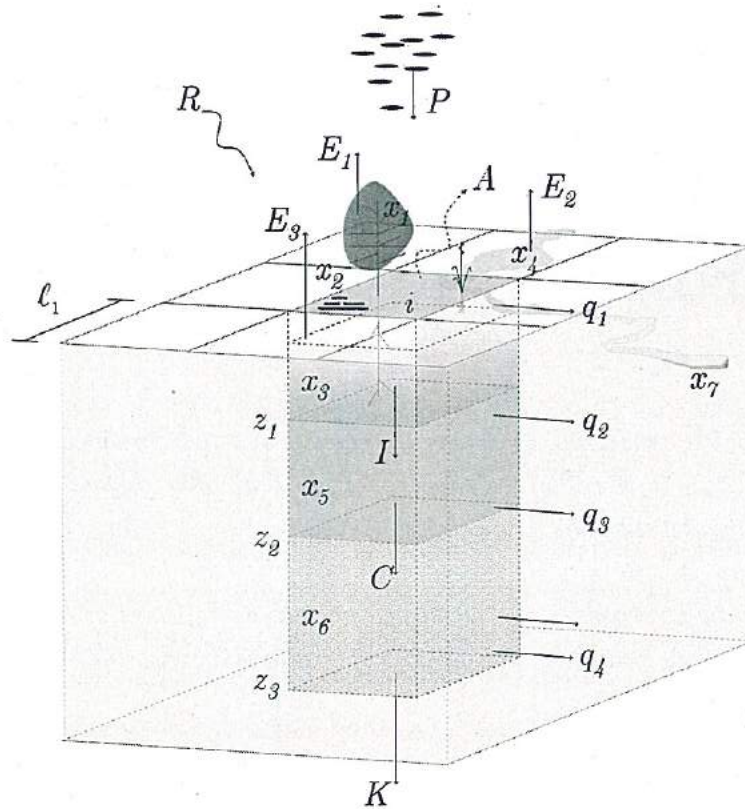


Figure 2.1: General model structure for a cell i at time point t draining to a stream section within a cell (graphic is not to scale).

2.2 Hierarchy of Spatial Scales

Dominant processes of the hydrological cycle at mesoscale span over several orders of magnitude (Blöschl and Sivapalan, 1995). In mHM, three levels (Fig. 2.2) of spatial discretization are differentiated to better incorporate and represent the spatial variability of input, state variables and water fluxes:

1. **Level-0:** Spatial discretization used to describe the sub-grid variability of relevant basin characteristics such as terrain elevation, slope, and aspect,

the main soil characteristics and horizons of a pedotop, main geological formations of a basin, and land cover characteristics. The cell size and cell index at this level are denoted by ℓ_0 and j , respectively.

2. **Level-1:** Spatial discretization used to describe dominant hydrological processes accounted in mHM at a mesoscale. The cell size and cell index at this level are denoted by ℓ_1 (such that $\ell_1 \gg \ell_0$) and i , respectively.
3. **Level-2:** Spatial discretization used to describe the spatio-temporal variability of the meteorological forcings, for example the formation of convective precipitation cells. The cell size at this level is denoted by ℓ_2 (such that $\ell_2 \geq \ell_1$).

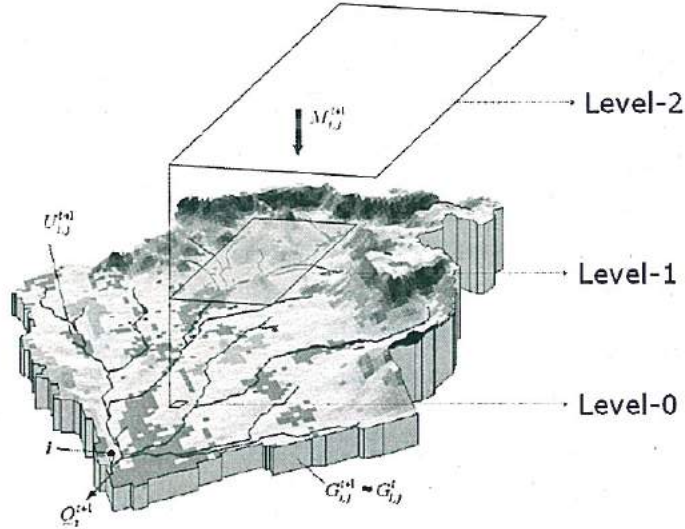


Figure 2.2: Hierarchy of data and modeling levels in mHM.

2.3 The Grid-based mHM Model

2.3.1 Model Formulation

A mesoscale basin is an open system that can be defined mathematically in various ways depending on how the spatio-temporal variability of the basin characteristics is described. If the basin characteristics can be assumed continuous in space, its media characteristics and boundary conditions would be

known at the point scale, and the governing process would be fully scalable, then a system of partial differential equations (PDE) would be suitable to describe the evolution of the dominant processes at this scale (Freeze and Harlan, 1969). Conversely, if these characteristics appeared to be discrete with unknown scaling laws, then a system of ordinary differential equations (ODE) may be appropriate to describe the temporal evolution of these processes at a given location i (Blöschl et al., 2008).

Since the continuity and the scalability assumptions are quite difficult to justify at the mesoscale, most conceptual hydrologic models (e.g. HBV, SAC-SMA, VIC) have adopted a ODE formulation, which may also include stochastic terms representing the uncertainty of the system (Young and Parkinson, 2002). In this study, a system of simultaneously ODEs was adopted for the formulation of mHM.

Let $Z = \{(x, y) | 1 \leq x \leq n, 1 \leq y \leq m\}$ denote a $n \times m$ integer rectangular lattice covering a spatial domain of a river basin Ω . The cell size of this lattice is denoted by ℓ_1 (i.e. at level 1). To ease the notation, the pair of coordinates (x, y) is replaced by a unique cell identifier i as shown in Fig. 2.1, where $i \geq 1 \forall (j, k) \in \Omega$, otherwise $i = 0$. A necessary condition of the lattice covering this domain is that there should be a unique point having the highest flow accumulation. This point is denoted hereafter as the basin's outlet. Moreover, let $\mathcal{M}\{\mathbf{f}, \mathbf{g}\}$ be a distributed mesoscale water balance hydrologic model that relates the state variables \mathbf{x} with some observable categorized as inputs \mathbf{u} and outputs \mathbf{y} . Here \mathbf{f} and \mathbf{g} denote a set of functional relationships that describe the evolution of the system and the quantification of model outputs respectively. \mathbf{u} is a set of fields (grids) representing the land cover, the physiological and the meteorological variables. Based on this the rate of change of the state variables at a given location i (Fig. 2.1) and point in time t are

$$\dot{\mathbf{x}}_i(t) = \mathbf{f}(\mathbf{x}_i(t), \mathbf{u}_i(t), \boldsymbol{\beta}_i(t)) + \boldsymbol{\eta}_i(t) \quad \forall i \in \Omega. \quad (2.1)$$

Observed outputs such as streamflow or ground water levels (\mathbf{y}) at given locations $l \in \Omega$ in time t are defined by

$$\mathbf{y}_l(t) = \mathbf{g}(\mathbf{x}(t), \mathbf{u}(t), \boldsymbol{\beta}(t)) + \boldsymbol{\epsilon}_l(t) \quad (2.2)$$

where $\boldsymbol{\beta}$ is a vector of location specific parameters. $\boldsymbol{\eta}$ is a vector of unmeasur-

able stochastic inputs, which can be interpreted as the degree of uncertainty originated by the lack of knowledge about the dominant processes during the formulation of \mathcal{M} . ϵ is a vector denoting the uncertainty of the system originated by defects on measurements of both the inputs and outputs.

It is worth noting that fields input u and outputs y can be measured or observed at given point in time or at predetermined time intervals. Conversely, the state variables and their rate of change (represented as $\dot{x} = \frac{dx}{dt}$) can only be inferred indirectly. As a result, it becomes impossible to estimate the characteristics probability density function (PDF) of η . The classical deterministic approach to solve this system of ODEs would be to assume that the stochastic term $\eta = 0$ in (Eq. 2.1) and then to embed all model uncertainties into the model parameters β and the measurement noise ϵ . The main disadvantage of this procedure is the impossibility to determine the causality of the various sources of errors. It is worth noting that this solution procedure, although disadvantageous, has been pursued by most of the existing hydrologic models. This approach was also pursued in this study for the sake of simplicity. There are, however, other possible alternatives to solve explicitly this system of stochastic ODE, for example through Bayesian analysis (Kavetski et al., 2006) or data assimilation (Vrugt et al., 2005). The application of any of these techniques within the mHM modeling framework is possible but not pursued in this study. The assumption stated above, although disadvantageous in other respects, would allow us to test the efficiency of the proposed model.

Under the above assumption, the state equations f for a given cell i in time point t (Fig. 2.1) are

$$\left. \begin{aligned} \dot{x}_{1i} &= P_i(t) - F_i(t) - E_{1i}(t) \\ \dot{x}_{2i} &= S_i(t) - M_i(t) \\ \dot{x}_{3i}^k &= (1 - \rho^k) I_i^{k-1}(t) - E_{3i}^k(t) - I_i^k(t) \\ \dot{x}_{4i} &= \rho^1 (R_i(t) + M_i(t)) - E_{2i}(t) - q_{1i}(t) \\ \dot{x}_{5i} &= I_i^2(t) - q_{2i}(t) - q_{3i}(t) - C_i(t) \\ \dot{x}_{6i} &= C_i(t) - q_{4i}(t) \\ \dot{x}_{7i} &= \hat{Q}_i^0(t) - \hat{Q}_i^1(t) \end{aligned} \right\} \quad \forall i \in \Omega \quad (2.3)$$

where k denotes here the index of a root zone layer, $k = 1, 2$. t is a time index for each Δt interval. ρ^k is an overall influx fraction accounting for the impervious cover within a cell. q denotes a surface runoff component, and

Q is the generated discharge. The complete description of the inputs, state variables, fluxes, and output variables can be found in the Notation section. The following sections provide the detail description and mathematical formulation of hydrological processes, that are accounted in mHM. The schematic representation of main components of mHM are shown in Fig. 2.3. The main differences and/or similarities between mHM and three commonly used hydrologic models are presented, after the description of the different mHM components, in Table 2.1.

2.3.2 Canopy Interception

Canopy interception is the amount of precipitation (i.e. liquid and/or solid phases) which is retained by the foliage and do not reach the ground. This process plays an important role on the water balance but is often neglected in hydrologic models (Fenicia et al., 2008). According to Dickinson (1984), the maximum water intercepted by the vegetation is proportional to the leaf area index L (cell sub-indices are omitted to ease the notation):

$$x_1^{\max}(t) = \beta_1 L(t) \quad (2.4)$$

consequently the throughfall is the difference between the precipitation and the interception, which can be estimated by

$$F(t) = \max \{P(t) + x_1(t-1) - x_1^{\max}(t), 0\} \quad (2.5)$$

where β_1 denotes proportionality constant in mm, normally assumed equal to 0.2 mm. P is the precipitation depth. The leaf area index (LAI) is a dimensionless ratio between the total upper leaf surface of the canopy and the surface of the reference area. This index depends on the land cover state (e.g. forest, impervious, permeable) and the vegetative cycle at a given place. LAI ranges from 0 to 8, where the extremes correspond to bare soils (e.g. in settlements) and dense forest, respectively.

2.3.3 Snow Accumulation and Melting

Snow accumulation (x_2) and melting (M) are modeled with a modified version of the degree day method (Linsley, 1943). This method assumes that the potential snow melt depth is proportional to both the temperature above a given

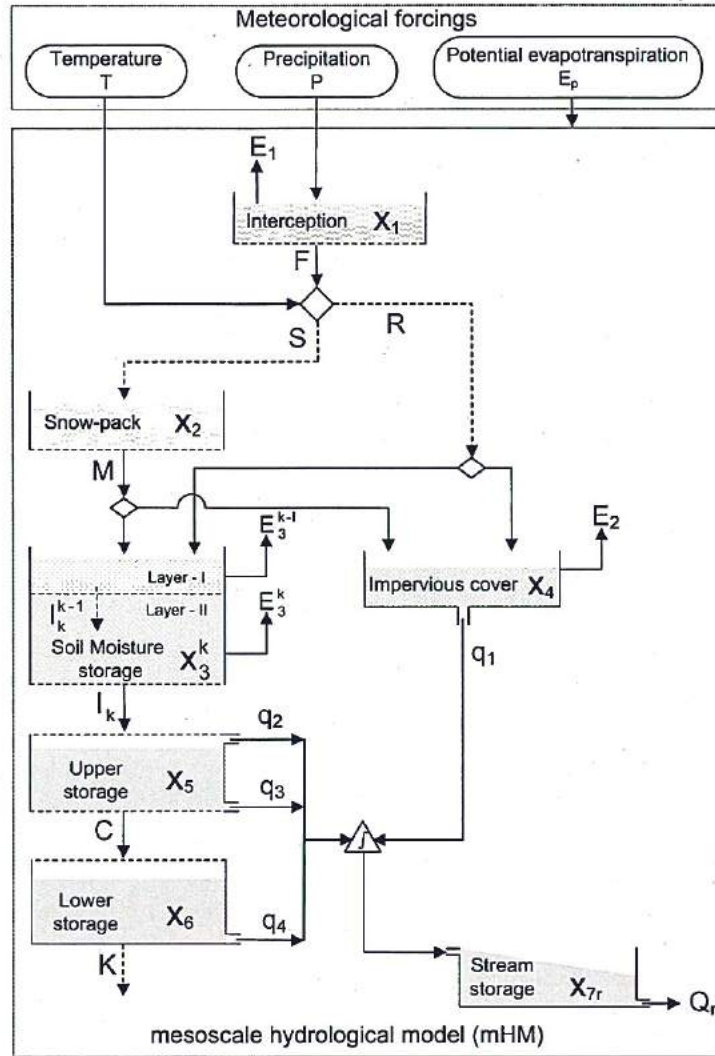


Figure 2.3: Schematic representation of different components accounted in mHM. Where, $X \equiv$ state variable, $E \equiv$ actual evapotranspiration, $q \equiv$ component of runoff, $S \equiv$ snow precipitation depth, $R \equiv$ rain precipitation depth, $F \equiv$ throughfall, $I \equiv$ infiltration capacity, $C \equiv$ percolation, $K \equiv$ gain/loss flux in a leaking cell, $Q_r \equiv$ net runoff produced at the outlet of a grid cell.

threshold β_2 and the amount of heat expelled from the rain in liquid phase. The latter proportionality relationship, however, is limited to avoid over-predicting snow melting rates during intense precipitation events. To estimate the equivalent depth of the snowpack, the throughfall is firstly separated into its liquid

(R) and solid phases (S) by

$$S(t) = \begin{cases} 0 & T(t) > \beta_2 \\ P(t) & \text{otherwise} \end{cases} \quad (2.6)$$

$$R(t) = \begin{cases} P(t) & T(t) > \beta_2 \\ 0 & \text{otherwise} \end{cases} \quad (2.7)$$

Melting rates at a given location i is given by (Hundechea and Bárdossy, 2004)

$$M(t) = \begin{cases} \min \{x_2(t-1), \varphi(t)(T(t) - \beta_2)\} & T(t) > \beta_2 \\ 0 & \text{otherwise} \end{cases} \quad (2.8)$$

here the modified degree-day factor $\varphi(t)$ in $[\text{mm d}^{-1} \text{ } ^\circ\text{C}^{-1}]$ is estimated by

$$\varphi(t) = \begin{cases} \beta_3(t) + \beta_4 R(t) & R(t) < \frac{\beta_5(t) - \beta_3(t)}{\beta_4} \\ \beta_5(t) & \text{otherwise} \end{cases} \quad (2.9)$$

where T denotes the average air temperature, β_3 is the degree-day factor during rainless days, β_5 denotes the maximum degree-day factor reached during rainy days, and β_4 is a positive proportionality factor denoting the rate of increase of the degree-day factor per unit of precipitation.

2.3.4 Soil Moisture Dynamics

mHM (Fig. 2.3) is composed of three subsurface layers. The depths of these three layers are denoted by z_i , $i = 1, \dots, 3$ respectively. The first layer represents the upper part of vadose or – the root zone ($0 \leq z \leq z_1$) – which responds to rainfall events and controls the surface runoff generation. This zone is, in turn, sub divided into two horizons ($\lambda = 2$) to better account for phenomena like soil freezing during winter season and the soil moisture redistribution and evapotranspiration during the summer season (Liang et al., 1996), as well as the alterations of the soil physical characteristics due to anthropogenic activities (e.g. bulk density due to tillage or land cover change). The depths of these subdivisions are denoted by z_1^l , $l = 1, \dots, \lambda$ respectively, and often obtained from soil and geologic maps.

The middle layer (Fig. 2.1) $z_1 < z \leq z_2$ comprises the lower part of the vadose zone that governs the fast and slow subsurface interflows generation. Finally, the third layer represents the saturated zone that controls the baseflow generation. Based on this conceptualization, the ratio between the influx and the efflux at the l^{th} horizon of the root zone is estimated based on a simplification of the Richards' equation proposed by Mahrt and Pan (1984); Liang et al. (1994) neglecting the soil water diffusivity. In case the model is applied in dry environmental conditions (e.g. arid river basin), capillary rise should be included in this equations. The soil water conductivity is based on the relationship proposed by Brooks and Corey (1964).

Under these conditions, the governing equation is

$$\frac{I^l(t)}{I^{l-1}(t)} = \left(\frac{x_3^l(t-1)/d^l - \theta_r^l}{\beta_6^l - \theta_r^l} \right)^{\beta_7^l(t)} \quad (2.10)$$

where $I_i^0(t) = R(t) + M(t)$ for $l = 1$. Here, x_3^l/d^l denotes the average water content [$\text{m}^3 \text{m}^{-3}$] in the l root zone horizon of a given cell and time point. The variable $d^l = z_1^l - z_1^{l-1}$ denotes the depth of each horizon. θ_r^l and β_6^l are the limits within which the soil moisture fluctuates. They denote the residual and the maximum soil moisture content, respectively.

It should be noted, however, that not all rainfall hitting the ground is contributing to the infiltration process because only a fraction of a grid cell area might remain permeable at a given time point. There are two reasons that may hinder the infiltration process.

The first reason depends upon the fraction of impervious surfaces $\rho_U(t)$ (e.g. paved surfaces, roofs) at a given time point estimated with the land cover information at level-0. In this case, the fractional area concept (i.e. fraction of a given grid cell that is located within the basin's boundaries) is employed to ensure that the basin's area is not altered.

The second reason is related to the ground temperature. Empirical evidence shows that freezing temperatures have a substantial impact on both the thermal and hydraulic properties of soils (Bastidas et al., 2005; Niu and Yang, 2006). Frozen soil is in general less permeable (i.e. smaller hydraulic conductivity) than unfrozen soil because the infiltration process mainly occurs through macropores. As a result of the increase of the soil ice content (i.e. water equivalent) in the upper root-zone horizon $\vartheta(t)$, a portion of the perme-

able areas $\rho_T(t)$ become semi- to completely impermeable during freeze-thaw cycles in winter and spring seasons (Koren et al., 1999; Niu and Yang, 2006). During these periods, the thermal conductivity of the soil would also increase. Changes of the mass and energy balances significantly alter the soil moisture dynamics of the top soil horizon which, in turn, lead to an increase of surface runoff. During extreme events, these changes would even decouple the moisture exchange between land surface and the atmosphere (Williams and Smith, 1989).

It is assumed that there is a critical value of soil ice content β_8 , above which the soil is practically impermeable. Consequently, the fraction of impermeable area $\rho_T(t)$ can be estimated as the probability that the soil ice content ϑ exceeds the threshold β_8 , formally:

$$\rho_T(t) = P[\vartheta(t) > \beta_8(t)] = 1 - \int_0^{\beta_8(t)} f(\vartheta) d\vartheta \quad (2.11)$$

Empirical evidence indicates that the spatial variability of ϑ can be described by a standard Gamma distribution (Koren et al., 1999), i.e. $f(\vartheta) \sim \Gamma(\xi, \beta_9)$, with $\xi = \frac{\vartheta}{\theta}$. Here, β_9 and θ are the shape and scale factors of the distribution respectively. In this case, (Eq. 2.11) is reduced to

$$\rho_T(t) = 1 - \frac{1}{\Gamma(\beta_9)} \int_0^v \xi^{\beta_9-1} e^{-\xi} d\xi \quad (2.12)$$

where, the scale parameter can be estimated by $\theta = \frac{E(\vartheta)}{\beta_9}$. Here $E(\cdot)$ denotes the expectation of the soil ice content on a given cell. Since the best estimate of this expectation at the time point t is $\vartheta(t-1)$, the upper limit of the integral becomes $v = \frac{\beta_8(t)}{\theta} = \frac{\beta_8(t)\beta_9}{\vartheta(t-1)}$.

Finally, the soil ice content can be estimated by

$$\vartheta(t) = x_3^1(t)(1 - f_l(t)) \quad (2.13)$$

where f_l denotes the fraction of unfrozen water in the first root zone layer. Since, in the present version of the mHM, the energy balance is not accounted, a simple non-linear relationship based on empirical evidence was employed. According to Patterson and Smith (1981), f_l reduces rapidly in the range from 0°C to -2°C , then, it tends asymptotically to a minimum value. Both, the rate of decrement $\frac{1-\beta_{12}}{\beta_{11}-\beta_{10}}$ and the minimum fraction of unfrozen water β_{12} are soil-

type dependent. Since soil temperature is not often available, the antecedent temperature index a_T is used as a proxy of the accumulated heat in the ground. The proposed relationship to estimate f_l is

$$f_l(t) = \begin{cases} \beta_{12} & a_T(t) < \beta_{10} \\ \beta_{12} + \frac{1-\beta_{12}}{\beta_{11}-\beta_{10}}(a_T(t) - \beta_{10}) & \beta_{10} \leq a_T(t) < \beta_{11} \\ 1 & \text{otherwise} \end{cases} \quad (2.14)$$

where a_T is estimated by

$$a_T(t) = a_T(t-1) + \beta_{13}(T(t) - a_T(t-1)) \quad (2.15)$$

where β_{13} denotes weighting multiplier ranging from 0.1 to 1. T denotes the daily mean air temperature.

2.3.5 Infiltration and Surface Runoff

The infiltration rate I generated by pervious surfaces within a given cell at time t can be estimated as

$$I^k(t) = (1 - \rho^k(t)) I^{k-1}(t) \left(\frac{x_3(t-1)}{d^k \beta_6^k} \right)^{\beta_7^k(t)} \quad (2.16)$$

where

$$1 - \rho^k(t) = \begin{cases} (1 - \rho_T(t))(1 - \rho_U(t)) & k = 1 \\ 1 & \text{otherwise} \end{cases} \quad (2.17)$$

Rainfall hitting impervious surfaces, on the contrary, would generate surface runoff only if a given retention threshold β_{14} is exceeded. Otherwise, surface ponding occurs. This parameter was not regionalized. Formally,

$$q_1(t) = \max \{ \rho(t)(R(t) + M(t)) + x_4(t-1) - \beta_{14}, 0 \} \quad (2.18)$$

The water balance, in this layer, is ensured by the fourth state equation in (Eq. 2.3).

2.3.6 Evapotranspiration

Three types of evaporation are considered in mHM (Fig. 2.3), namely: Evaporation from the canopy E_1 , evaporation from free-water and impervious surfaces E_2 , and evapotranspiration from the root zone layer E_3 . The total evapotranspiration within a cell is the sum of these three components, but should never exceed the potential evapotranspiration (PET) E_p . The attempt to satisfy the PET is carried out sequentially starting from the canopy layer.

The evaporation component originated from the canopy on a grid cell is estimated as according to Deardorff (1978)

$$E_1(t) = \left(\frac{x_1(t)}{x_1^{\max}(t)} \right)^{2/3} E_p \quad (2.19)$$

The evaporation from free-water bodies and/or ponding waters on impervious areas is proportional to the ratio of the current amount of impounded water x_4 and its maximum retention capacity β_{14} , given by

$$E_2(t) = \frac{x_4(t)}{\beta_{14}} \left(\frac{E_p(t)}{f_p(t)} - E_1(t) \right) \quad (2.20)$$

where f_p denotes the time dependent evaporation-pan coefficient.

Finally, the evapotranspiration rate from the root zone depends not only on the evaporative demand of the atmosphere but also on its relative soil water content and the vegetation type. This component can be estimated by the relationship proposed by (Denmead and Shaw, 1962) such that

$$E_3^k(t) = \begin{cases} \alpha \beta_{17}^k (E_p'(t)) & k = 1 \\ \alpha \beta_{17}^k (E_p'(t) - \sum_{l=1}^{k-1} E_3^{l-1}(t)) & \text{otherwise} \end{cases} \quad (2.21)$$

with

$$\alpha = \begin{cases} 0 & x_3^k(t-1) \leq \beta_{15}^k \\ \frac{x_3^k(t-1) - \beta_{15}^k}{\beta_{16}^k - \beta_{15}^k} & \beta_{15}^k < x_3^k(t-1) \leq \beta_{16}^k \\ 1 & \text{otherwise} \end{cases} \quad (2.22)$$

and

$$E_p'(t) = E_p(t) - E_1(t) - E_2(t) \quad (2.23)$$

where k denotes the root zone horizon. β_{15} is the permanent wilting point whereas β_{16} is the soil moisture limit above which the actual transpiration is equated to the PET. β_{17}^k denotes the fraction of roots in the k^{th} horizon, with $\sum_k \beta_{17}^k = 1$.

2.3.7 Subsurface Storage and Discharge Generation

At the mesoscale, lateral flows—not shown in Fig. 2.1—originating from a given cell to a neighboring one are assumed negligible with respect to the vertical components (I , C and K) (Zhu and Mohanty, 2002). Three subsurface storages are considered in mHM to simulate the fast interflow q_2 , the slow interflow q_3 , and the baseflow q_4 . It is worth noting that q_k , $k = 1, \dots, 4$ are afterwards aggregated to generate the total runoff of a given cell.

The fast interflow refers to the intermittent movement of water from the unsaturated zone to the stream channel in a given cell. This flow occurs only if the accumulated influx of water originated from the root zone exceeds the maximum holding capacity β_{18} of the second reservoir. This surface runoff component q_2 can be estimated at any point in time t by

$$q_2(t) = \max \{ I(t) + x_5(t-1) - \beta_{18}(z_2 - z_1), 0 \} \beta_{19} \quad (2.24)$$

where β_{19} denotes a fast-recession constant.

The slow interflow refers to the almost permanent flow of water that also originates from the unsaturated zone. It is estimated as the outflow of a nonlinear reservoir by

$$q_3(t) = \beta_{20} (x_5(t-1))^{\beta_{21}} \quad (2.25)$$

where β_{20} denotes a slow-recession constant and β_{21} is an exponent that quantifies the degree of nonlinearity of the cell response.

The groundwater recharge or percolation C is estimated as a linear reservoir by

$$C(t) = \beta_{22} x_5(t-1) \quad (2.26)$$

where β_{22} denotes the percolation rate.

Currently no capillary flux is taken into account. The mass balance in the second soil layer (i.e. reservoir) is ensured by the fifth state equation shown in (Eq. 2.3).

2.3.8 Baseflow

The last subsurface layer (Fig.) $z_2 < z \leq z_3$ represents the saturated zone which is assumed to generate entirely the base-flow q_4 . This process is conceptualized as a leaking linear reservoir whose outflow can be estimated as

$$q_4(t) = \beta_{23}x_6(t-1) \quad (2.27)$$

with the gain/loss flux K given by

$$K(t) = \beta_{24}C(t) \quad (2.28)$$

where β_{23} is a base-flow recession rate and β_{24} denotes the fraction of the groundwater recharge that might be gained or lost either as deep percolation or as inter-catchment groundwater flow in nonconservative catchments. These two fluxes may occur if the substratum is composed of geological formations such as karstic, limestone, and/or fractured quasi-impermeable insoluble rocks (Le Moine et al., 2007). A value of β_{24} equal to zero corresponds to those basins where the watertightness hypothesis holds.

2.3.9 Discharge Attenuation and Flood Routing

mHM generates time series of streamflow values q for every cell i as the aggregate of all runoff components described before, hence, $q(t) = \sum_{k=1}^4 q_k(t)$. These runoff components, however, should not be consider as produced at the center of a grid cell but as distributed non-uniformly over its area in accordance with the antecedent distribution of soil moisture and the soil moisture capacity. To take into account this effect in mHM, the total streamflow q is convoluted with a triangular unit hydrograph (TUH) $\mu(\beta_{25}, \Delta t)$ to produce the hydrograph Q at the outlet of every cell (i_o). Here, the TUH simulates the routing within the grid cell. Formally, Q can be estimated by

$$Q(t) = \sum_{k=1}^{\delta} q(t - \delta + k)\mu(k) \quad (2.29)$$

with $\sum_{k=1}^{\delta} \mu(k) = 1$ and $\delta = \frac{\beta_{25}}{\Delta t} - 1$. Here β_{25} denotes the duration of the TUH, usually taken as an even number for practical reasons. This parameter is related to the length, land cover, and the slope of the drainage within a grid

cell. Δt denotes the simulation time interval.

It may be noted that, if the modeling cell size is smaller than certain threshold (e.g. $\ell_1 \leq 4\text{km}$) or modeling time step is large (in order of days) then this component (or hillslope routing) becomes not significant and adjusted within surface flow and fast- and slow-interflow recession constants (Blöschl et al., 2008). Conversely, if the cell size exceeds certain threshold limit or modeling time step are short (in order of hours), this component becomes specially important because it represents the differences Of travel time of runoff occurring within every cell (Wood et al., 1997).

The hydrograph generated at each cell are then routed through the drainage network at level-1 towards the basin's outlet. The drainage network at level-1 is conceptualized as a graph whose nodes are hypothetically located at the center of each grid cell connected by links that represent the river reaches. The flow direction of a link correspond to the direction towards a neighboring cell in which the net flow accumulation (outflows minus inflows) attains its maximum value. The net flow accumulation across a cell's boundary at level-1 is estimated based on flow direction and flow accumulation obtained at level-0 (Olivera et al., 2002; Reed, 2003). Fig 2.4 presents the graphical representation of river network upscaling from level-0 (i.e. input data scale) to level-1 (i.e. modeling scale), adopted in mHM. It is worth mentioning that runoff from a given cell can flow to its neighboring cells in multiple directions (Guo et al., 2004). At the mesoscale, however, it is often assumed, for the sake of simplicity, that all runoff leaving a given cell would exit through a major direction (O'Donnell et al., 1999).

A river reach represents those segments of the river network within the boundaries of a grid cell at level-1. The river reach length, its mean slope, and the potential floodplain areas within every grid cell i are also estimated based on level-0 information. The intersections between river reaches and cell boundaries are denoted as inflow or outflow points depending on the flow direction.

Hydrograph routing in river reaches are carried out with the Muskingum algorithm (Cunge, 1969). This simplification of the St. Venant equations is justified in mHM because the potential areas of application of this model would hardly exhibit abruptly changing hydrographs with supercritical flows (Chow, 1964). According to the Muskingum algorithm, the total reach storage as a flood wave propagates downstream is estimated by (cell subindexes required for clearness)

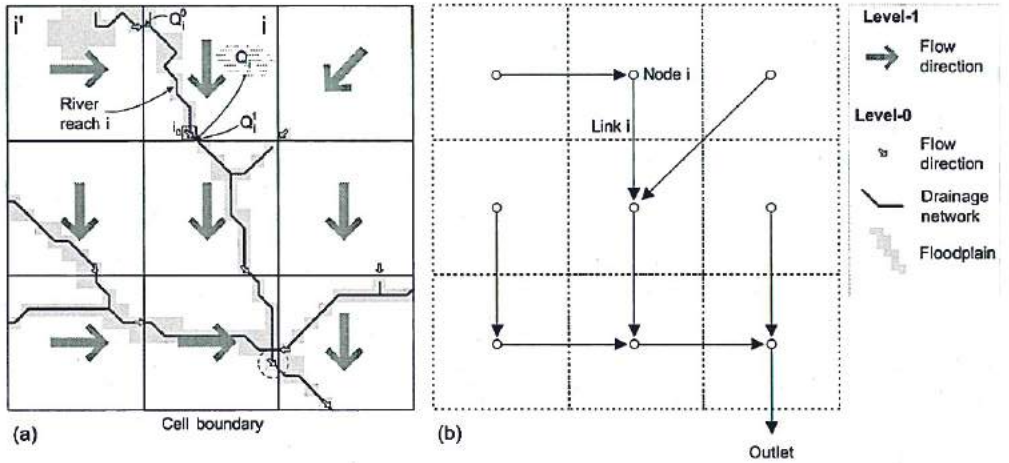


Figure 2.4: Panel (a): Schematic derivation of a drainage network at the level-1 based on level-0 flow direction and flow accumulation. The dotted line circle denotes the point with the highest flow accumulation within a grid cell. Panel (b): Topology of the drainage routing network at level-1.

$$x_{7i}(t) = \beta_{26i}Q_i^1(t) + \beta_{26i}\beta_{27i} (Q_i^0(t) - Q_i^1(t)) \quad (2.30)$$

where

$$Q_i^0(t) = Q_{i'}(t) + Q_{i'}^1(t) \quad (2.31)$$

here Q_i^0 and Q_i^1 denote the discharge entering and leaving the river reach located on cell i respectively. $Q_{i'}$ is the contribution from the upstream cell i' based on (Eq. 2.29). β_{26} denotes the Muskingum travel time parameter. β_{27} is a dimensionless attenuation parameter.

Following a routing sequence obtained from the flow directions at level-1, $Q_i^1(t)$ can be found by combining (Eq. 2.30) with the last state equation shown in (Eq. 2.3), thus

$$Q_i^1(t) = Q_i^1(t-1) + \nu_1 (Q_i^0(t-1) - Q_i^1(t-1)) + \nu_2 (Q_i^0(t) - Q_i^0(t-1)) \quad (2.32)$$

where

$$\nu_1 = \frac{\Delta t}{\beta_{26i}(1 - \beta_{27i}) + \frac{\Delta t}{2}} \quad (2.33)$$

$$\nu_2 = \frac{\frac{\Delta t}{2} - \beta_{26i}\beta_{27i}}{\beta_{26i}(1 - \beta_{27i}) + \frac{\Delta t}{2}} \quad (2.34)$$

$$(2.35)$$

subject to

$$\frac{1}{2(1 - \beta_{27})} \leq \frac{\beta_{26}}{\Delta t} \leq \frac{1}{2\beta_{27}} \quad (2.36)$$

In case that man-made reservoir belongs to the drainage network, the total reservoir capacity and minimum release rates can be specified for each grid cell so that the routing can be performed at each grid cell.

2.4 mHM Model Parameters

The mHM model as described above consists of a total 27 parameters (i.e. β_p , $p = 1, 2, \dots, 27$). Out of which 25 parameters are associated to each modeling cell (at level-1) to describe the spatio-temporal dynamics of the accounted hydrological processes, and the remaining two parameters are for the flow routing process within a river network. A short summary of these model along with their units is provided in Table 2.2. The method to estimate the spatial fields of these *effective parameters* is presented in the next chapter.

Table 2.1: Main differences between mHM and other distributed hydrologic models.

Item	Description	mHM	HBV-IWS	VIC-3L	WASIM-ETH
Code	Open source	yes	yes	yes	no
	Language	Fortran 95	FORTRAN 77	C	C++
Input layers	ℓ_0	DEM, soil types, land cover	-	-	-
	ℓ_1	Hydrological processes	all grids	all grids ^a	all grids
	ℓ_2	Meteorological forcings	-	-	-
Regionalization		all parameters with ℓ_0 data, then up-scaled at ℓ_1	5 parameters	-	-
Meteo.	daily/night variation	yes	-	yes	yes
	PET	Hargreaves-Samani ^c with slope-aspect correction ^d	Hargreaves-Samani ^c	Penman-Monteith ^b	Penman-Monteith ^b
	Interpolation	EDK ^e	EDK ^e	simple average	IDW ^e
Canopy	Interception	Dickinson ^f	-	Dickinson ^f	simple bucket
	LAI	weekly-monthly	-	monthly/seasonal	seasonal
	Evaporation	Deardorff ^g	-	Deardorff ^g	-
Snowmelt		degree-day ^h	degree-day ^h	energy balance	degree-day ⁱ
Soil moisture	Layers	2	1	3	n
	Frozen soil	based on ATI ^m	-	energy balance	-
	Evaporation	nonlinear ^o	Bergström ^k	Liang et al. ^r	nonlinear ^o
	Surface runoff	sealed areas	sealed areas	Saturation-infiltration-excess runoff	-
	Infiltration	Mahrt-Pan, Brooks-Corey ^s	Bergström ^k	Zhao et al., Liang-Xie ⁿ	Green-Ampt
	surface runoff				
Vadose zone	Fast interflow	linear reservoir	linear reservoir ^k	-	-
	Slow interflow	nonlinear reservoir	nonlinear reservoir	-	Richards ^l
	Percolation	linear reservoir	linear reservoir ^k	Brooks-Corey ^j	Richards ^l
Saturated zone	Baseflow	cell, linear reservoir, leakage	lumped linear reservoir	Zhao ⁿ , Todini ^p	lumped nonlinear reservoir, 2D groundwater model
Routing		ℓ_1 , cell-cell TUH ^q Muskingum	lumped TUH Muskingum	cell-cell TUH time delay	kinematic-wave Manning

^a Land cover types is given as fractions in each cell

^b Monteith and Unsworth (2007)

^c Hargreaves and Samani (1985)

^d Shevenell (1999)

^e External drift kriging / inverse distance weighting

^f Dickinson (1984)

^g Deardorff (1978)

^h Linsley (1943), includes a precipitation-intensity correction factor

ⁱ Linsley (1943)

^j Brooks and Corey (1964)

^k Bergström (1995), Bergström et al. (1997)

^l Richards (1931)

^m Antecedent temperature index (ATI)

ⁿ Zhao et al. (1980), Liang and Xie (2001)

^o Related to soil moisture, wilting point and field capacity

^p Todini (1996)

^q Triangular unit hydrograph

^r Liang et al. (1994)

^s Mahrt and Pan (1984), Brooks and Corey (1964)

Table 2.2: List of mHM model parameters.

Parameter	Unit	Description
β_1	-	Thickness of waterfilm on the canopy surface.
β_2	$^{\circ}\text{C}$	Threshold temperature for phase transition snow and rain.
β_3	$\text{mm d}^{-1} ^{\circ}\text{C}$	Degree day factor during rainless days.
β_4	$\text{mm d}^{-1} ^{\circ}\text{C}$	Rate of increase of the degree-day factor per unit of precipitation.
β_5	$\text{mm d}^{-1} ^{\circ}\text{C}$	Max. degree-day factor reached during rainy days.
β_6^k	mm	Max. soil moisture content of k^{th} root zone layer.
β_7	-	Parameter that determines the relative contribution of rain or snowmelt to runoff.
β_8	mm	Critical value of soil ice content in first root zone layer above which the soil is practically impermeable.
β_9	-	Shape factor of the gamma distribution that statistically estimates the virtual impermeable area due to frozen soil.
β_{10}	K	Antecedent Temperature Index (ATI, proxy for soil temperature) threshold below which unfrozen water content reach its minimum value.
β_{11}	K	ATI threshold above which no frozen water exist.
β_{12}	-	Min. value of unfrozen water content estimated as the fraction of total total water content of first root zone layer.
β_{13}	-	Weighting multiplier to estimate ATI from air temperature.
β_{14}	mm	Max. ponding retention in impervious areas.
β_{15}	-	Permanent wilting point, estimated as the fraction of maximum soil moisture content.
β_{16}	-	Soil moisture limit above which the actual evapotranspiration is equated with the potential evapotranspiration, estimated as the fraction of max. soil moisture content.
β_{17}	-	Fraction of roots in the first root zone layer.
β_{18}	mm	Max. water holding capacity of the unsaturated zone.
β_{19}	d	Fast recession constant.
β_{20}	d	Slow recession constant.
β_{21}	-	Exponent that quantifies the degree of nonlinearity of the cell response.
β_{22}	d	Effective percolation rate.
β_{23}	d	Baseflow recession rate.
β_{24}	-	Fraction of the groundwater recharge that might be gained or lost either as deep percolation or as intercatchment groundwater flow in nonconservative catchments.
β_{25}	h	Duration of triangular unit hydrograph accounting for the discharge attenuation within the cell.
β_{26}	h	Muskingum travel time parameter.
β_{27}	-	Muskingum attenuation parameter

Chapter 3

Distributed Model Parameterization¹

"If I have seen further, it is by standing on the shoulders of giants"

Sir Isaac Newton

3.1 Problem Description

The spatial heterogeneity and process complexity of surface and subsurface flow imply that any spatially explicit hydrological model at the mesoscale is only a conceptual approximation of hydrological processes (Beven, 2001a; Kirchner, 2006). Modeling of these processes would, therefore, require substantial simplifications and generalizations. Model parameters that governs hydrological processes would tend to compensate for an unaccounted spatio-temporal heterogeneity caused by the discretization, and due to the errors induced by the numerical solution of the governing differential equations, as well as, due to the simplification and assumptions made during the conceptualization of hydrological processes (Beven, 2001a; Blöschl, 2001; Kirchner, 2006). As a result, these parameters (e.g. β of mHM) at a mesoscale lose their physical meanings and become "*effective parameters*" (Kirchner, 2006). Since these effective parameters are not directly observable or easily inferred from measurement data, they must be estimated through a model calibration process (Beven, 2001a;

¹This chapter is a modified and an extended version of the manuscript: Samaniego, L., Kumar, R., and S. Attinger (2010). Multiscale parameter regionalization of a grid-based hydrologic model at the mesoscale. *Water Resour. Res.*, 46, W05523.

Gupta et al., 2002). Some degree of calibration is, therefore, generally required for any hydrologic model when applied at a mesoscale level.

In case of a spatially distributed model the calibration process is challenging mainly due to its highly parameterized nature. For instance, the proposed distributed mHM model requires an estimate on the spatial fields of 27 model parameter (β) to explain the spatial variability of incorporated hydrological processes. Calibrating mHM with such a significant number of free parameters for every grid cell would lead to the model overparameterization problem. This would not only impose a severe restrictions on the use of available optimization algorithms for a model calibration (Pokhrel et al., 2008), but also would tend to increase the predictive uncertainty of the model due to the equifinality of feasible parameter sets (Beven, 2001a), as discussed in the introductory chapter. Without addressing the solution to the overparameterization problem the practical implementation of a distributed model in mesoscale river basins would be limited.

Considerable research efforts have been devoted during the recent years, different parameterization methods have been developed mostly aimed at reducing the dimensionality of the calibration problem and therefore making it solvable by existing optimization algorithms. One such method that is commonly used in hydrological modeling studies at a mesoscale is based on the Hydrological Response Units (HRU). The basic working methodology and the inherent advantages and limitations of this approach were discussed in the introductory chapter.

An another approach for distributed model parameterization is founded on the concept of parameter regionalization. This was also briefly explained in the introductory chapter. Since the proposed parameterization for obtaining the spatial fields of the mHM model parameters is mainly based on the concept of regionalization method, a detail review on this method is provided in the following section. It may be noted that some parts of the text provided in the following review section may overlap with those written in the introductory chapter. This was unavoidable and was necessary for better understanding and readership of the proposed parameterization technique, as well as, for recognizing the differences between the proposed method and the currently used standard regionalization method.

3.2 Regionalization of Hydrologic Model Parameters

Regionalization in a broad sense is the method to transfer the information (in our case model parameters) from one location to the another (Blöschl and Sivalapan, 1995). Regionalization of model parameters in hydrological modeling studies have been pursued in various ways for various purposes:

- to reduce model overparameterization or the dimensionality of the parameter estimation problem (Pokhrel et al., 2008, 2009),
- to constrain the parameter search space to realistic ranges (Hundecha and Bárdossy, 2004; Göttinger and Bárdossy, 2007),
- to facilitate the transfer of model parameters from gauged to ungauged locations (James, 1972; Magette et al., 1976; Mosley, 1981; Jakeman et al., 1992; Post and Jakeman, 1996; Sefton and Howarth, 1998; Abdulla and Lettenmaier, 1997; Seibert, 1999; Koren et al., 2000; Merz and Blöschl, 2004; Young, 2006; Wagener and Wheeler, 2006; Parajka et al., 2007; Hundecha et al., 2008; Oudin et al., 2008; Samaniego et al., 2010a).

A variety of regionalization approaches has been developed and tested with a varying degree of success, which reviewed from available literature can be categorized in two main groups: First, parameter regionalization carried out after model calibration, or simply *post regionalization*; and second, parameter regionalization carried out simultaneously with a dual objective to establish a functional relationship (or transfer functions) between model parameters and catchment characteristics, and additionally to obtain the fields of model parameters via transfer functions (Hundecha and Bárdossy, 2004), or simply *Simultaneous regionalization*. These transfer-function parameters are also called as global or super parameters (Pokhrel et al., 2008).

The **post regionalization** technique being commonly used (Post and Jakeman, 1996; Abdulla and Lettenmaier, 1997; Seibert, 1999; Merz and Blöschl, 2004; Parajka et al., 2005; Young, 2006; Wagener and Wheeler, 2006; Parajka et al., 2007; Oudin et al., 2008) for model parameter regionalization follows a general two-step procedure: a) estimation of a set of model parameters for

a number of gauged locations or basins independently, followed by b) an attempt to link statistically (e.g. multivariate regression, neural network) model parameters obtained independently for each basin to a set of catchment characteristics. These statistical (or regional) relationship and available catchment characteristics can then be used to derive the estimates of model parameters at ungauged locations (Wagener and Wheeler, 2006). This technique, while intuitive and simple to implement, however, quite disadvantageous due to the following reasons.

First, the parameter regionalization uses a unique set of model parameters to establish a functional relationships and thus do not account for the *equifinality* (Beven, 2001a) of parameters set in the regionalization procedure. Therefore, the strength of so-established regional relationships directly depends upon the parameter sets selected among the many optimum parameter sets. These relationships may provide inconsistent results for other parameter sets and therefore the regional relationships are likely to be weak or inconsistent (Merz and Blöschl, 2004; Hundecha and Bárdossy, 2004; Götzinger and Bárdossy, 2007). Second, a set of calibrated model parameters can be a good solution to minimize a given error function used in calibration but it might be a bad one to perform regionalization analysis because it may not conform with the physical range expected for a given parameter. Or in other words, it might be only an artifact of the calibration process. And third, because an interaction among both parameters and regionalization functions is not considered during the model calibration process (Parajka et al., 2005; Heuvelmans et al., 2006; Wagener and Wheeler, 2006; Boughton and Chiew, 2007), which imply that the regionalized relationship and transfer function parameters so obtained could be a wrong estimate (Kim and Kaluarachchi, 2008).

The **simultaneous regionalization** technique has been proposed to address the shortcomings of the previous approach as well as to account for the spatial variability of model parameters (Fernandez et al., 2000; Hundecha and Bárdossy, 2004; Vogel, 2005; Götzinger and Bárdossy, 2007; Kim and Kaluarachchi, 2008; Hundecha et al., 2008; Bastola et al., 2008; Pokhrel et al., 2008; Pokhrel and Gupta, 2009). In the simultaneous regionalization technique, both steps of post-regionalization are implemented concurrently, instead of treating these two steps as independent, to simultaneously strengthen the regionalization relationships or transfer functions and estimating the model pa-

rameters (Fernandez et al., 2000) thereby mitigating the effect of strong model parameter covariance. The basic procedure is as follows: 1) select a group of gauged basins, 2) establish a prior functional relationships or transfer functions between model parameters and catchment characteristics, 3) calibrate the transfer function parameters coupled with a hydrologic model, and 4) cross-validate the results in a gauged basin that was not used in the calibration procedure.

Early applications of this method were reported by Fernandez et al. (2000), and Vogel (2005). In both cases, authors reported that the simultaneous-regionalization resulted in strong regional regression relationships between model parameters and catchment characteristics, although it did not improved the performance of regionalized model for streamflow simulations in cross-validated catchments. In these studies, however, many of the catchment characteristics employed for regionalization functions required an analysis of stream flow data which limits this method for the predictions in ungauged locations. More recently, Kim and Kaluarachchi (2008) followed the similar approach, but without using streamflow characteristics as predictors. Here the authors reported an improvement in the streamflow simulations using simultaneous-regionalization technique as compared to those obtained through the two step post-regionalization method. However, in all of the above three studies the authors calibrated both unknown model parameters and transfer function parameters which in fact is a redundant because model parameters are internally linked with transfer function parameters (see step-2 of the simultaneous-regionalization technique described above). As a result, use of this approach in the case of a spatially distributed model is not reasonable since it does not solve the overparameterization problem.

A variant of this method was used by Hundecha and Bárdossy (2004), where authors employed standard regionalization method for estimating model parameters of a semi-distributed conceptual model (HBV-IWS). The model was calibrated for the estimation of transfer function parameters instead of the model parameters itself and the spatial variability of the catchment characteristics was grouped into homogenous areas or zones based on land cover classes, soil types and elevation. A follow up of this study was proposed by Göttinger and Bárdossy (2007), in which only the top-soil reservoir of the HBV-IWS model was conceived as spatially distributed. In this case, the authors intro-

duced monotony and Lipschitz conditions into the optimization problem to ensure the continuity of the model parameters in neighboring cells which share similar properties. In both studies models were able to reproduce quite well the discharge hydrograph. However, in both cases reasonable soil moisture patterns are unlikely to be obtained, since this regionalization technique employs discrete classes as basin predictors. More recently, Bastola et al. (2008) followed the similar approach for regionalization of the semi-distributed hydrologic model (TOPMODEL) parameters. A series of studies have been reported by Pokhrel et al. (2008); Pokhrel and Gupta (2009) and Pokhrel et al. (2009) following the same regionalization technique to obtain the spatial field of distributed HL-DHM model parameters. These studies were mainly aimed at reducing the model overparameterization problem, while retaining the predictive ability of the model for streamflow simulations. The relationships between the model parameters and catchment characteristics proposed by Koren et al. (2000) were used to derive a priori parameter estimates. However, the transfer function parameters were further refined by the calibration process to improve the model predictions.

The regionalization techniques reported in recent literature share a common feature in respect that the catchment characteristics used for establishing functional relationships are defined at the same scale that of modeling units (e.g. grid cells). Or in other words, the catchment characteristics are pre-processed (e.g. through an aggregation or upscaling procedures) to the modeling scale before the regionalization procedure is employed. As a result these methods, hereafter denoted as the **standard regionalization technique (SR)**, do not account for the sub-grid variability of the catchment characteristics. Many hydrological studies have demonstrated the importance of such sub-grid variability which are intimately related to the several small scale hydrological processes including the runoff generation process at hillslope (Barling et al., 1994; Becker and McDonnell, 1998; Grayson and Blöschl, 2000; McDonnell et al., 2001; Zehe and Blöschl, 2004).

Moreover, the recent study conducted by Kling and Gupta (2009), showed the impact of ignoring the sub-grid scale variability in parameter regionalization. The authors concluded that the noise induced due to the pre-aggregation of catchment characteristics can be so high that it can diminish the regionalization relationships even when a theoretically strong relationship exists.

In this study, a multiscale parameter regionalization (MPR) technique is proposed to overcome the issues related to the standard regionalization method as mentioned above. This approach is a kind of a simultaneous-regionalization but it differs in many important aspects from those found in the reviewed literature. Foremost in case of MPR, the regionalization is performed at a finer resolution (i.e. data input level) to account for the sub-grid variability of the catchment characteristics such as soil texture, land cover, hydraulic conductivity of the geological formation, among others. Subsequently, the spatial fields of effective model parameters required for capturing the spatial variability of dominant hydrological processes in mHM at a coarser grid are obtained with appropriate upscaling operators. Fig. 3.1 presents the schematic comparison of the proposed MPR method with the SR method and also with the HRU parameterization method.

3.3 Multiscale Parameter Regionalization (MPR)

The MPR technique focus on two levels of spatial resolution: level-0 and level-1. The difference between these two spatial scales were discussed in Section 2.2 in the previous chapter. To shortly summarize that these two scales are the input data scale (level-0) containing gridded information on basin physical characteristics (or predictors in regional relationships), and the modeling scale (level-1) for describing the spatial variability of hydrological processes incorporated in the mHM model.

It is worthwhile mentioning here that the basis of the MPR method is the fact that we are not interested in estimating *aggregated basin characteristics* having little or no information regarding the spatial variability of the natural factors that regulate the hydrological process at the sub-grid scale, but rather than that in estimating *effective model parameters* that capture the emergent properties of these processes at a modeling scale (level-1).

Consequently, to achieve so, the MPR technique requires two phases to estimate the effective values of mHM model parameters β^1 (for details, see Section 2.4) at modeling scale (level-1). These are namely: 1) regionalization, and 2) upscaling. These phases are graphically depicted in Fig. 3.2.

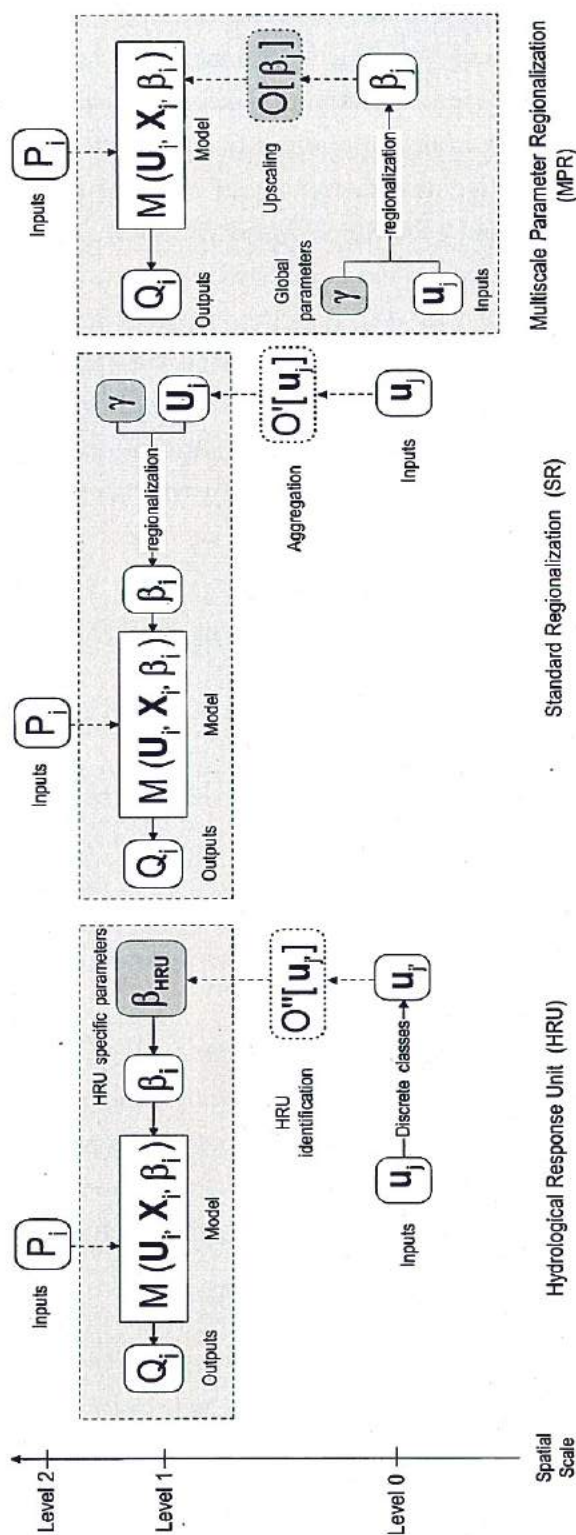


Figure 3.1: Schematic comparison between Multiscale Parameter Regionalization (MPR) and other two parameterization approaches: Hydrological Response Unit (HRU) and Standard regionalization (SR). In case of HRU method and regionalization based methods (i.e. SR and MPR) a set of HRU specific parameters β_{HRU} and global parameters γ is obtained through calibration, respectively.

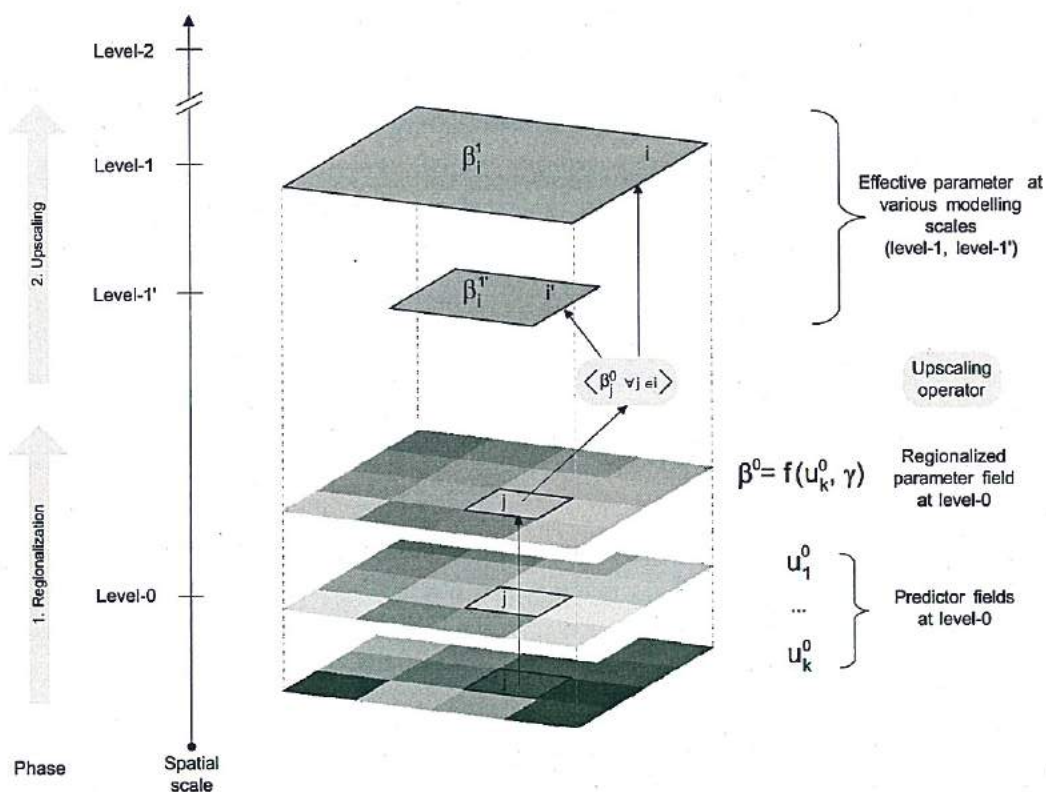


Figure 3.2: Estimation of effective regionalized parameters β^1 at level-1 based on regionalized model parameters β^0 at level-0. Note that global parameters γ are common for the effective parameters at level-1 and level-1'. Given the level-0 information and a modeling scale, say at level-1, γ can be found via calibration.

3.3.1 Parameter Regionalization

The first phase of MPR consists on establishing *a priori* relationships between the fields of model parameter β^0 and distributed basin predictor u^0 at level-0 (Fig. 3.2). These spatio-temporal fields are merged together through linear or nonlinear transfer functions $f(\bullet)$ and scalar values denoted hereafter as *global parameters* γ .

The general formulation of a regionalization or transfer function $f(\bullet)$ can be given by

$$\beta_{ij}^0(t) = f_i(u_j^0(t), \gamma) \quad (3.1)$$

where $\beta_{lj}^0(t)$ denotes the l -th model parameters defined at the cell j at level-0 in time point t , $l = 1, \dots, p$, with p denoting the total number of model parameters. \mathbf{u}_j^0 denotes a v -dimensional predictor vector for cell j . γ is a s -dimensional vector of global parameters, with s denoting the total number of free parameters to be calibrated.

Global parameters γ are hypothesized as quasi-scale-independent scalar values that remain fixed across the whole modeling domain Ω . These global parameters along with the transfer functions and different basin attributes \mathbf{u}^0 estimate the fields of model parameters β^0 at level-0. These functions are based on process understanding and/or empirical evidences (e.g. pedo-transfer functions²). Commonly, static morphological variables of a catchment such as terrain properties – elevation, slope, aspect; soil texture properties – sand, silt, clay, bulk density; geological characteristics – hydraulic conductivity, as well as the dynamic variables – land cover classes, available at level-0 scale can be used as basin predictors (Abdulla and Lettenmaier, 1997; Koren et al., 2000; Hundecha and Bárdossy, 2004).

The main objectives of this phase is to reduce model overparameterization, to ease the transferability of global parameter sets from gauged to ungauged catchments (Samaniego et al., 2010a), and to increase the overall model performance. Furthermore, some model parameters β^0 may be time-dependent due to its linkage with dynamic basin predictors such as land cover.

3.3.2 Estimation of Effective Parameter

The second phase of MPR consists in upscaling of the l^{th} regionalized model parameters $\beta_l^0(t)$ from level-0 to the modeling level-1 (cell i) in a way that the resulting parameter $\beta_{li}^1(t)$ becomes an effective parameter that encapsulates the emerging features of a given process at this scale. The schematic representation of this phase is shown in Fig. 3.2.

The general form of an upscaling operator O applied to the l -th model parameter at level-1 ($\beta_{li}^1(t)$, $l = 1, \dots, p \quad \forall i \in \Omega$) is given by:

$$\beta_{li}^1(t) = O_l \left\langle \beta_{lj}^0(t) \quad \forall j \in i \right\rangle_i \quad (3.2)$$

²Pedo-transfer functions (PTFs) emerged as relationship between soil hydraulic parameters (e.g. saturated water content, saturated hydraulic conductivity, etc.) and the easier measurable properties usually available from soil survey (e.g. percentage of sand, silt and clay; organic matter content, etc.) (Pachepsky et al., 2006)

where p denotes the total number of model parameters, i and j are indices related to grid cells at level-1 and level-0, respectively. $O_l(\bullet)$ is the upscaling operator applied to the model parameter l .

The main challenge in this phase is therefore to find the best, often non-linear aggregation or upscaling rules, hereafter denoted as upscaling operators. Each process and its related effective parameters, however, would have to be analyzed in a case by case approach, since no generally agreed upon upscaling theory exists for dominant hydrologic process at the mesoscale. Consequently, the upscaling operators can be considered as an approximation to account the influence of the subgrid variability on model parameters.

Moreover, these operators should also take into account the characteristics of the sub-grid variability of a given parameter (i.e. second and higher moments) and its propagation via non-linear equations describing the hydrological system. If this is not done properly, significant biases in predicted variables would be introduced. The reason for that stems from the fact that predicting the evolution of an aggregated variable x^1 at a larger scale through a non-linear process $\mathcal{P}(x^1)$ may be quite different from predicting the evolution of the subgrid-scale variability of variable x^0 , since

$$\overline{\mathcal{P}(x_j^0)} \neq \mathcal{P}(x_i^1), \quad \forall j \in i \quad \forall i \in \Omega \quad (3.3)$$

where

$$x_i^1 = \overline{x_j^0}. \quad (3.4)$$

with overbar denoting the arithmetic mean. The magnitude of the difference between the $\overline{\mathcal{P}(x_j^0)}$ and $\mathcal{P}(x_i^1)$ would depend mainly on the temporal gradient of the function \mathcal{P} and the variance of x (Nykanen et al., 2001). This point is also schematically illustrated in Fig. 3.3, which considers the nonlinear evolution of a variable x^0 from sub-grid scale (level-0) to x^1 at modeling scale (level-1) through a non linear process \mathcal{P} and simple upscaling operator (i.e. arithmetic mean) by two different ways.

3.3.3 Implementation of MPR in mHM

Foremost, it should be emphasized here that the working framework of MPR is general and therefore it is not only limited for the mHM model parameter-

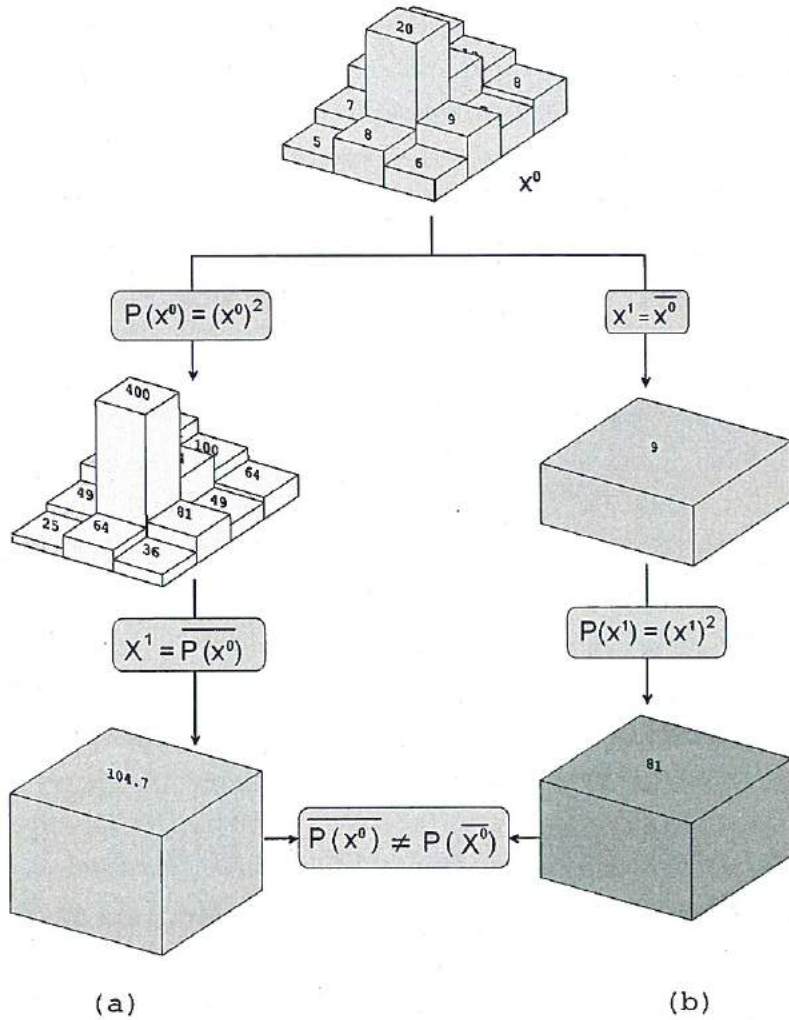


Figure 3.3: Nonlinear evolution of a variable x^0 from sub-grid scale (level-0) to x^1 at modeling scale (level-1) through a non-linear process \mathcal{P} [$\mathcal{P}(x) = x^2$] and arithmetic mean as an upscaling operator by two different ways [MPR (a) and SR (b)]. Depending upon the nonlinear function \mathcal{P} and the magnitude of sub-grid scale variance of x^0 , the effective values of the variable x^1 at higher scales can be very different by two different upscaling sequences. The plot is based on the concept of Nykanen et al. (2001).

ization. It can be applied to any spatially distributed model that employ the regionalization technique for estimating the fields of model parameters. In this study, however, the MPR technique is implemented only for parameterizing mHM. Although the description of study area and detail analysis of required

input data for establishing MPR within mHM is provided in the next chapter, for better readership the basic framework of implementation of MPR in mHM is provided in this chapter for better readership.

The basin predictors at level-0 used for establishing the regionalization functions between them and model parameters are described in Table 3.1. In this table, u denotes a field describing the spatial variability of a given basin predictor. All these predictors, with the exception of land cover, leaf area index (LAI), and fraction of impervious cover on the floodplains, are time independent.

Table 3.1: Description of basin predictors used in MPR.

Variable	Description
u_1	Land cover class (time dependent).
u_2	Leaf area index (LAI) (time dependent).
u_3	Fraction of impervious cover on the floodplains (time dependent).
u_4	Sink free digital elevation model (DEM).
u_5	Terrain slope based on the DEM.
u_6	Aspect based on the DEM.
u_7	Flow directions based on the DEM.
u_8	Flow accumulation based on the DEM.
u_9	Length of the reach segment in cell i at level-1.
u_{10}	Slope of the reach segment in cell i at level-1.
u_{11}	Length of flow path based on flow direction (u_7).
u_{12}	Mean clay percentage in the root zone.
u_{13}	Mean sand percentage in the root zone.
u_{14}	Mineral bulk density in the root zone (Rawl, 1983).
u_{15}	Mean clay percentage in the vadose zone.
u_{16}	Mean sand percentage in the vadose zone.
u_{17}	Mineral bulk density in the vadose zone (Rawl, 1983).
u_{18}	Hydraulic conductivity of major geological formation.
u_{19}	Fraction of karstic formations within a cell i at level-1.

Not all parameters of mHM required to be regionalized because not all of them exhibit spatial variability at the mesoscale level and thus one that does not show the spatial variability can be regarded as global parameters, and have same value in a spatial domain. Among these parameters are: $\beta_2, \beta_4, \beta_9, \beta_{11}, \beta_{12}, \beta_{14}$ (for definition, see Section 2.4). The other model parameters were regionalized, the sources and the predictors used for these regionalization are presented in Table 3.2.

Table 3.2: Predictors used in the regionalization functions. All model parameters β_l^0 are regionalized at level-0, $l = 1, \dots, 28$. Superscript index 0 is not shown to ease notation.

Process	Model Parameter	Predictor variables	Reference(s)
Interception	β_1	LAI	Dickinson (1984); Fenicia et al. (2008)
Snow accum. & Melting	β_2, β_4	—	—
	β_3, β_5	Land cover	Hundecha and Bárdossy (2004); Göttinger and Bárdossy (2007)
Infiltration root zone	β_6	Soil texture, land cover	Zacharias and Wessolek (2007)
	β_7	Soil texture, land cover	Brooks and Corey (1964); Uhlenbrook et al. (2004)
	β_8	Soil texture, land cover	Koren et al. (1999)
	$\beta_9, \beta_{11}, \beta_{13}$	—	—
	β_{10}, β_{12}	Soil texture	Patterson and Smith (1981)
Surface Runoff	β_{14}	—	—
EVT root zone	β_{15}, β_{16}	Soil texture, land cover	Kutilek and Nielsen (1994)
	β_{17}	Land cover	Kutilek and Nielsen (1994)
Fast interflow	β_{18}	Soil texture, land cover	Booij (2005); Uhlenbrook et al. (2004)
	β_{19}	Slope	Booij (2005); Uhlenbrook et al. (2004)
Slow interflow	β_{20}	Soil texture	Booij (2005); Uhlenbrook et al. (2004)
	β_{21}	Soil texture, elevation	Booij (2005); Göttinger and Bárdossy (2007)
Baseflow	β_{22}	Soil saturated hydraulic conductivity	Liang et al. (1994)
	β_{23}, β_{24}	Geological formations	Le Moine et al. (2007)
Routing	β_{25}	Length, slope and land cover of drainage path within the cell	—
	β_{26}	Length, slope and fraction of impervious area of floodplains of the reach segment	Tewolde and Smithers (2006)
	β_{27}	Slope of the reach segment	Tewolde and Smithers (2006)

There are a number of possible operators or upscaling functions that can be used within the MPR method. Their selection and type, however, should be based on conceptual and/or process understanding, and subject to evaluation. Additionally, parsimonious relationships should be preferred to complex ones. In this study, five kinds of upscaling operators were tested, namely: the majority operator \mathcal{M} , the arithmetic mean \mathcal{A} , the maximum difference \mathcal{D} , the geometric mean \mathcal{G} , and the harmonic mean \mathcal{H} . The detail mathematical formulation of these equations are provided in Table 3.3.

The performance of several types of upscaling operators in MPR were studied during the calibration and evaluation phases. Most of these operators and

Table 3.3: Types of upscaling operators to derive an effective parameter at level-1 based on regionalized parameters at level-0. $|\cdot|$ denotes the cardinality of the set.

Name	Notation	Estimation	Condition
Arithmetic mean	\mathcal{A}	$\beta_i^1(t) = \mathcal{A}(\beta_j^0(t))_i = \frac{1}{n} \sum_j \beta_j^0(t)$	$\forall j \in i$
Maximum difference	\mathcal{D}	$\beta_i^1(t) = \mathcal{D}(\beta_j^0(t))_i = \max(\beta_j^0(t)) - \min(\beta_j^0(t))$	$\forall j \in i$
Geometric mean	\mathcal{G}	$\beta_i^1(t) = \mathcal{G}(\beta_j^0(t))_i = (\prod_j \beta_j^0(t))^{\frac{1}{n}}$	$\forall j \in i$
Harmonic mean	\mathcal{H}	$\beta_i^1(t) = \mathcal{H}(\beta_j^0(t))_i = \frac{n}{\sum_j \frac{1}{\beta_j^0(t)}}$	$\beta_j^0(t) > 0, \forall j \in i$
Majority	\mathcal{M}	$\beta_i^1(t) = \mathcal{M}(\beta_j^0(t))_i = b$	$\forall j \in i \quad \{ \beta_j^0(t) = b \} \rightarrow \max \quad b \in \mathbb{N}$

relationship between catchment characteristics and parameter fields at level-0 are based on process understanding and/or empirical evidence. For instance the harmonic mean was used for the soil-related parameters, as suggested by Zhu and Mohanty (2002). A summary of the mHM model parameter regionalization with their corresponding upscaling operators are presented in Table 3.4.

Table 3.4: Regionalization (or transfer) functions and upscaling operators used in the mHM. For simplicity three land cover classes, two soil layers, and two geological formations are employed. Forest $\equiv 1$, impervious cover $\equiv 2$, and permeable cover $\equiv 3$. Time index t only used for time dependent parameters. Superscript indexes of β (0,1) are not shown to ease notation. Subindexes i and j denote cells at level-1 and level-0, respectively. $\|\beta_j\|_i$ denotes a locally normalized field values located within the cell i , i.e. $\|\beta_j\|_i = \frac{\beta_j}{\max \beta_j} \forall j \in i$. \bullet is a globally normalized field.

Process	Param.	Operator	Regionalization Function
Interception	1	$\beta_{1i}(t) = \mathcal{A}(\gamma_1 u_{2j}(t))_i$	
Snow	2	$\beta_{2i} = \gamma_2$	
ac-			
cum. &			
Melt-			
ing			
	3	$\beta_{3i}(t) = \mathcal{A}(\beta_{3j}(t))_i$	$\beta_{3j}(t) = \begin{cases} \gamma_3 & u_{1j}(t) = 1 \\ \gamma_4 & u_{1j}(t) = 2 \\ \gamma_5 & u_{1j}(t) = 3 \end{cases}$
	4	$\beta_{4i} = \gamma_6$	

Table continue ...

Process	Param.	Operator	Regionalization Function
	5	$\beta_{5i}(t) = \mathcal{A}(\beta_{5j}(t))_i$	$\beta_{5j}(t) = \begin{cases} \gamma_7 & u_{1j}(t) = 1 \\ \gamma_8 & u_{1j}(t) = 2 \\ \gamma_9 & u_{1j}(t) = 3 \end{cases}$
Infiltration root zone	6	$\beta_{6i}^k(t) = \mathcal{H}(\beta_{6j}^k(t))_i$	$o_j(t) = \begin{cases} \gamma_{10} & u_{1j}(t) = 1 \\ \gamma_{11} & u_{1j}(t) = 2 \\ \gamma_{12} & u_{1j}(t) = 3 \end{cases}$ $e_j^k(t) = \begin{cases} \frac{1}{\frac{o_j(t)}{o_o} + \frac{1-o_j(t)}{u_{14j}}} & k = 1 \\ u_{14j} & k = 2 \end{cases}$ $\beta_{6j}^k(t) = \begin{cases} \gamma_{13} + \gamma_{14}u_{12j} + \gamma_{15}e_j^k(t) & u_{13j} < f_s \\ \gamma_{16} + \gamma_{17}u_{12j} + \gamma_{18}e_j^k(t) & \text{otherwise} \end{cases}$
	7	$\beta_{7i}^k(t) = \mathcal{H}(\gamma_{19} e_j^k(t))_i$	
	8	$\beta_{8i}(t) = \begin{cases} \mathcal{H}(\gamma_{20} + \gamma_{21} \frac{u_{13j}}{100})_i & \mathcal{M}(u_{1j}(t))_i = 1 \\ \mathcal{H}(\gamma_{20} + \gamma_{22} \frac{u_{13j}}{100})_i & \mathcal{M}(u_{1j}(t))_i = 2 \\ \mathcal{H}(\gamma_{20} + \gamma_{23} \frac{u_{13j}}{100})_i & \mathcal{M}(u_{1j}(t))_i = 3 \end{cases}$	
	9	$\beta_{9i} = \gamma_{24}$	
	10	$\beta_{10i} = \mathcal{H}(\gamma_{25} - \gamma_{26} \frac{u_{12j}}{100})_i$	
	11	$\beta_{11i} = \gamma_{27}$	
	12	$\beta_{12i} = \mathcal{H}(\gamma_{28} + \gamma_{29} \frac{u_{12j}}{100})_i$	
	13	$\beta_{13i} = \gamma_{30}$	
Surface Runoff	14	$\beta_{14i} = \gamma_{31}$	
EVT root zone	15	$\beta_{15i}^k(t) = \mathcal{H}(\gamma_{32} \beta_{6j}^k(t))_i$	
	16	$\beta_{16i}^k(t) = \mathcal{H}(\gamma_{33} \beta_{6j}^k(t))_i$	
	17	$\beta_{17i}(t) = \mathcal{A}(\beta_{17j}(t))_i$	$\beta_{17j}(t) = \begin{cases} \gamma_{34} & u_{1j}(t) = 1 \\ \gamma_{35} & u_{1j}(t) = 2 \\ \gamma_{36} & u_{1j}(t) = 3 \end{cases}$
Fast interflow	18	$\beta_{18i} = \mathcal{H}(\gamma_{37}(1 + \ \Theta_j\))_i$	$\Theta_j = \begin{cases} \gamma_{13} + \gamma_{14}u_{6j} + \gamma_{15}u_{17j} & u_{16j} < f_s \\ \gamma_{16} + \gamma_{17}u_{6j} + \gamma_{18}u_{17j} & \text{otherwise} \end{cases}$
	19	$\beta_{19i} = \mathcal{A}(\gamma_{38}(1 + \ u_{5j}\))_i$	
Slow interflow	20	$\beta_{20i} = \mathcal{A}(\gamma_{39} + \gamma_{40}(1 + \ \kappa_j\) + \gamma_{41}(1 + \ \mathcal{D}(u_{4j})\))_i$	$\kappa_j = \gamma_{42}e^{\gamma_{43}u_{16j} - \gamma_{44}u_{15j}}$
	21	$\beta_{21i} = \mathcal{A}(\gamma_{45}(1 + \ \mathcal{D}(u_{4j})\))_i$	
Baseflow	22	$\beta_{22i} = \mathcal{A}(\gamma_{46}(1 + \ \kappa_j\))_i$	
	23	$\beta_{23i}(t) = \begin{cases} \gamma_{47} & \mathcal{M}(u_{18j}(t))_i = 1 \\ \gamma_{48} & \mathcal{M}(u_{18j}(t))_i = 2 \end{cases}$	
	24	$\beta_{24i}(t) = 1 + (-1)^{\gamma_{49}} \gamma_{50} \mathcal{M}(u_{19j})_i$	

Table continue ...

Process	Param.	Operator	Regionalization Function
Routing	25	$\beta_{25i}(t) = 9 \langle \Upsilon_j(t) \rangle_i$	$\psi_{j'} = \begin{cases} \gamma_{51} & u_{1j}(t) = 1 \\ \gamma_{52} & u_{1j}(t) = 2 \\ \gamma_{53} & u_{1j}(t) = 3 \end{cases}$
			$\Upsilon_j(t) = \sum_{j' \in \{j \rightarrow i_o\}} \psi_{j'} \frac{(u_{11j'})^{\gamma_{54}}}{(u_{5j'})^{\gamma_{55}}}$
			26 $\beta_{26i}(t) = \gamma_{56} \ u_{9i}\ (1 - \ u_{3i}\)^{\gamma_{57}} \ u_{10i}\ ^{\gamma_{58}}$
			27 $\beta_{27i}(t) = \gamma_{59} \ u_{10i}\ $

3.3.4 Remarks on the MPR Technique

1. The regionalization in MPR is carried out at the lowest spatial resolution supported by the input data (i.e. level-0). This contributes to preserving the spatial variability of both the predictors and the regionalized parameters, as well as, it allows for incorporating the sub-grid scale dynamics of hydrological processes. This characteristic not only distinguishes this approach from standard regionalization methods (Fig. 3.1) but also minimizes the bias introduced by simple aggregation of predictors that often introduces a significant noise leading to the deterioration in functional relationships between them and model parameters (Kling and Gupta, 2009). In contrast with MPR, basin predictors in standard regionalization techniques are firstly aggregated from level-0 to level-1, and afterwards parameter regionalization is performed at a modeling scale [e.g. Hundecha and Bárdossy (2004), Pokhrel et al. (2008)].

Furthermore, the rationale behind performing regionalization at lowest spatial resolution of input data is motivated by the fact that most of the spatially distributed hydrologic models or even land surface models (e.g. VIC model) employ a pedotransfer functions for inferring soil related hydraulic parameters (e.g. saturated hydraulic conductivity, saturated soil moisture content), which are mainly derived from the point scale or soil core data from field measurement. The functional relationship between hydraulic parameter and soil properties in such cases exhibit complex and non-linear relationships (Pachepsky et al., 2006), and therefore the estimate of these parameters at coarser modeling scale (level-1) may be quite different with the MPR and the SR method due to difference in upscaling sequences, as discussed before (see Section 3.3.1 and also Fig. 3.3)

2. MPR greatly reduces the level of model complexity in terms of number

of free parameters estimated through calibration process, as denoted by the following inequality

$$p \times n_{\Omega} \gg s \quad (3.5)$$

where n_{Ω} denotes the number of cells contained within the basin Ω . For example, if a hydrologic model requires $p = 27$ parameters per cell (e.g. mHM) and would be calibrated without regionalization in a basin covering an area 1000 km^2 with a resolution of 1 km^2 (i.e. $n_{\Omega} = 1000$ cells), then the optimization algorithm would have to search for a good solution to an optimization problem with $27 \times 1000 = 27\,000$ degrees of freedom, a daunting computational task!

Conversely, if MPR would be applied within mHM, then merely $s = 59$ global parameters γ would have to be estimated. Consequently, MPR becomes quite advantageous during model calibration because sampling in a lower dimensional space improves dramatically the convergence speed of any optimization algorithm (Pokhrel et al., 2008).

3. MPR as a parametrization method is also advantageous with respect to the Hydrologic Response Unit (HRU) concept (Flügel, 1995; Blöschl et al., 2008; Das et al., 2008) because it employs continuous and dynamic regionalization functions rather than a static categorical classification which induces bias and do not necessarily preserve existing local relationships. Additionally, it is more parsimonious than the HRU technique. For instance, if the HRU concept would be employed, at least 10 to 20 HRUs or even more, would be required to represent the spatial variability of a typical mesoscale basin (Das et al., 2008). This would imply an optimization problem with at least 270 DOF for a hydrologic model having 27 parameters (e.g. in mHM) per HRU. MPR, on the contrary, would require only 59 global parameters to take into account the full spatial variability of the basin predictors without requiring any ad hoc classification.

It may be noted that the first phase of MPR (i.e. parameter regionalization) can also be performed with the static or dynamic basin characteristics of pre-classified HRUs. However, this procedure would anyhow require a categorical classification for identifying HRUs, which in-turn induces a bias in parameterization. Moreover, the HRU method using regionalized

functions may not solve a overparameterization problem – i.e. it still requires 59 parameters for each HRU.

4. The MPR method, because of its two phase parameterization approach, allows to generate effective parameters β^1 at various modeling scales, using the same upscaling operators, and without re-calibrating the global parameters γ (Fig. 3.2). Global parameters are expected to be time-invariant and quasi scale-independent. This is quite advantageous because this would allow us to perform the tedious calibration procedure, which requires several thousands iterations for obtaining good parameter sets at a larger scale and then to transfer the global parameters to a finer scale where more detailed information is required. Or in other words it will reduce considerably model time complexity. Furthermore, this would also allow us to link the hydrological model components to a regional climate model normally running at much larger scales, for various purposes, for instance, to explore the sensitivity of future climate conditions on different water fluxes.

It may be noted, however, that shifting global parameters from one scale to another always induces bias and violate the fundamental hydrological continuity principle [i.e. mass conservation on a given control volume (Dooge, 1986)]. This problem is widely recognized in catchment hydrology as a scaling problem [e.g. Blöschl and Sivapalan (1995)]. Large deviations in the conservation of water fluxes due to shift in global parameter across scales would, therefore, be a clear indication of a biased and poor regionalization technique.

5. In the first phase of MPR that is regionalization which attempts to establish a regional relationship between model parameters and basin predictors including the dynamic catchment characteristics such as land-cover properties. As a result MPR offers a possibility to simulate the effect of changes in land cover and/or agricultural management practices on regional water balance (Hundecha and Bárdossy, 2004). Moreover, the regionalization phase of the MPR method also allows us to make usage of mHM with the MPR parameterization method for the prediction in ungauged or data-scare basins (Samaniego et al., 2010a).

Chapter 4

Applications of mHM in a Mesoscale River Basin ¹

"Data, Data, Data! He cried impatiently. I can't make bricks without clay"

Sherlock Holmes

"Models are to be used, not to be believed in!"

James. C. I. Dooge

4.1 Introduction

In this chapter, a detailed application of the proposed spatially distributed mesoscale hydrologic model (mHM) with the multiscale parameter regionalization (MPR) method is presented. All applications of mHM presented in this study are carried out in a mesoscale river basin belonging to Neckar river which is located in the south and south-west of Germany. The selection of this area as a study site was mainly based on the following reasons.

Firstly and the most importantly because of the previous study conducted by Samaniego (2003) for the same region who had reported regarding the fast transformations of land use/cover of the region, from cropland or grassland to built-up area or industrial usages, during the last decades due to anthropogenic

¹This chapter is a modified version of the manuscript: Samaniego, L., Kumar, R., and S. Attinger. A parsimonious spatially distributed hydrologic model for water resources management at the mesoscale. (Manuscript to be submitted).

reasons. This will clearly have sooner or later implications on natural hydrological processes of the region. Secondly because the river flows in the region for most of its part are natural and not affected by hydraulic structures. This had led to implement mHM without any modification in its conceptual structure or inclusion of other dominant modules. And, finally the study basin has long time series of observed hydro-meteorological dataset and other required data sets which are readily available in digitized forms, to set up the mHM model in this area. These data sets, for instance, include digitized terrain elevation map, a series of land cover maps, soil and geological maps with their respective characteristics.

4.2 General Description of the Study Area

The study area belongs to Neckar river located in the south and the south-west part of Germany in the state of Baden-Württemberg (Fig. 4.1). The 367 km long reach of the Neckar is right tributary of the River Rhine. The study basin covers only 28% of the whole Neckar river basin and defined by upstream of the Plochingen Gauging station with a drainage area of approximately 4000 km². Major urban settlements in and around the study region are: Stuttgart, Tuebingen and Rottweil. The region is bounded by the Black Forest in the western side and the Swabian Jura on its south-eastern edge and extends over wide range of landscape features with highly varying altitudes. Topographic elevation ranges from 240 m.a.s.l. to 1010 m.a.s.l. with a mean elevation of about 550 m.a.s.l. Although maximum slopes in parts of Black Forest are as high as 50°, the mean slope in the region is generally mild, with 90% of the slopes are within a range of 0° to 15°.

The geologic formations in the study regions are from the Jurassic and the Triassic periods which are predominantly composed of altered-keuper, claystone-jura, claystone-keuper, loess, sandstone and shelly limestone. Some parts of the study basin lying in the foothill of the Swabian Jura are composed of limestone-jura formations or karstic formations. These karstic formations mainly originated from groundwater flow erosions act as interconnected subsurface reservoirs causing considerably large amount of subsurface water transfer from one catchment to another catchment and therefore would present huge discrepancies in water budget calculations for the region.

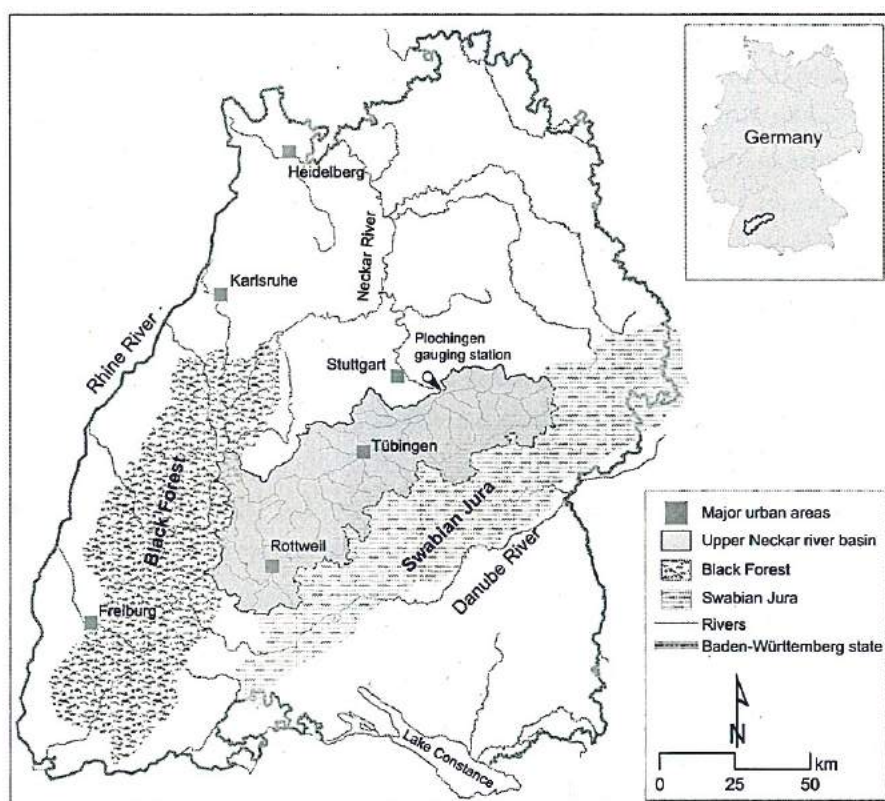


Figure 4.1: Overview of the upper Neckar river basin located within the state of Baden-Württemberg, Germany.

The soil in the study area is highly variable with shallow podsoles and grey brown podsoles formed by weathered variegated sandstones in the western portion (near the Black Forest) to the layers of loess, sandy soils as well as heavy clay originated from shelly limestone and keuper formations on the eastern side of the catchment. This variability is a direct consequence of geological variations.

The vegetation in the study area is mainly dominated by forest of spruce, fir and beech, whereas, the fertile areas on the either banks of the Neckar and foothills of the Swabian Alps are mostly used for agriculture, pasture and meadows. On slopes to the south are partly used for cultivation of wine yards and fruits and partly are covered with ash, beech and elm and lime trees. The barren soils on top of the Swabian Jura are covered with heath and juniper, whereas pastures and meadows are found on heavy-clay soil in the foreland

between keuper and the Alb.

The climate of the study area is characterized by moist with mild winters according to the Köppen notation (Köppen and Geiger, 1939), and is dominated by both continental as well as oceanic weather systems. The impact of the Atlantic Ocean is relatively higher, due to western wind flowing through the region. The daily mean air temperature is approximately 8 °C, ranging between approximately -19 °C and 27 °C with the coldest and warmest months being January and July, respectively (Samaniego, 2003). All above statistics are based on daily data for the time period from 1961 to 1990 (source: DWD). Heavy snow fall events during the winter season are particularly noticed in the upper part (i.e. northwest and southeast parts) of the catchment. Soil freezing may occur during the winter at higher altitudes (e.g. in area of Black Forest). The precipitation events in study area may occur whole year around, however, it exhibit a large variation in both space and time. Mean annual precipitation in the region ranges from 650 mm near Stuttgart to 1800 mm in the Black Forest with the spatial mean of 900 mm (Bárdossy et al., 1999). The wettest and the driest months being June and October, respectively.

The above description of study area was mainly based on the previous studies of Samaniego (2003) and Das (2006), whom conducted their studies in the same study area.

4.3 Data Availability and Processing

The required input data to implement mHM in the study basin were obtained from different agencies and state authorities including German Weather Service (DWD) and the State Agency for Environmental Protection (LUBW, Baden-Württemberg). These data can be broadly grouped into three categories: physiographical characteristics, land cover types and, meteorological variables.

4.3.1 Physiographical Characteristics

The physiographical characteristics of a river basin contain information regarding terrain elevation, soil properties and geological formations. Terrain elevation map also known as digital elevation model (DEM) with a spatial resolution of 50 m × 50 m were obtained from LUBW, Baden-Württemberg. It

was subsequently re-sampled to a spatial resolution of $100\text{ m} \times 100\text{ m}$ in an ArcGIS toolbox using a nearest neighborhood sampling technique. The DEM map was further processed to produce a "sink free DEM" map, that ensures a given drainage basin must have only one single pour point. From the sink free DEM different characteristics such as flow direction, flow accumulation, stream network, slope, aspect, was derived. Subsequently, the watershed boundary corresponding to the outlet of the study area (i.e. Plochingen gauging station; N3 530 930 m and E5 396 740 m in the Gauss-Krueger-3 coordinate system) was delineated. The drainage area of the delineated watershed was cross-checked with the official drainage map (Hydrological Atlas Map of Germany, HAD). Fig. 4.2 shows some of these physical characteristics of the study area.

A digitized soil map for the study area at the scale of 1 : 200 000 (BÜK 200) was obtained from LUBW, Baden-Württemberg, and subsequently processed to $100\text{ m} \times 100\text{ m}$ raster map in an ArcGIS toolbox. The soil map was grouped into 20 major soil classes based on the soil textural information and the root zone depth. The spatial variation of the sand and clay contents within the study area are depicted in Fig. 4.3. These contents for different soil classes are based on the look up table from AG Boden (1994). Mineral bulk density for each soil class using their soil textural information was estimated by the relationship proposed by Rawl (1983) .

A digitized geological map for the study area at the scale of 1 : 600 000 was obtained from LUBW, Baden-Württemberg, and was subsequently processed to $100\text{ m} \times 100\text{ m}$ raster map in an ArcGIS toolbox. Although there exists a significant variation in the geological formation within the study area (Fig. 4.4), in the present study only karstic (i.e. areas that belongs to only Limestone-Jura formations) and non-karstic formation were distinguished for the geological formations. This differentiation was necessary since the karstic formations could present huge abnormalities in water budget calculations. The groundwater flow in presence of karstic aquifer is accounted in mHM in a simplified way (for detail see Section 2.3.7 in Chapter 2) since these formations are mainly located around the boundary of the study area for which no measurements regarding the inter-catchment groundwater flow are available. It is worthwhile pointing here that the presence of karstic formations could be one of the potential source of errors in modeling for the closure of water balance in these regions.

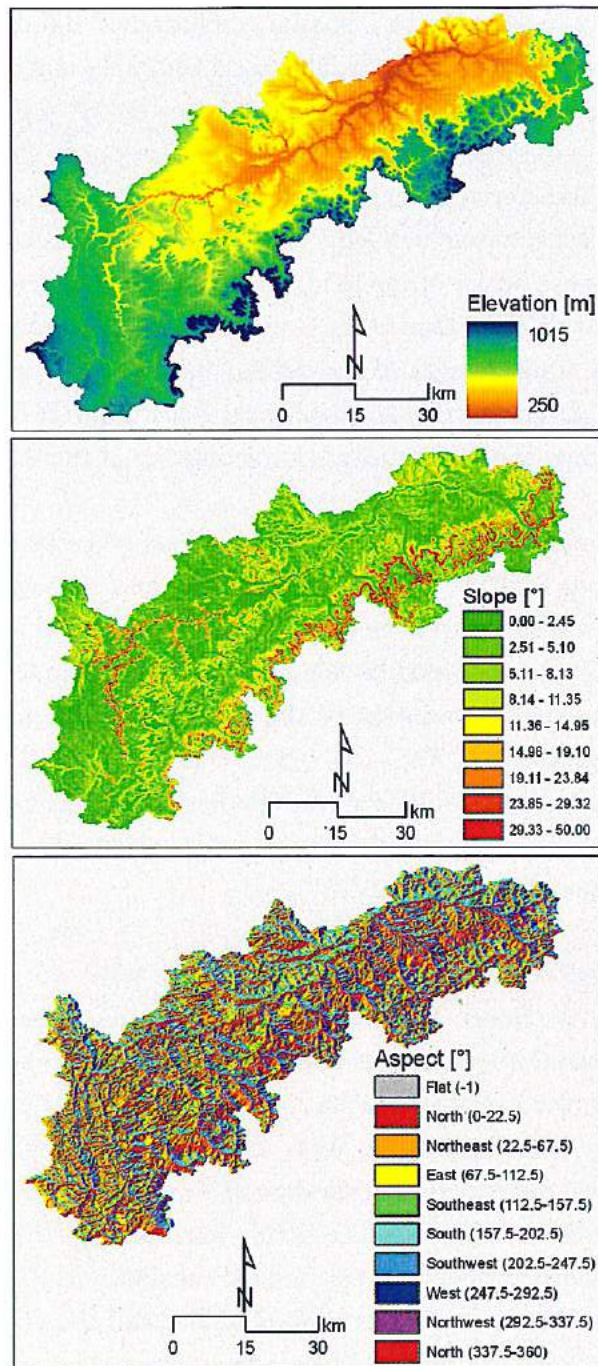


Figure 4.2: Physiographical characteristics map for the study area. From top to bottom: Terrain elevation, slope and aspect. Source: 100 m× 100 m, LUBW.

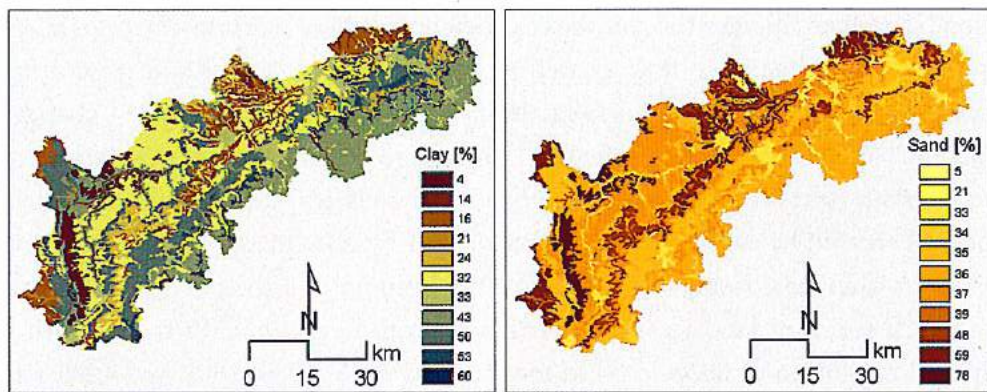


Figure 4.3: Variation in soil textural properties within the study area: clay (left panel) and sand content (right panel). Source: 1 : 200 000 (BÜK 200), LUBW; resampled to 100 m × 100 m.

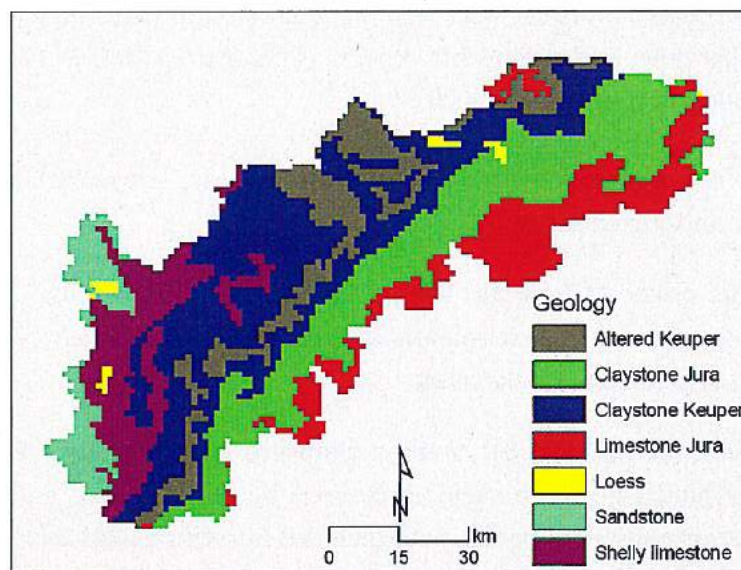


Figure 4.4: Variation in geological formation within the study area. The karstic formation corresponds to Limestone-Jura. Source: 1 : 600 000, LUBW; resampled to 100 m × 100 m.

4.3.2 Land Cover Characteristics

In addition to the physiographical characteristics, land cover plays an important role in modulating the movement and the storage of water within a river basin through various processes such as canopy interception, evapotranspira-

tion, as well as changes the soil water relation capacity, which in-turn can effect surface and sub-surface flow as well as the infiltration and runoff generation processes. The study area, during the last decades, has experienced changes in land cover/uses from permeable covers (e.g. croplands or grasslands) to impervious areas (e.g. urban areas or industrial usages) mainly due to anthropogenic activities as per the study conducted by Samaniego (2003). In some places within this basin, this transition has been up to 1.5% per year. For this reason a series of land cover maps derived from Landsat TM5 scenes with a spatial resolution of 30 m \times 30 m for the year 1975, 1984, 1989 and 1993 was used in this study. These maps for the study area were further classified by an algorithm proposed by Bárdossy and Samaniego (2002) and subsequently re-sampled in an ArcGIS toolbox into raster maps of 100 m \times 100 m spatial resolution. Different land cover classes, ranging from urban settlements to agricultural areas to forests, were then aggregated into three main categories: Forest, impervious and permeable covers. This aggregation is based on the previous study of Samaniego (2003):

Forest (Class 1): composed of permeable areas covered by coniferous, deciduous, and mixed forest,

Impervious cover (Class 2): mainly composed of impervious areas with land usages such as settlements, industrial parks, highways, airport runways, and railway tracks, and

Permeable cover (Class 3): mainly composed of permeable areas covered fallow lands, or those surfaces covered by crops, grass, and orchards. Wetlands and water bodies were included into this class because they are insignificant in this region.

The land cover maps showing the changes in land cover for the year 1975, 1984 and 1993 in the study area are depicted in Fig. 4.5.

Another important land cover property is leaf area index (LAI), which has major implications on various simulated hydrological processes such as canopy interception storage, root zone soil moisture, plant root water uptake, amongst others. The time series of LAI mainly shows the plant phenology and is variable in both space and time. It exhibits strong seasonal characteristics, which means while the annual cycle of LAI is fixed it shows a strong temporal

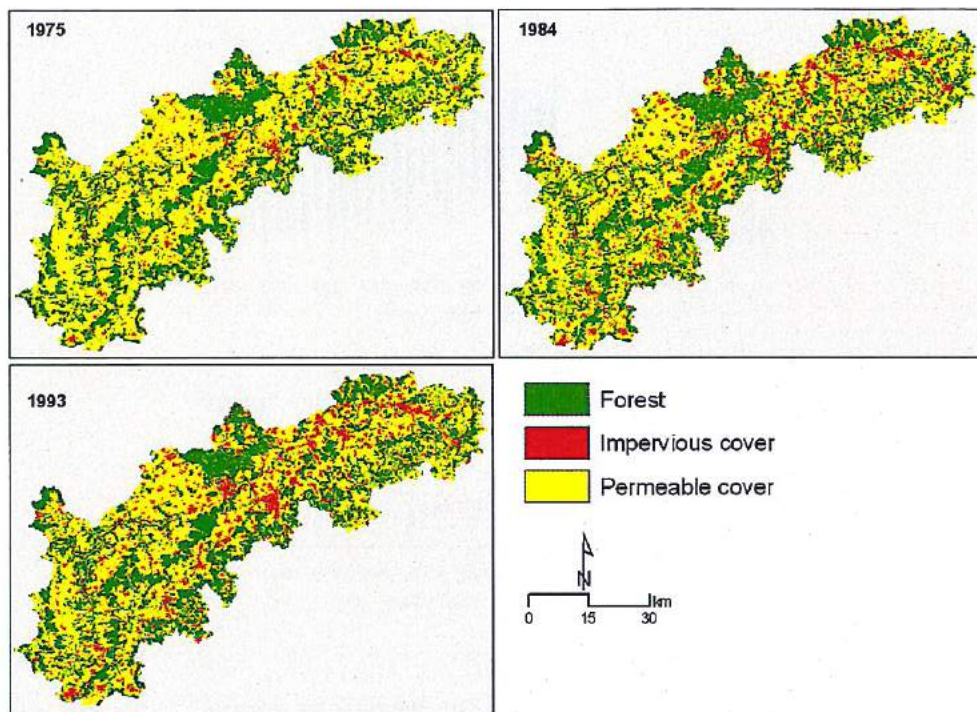


Figure 4.5: Land cover maps for the study area for the year 1975, 1984 and 1993. Source: 30 m \times 30 m, Landsat TM5 scenes; resampled to 100 m \times 100 m

seasonal variations. It can be directly measured using LAI meters during the field campaigns. However, it is not feasible to estimate LAI with direct measurement techniques over a large spatial domain both due to the financial and the practical limitations. Often indirect remotely sensed measurement techniques are used as alternatives. In this study, weekly LAI data at the spatial resolution of 500 m \times 500 m during the period from 2001 to 2007 were obtained freely from Moderate Resolution Imaging Spectroradiometer (MODIS, NASA; <https://wist.echo.nasa.gov/api/>). These data were subsequently processed for each land cover class and the spatio-temporal variability of LAI was approximated by merging the maps of land cover (based on Landsat TM5) with the long-term weekly LAI values. Fig. 4.6 briefly depicts the temporal variation of weekly LAI data for three main land cover classes averaged over the study area.

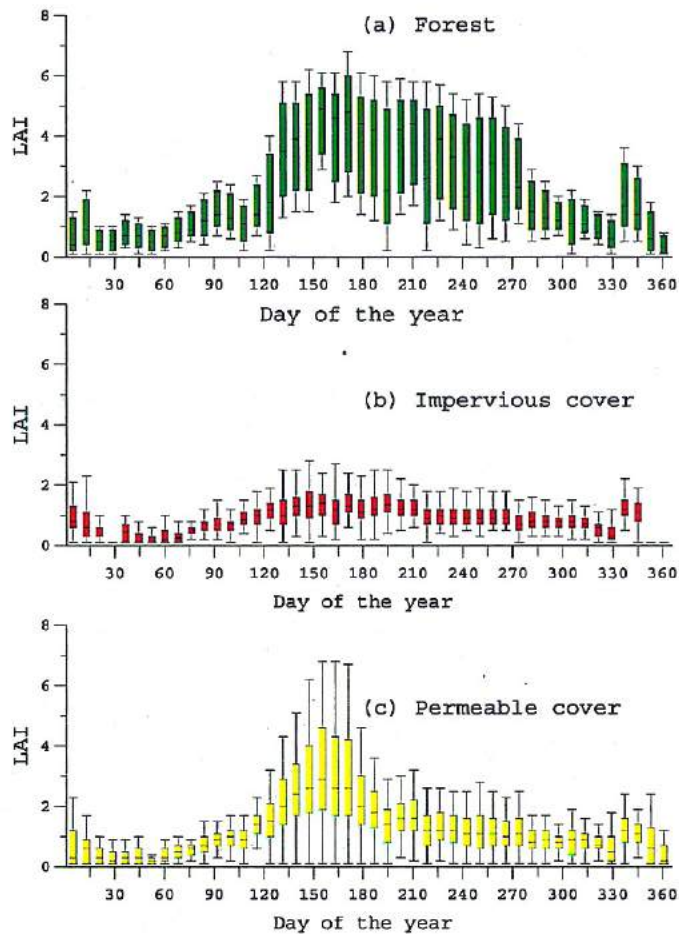


Figure 4.6: Long term yearly distribution of LAI for three land cover classes: Forest, impervious cover and permeable areas. Source: weekly LAI-MODIS data from 2001 to 2007.

4.3.3 Meteorological Variables

Meteorological variables, in general and precipitation and temperature in particular are the main driving forces for hydrological processes such as soil moisture, runoff generation, infiltration, evapotranspiration, snow melt, occurring within a basin. Both variables exhibit a large variability in both space and time. As a result, hydrological response simulated by a model depicts a similar behavior in both dimensions. These variables are directly measured at meteorological or climate stations at a point scale by conventional gadgets. There are also indirect procedures to infer these variables including rainfall

estimates through either radars or satellites (e.g. Tropical Rainfall Measuring Mission (TRMM), NASA). However rainfall amounts directly measured at meteorological stations is often used to remove bias in precipitation estimate inferred by an indirect procedure.

The measurements of daily total precipitation from 294 stations and daily average, maximum and minimum air temperature from 157 climatic stations distributed within and around the study area (Fig. 4.7) were obtained from DWD for the period from 1979 to 2001.

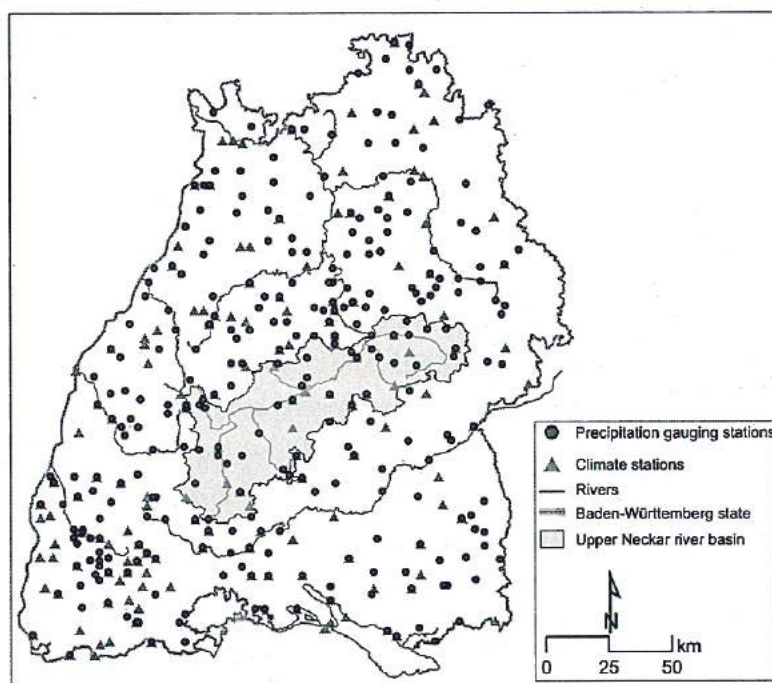


Figure 4.7: Location of precipitation and temperature stations in and around the study area. Source: DWD.

Since these input meteorological data are measured at point scale, and for driving a distributed hydrological model with these variables their areal average estimates over a modeling grid cells are required. There exist several interpolation techniques such as simple isohyetal, Thiessen-polygons, arithmetic mean, inverse distance method, amongst others, in this study an external drift kriging (EDK) method (Ahmed and Marsily, 1987) was used for the spatial interpolation of all meteorological variables. The EDK method is based on the geostatistics and its *intrinsic hypothesis* that assumes the expected value of

regionalized variables (e.g. precipitation) is constant all over the domain of the study and the variance of the difference in the values of the regionalized variable corresponding to two different locations (i.e. distance between rain gauges) depends only on the vector separating them. EDK offers several advantages over other traditional methods and some of them can be listed as : a) it ensures the spatial continuity of the variable under investigation over the large distance, if it or till it exist, b) it is best linear unbiased estimators and, c) it offers a possibility to incorporate the effects of additional variables that shows a relationship with meteorological variables. For instance the variation of either precipitation or temperature due to terrain elevation.

To apply the krigging method for the spatial interpolation of meteorological variables, a theoretical variogram model is required to fit the experimental variogram. The experimental variogram is computed by considering the difference between observations separated by a given distance. Based on the previous studies conducted by Bárdossy et al. (1999) and Samaniego (2003) for the same region, an isotropic theoretical variogram (i.e. variogram that depends on the scalar separation distance and not on the direction) composed of a pure nugget effect and a spherical variogram was used in this study. Fig. 4.8 depicts a sample of the experimental variogram and the corresponding fitted theoretical variogram derived from the daily time series of precipitation and the daily average air temperature obtained from their respective stations for the whole observational period (i.e 1979 to 2001). Since both precipitation and air temperature has fairly good relationship with the topography (Bárdossy et al., 1999), the terrain elevation was used as an external drift in the EDK interpolation method. The daily time series of total precipitation and average, maximum and minimum air temperature for whole observational period were subsequently interpolated on $1 \text{ km} \times 1 \text{ km}$ spatial resolution with the EDK method ². Fig. 4.9, as an example, shows the spatial distribution of the long term mean (1991 to 2001) of daily meteorological variables obtained through the EDK method. For more details on the EDK interpolation method may please refer to (Ahmed and Marsily, 1987; Bárdossy et al., 1999; Samaniego, 2003).

²The initial version of fortran code for external drift krigging was obtained from Dr. Luis E. Samaniego, and later modified by the author.

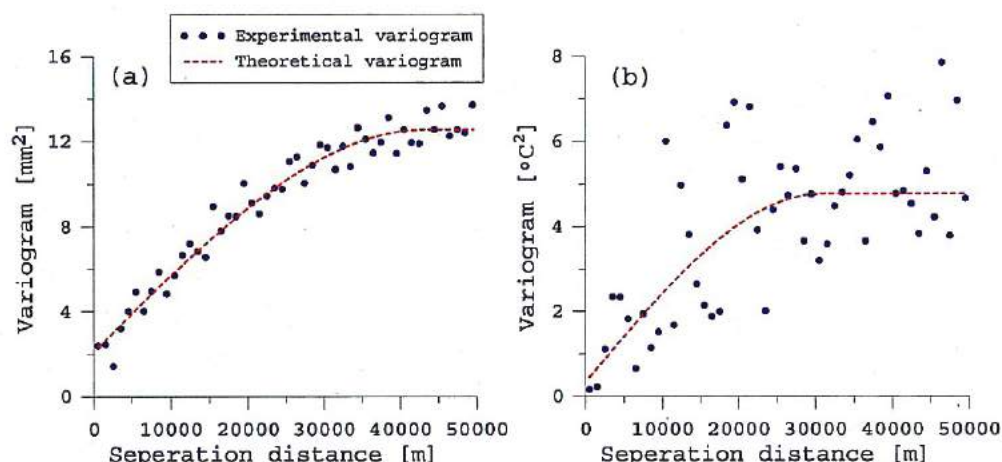


Figure 4.8: Experimental and fitted theoretical variogram for the daily total precipitation [left panel: (a)] and the daily average air temperature [right panel: (b)] for the study region. Source: Daily time series data for the period from 1979 to 2001, DWD.

Potential Evapotranspiration

Another meteorological variable which is required to run mHM is the estimate on potential evapotranspiration. Evapotranspiration is the combination of evaporation occurring from soil, open water bodies, vegetation surface, and transpiration from vegetation. It thus represents the process by which water is returned back to the atmosphere. This process plays an important role in the natural water cycle and it is mainly driven by the solar energy as the source for the latent heat of vaporization and the prevailing meteorological conditions such as wind velocity, relative humidity, to transport the water vapor away from the evaporating bodies. Additionally, the characteristics of evaporating surfaces such as vegetation cover, plant phenological properties, and terrain characteristics such as slope, aspect, and water availability also influence the evapotranspiration process.

If there is sufficient moisture available to completely meet the evapotranspiration needs of a well vegetated surface then the resulting evapotranspiration or an equivalent amount of water is called potential evapotranspiration (PET). Actual evapotranspiration is always equal or lower than this potential limit and depends mainly on water available for meeting the evaporation and/or transpiration demands. Actual evapotranspiration is usually obtained via sim-

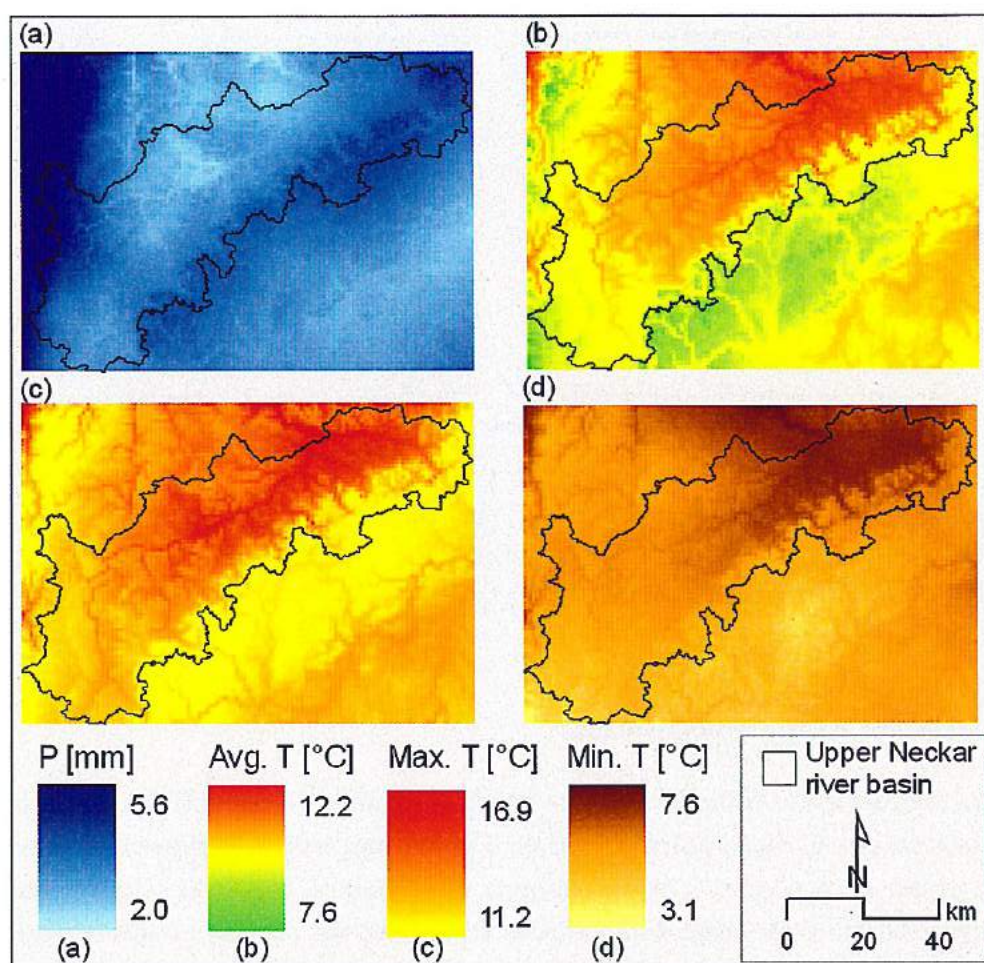


Figure 4.9: Spatial distribution of the long term mean of daily total precipitation [panel: (a)] and daily average, maximum and minimum air temperature [panel: (b), (c) and (d), respectively] in and around the study area estimated using the EDK method. The long term means were calculated from the daily interpolated values at $1 \text{ km} \times 1 \text{ km}$ spatial resolution for the period from 1991 to 2001 (DWD).

ulations from hydrological models. An estimate on PET is always required for modeling purposes since it is the upper limit of the actual evapotranspiration. Many methods are available for an estimation of PET which ranges from data intensive physically based Penman-Monteith method (Monteith, 1965) to less data demanding the Blaney and Criddle (Blaney and Criddle, 1950) method or the Hargreaves and Samani (Hargreaves and Samani, 1985) method. The

Penman-Monteith method, based on the physical approach, can be the first choice to estimate PET. However, this approach requires a large amount of input information including air temperature, relative humidity, wind speed, amongst other meteorological variables. Some of these meteorological variables are often not available at all climate stations for the longer time period. Furthermore, to estimate the spatio-temporal distribution of meteorological variables, in particular wind speed and relative humidity, poses a significant problem as they show large spatial variability within a small spatial domain and depends on local conditions. Under these limitations and based on the previous studies conducted by Das (2006) and Hartmann (2003) for the same area, the Hargreaves and Samani method for the estimation of PET was used in this study. This method estimates PET at a given geographical location based on only the average, maximum, and minimum air temperature data. Study conducted by Hargreaves (1994) reported a very good correspondence between PET estimated by the Hargreaves and Samani method and the Penman-Monteith method for several lysimeter data over the broad range of climatological conditions.

The Hargreaves and Samani method estimates potential evapotranspiration E_p^* as a function of air temperature and extraterrestrial radiation as

$$E_p^* = 0.0023cR_a(T_{avg} + 17.8)(T_{max} - T_{min})^{0.5} \quad (4.1)$$

where T_{avg} , T_{max} and T_{min} denotes the average, minimum and maximum air temperature, respectively. R_a represents the extraterrestrial radiation, which is a function of the day of the year starting from the first day of an year (i.e. 1-1-yyyy) and also depends on the latitude of a location (Allen et al., 1998). $c = 0.408$ is a constant used to convert the radiation to an evaporation equivalent of water expressed in millimeter.

The daily time series of PET were estimated by the Hargreaves and Samani method using EDK interpolated air temperature data on the spatial resolution of $1 \text{ km} \times 1 \text{ km}$ spatial resolution for the whole observational period (1979 to 2001). Fig. 4.10, as an example, shows the spatial distribution of the long term mean of daily total E_p in and around the study area.

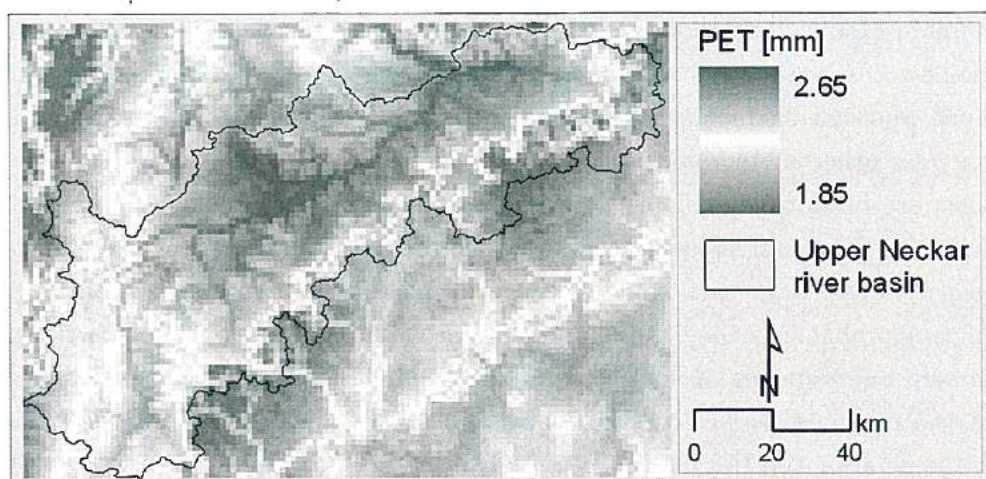


Figure 4.10: Spatial distribution of the long term mean of daily total potential evapotranspiration E_p in and around the study area. Daily time series of the E_p estimated through Hargreaves and Samani method (Hargreaves and Samani, 1985) for the period from 1991 to 2001 were used for the calculation of long term mean. Source: DWD.

Adjustments and Disaggregation of Meteorological Forcings

Adjustments of meteorologic forcings can be done to better represent their spatio-temporal distributions. For example, if mHM is to run with time intervals less than 24 h and if no hourly information is available, then the daily meteorological forcings can be disaggregated proportionally to their long term daytime/nighttime fluctuations. In this study such long term mean daily-night fractions were estimated from the hourly data of 160 stations (data obtained from DWD) located in and around the Study during the period from 1994 to 2003. These fractions were estimated on monthly timescale (Fig. 4.11).

Empirical evidence showed that the potential evapotranspiration is significantly influenced by elevation and aspect (Shevenell, 1999). The variability due to elevation is indirectly considered in the interpolation of temperature using EDK, whereas the variability induced by the orientation was accounted in the multiscale parameter regionalization framework. The correction on potential evapotranspiration E_p^* can be given by

$$E_p = \beta_{28} E_p^* \quad (4.2)$$

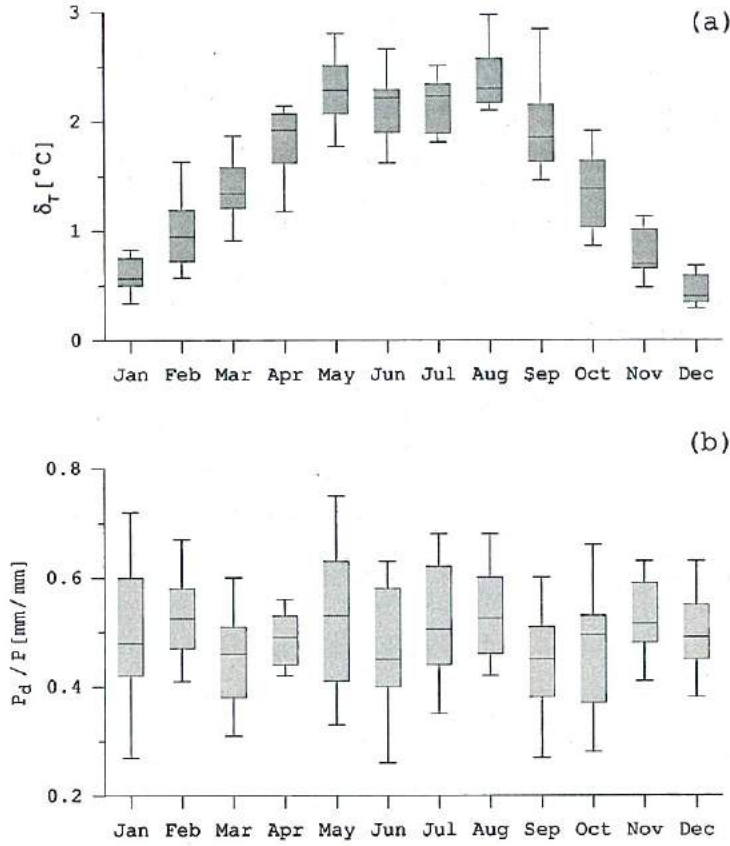


Figure 4.11: Panel (a): Box plots with the yearly fluctuations of the day-time/nighttime air temperature ($T = \bar{T} \pm \delta_T$) with respect to the average daily air temperature (\bar{T}) respectively. Panel (b): Box plots with the yearly variations of the daytime precipitation depth (P_d) with respect to the daily precipitation (P). Daytime comprises the time between (8:00-18:00) h. Data source: Hourly data from 1994 to 2003, DWD.

where, β_{28} at level-1 is incorporated in the MPR framework. The effective value of β_{28i} for i^{th} cell in MPR is obtained from their corresponding β_{28j} of j^{th} cells at level-0 and upscaling operator \mathcal{A} such that

$$\beta_{28i} = \begin{cases} \mathcal{A} \left\langle \gamma_{60} + \frac{\gamma_{61} - \gamma_{60}}{\gamma_{62}} u_{6j} \right\rangle_i & u_{6j} < \gamma_{62} \\ \mathcal{A} \left\langle \gamma_{60} + \frac{\gamma_{61} - \gamma_{60}}{360 - \gamma_{62}} (360 - u_{6j}) \right\rangle_i & \text{otherwise} \end{cases} \quad (4.3)$$

Here u_6 is aspect at sub-grid scale and γ_\bullet being global parameters. It may be noted that now there are total 28 mHM model parameters (β) and 62 global pa-

rameters (γ). In case of surfaces covered by water bodies or impounded water, the daily E_p estimate is further adjusted with the pan-evaporation coefficient to better represent the maximum free-water surface evaporation rate. Additionally, if mHM is implemented to run at hourly time scale the daily E_p was disaggregated according to its long-term the day-night variations. This disaggregation is carried out to better describe the daily soil moisture dynamics. For each month, long term mean day-night fractions were estimated from hourly records from 1994-2003 at 49 climate stations (data obtained from DWD) located in and around the study area. The Penman-Monteith approach Monteith (1965) was used for estimated hourly PET. Fig. 4.12, as an example, shows the long term diurnal cycle of PET in the month of January and July.

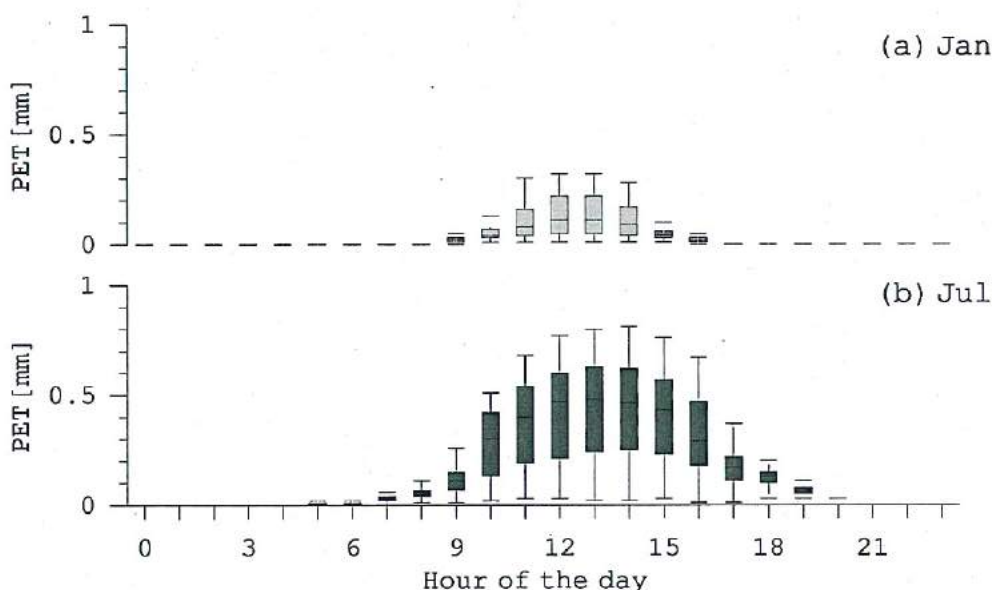


Figure 4.12: Long-term diurnal cycle of the PET for January and July. The proportion of daytime PET with respect to the daily total is 91.7% in summer whereas in winter is 100%. Daytime ranges from 6:00 to 18:00h. Daily mean PET in winter and summer are 0.62 mm and 3.3 mm respectively according to the Monteith (1965). Data source: Hourly data from 1994 to 2003, DWD.

4.3.4 Discharge Data

River discharge plays a central role in the hydrological cycle as it integrates all the hydrological processes (e.g. soil moisture, infiltration, runoff) occur-

ring within a basin, and at the same time it also serves as an indicator for climatic change and variability as it reflect changes in precipitation and evapotranspiration. Furthermore, the estimates on the river discharge are commonly required for water resources application purposes, including the design of hydraulic structure (e.g. dams, reservoirs, etc.), flood protection, irrigation and water management for both ecosystem and human use. River discharge data can be readily measured. It has been long used for the calibration and evaluation purposes of hydrologic models and as well as for land-surface models.

The time series of daily mean discharge data at the outlet (i.e Plochingen gauging station) as well as at several interior locations within the study area for the period from 1979 to 2001 were collected from LUBW, Baden-Württemberg. The mean daily discharge at the outlet for this period was estimated as approximately $50 \text{ m}^3 \text{ s}^{-1}$. At the outlet of the study area, high flows or floods are mainly observed during the month of February, whereas, low flows occurs mostly in in October and at the beginning of November. The highest daily discharge was noticed during May 1978 as approximately $1030 \text{ m}^3 \text{ s}^{-1}$, according to the discharge records of the outlet station for the period of 1961 to 2001 (Das, 2006).

Since the main aim of this chapter is to show preliminary applications of mHM, the simulation results of only two interior locations: Horgen-Kläranlage and Horb, whose drainage areas are approximately 210 km^2 and 1120 km^2 , respectively (Fig. 4.13), are presented in this chapter. In the subsequent chapters, however, discharge data from many other interior locations are used to evaluate the model performance. These data too were acquired from the same state authority. The locations and description of those interior gauging stations will, therefore, be presented afterwards.

4.4 Global Parameter Identification

Once the functional relationship between model parameters and basin predictors were established either based on past modeling exercises or on empirical evidences such as pedo-transfer functions (see 3.2), this step also provides a priori estimate on global parameters γ . These a priori estimates, however, are required to be refined so as to match as closely as possible the dynamic behavior of the modeled responses with those of the the observed behavior of

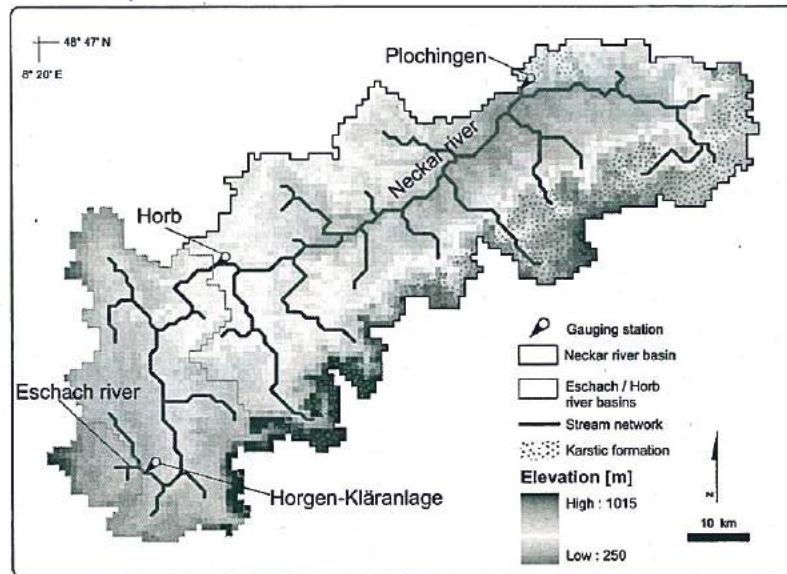


Figure 4.13: Location of the interior gauging stations within the Upper Neckar river basin.

a catchment. This refinement is usually achieved via the calibration process. The calibration of a hydrological model can be achieved either manually or the so-called the *trial and error* procedure or through an automatic calibration procedure using an automatic optimization algorithm and computer power. In case of a spatially distributed model or even simple lumped model, the second approach is often preferred mainly because the calibration process requires several thousands of model runs to find a good set of model parameters. Manual procedure for such cases may be a very tedious and time consuming. Moreover, the manual calibration procedure requires considerable training and practice, and expertise and subjective decisions of the modeler, which in most cases can not be easily transferred from one person to another.

Great deal of research have been devoted during the recent past for developing efficient and effective optimization algorithms. As a result several global optimization algorithms exist including population based genetic algorithms, combinatorial algorithms simulated annealing (Kirkpatrick et al., 1983), shuffled complex evolution method (Duan et al., 1992), dynamically dimensioned search algorithm (Tolson and Shoemaker, 2007), amongst others. For a detail review on different search algorithms used in hydrological modeling studies readers may refer to Gupta et al. (2002). In this study and for most of the ap-

plications of mHM presented in this chapter, a good sets of global parameters γ were identified with a split-sampling technique using a constrained optimization algorithm based on simulated annealing (SA) (Kirkpatrick et al., 1983). The SA algorithm utilizes the principles of statistical physics regarding the behavior of a large number of atoms at low temperature for finding minimal cost solutions (in our case global parameters) to large optimization problems by minimizing the associated energy (i.e. objective function or error function). In the annealing process of SA, the temperature is first raised, then decreased gradually to a very low value, while ensuring that one spends sufficient time at each temperature value. This process yields stable low energy states. Geman and Geman (1984) provided a proof that SA, if annealed sufficiently slowly, converges to the global optimum. As a result, temperature, is one of the crucial control parameter in SA. The following estimation procedure was used in this study

Algorithm 1:

1. Randomly select an initial set of global parameters γ within their predefined ranges and constraints.
2. Estimate model parameters β^0 at level-0, using [Eq. (3.1)].
3. Estimate effective model parameters β^1 at level-1, using [Eq. (3.2)].
4. Set an initial annealing temperature τ (a priori estimate).
5. Calculate the current objective function Φ [Eq. (4.4)].
6. Randomly select an index (ι) with $1 \leq \iota \leq s$.
7. Randomly modify the element γ_ι of the vector γ and formulate a new vector γ^* .
8. Estimate fields of model parameters β^{0*} and corresponding effective model parameters β^{1*} using [Eq. (3.1)] and [Eq. (3.2)], respectively.
9. Calculate the new objective function Φ^* .
10. If $\Phi^* \leq \Phi$ then replace γ by γ^* . Else calculate $\pi = \exp(\frac{\Phi - \Phi^*}{\tau})$. With the probability π , replace γ by γ^* .

11. Repeat steps (6)-(10) M times with M being the length of the Markov chain of SA (Aarts and Korst, 1990).
12. Reduce the annealing temperature τ and repeat steps (6)-(11) until the objective function Φ achieves a minimum.

The formulation of objective function that measures the closeness of observed and simulated responses (typically the streamflow hydrograph) is crucial for the successful calibration. Often, the use of different objective functions results in different final parameter sets and thereby different model simulations, which may fit specific aspects of the hydrograph at the expense of others.

The overall model efficiency Φ in this study was estimated as a weighted combination of four estimators based on the Nash-Sutcliffe efficiency (NSE) between observed and simulated streamflows using three different time scales (daily, monthly and yearly) as well as the logarithm of the daily streamflow to de-emphasize the effects of the peak flows over the low flows (Oudin et al., 2006). These objective functions are denoted by ϕ_n , $n = 1, 4$. The overall objective function to be minimized is then

$$\Phi = \left(\sum_n w_n^p (1 - \phi_n)^p \right)^{\frac{1}{p}} \quad (4.4)$$

where $p > 1$, and $\sum_{n=1}^4 w_n = 1$. Here p is an exponent according to the compromise programming technique (Duckstein, 1984) and w_n denote the degree of importance of each objective. High values of p , say $p = 6$, should be chosen to avoid substitution of objective function values at low levels. In this study, the estimators related with daily streamflows were twice as important as the long-term ones, thus $\{w_n\} = \{\frac{1}{3}, \frac{1}{6}, \frac{1}{6}, \frac{1}{3}\}$. The NSE for a given time scale t (say day, month or year) is given by

$$\phi_n = 1 - \frac{\sum_{t=1}^T (Q_n(t) - \hat{Q}_n(t))^2}{\sum_{t=1}^T (Q_n(t) - \bar{Q}_n(t))^2} \quad (4.5)$$

where, T is the total number of observations, $\bar{Q}_n(t)$ is the mean value of the observations time series over the calibration period. The index n denotes here the daily, monthly, yearly, and the transformed $\ln(Q(t))$ streamflow discharges. Q and \hat{Q} are the observed and simulated streamflows at a given time scale.

Appropriate ranges (i.e. maximum and minimum values) were assigned to each global parameter γ based on either the empirical evidences (e.g. pedo-transfer function derived values) or from the modeling experiences. Table 4.1 shows initial ranges and *a priori* estimates for global parameter γ for the study basin used in this study. These global parameters were forced to stay within the assigned ranges during calibration. Other physically significant constraints were also applied to some of the model parameters β^1 . For examples, the parameter "saturated water content" at modeling grid cell (level-1) was always kept higher than the parameter "wilting point", and the parameter "recession constant" for the fast interflow was always higher than the "recession constant" of the slow and fast interflows as well as of the base flow.

Table 4.1: Range and a priori guess of transfer function parameters (γ) for the Upper Neckar river basin.

Parameter	Min.	Max.	Guess	Parameter	Min.	Max.	Guess
γ_1	0.10	0.50	0.2	γ_{32}	0.1	0.6	0.1
γ_2	-1.0	1.0	0.0	γ_{33}	0.8	0.95	0.80
γ_3	1.0	4.0	1.0	γ_{34}	0.1	0.3	0.2
γ_4	1.0	4.0	1.0	γ_{35}	0.8	1.0	0.8
γ_5	1.0	4.0	1.0	γ_{36}	0.6	0.8	0.6
γ_6	0.1	0.8	0.1	γ_{37}	1.0	40.0	1.1
γ_7	3.0	8.0	3.0	γ_{38}	1.0	10.0	4.0
γ_8	3.0	8.0	3.0	γ_{39}	1.0	30.0	10.0
γ_9	3.0	8.0	3.0	γ_{40}	0.0	30.0	10.0
γ_{10}	4.0	7.0	5.0	γ_{41}	0.0	30.0	10.0
γ_{11}	0.0	0.1	0.0	γ_{42}	50.0	60.0	54.0
γ_{12}	1.5	3.0	2.0	γ_{43}	-0.10	-0.05	-0.07
γ_{13}	0.7	0.8	0.788	γ_{44}	0.160	0.170	0.165
γ_{14}	0.0005	0.0015	0.0010	γ_{45}	0.0	1.0	0.5
γ_{15}	-0.27	-0.25	-0.263	γ_{46}	1.0	100.0	10.0
γ_{16}	0.8	0.9	0.890	γ_{47}	10.0	10000.0	200.0
γ_{17}	-0.0015	-0.0005	-0.0010	γ_{48}	10.0	10000.0	200.0
γ_{18}	-0.35	-0.30	-0.322	γ_{49}	0	1	0
γ_{19}	1.0	5.0	3.0	γ_{50}	0.5	1.5	1.0
γ_{20}	25.0	35.0	30.0	γ_{51}	0.0001	0.0020	0.0010
γ_{21}	30.0	70.0	50.0	γ_{52}	0.0001	0.0020	0.0010
γ_{22}	30.0	70.0	50.0	γ_{53}	0.0001	0.0020	0.0010
γ_{23}	30.0	70.0	50.0	γ_{54}	0.75	1.00	0.80
γ_{24}	1.0	5.0	3.0	γ_{55}	0.35	0.40	0.385
γ_{25}	270.0	274.0	272.5	γ_{56}	0.1	10.0	2.0
γ_{26}	0.5	3.5	1.5	γ_{57}	0.0	1.0	0.5
γ_{27}	270.0	273.0	273.0	γ_{58}	0.0	1.0	0.5
γ_{28}	0.15	0.25	0.20	γ_{59}	0.0	0.5	0.2
γ_{29}	0.1	0.3	0.2	γ_{60}	0.9	1.0	0.95
γ_{30}	0.1	1.0	0.20	γ_{61}	1.0	1.2	1.05
γ_{31}	0.0	1.0	0.05	γ_{62}	175.0	195.0	180.0

4.5 Evaluation Criteria

A number of statistical criteria, in addition to NSE of daily discharge and the logarithmic transformed daily discharge, were used to assess and compare the performance of models. These criteria include: Bias, Root Mean Square Error (RMSE) and Pearson correlation coefficient (r). They can be formally estimated as:

$$Bias = \frac{1}{T} \sum_{t=1}^T (\widehat{Q}_t - Q_t) \quad (4.6)$$

$$RMSE = \sqrt{\frac{1}{T} \sum_{t=1}^T (\widehat{Q}_t - Q_t)^2} \quad (4.7)$$

$$r = \frac{1}{T-1} \sum_{t=1}^T \left(\frac{(\widehat{Q}_t - \overline{\widehat{Q}})}{S_{\widehat{Q}}} \right) \left(\frac{(Q_t - \overline{Q})}{S_Q} \right) \quad (4.8)$$

where T is the total number of observations, t accounts for the time steps, and \widehat{Q}_t and Q_t are simulated and observed variables respectively (e.g. either daily streamflow or monthly values). $\overline{\widehat{Q}}$ and \overline{Q} are the mean of the simulated and observed variables over the period of T , respectively. $S_{\widehat{Q}}$ and S_Q denote the standard deviation of the simulated and observed variables, respectively.

Additionally, the Spearman's rank correlation coefficient (ρ), was also used to assess the performance of model. ρ is a non-parametric statistic that does not requires any assumption about the frequency distribution of the underlying variables. This statistic can be calculated with the same mathematical formula used for estimating r (Eq. 4.8), but with the series of the ranks of variables.

4.6 Application of mHM in the Upper Neckar River Basin

mHM with MPR parameterization were implemented in the study basin to simulate the observed streamflow time series at the Plochingen gauging station and the other state variables and water fluxes such as the spatio-temporal evolution of the root zone soil moisture distribution over the whole catchment, snow covers, amongst others. The distributed nature of the model also facilitated to generate streamflow time series at various interior locations within

the catchment. Two interior gauging stations, as described before, were used to cross-validate the model performance. Note that the discharge data of these two locations were not used during the model calibration process.

Applications of mHM presented in this chapter were performed with the spatial discretization of $1 \text{ km} \times 1 \text{ km}$ for both level-2 (meteorological forcings) and level-1 (modeling scale) of the model runs. The level-0 data was set at the resolution of $100 \text{ m} \times 100 \text{ m}$. The model runs were carried out at the hourly time step. Consequently, the required meteorological variables were statistically disaggregated into hourly time steps based on their long-term daytime/nighttime fluctuations, as described before. The hourly simulated discharge series produced at each grid node were aggregated to the daily values to compare them with the observed gauged data. It may be noted, however, that the spatial resolution at level-1 can vary from $2 \text{ km} \times 2 \text{ km}$ to as big as $32 \text{ km} \times 32 \text{ km}$. The detailed applications of mHM for the coarser resolution are presented in the next chapter.

The upscaled cell to cell flow routing network derived using the flow direction and flow accumulation information of level-0 input data scale to the modeling scale (say, level-1 at 2 km) matched quite well with the observed river network. As an example, Fig. 4.14 shows the upscaled river network for the upper portion of the study area. Furthermore, the upstream drainage area belonging to a particular discharge gauging station obtained after upscaled river network were also in the range of the reported official drainage area (hydrological year-books, LUBW). It is worthwhile to emphasize here that this delineation of flow routing network at a modeling scale was automatically carried out during the initialization of mHM, and therefore requires no manual adjustments.

The standard split-sampling model calibration procedure was subsequently followed. The model calibration was performed during the period from 1979-11-01 to 1988-10-31 using the daily discharge data of the outlet (i.e. Plochingen gauging station) of the catchment. Six months spin up time was used to establish reliable initial conditions for the state variables. This period, however, was not accounted for in the overall objective function. The subsequent period until 2001-10-31 was used as the evaluation period.

An adaptive version of simulated annealing algorithm was used to generate 50 000 global parameters sets which were ranked according to their overall performance index (Eq. 4.4). It is worth noting that the very best parame-

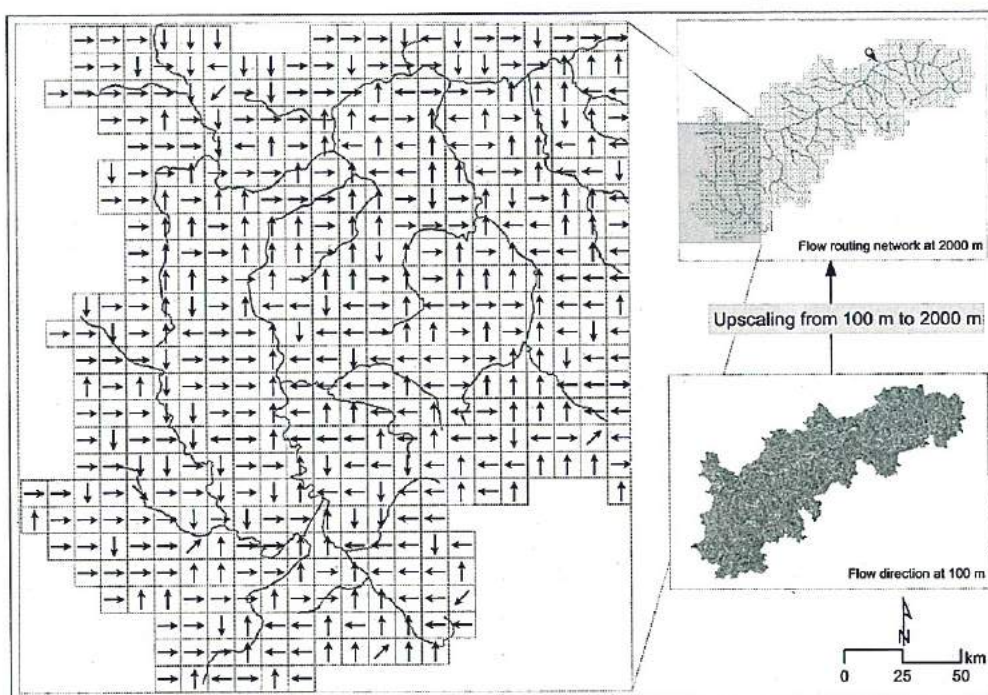


Figure 4.14: Upscaling of river network on modeling scale at 2000 m from 100 m flow direction and flow accumulation data. The upscaled flow routing network for the upper portion of the study area is depicted in left portion of this figure.

ter sets ($\Phi_1 \geq 0.8$) seems to share the same locus on the parameters space (Fig. 4.15). The probability density functions obtained for each parameter γ are skewed and in some cases exhibited large ranges of variation (Table 4.2).

4.6.1 Streamflow Prediction

The usual way to verify the output from a hydrologic model is to plot observed versus simulated discharge. Due to the equifinality of many good parameter sets (Fig. 4.15), however, it is more appropriate to estimate the mean value of an ensemble of simulations carried out with the best parameters sets. In this study, the best thousand sets were used for this purpose. Using these parameter set, the deterministic model prediction was given by the mean of the ensemble and the variability of model outputs were estimated by the 5% and 95% percentile ranges ($P_5 - P_{95}$). It may be noted, however, that so-derived variability bounds are not confidence bounds in a statistical sense,

Table 4.2: Statistics of the good sets of transfer function parameters.

Param	Min	Max	Mean	Std. Dev.	Param	Min	Max	Mean	Std. Dev.
γ_1	0.150	0.271	0.165	0.023	γ_{32}	0.436	0.600	0.577	0.020
γ_2	-0.997	-0.473	-0.938	0.072	γ_{33}	0.886	0.970	0.961	0.010
γ_3	1.003	3.872	2.565	1.042	γ_{34}	0.101	0.297	0.182	0.063
γ_4	2.664	3.978	3.705	0.215	γ_{35}	0.823	1.000	0.983	0.021
γ_5	2.645	3.949	3.614	0.224	γ_{36}	0.601	0.722	0.639	0.022
γ_6	0.348	0.798	0.744	0.046	γ_{37}	13.450	20.800	18.258	0.915
γ_7	3.000	7.891	6.559	1.318	γ_{38}	1.218	3.683	2.218	0.281
γ_8	6.179	7.989	7.828	0.124	γ_{39}	10.000	29.920	25.227	3.099
γ_9	5.488	7.988	7.724	0.304	γ_{40}	12.790	29.980	25.704	3.471
γ_{10}	4.029	6.993	5.757	0.941	γ_{41}	2.962	29.990	22.491	4.802
γ_{11}	0.001	0.099	0.052	0.020	γ_{42}	52.000	55.960	54.409	1.018
γ_{12}	1.530	2.966	2.410	0.195	γ_{43}	-0.089	-0.050	-0.063	0.009
γ_{13}	0.700	0.750	0.705	0.008	γ_{44}	0.162	0.170	0.166	0.001
γ_{14}	0.001	0.001	0.001	0.000	γ_{45}	0.011	0.343	0.169	0.025
γ_{15}	-0.270	-0.255	-0.268	0.002	γ_{46}	63.320	99.960	91.876	6.779
γ_{16}	0.818	0.900	0.868	0.014	γ_{47}	76.140	993.800	512.559	171.763
γ_{17}	-0.001	-0.001	-0.001	0.000	γ_{48}	51.800	715.400	230.815	83.491
γ_{18}	-0.350	-0.304	-0.334	0.009	γ_{49}	0.000	1.000	0.006	0.077
γ_{19}	1.034	2.090	1.345	0.149	γ_{50}	0.852	1.499	1.348	0.108
γ_{20}	27.500	33.500	30.000	2.050	γ_{51}	0.001	0.002	0.002	0.000
γ_{21}	44.240	69.880	64.099	4.050	γ_{52}	0.000	0.001	0.001	0.000
γ_{22}	30.270	67.360	50.127	11.349	γ_{53}	0.000	0.001	0.001	0.000
γ_{23}	30.700	69.880	55.799	12.379	γ_{54}	0.802	0.999	0.949	0.040
γ_{24}	2.010	4.551	2.736	0.414	γ_{55}	0.351	0.400	0.384	0.008
γ_{25}	272.000	273.000	272.500	0.050	γ_{56}	1.022	9.985	6.871	2.906
γ_{26}	0.501	3.498	1.870	0.902	γ_{57}	0.018	0.998	0.702	0.165
γ_{27}	270.000	272.300	270.510	0.359	γ_{58}	0.118	1.000	0.646	0.196
γ_{28}	0.180	0.220	0.200	0.005	γ_{59}	0.129	0.370	0.274	0.036
γ_{29}	0.100	0.300	0.176	0.062	γ_{60}	0.940	1.000	0.992	0.008
γ_{30}	0.116	0.964	0.458	0.153	γ_{61}	1.000	1.073	1.007	0.010
γ_{31}	0.017	0.908	0.314	0.179	γ_{62}	175.100	194.800	187.485	4.183

i.e. they are not expected to include in all cases a given percentage of the observations. Fig. 4.16 and Fig. 4.17 shows the performance of mHM for daily discharge simulations at the Plochingen gauging station for couple of water years in the calibration and the validation periods. The ensemble mean and the ($P_5 - P_{95}$) variability bounds of the simulations indicated that mHM is able to reproduce quite well the dominant process occurring in the Upper Neckar basin. Table 4.3 presents the summary statistics for the daily discharge simulations. The NSE obtained during the calibration and evaluation period were 0.89 ± 0.02 and 0.87 ± 0.03 , respectively, at the ($P_5 - P_{95}$) variability bounds. The bias during the calibration period is approximately $-0.03 \text{ m}^3/\text{s}$, whereas the root mean squared error (RMSE) is $18 \text{ m}^3/\text{s}$, i.e. approximately one third of the mean streamflow. As a result of the satisfactory fit, most of the observed values fall within these ($P_5 - P_{95}$) variability bands.

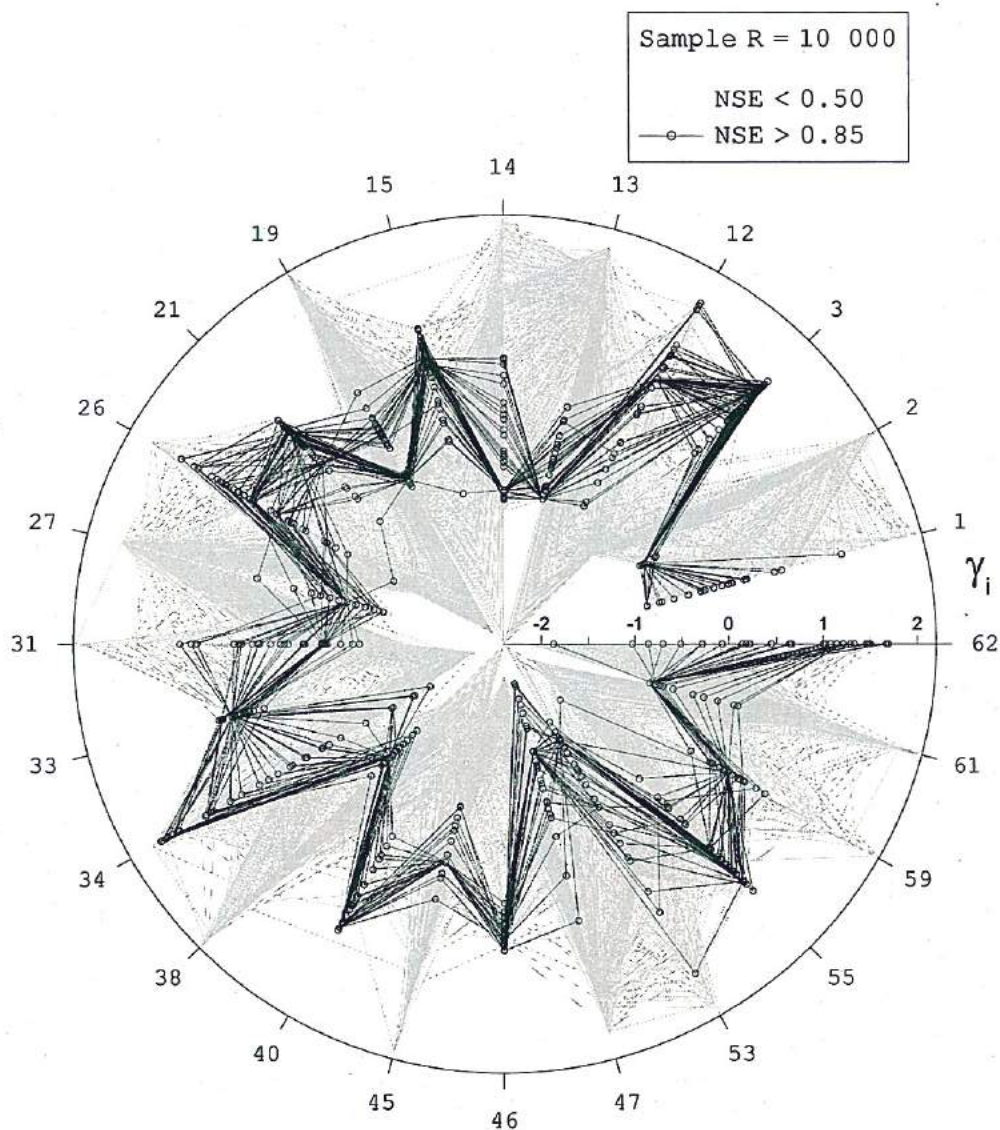


Figure 4.15: Variability of a subset of transfer function parameters γ . All parameters were standardized with the statistics reported in Table 4.2. Sets of good parameters are those whose NSE values are greater than 0.85 (in red colour).

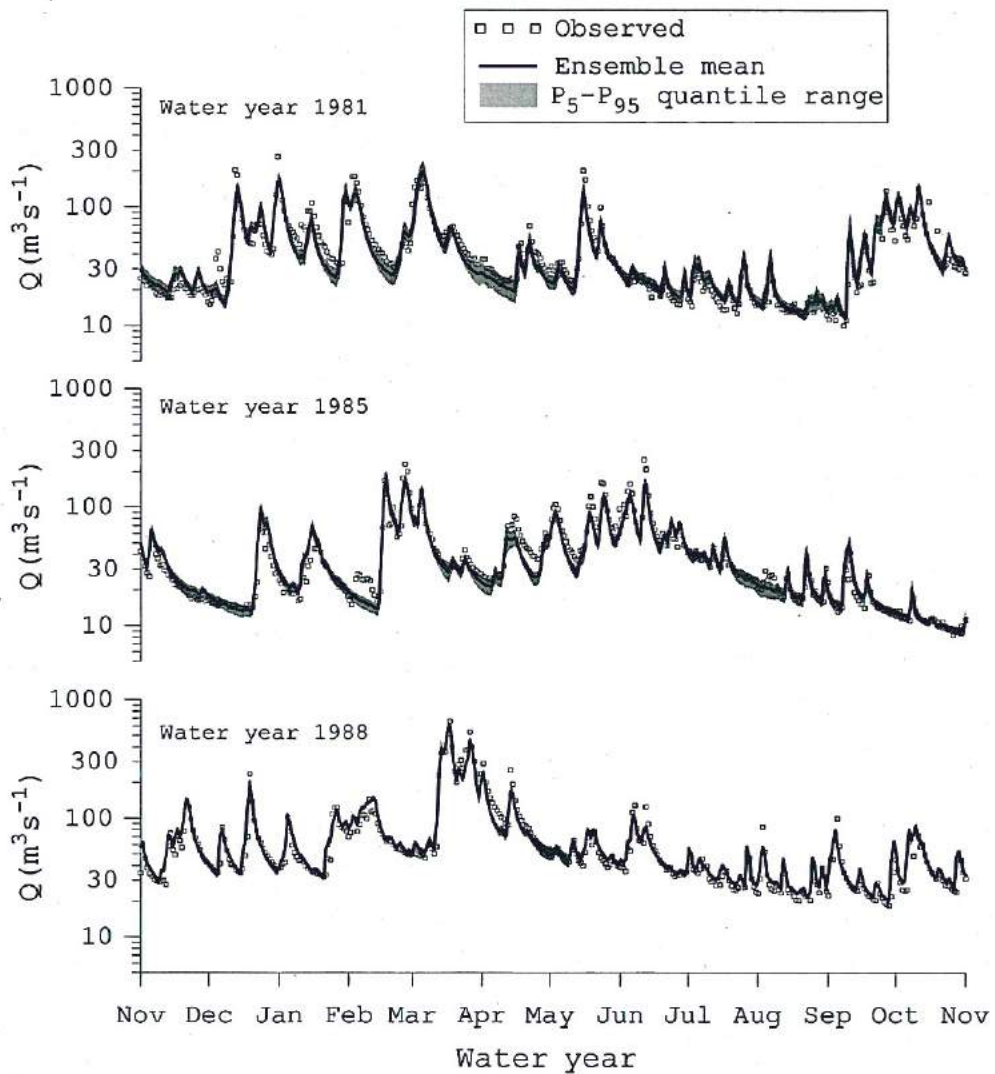


Figure 4.16: Comparison of the observed and the ensemble values for the streamflow at Plochingen during the selected calibration water years. The ensemble mean and the ($P_5 - P_{95}$) percentile limits of the simulations were estimated with the best thousand solutions.

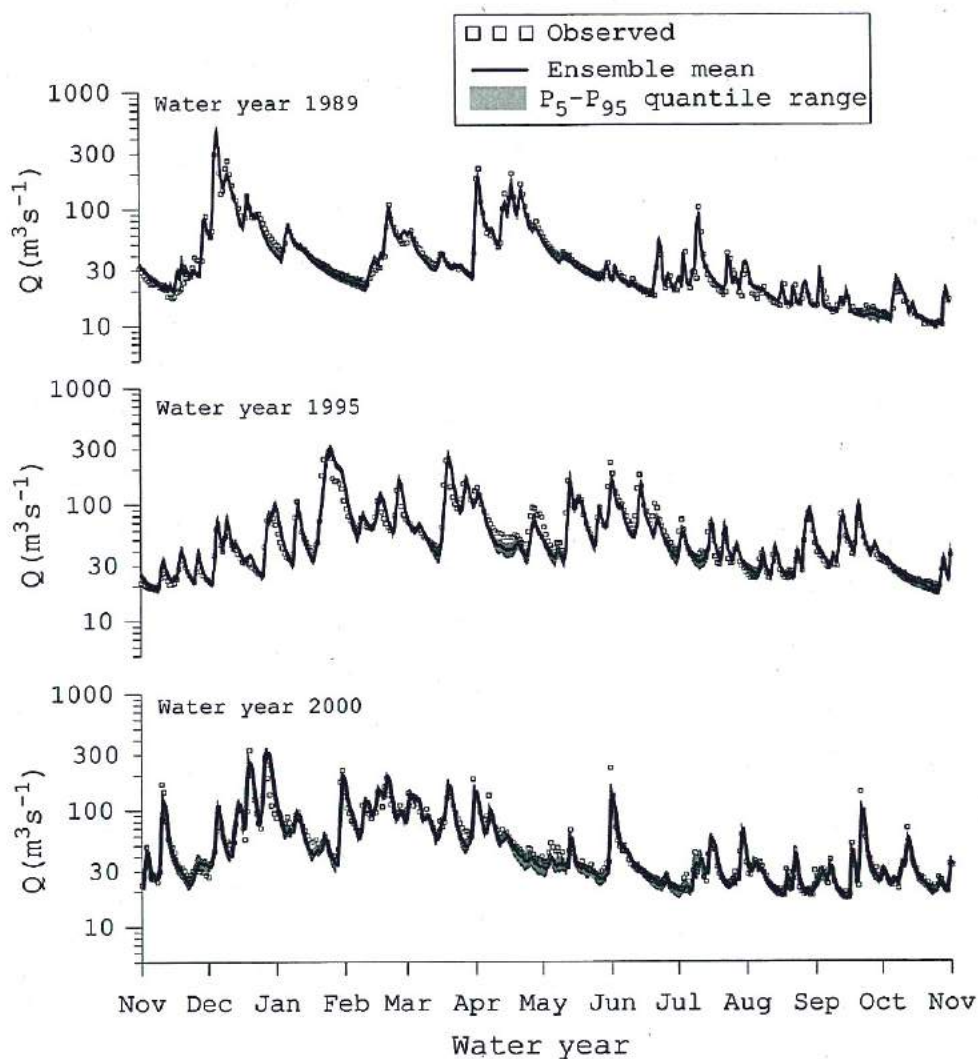


Figure 4.17: Comparison of the observed and the ensemble values for the streamflow at Plochingen during the selected evaluation water years. The ensemble mean and the ($P_5 - P_{95}$) percentile limits of the simulations were estimated with the best thousand solutions.

Table 4.3: Ensemble mean value and 5% and 95% percentile ranges ($P_5 - P_{95}$) obtained for six estimators for daily discharge simulations at Plochingen during the calibration and evaluation periods. Best thousand parameter sets were used for estimating these statistics.

Estimator	Unit	Calibration		Evaluation	
		Mean	$P_5 - P_{95}$	Mean	$P_5 - P_{95}$
Bias	m^3s^{-1}	-0.03	(-1.05 - 1.05)	-0.1	(-1.2 - 0.8)
RMSE	m^3s^{-1}	18.06	(17.53 - 19.08)	13.86	(13.21 - 15.36)
NSE (Q)	-	0.89	(0.87 - 0.91)	0.87	(0.86 - 0.90)
NSE (lnQ)	-	0.88	(0.85 - 0.90)	0.86	(0.84 - 0.89)
r	-	0.95	(0.94 - 0.96)	0.94	(0.92 - 0.95)
rho	-	0.94	(0.93 - 0.96)	0.94	(0.92 - 0.95)

The results provided above were based on the performance (e.g. NSE) of the model over the whole modeling period. The model performance generally varies over the modeling period from one year to another. To gain more insight into the model performance, the NSE between observed and simulated discharge as well as for their logarithmic transformation were estimated year wise for the best sets of global parameters. Fig. 4.18 depicts the results for these simulations. In general the model performance with respect to both statistics were in the range of 0.70 to 0.95, which indicates a quite good correspondence between observed and simulated values. However, the performance during the water years of the evaluation period were, on average, inferior than that obtained during the calibration period. This is quite normal and generally noticed in many hydrological modeling studies. The reason for this is that the model was trained to match the observed streamflow during the calibration period, and as a result it performed better in this period. A sharp decrease in the model performance was noticed during the water year 1996, which was relatively a dry year as compared to other years. For other years the model performance were quite satisfactory since both statistics were on average greater than 0.80. Monthly and annual water balances were also closed significantly well. The Pearson's correlation coefficient (r) between the monthly observed and calculated discharges at the Plochingen station during the evaluation period was on average equal to 0.95 ± 0.025 at the ($P_5 - P_{95}$) bounds (Fig. 4.19). Other runoff characteristics like total seasonal drought-spell duration (TDD), frequency of high flows, and volume of peak flows were also effectively reproduced by this

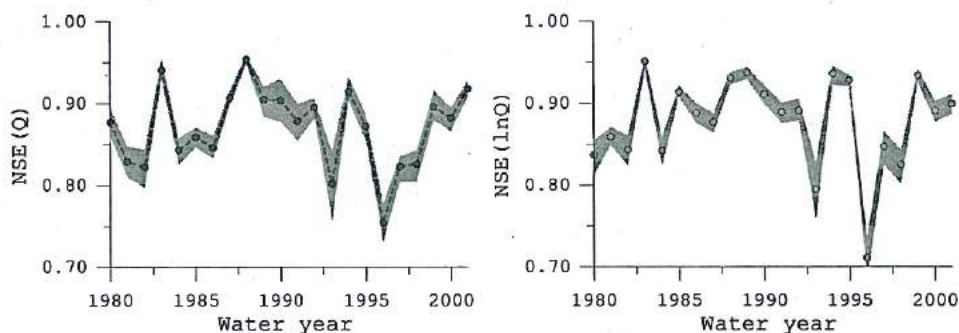


Figure 4.18: Yearly evolution of the NSE obtained between observed and simulated discharge (left panel) as well as between for their logarithmic transformation (right panel) during whole modeling period at Plochingen. Gray shaded region represents ($P_5 - P_{95}$) percentile limits of NSEs whereas, dotted line with filled circle denotes their ensemble mean.

model. For example, the Pearson's correlation coefficient r for the TDD characteristic was on average equal to 0.60 ± 0.11 at the ($P_5 - P_{95}$) bounds. The in-depth analysis of these extreme flow characteristics will be reported in next chapters.

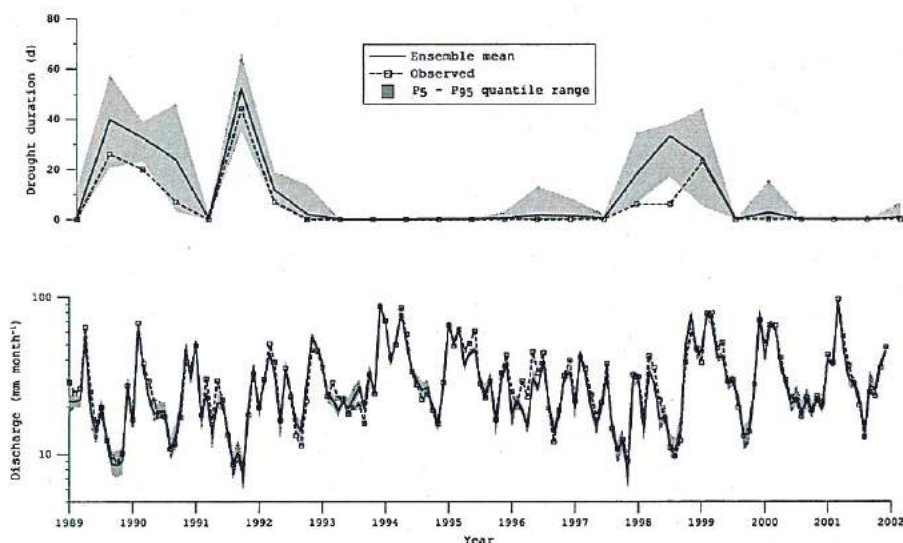


Figure 4.19: Monthly discharge and seasonal total drought duration in the evaluation period at Plochingen.

The cross-validation results obtained for the streamflow predictions at an interior Horb gauging station showed a good match between observed and simulated values. Both ensemble NSE (Q) and NSE (lnQ) mean values obtained for the daily discharge simulation during the modeling period (1979-2001) were above 0.80 (Table 4.4). Other statistics were also in reasonably good range. For instance, both the Pearson's correlation coefficient r and the Spearman Rank correlation coefficient ρ were above 0.90. A positive bias of approximately 1 m³/s was noticed. Monthly simulated discharge also showed a good correspondence with the observed values since the ensemble mean NSE values was greater than 0.90. The performance of mHM for this interior location were slightly inferior than that obtained for the outlet gauging station. This was expected as the discharge data of this station were not used for the model calibration. However, the NSE (Q) and NSE (lnQ) values obtained for the daily discharge simulations at this interior location were at most 10% lower than that obtained at the outlet station. It shows the robustness of mHM to provide reliable and reasonable estimate on streamflow at interior un-gauged locations, once calibrated with information from a catchment outlet. The visual inspection of discharge hydrograph also confirmed the above results (Fig. 4.20).

Table 4.4: Ensemble mean value and 5% and 95% percentile ranges ($P_5 - P_{95}$) obtained for six estimators for daily discharge simulations at an interior Horb gauging station during the modeling period (1980-2001).

Estimator	Unit	Mean	$P_5 - P_{95}$
Bias	m ³ s ⁻¹	1.08	(0.74 - 1.41)
RMSE	m ³ s ⁻¹	7.01	(6.79 - 7.28)
NSE (Q)	-	0.86	(0.83 - 0.87)
NSE (lnQ)	-	0.84	(0.82 - 0.87)
r	-	0.92	(0.91 - 0.94)
ρ	-	0.93	(0.91 - 0.95)

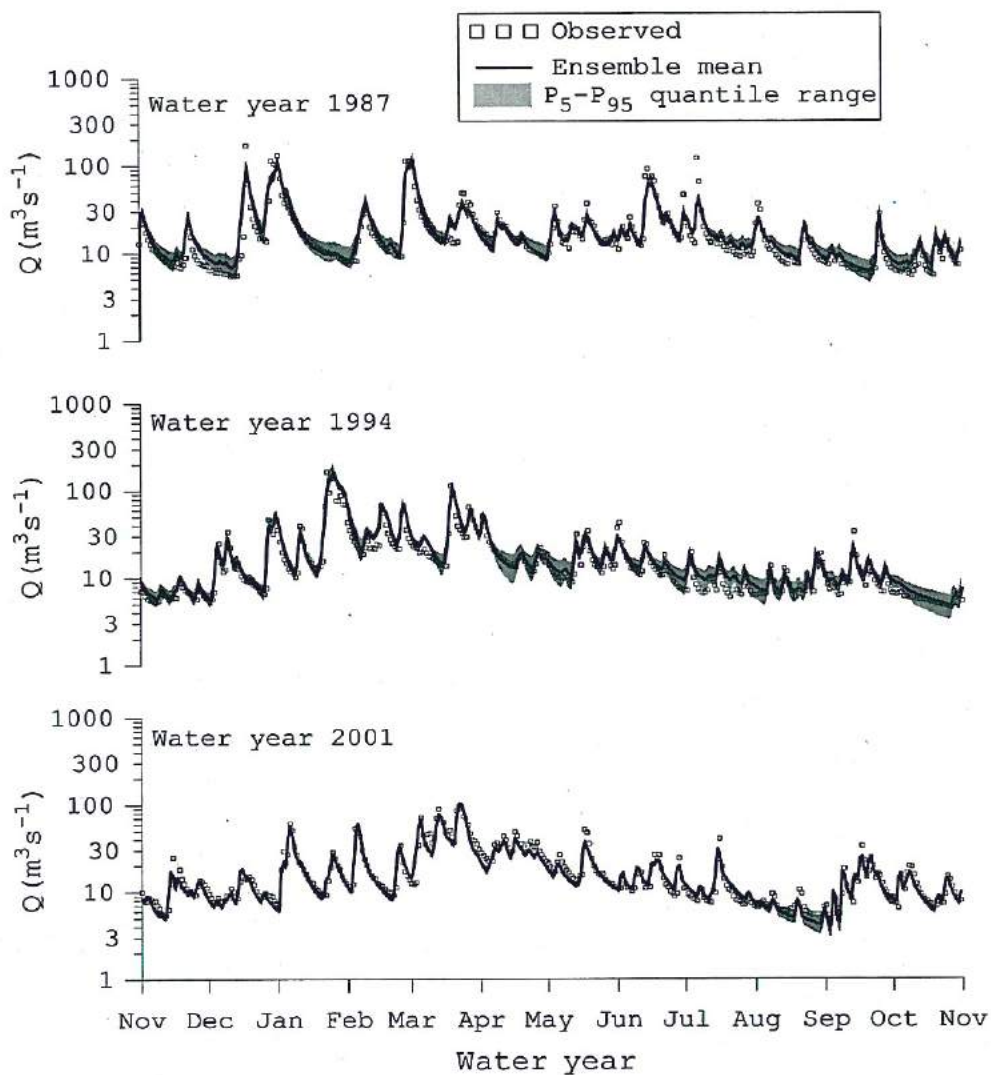


Figure 4.20: Comparison of the observed and the ensemble values for the streamflow at an interior Horb gauging station during the selected water years. The ensemble mean and the ($P_5 - P_{95}$) percentile limits of the simulations were estimated with the best thousand solutions.

4.6.2 Prediction of Spatial Patterns of Soil Moisture and Snow Cover

Due to the large uncertainty of input data, model structure and in the estimation of model parameters at a mesoscale, it is advisable to evaluate or at least perform a plausibility test of a model for not only with the streamflow time series data, but also with other relevant state variables such as the spatio-temporal distribution of the soil moisture, snow covers, groundwater table levels. Direct measurement of state variables in a mesoscale river basin at a finer spatial resolution is very costly and time consuming. Remotely sensed data offers a cost-effective source of data. In this study, two state variables namely: top thin root zone soil moisture and snow cover, simulated by mHM were cross-checked against the indirect proxies data obtained from remotely sensed data. Although the spatial pattern of model simulated snow cover can be directly compared with the remote sensing data sets such as snow cover products obtained from the Moderate Resolution Imaging Spectroradiometer (MODIS), evaluation of the soil moisture patterns is very difficult task since it is often partially related with the remotely sensed data. In this study, the land surface temperature (LST) derived from observations of the MODIS (data freely available at <https://wist.echo.nasa.gov>) was used for plausibility tests of the spatial patterns of model simulated soil moisture content in the top root zone horizon. This MODIS product along with the normalized difference vegetation index (NDVI) are often employed as predictors of soil moisture in the so-called "triangle method" (Carlson, 2007).

The daily time series of snow cover and LST data for the year 2001 were obtained from the MODIS server. These data were subsequently geo-referenced and extracted for the study area using an ArcGIS toolbox. It may be noted that the MODIS data are generally affected by the presence of clouds. It means that in cloudy day or parts of study area covered by cloud, there are no observation for both MODIS products. Although there exist several algorithms to filter cloud covers [see e.g. Parajka and Blöschl (2008)], no attempts were made in this study to filter the cloud covers. This was mainly because MODIS is in operational from mid 2000 and the present study was conducted only up to the year 2001. In the overlapping period of this study with the MODIS operational period there is only one winter season when snow-fall was noticed.

4.6.2.1 Soil Moisture Simulation

Soil moisture is a crucial state variable for the appropriate representation of hydrologic as well as land-atmosphere processes at the meso and/or macro scales because of its long temporal memory (Vinnikov et al., 1996; Bastidas et al., 2005). Accordingly, it influences not only runoff generation mechanisms but also the vegetation growth and other various near-surface atmospheric processes such as cloud formation, partition of latent and sensible heat energy (Vinnikov et al., 1996). Experiments with regional and global climate models have also corroborated that the evolution of the weather and climate strongly depend on the initial soil moisture conditions (Fennessy and Shukla, 1999).

A quite strong negative correlation was found by comparing the series of images of LST and the mHM simulated soil moisture fraction in the top soil horizon (i.e. the ratio between the actual to maximum water content) as depicted in Fig. 4.21. One of the good set of global parameters (γ) was used for these simulations. It can be observed from Fig. 4.21 that the areas within the study basin where LST is higher, the model simulated soil moisture is smaller and vice-versa. The range of the Pearson correlation coefficient (r) calculated between soil moisture fraction and LST on daily time scale for 30 summer consecutive days in the year 2000 varied between $(-0.85, -0.30)$. The ensemble mean and variability bounds ($P_5 - P_{95}$) of r values between MODIS derived LST data and the mHM simulated daily spatial dynamics of soil moisture patterns obtained with all good parameter sets are depicted in Fig. 4.22. It can be noted that during the investigation period there was no observation available from MODIS derived LST data, due to cloud cover. Consequently these days or the cloud affected areas were not accounted in the calculation of the r values. This figure depicts a quite good negative correlation r between model simulated soil moisture patterns and MODIS derived LST, with average ensemble mean r value of approximately 0.62. These results also indicated the existence of strong coupling between the top thin root zone soil moisture and the streamflow generation. The corresponding daily discharge simulations for these investigation period are provided in Fig. 4.23. For most of the investigated days, the observed discharge was covered within the model simulated ($P_5 - P_{95}$) variability bounds. And the NSE values during this period was at least 0.90.

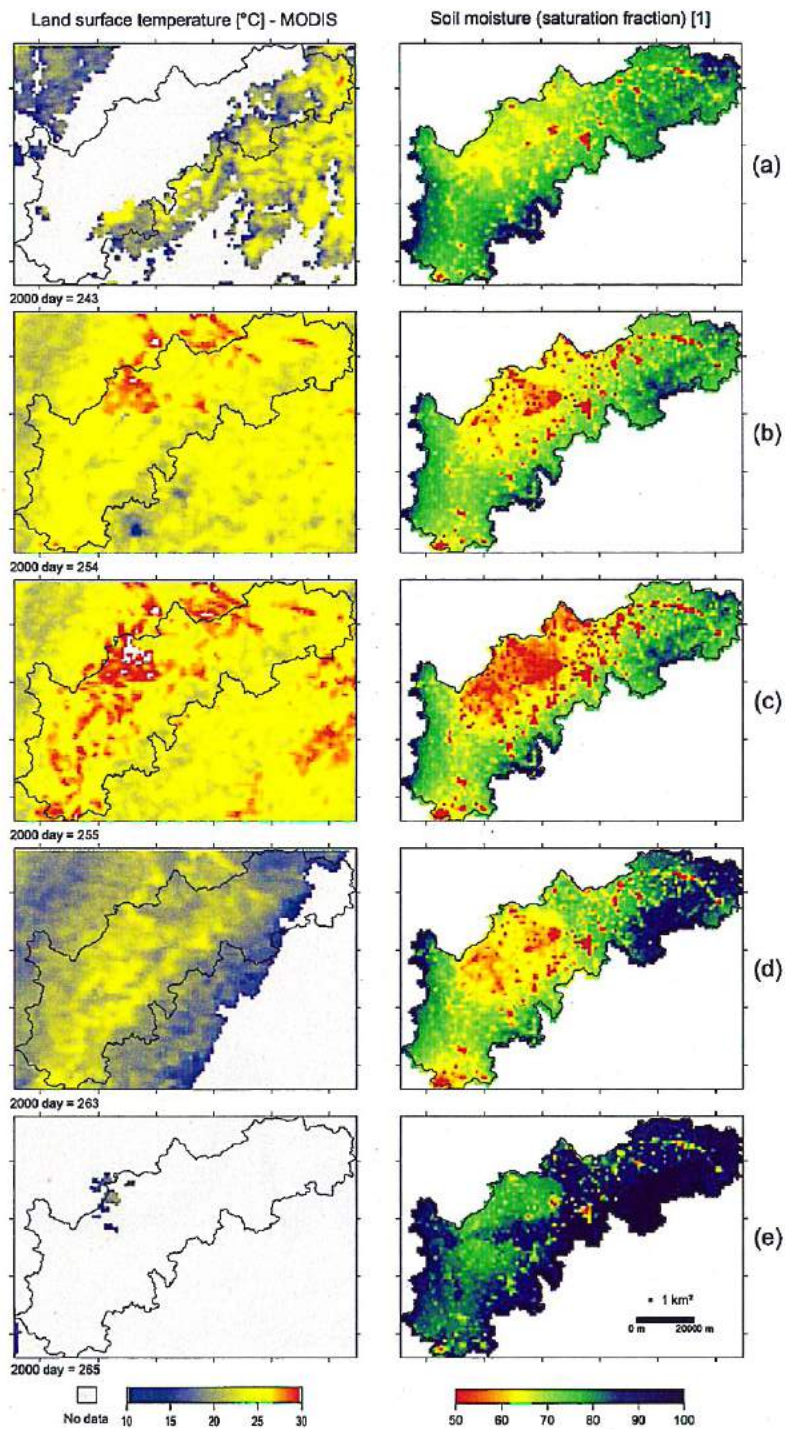


Figure 4.21: Panels (a)-(e): Plausibility test of soil moisture patterns for five summer days in year 2000. LST patterns are depicted as a proxy of soil moisture.

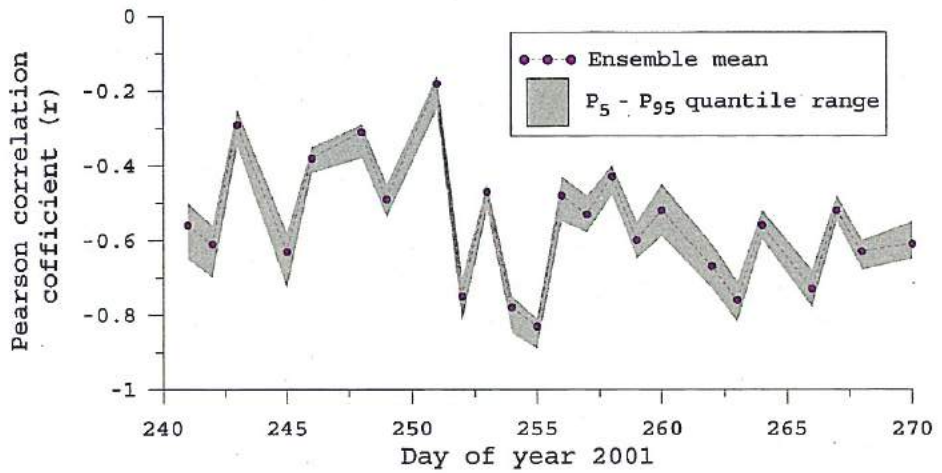


Figure 4.22: Ensemble model simulation of soil moisture patterns compared with MODIS derived LST during 30 summer days in year 2000. The ensemble mean and the ($P_5 - P_{95}$) percentile limits of the simulations were estimated with the best thousand solutions.

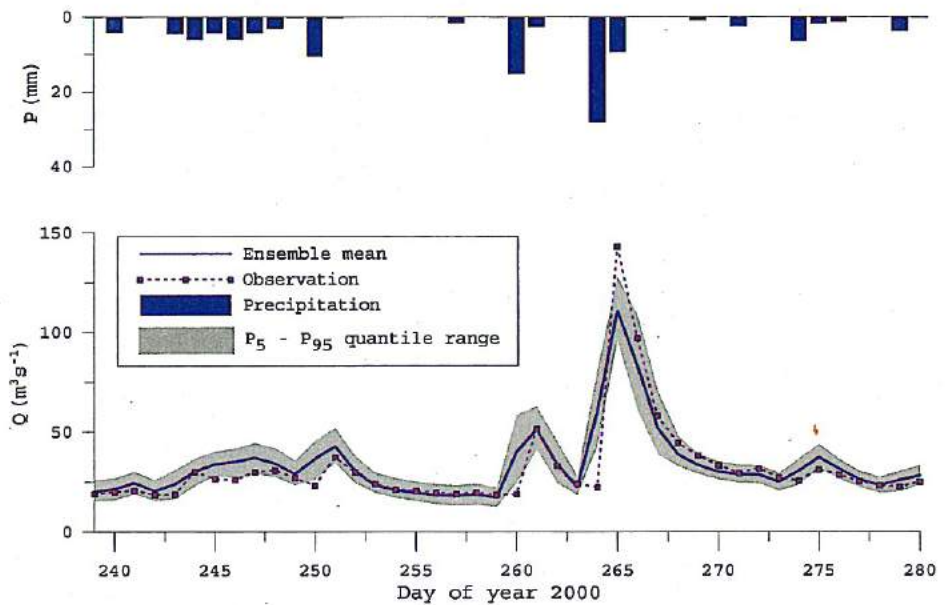


Figure 4.23: Daily discharge simulations at Plochingen during the plausibility test of soil moisture patterns in year 2000. The ensemble mean and the ($P_5 - P_{95}$) percentile limits of the simulations were estimated with the best thousand solutions.

4.6.2.2 Snow Cover Simulation

Another important component of hydrologic balance is a spatio-temporal dynamics of snow cover that effects the basin response during the winter and spring seasons in many regions of the world, in particular in mountainous regions (Parajka and Blöschl, 2008). The spatio-temporal pattern of the mHM simulated snow covers was compared with the MODIS derived snow covers for three winter days for the year 2001 (Fig. 4.24). One of the good set of global parameter (γ) was used for this plausibility test. A threshold of 1.0 mm for model simulated snow accumulation was used for the identification of snow covered pixels. Below this threshold limit all modeling cells was categorized under non-snow cover pixels.

The visual inspection between model simulated spatial pattern of snow cover and the MODIS imageries on snow covers, as depicted in Fig. 4.24 revealed that mHM, albeit having simple algorithm (i.e based on the temperature index method) for snow accumulation and melting process, catches reasonably well the spatial patterns of snow cover that are observed by MODIS. The model simulated daily discharge time-series also matched quite well with their corresponding observed values. The NSE value for this discharge simulations during this period was above 0.90. However, most of the days in this investigated period, MODIS data were affected by the cloud cover. The in-depth analysis regarding cloud removal algorithms is out of scope of the present study and therefore left for the future investigation.

4.6.3 Effects of Frozen Soil on Streamflow Predictions

Ground surface temperature play a significant role in the streamflow generation during freezing-spells in winter. To study the effect of frozen soil on model responses, in particular streamflow, model simulations were performed out at the Horgen-Kläranlage gauging station. The drainage area of this gauging station belongs to the Eschach river which is located in vicinity of Black Forest (Fig. 4.13). In these regions during the winter season the air temperature stays below 0°C for several days. As a result, soil freezing can occur in these areas. The results of the model simulations shows that the freezing spells during the winter has the impact on the streamflow simulations, in particular during the recession phase of the hydrograph (Fig. 4.25). Streamflow variations of up to 50% less than the observed value were obtained if the freezing and thawing

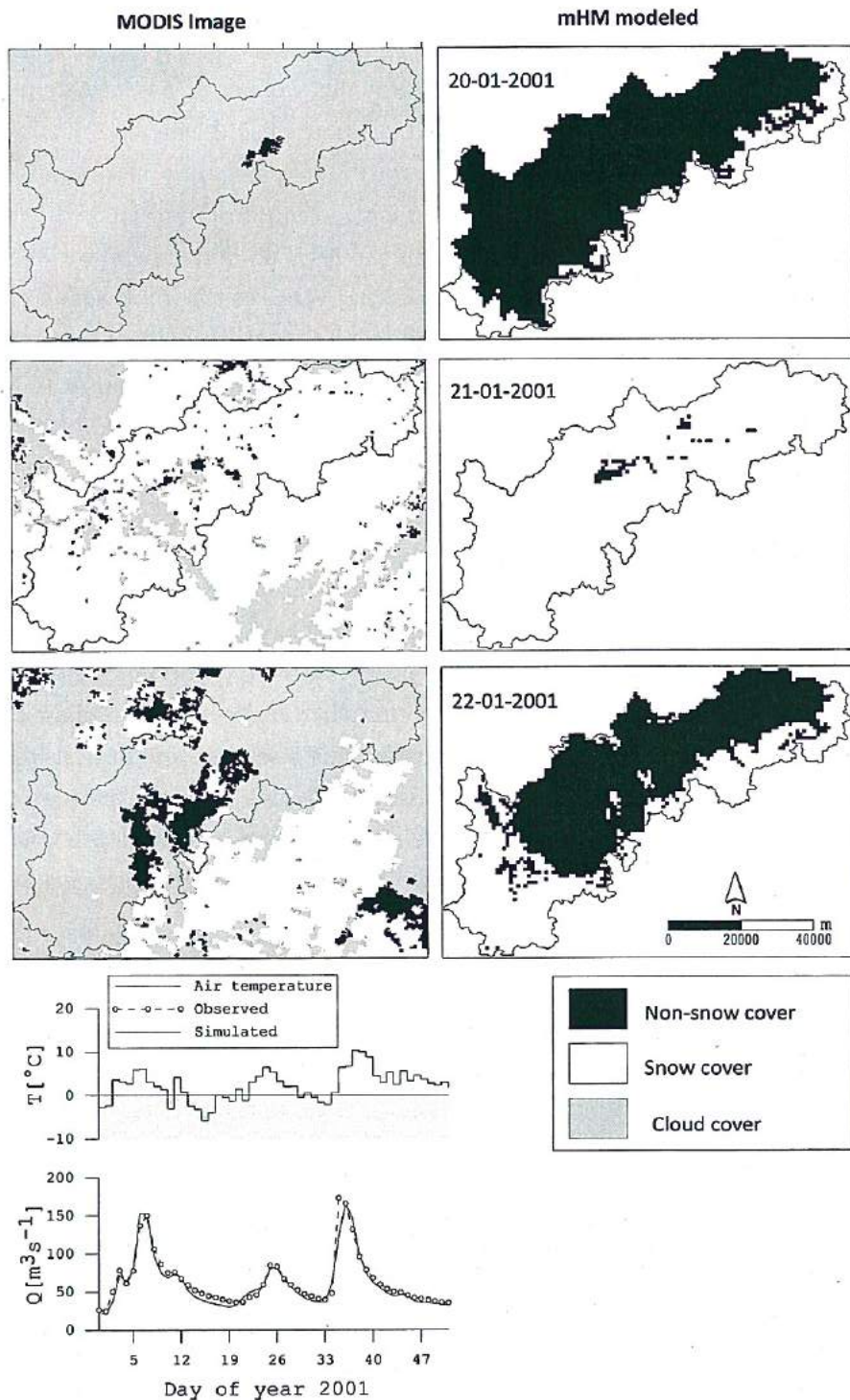


Figure 4.24: Plausibility test for the mHM simulated snow cover with the MODIS derived snow cover data on the selected days of year 2001 for the study area.

process was not included in the model. The spatial distribution of the semi-impermeable areas during a typical freezing-thawing cycle in winter was rapidly changing from day to day in accordance with the spatial distribution of the antecedent temperature index (Fig. 4.26). The latter was derived from the air temperature and used as a proxy for the soil temperature. It is worth mentioning that the discharge series shown in Fig. 4.25 constitute a cross-validation test because the observations at the gauging station "Horgen-Kläranlage" were not taken into account during the calibration phase. The NSE values between observed and simulated values as well as for their logarithmic transformed values of 0.83 and 0.82, respectively were obtained for the evaluation period at this gauging station. This result further indicated the robustness of the mHM model with multiscale parameter regionalization technique in the sense that the model might also be quite suitable for streamflow prediction in ungauged locations. However no attempts have been made in this study to evaluate the model for streamflow predictions outside of the study area.

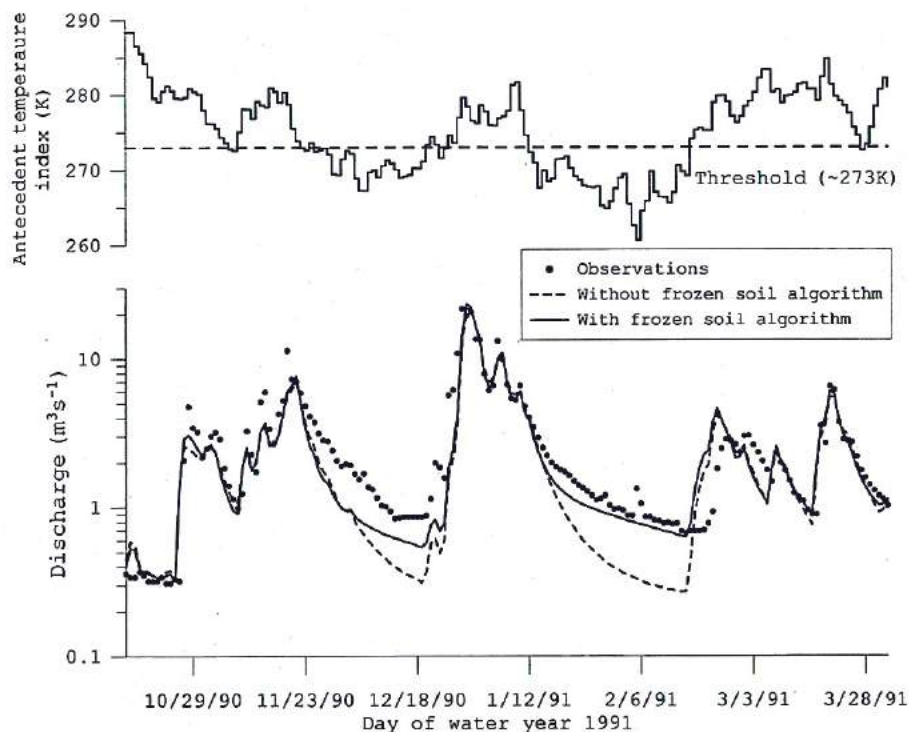


Figure 4.25: Effect of the frozen soil algorithm on the daily discharge hydrograph of the Eschach river at Horgen-Kläranlage gauging station.

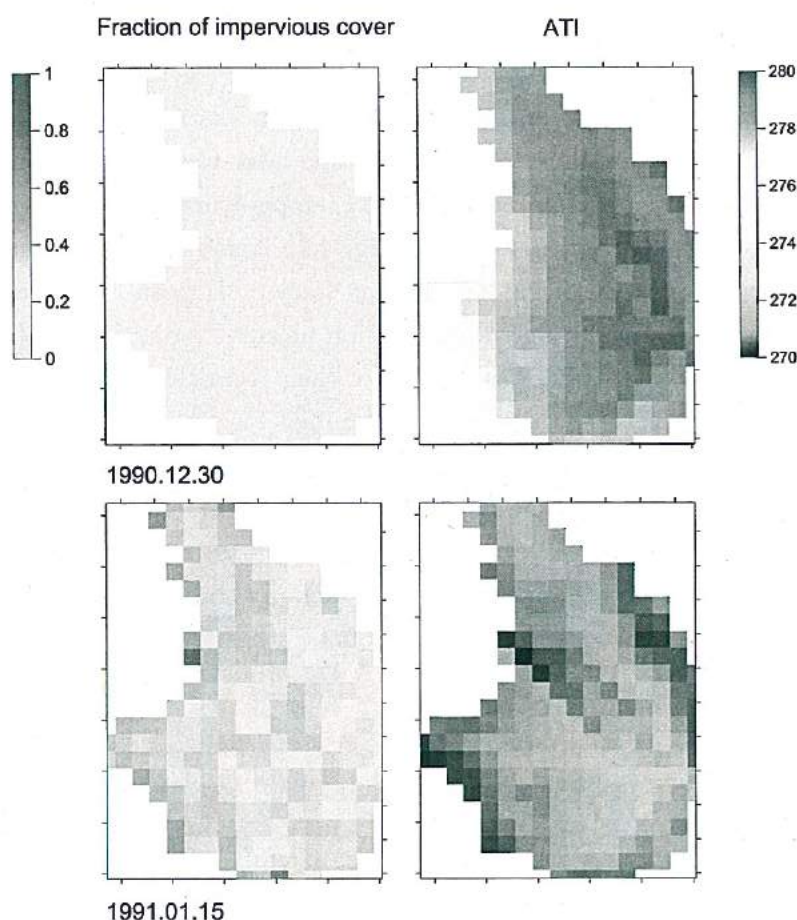


Figure 4.26: Spatial variation of the fraction of semi-impervious area due to frozen soil conditions in the Eschach river basin.

4.6.4 Effects of Canopy Interception on Streamflow Predictions

Several studies underline the importance of interception as one of the key processes affecting the water balance at the mesoscale (Fenicia et al., 2008). Often this process in hydrologic models is either disregarded or taken as a fixed percentage of the precipitation, so as to reduce the model complexity in terms of number of calibration parameters. With the increasingly availability of remotely sensed data on the vegetation cover (e.g. LAI, NDVI), it become possible to easily incorporate the interception processes in a spatially distributed hydrologic model (mHM).

A simple but an effective numerical experiment was conducted to study the effect of canopy interception storage on the streamflow simulations. The mHM model runs were performed with and without interception process for the water year 2001 with modeling spatial scale (level-1) of $4 \text{ km} \times 4 \text{ km}$. The lower scale (level-0) for the regionalization of the maximum interception capacity parameter (i.e. β_1 multiplied by LAI) for different land cover classes was fixed at the spatial resolution of $100 \text{ m} \times 100 \text{ m}$.

The results of this experiment clearly demonstrated the impact of neglecting the interception process and thereby not considering the spatio-temporal variability of canopy storage. Fig. 4.27 shows the model performance for daily discharge simulation during the summer season of the year 2001. It can be noticed from this figure that if canopy interception process is not accounted in modeling process a systematic bias between daily observed and simulated discharge can be produced, in particular overestimation of simulated discharge values. Whereas, when the interception process is accounted it can reduce the bias and the simulated values can match better the observed discharge values. The NSE values obtained for the daily discharge simulations during this season with interception process was, on average, 5% higher than that obtained without taking the interception process into the account. The reason for this poor performance, when not accounting the interception process, can be attributed to not accounting the spatio-temporal variability of canopy interception storage (Fig. 4.27), which in the full vegetation growth period can be very high (e.g. in months of May to July).

4.6.5 Comparison of mHM with the HBV model

Although there are several similarities between the HBV model (Lindström et al., 1997) and the proposed mHM model, the main differences are the inclusion of top-thin root zone soil layer, the soil freezing and thawing process and most importantly the parameterization approach. The question than normally arises whether the inclusion of these modules help to improve the predictions of streamflow and also the spatio-temporal patterns simulated water fluxes and state variables such as soil moisture. For this purpose, the simulations of the HBV model were compared with those obtained from the proposed mHM model.

The distributed version of the HBV model (i.e. HBV-IWS) used in this study is

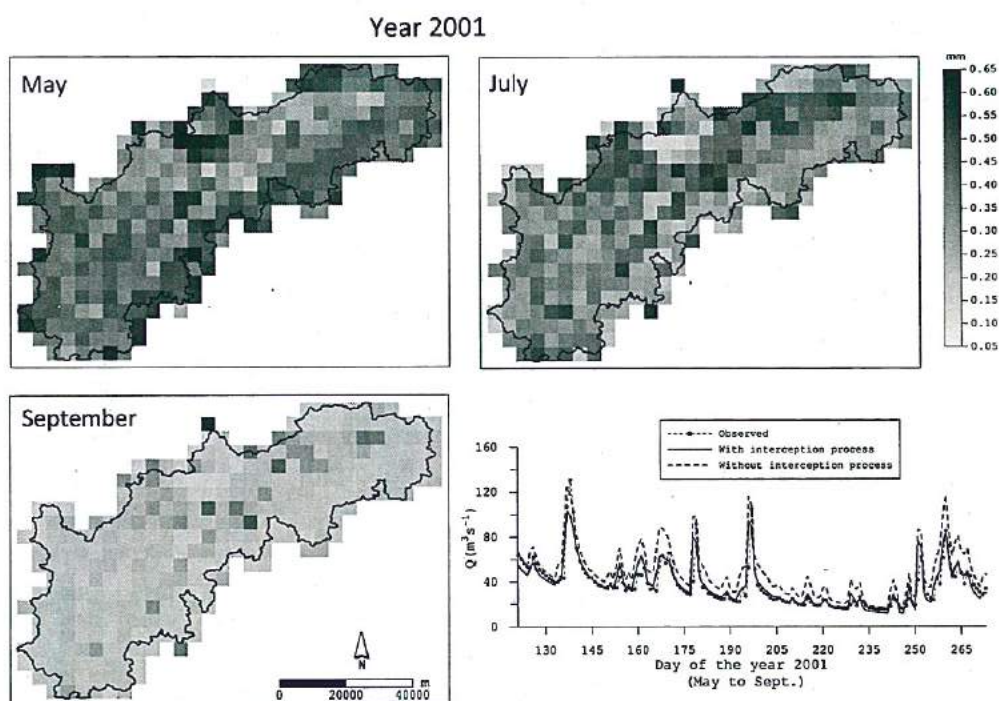


Figure 4.27: Spatio-temporal variability of daily mean maximum canopy interception storage during three summer months (i.e. May, July and September) of the year 2001. Additionally the model performance during these period for daily discharge simulations with and without interception process at the Plochingen is also shown.

based on the study of Das (2006). In summary, the HBV-IWS model also uses a grid cell (1 km \times 1 km) as a primary hydrological unit to simulate different hydrological processes such as snow accumulation and melting, soil moisture, infiltration. The runoff generation is, however, estimated on the sub catchment level and the flow generated from each sub-catchment are routed through the river network using the Muskingum algorithm. The model parameterization for the hydrological processes is based on the hydrological response units (HRU) method, whereas the runoff generation parameters are lumped to the sub-catchment level. A total 28 HRUs based on 7 soil type and 4 land cover classes were used to describe the spatial dynamics of hydrological processes and a total 13 sub-catchments depending on the available gauging stations were used to set up the HBV-IWS model (Das, 2006). Detail description of this model is, however, out of scope of this thesis, interested readers may refer to Das (2006).

It is worthwhile emphasizing here that the following comparison between mHM and HBV-IWS (hereafter denoted as only HBV) is not aimed at pointing out the deficiencies in the HBV model, since the HBV model has been used for last several decades in many catchments throughout the world (Lindström et al., 1997). The comparison done in this study was to specifically observe the effects of the inclusion of new modules in mHM. It may be also noted that the basic conceptualization of hydrological processes in HBV is quite robust, and therefore was also adopted in the basic formulation of mHM.

Both models were first tested for the streamflow predictions at Horb gauging station. In general, the mHM model significantly improves the streamflow predictions compared with those obtained with a distributed implementation of the HBV model (Fig. 4.28). In the evaluation period, yearly evaluated NSE values obtained with mHM are usually greater than those obtained with HBV. The mean NSE obtained for both models in this period was 0.86 and 0.79, respectively.

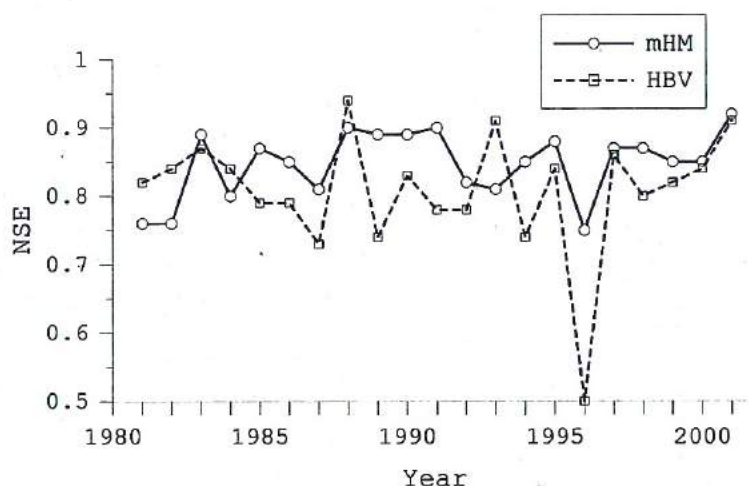


Figure 4.28: Evolution of annual NSEs between observed and models (i.e. mHM and HBV) simulated daily discharge at the Horb gauging station during the modeling period.

Comparing the simulation results of both models it can be appreciated that mHM is better than the standard HBV model at predicting the recession phase of the hydrograph after a freezing-spell has occurred during the winter season (Fig. 4.29). In summer, it was also noticed that HBV tended to under predict peak flows, and quite often; a decoupling between observed and simulated

values during the recession phase of the hydrograph was detected afterwards (Fig. 4.29).

The model performance (e.g. NSE) varies over the modeling period for both models (Fig. 4.28). However, this variability is quite small in case of the mHM model as compared to the HBV model performance. A possible reason for the variability of the NSE is likely related to the quality of the precipitation data in summer. During this season, the occurrence of convective events are often not registered by the climatological network due to their small spatial scale.

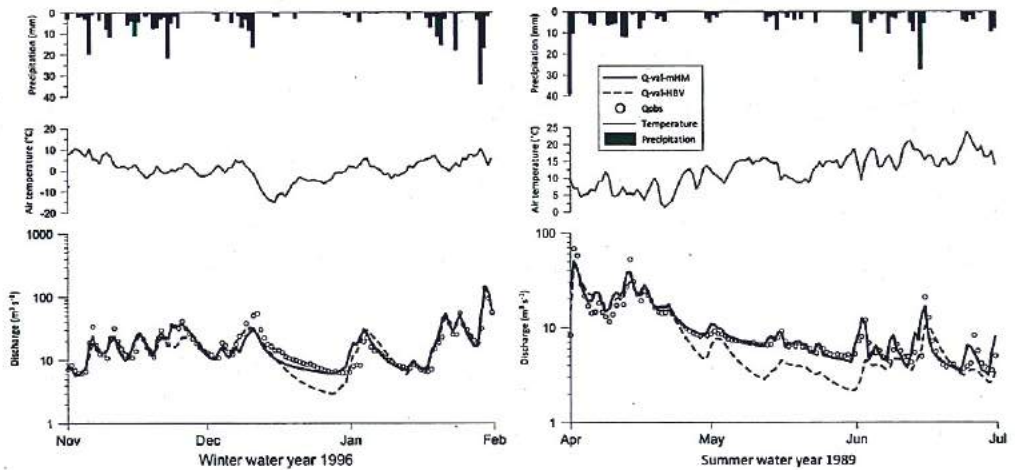


Figure 4.29: Comparison between HBV and mHM during selected winter (a) and summer (b) seasons at Horb gauging station.

The proposed modifications of the soil moisture accounting routines (e.g. inclusion of pedo-transfer functions, regionalization at sub-grid scale, amongst others) in mHM produced much better results with respect to the soil moisture distribution that are obtained by HBV with the HRU parameterization method as depicted in Fig. 4.30. The pearson's correlation coefficient between the LST patterns and the saturation fraction for both approaches (i.e. the HRU and the proposed MPR) are -0.36 and -0.72 on the day 255 of year 2000. The performance of mHM for the soil moisture simulations in terms of r statistics between it and MODIS-LST data were, on average, at least 50% higher than those obtained through the HRU method including all investigated days, when MODIS data were available. The relatively poor performance of HRU is mainly because it uses a categorical classification to identify HRU and their related

parameters within a basin. Since the geographic locations of modeling cells in the HRU method are not explicit, the neighboring cells can have very different soil parameters even though the soils properties were same. More in-depth analysis on this aspect and the influence of other regionalization techniques on the soil moisture patterns will be presented in next chapter.

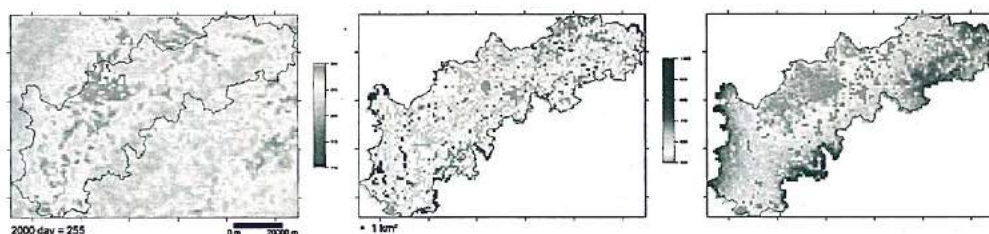


Figure 4.30: Comparison of the top-layer soil moisture distribution for the day 255 of the year 2000. From left to right: LST (MODIS), soil moisture obtained with HBV and mHM, respectively.

4.6.6 Model Time Complexity and Coding

Before concluding this chapter, a short summary on the computational requirements of mHM and its coding are presented here. The heavy computational time can hinder the application of any spatially distributed hydrologic model in a mesoscale catchment. Several thousands of iteration are required to search a “good” set of model parameter in an automatic calibration process. Moreover, for real time flow forecasting an efficient model would be required that have lower running time complexity and at the same time model can provide a reasonable estimate on required information. For mHM, the total time required to carry out the simulation shown in Fig.4.19 was on average 6 min using a single node of a Linux cluster with 32 AMD Dual Core OpteronTM885, 64-bit Processors. This implies an average of 7×10^{-3} s/cell/year. The source code of mHM was entirely written on the standard Fortran 2003 computer language using the PGI Visual FortranTM compiler. The code is written in a modular approach, which offers the flexibility to easily incorporate new processes.

Chapter 5

Comparison of Regionalization Methods ¹

“Every theory is based on physical concepts expressed through mathematical idealizations. They are introduced to give an adequate representation of the physical phenomena. No physical concept is sufficiently defined without the knowledge of its domain of validity”

Leon Rosenfeld

5.1 Introduction

This chapter mainly presents the results of a comparison of the proposed multi-scale parameter regionalization (MPR) with the standard regionalization (SR) method. Both parameterization methods were implemented in the mHM model and several numerical experiments were designed to test the efficiency of a particular parameterization method for the transferability of model parameters across scales and locations other than that used for model calibration, the preservation of spatial patterns of relevant state variables and water fluxes, the conservation of mass balance on a given control volume, amongst others. This chapter is divided into two main sections. First section deals with the design of numerical experiments, following to which in the next section results of the systematic comparison between the MPR and SR methods is presented.

¹This chapter is a modified and extended version of the manuscript: Samaniego, L., Kumar, R., and S. Attinger (2010). Multiscale parameter regionalization of a grid-based hydrologic model at the mesoscale. Water Resour. Res., 46, W05523.

5.2 Numerical Experiments and Evaluation Criteria

Various numerical experiments were carried out to evaluate the performance of a parametrization technique with respect to the following criteria.

1. Sensitivity of model efficiency measures to the spatial resolution of basin predictors at level-0,
2. Sensitivity of model efficiency measures to global parameters γ calibrated at modeling scales and/or locations different from that currently used.
3. Degree of disruption of the mass balance in a control volume at level-1 caused by the transfer of global parameters γ from modeling scales and/or locations different from that currently used.
4. Preservation of spatial patterns of the state variables at various modeling scales (i.e. level-1).

5.2.1 Effect of the Sub-grid Variability

The purpose of this numerical experiment was to assess the effect of the sub-grid variability of predictors (i.e. level-0) on model efficiency, given a predefined modeling level-1. Aggregated statistics based on streamflow only [e.g. the root mean squared error (RMSE) or the Nash Sutcliffe Estimator (NSE)] may not be sufficient to identify these effects mainly due to the nonlinearity of the system. For this reason, the spatial variability statistic \bar{r} based on water fluxes or state variables was also estimated in the following algorithm.

Algorithm 2:

1. Set the spatial resolution of level-1, e.g. $\ell_1 = 2$ km
2. Set a spatial resolution for level-0 data, ℓ_0 .
3. Calibrate the model at level-1 based on level-0 information using Algorithm 1.
4. Estimate model efficiency at level-1 (e.g. bias, RMSE, NSE).
5. Estimate the spatial variability statistic \bar{r} [Eq. (5.1)].
6. Repeat (2) to (5) for various spatial resolutions of input data or basin predictors, e.g. $\ell_0 = (100, 500, 1000, 2000)$ m.

Here \bar{r} denotes the expectation of r estimated as

$$\bar{r} = E \left[r(\mathbf{x}_i^{(100)}(t), \mathbf{x}_i^{(J)}(t)) \right]_t \forall i \in \Omega, \forall t \quad (5.1)$$

where r is the spatial correlation of two fields in time t . It should be noted that, the correlation coefficient r is estimated over the space for each point in time t . $\mathbf{x}_i^{(J)}(t)$ denotes the value of a state variable or a water flux at cell i (level-1) in time point t estimated with effective parameters obtained with level-0 information at a spatial resolution $\ell_0 = J$. J is the level-0 discretization with $J = (100, 500, 1000, 2000)$ m. The simulation with $\ell_0 = 100$ m was used as a baseline for the estimation of \bar{r} . It may be noted that this particular experiment is only valid for testing the MPR method.

5.2.2 Transferability of Global Parameters across Modeling Scales

The transferability of global parameters may introduce bias either because of the unaccounted spatial heterogeneity of basin predictors or because of the assumptions required to define the regionalization functions and the upscaling rules. The procedure depicted in Fig. 5.1 was employed to test the mass conservation on a given control volume.

Algorithm 3:

1. Set the spatial resolution of level-0 ($\ell_0 \times \ell_0$) and level-1 ($\ell_1 \times \ell_1$). The latter is denoted as the **control** scale. Level-2 scale is set equal to that of level-1. E.g. $\ell_0 = 100$ m and $\ell_1 = 8$ km.
2. Find global parameters $\gamma^{(\ell_1)}$ at the control scale (use Algorithm 1), e.g. if $\ell_1 = 8$ km then find $\gamma^{(8)}$ as shown in Fig. 5.1.
3. Set a new modeling level-1' for evaluation such that $\ell'_1 < \ell_1$, e.g. $\ell'_1 = 2$ km.
4. Simulate fluxes at level-1' using the set of global parameters obtained for the control scale in (2) (e.g. $\gamma^{(8)}$).
5. Estimate global efficiency measures of the model at level-1' (e.g. RMSE, NSE).
6. Integrate water fluxes obtained in (4) [Eq. (5.2)] from level-1' to level-1 and estimate the statistic r_f [Eq. (5.3)].

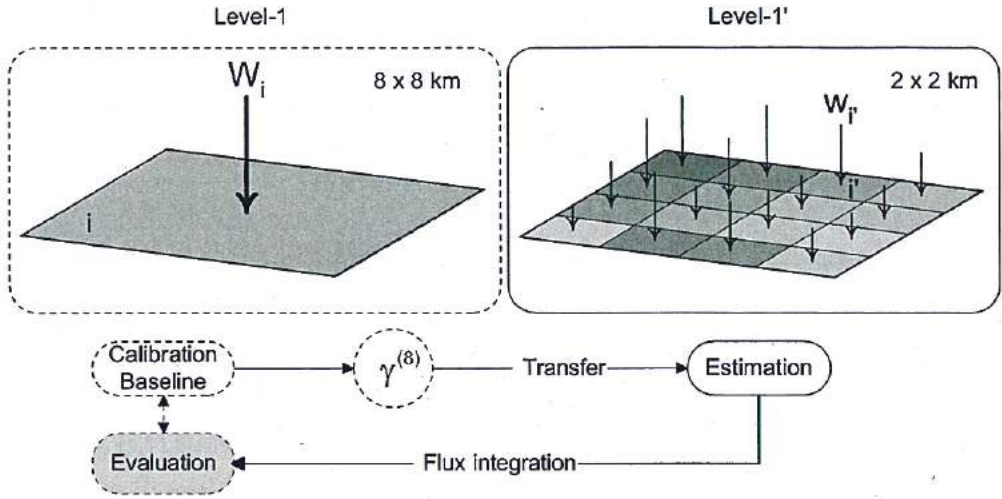


Figure 5.1: Evaluation scheme for the evaluation of the continuity principle between two modeling scales. In this example, level-1 is the control scale at 8×8 km whereas the level-1' is the simulations scale at 2×2 km. Here $\gamma^{(8)}$ denote global parameters (scalars) calibrated at level-1. $W_i(t)$ and $w_{i'}(t)$ is the estimated water fluxes at each scale, respectively.

7. Repeat (3) to (7) for various spatial resolutions of level-1.

It is worth noting that in MPR, model parameters β^1 are not transferred from one modeling scale ℓ_1 to a different one at level-1, but the global parameters $\gamma^{(\ell_1)}$. Based on them, regionalized fields of parameters β^0 at level-0 can be upscaled to any modeling scale (level-1) as indicated in step (4) of Algorithm 3 (Fig. 3.2). This algorithm basically consists in finding the absolute deviations between fluxes of every cell i at a control scale defined a priori (e.g. $\ell_1 = 8$ km) and the corresponding integral of water fluxes obtained at the finer scale (e.g. $\ell_1 = 2$ km). In this case, both simulations (i.e. at coarser and finer modeling scales) have to be forced by the same meteorological drivers and employ the same global parameters γ , which can be obtained at the coarser resolution via calibration. This implies that model parameters at level-0 (β^0) are common for both modeling scales. Formally, the absolute deviations at point in time t can be calculated by

$$\left| W_i(t) - \int_i w_{i'}(t) \right| \rightarrow 0 \quad i' \in i \quad \forall i \in \Omega \quad (5.2)$$

where $W_i(t)$ and $w_{i'}(t)$ denote the fluxes at time t estimated at the coarser and

finer cells i and i' respectively. Ω represents the domain of a simulation.

A possible estimator for the conservation of mass at every grid i over a time interval is the NSE between the water fluxes obtained at the coarser scale $W_i(t)$ (used as baseline values since no observations exist) and the aggregated flux at grid i denoted as $\int_i w_{i'}(t)$. In this case, a negative NSE value indicates a complete mismatch between these two variables. If the principle of continuity is fully satisfied, then the expectation of the NSE statistic denoted by r_f would tend to one, formally,

$$r_f = E \left[\text{NSE}(W_i(t), \langle w_{i'}(t) \rangle)_i \right] \rightarrow 1 \quad (5.3)$$

where E is the expectation of the NSE evaluated at every cell i . Larger deviations of r_f from its ideal value (i.e. 1) would indicate that the global parameters obtained with a given regionalization technique can not be transferred to other modeling scales.

5.2.3 Preservation of Spatial Patterns

The spatial similarity of two fields at two different scales can be estimated with the averaged spatial correlation coefficient r_s given by

$$r_s \equiv r_s(\mathbf{x}_j^{(\ell_0)}, \mathbf{x}_i^{(\ell_1)}) \quad \forall j \in i \quad \forall i \in \Omega \quad (5.4)$$

where $\mathbf{x}_j^{(\ell_0)}$ and $\mathbf{x}_i^{(\ell_1)}$ two fields at scale ℓ_0 and ℓ_1 , respectively.

5.3 Implementation of MPR and SR within mHM

Both MPR and SR were used to parameterize mHM model parameter and the study was performed in the Upper Neckar river basin (for details, refer to Chapter 4). The detail description for the implementation of MPR within mHM was previously presented in Chapter 3. The main difference between both methods is their upscaling sequence. In the SR method, basin predictors were first upscaled from level-0 to required modeling scale at level-1 and than the regionalization of mHM model parameters was performed. Whereas, in the MPR method the regionalization was first performed at the level-0 and than upscaling operators were used to estimate the effective value of model parameters at level-1. To make a fair comparison between both methods, model

parameters in SR were regionalized with the same functional relationships as those used in MPR (see Chapter 3: Table 3.2). As a result, both methods have in total same number of global parameters $\gamma = 62$, which have to be estimated by the calibration process.

This case study was performed during the period from water year of 1980 to 2001. This period was divided into two parts: 1980 to 1988 as a calibration period and 1989 to 2001 as an evaluation period. Good sets of model parameters γ for both MPR and SR were identified using simulated annealing algorithm following the Algorithm-1, as described in previous chapter. All above mentioned numerical experiment includes several different spatial discretization at all three levels which can be summarized as

Level-0: To test the influence of the sub-grid variability on the parametrization scheme, four spatial resolutions were selected: $\ell_0 = (100, 500, 1000, 2000)$ m.

Level-1: Several modeling resolutions were considered to test the performance of mHM with both regionalization techniques (i.e. MPR and SR). The selected modeling resolutions were: $\ell_1 = (2, 4, 8, 16, 32)$ km.

Level-2: In this study, the meteorological data was derived at the same resolution as the modeling scale (i.e. $\ell_2 \equiv \ell_1$).

The EDK interpolated $1 \text{ km} \times 1 \text{ km}$ meteorological variables were upsampled to the required modeling resolution $(2, 4, 8, 16, 32)$ km. The spatial similarity of the meteorological fields (i.e precipitation, temperature, and PET) across spatial resolutions was analyzed with the averaged spatial correlation coefficient $\bar{r} = E[r(\mathbf{u}_i^{(2)}(t), \mathbf{u}_{i'}^{(J)}(t))]$, $\forall t, i \in \Omega^{(2)}, i' \in \Omega^{(J)} i \in i'$, where J denoting the discretization ℓ_1 of the spatial domain Ω , and $J = \{2, 4, 8, 12, 32\}$ km. Based on this statistic it can be concluded that the relationship of the cross-scale spatial variability \bar{r} with the spatial discretization is nonlinear. Additionally, its variance increases with the discretization (Fig. 5.2). Fig. 5.3 depicts an example of the reduction of the spatial variability of the precipitation fields for a particular day.

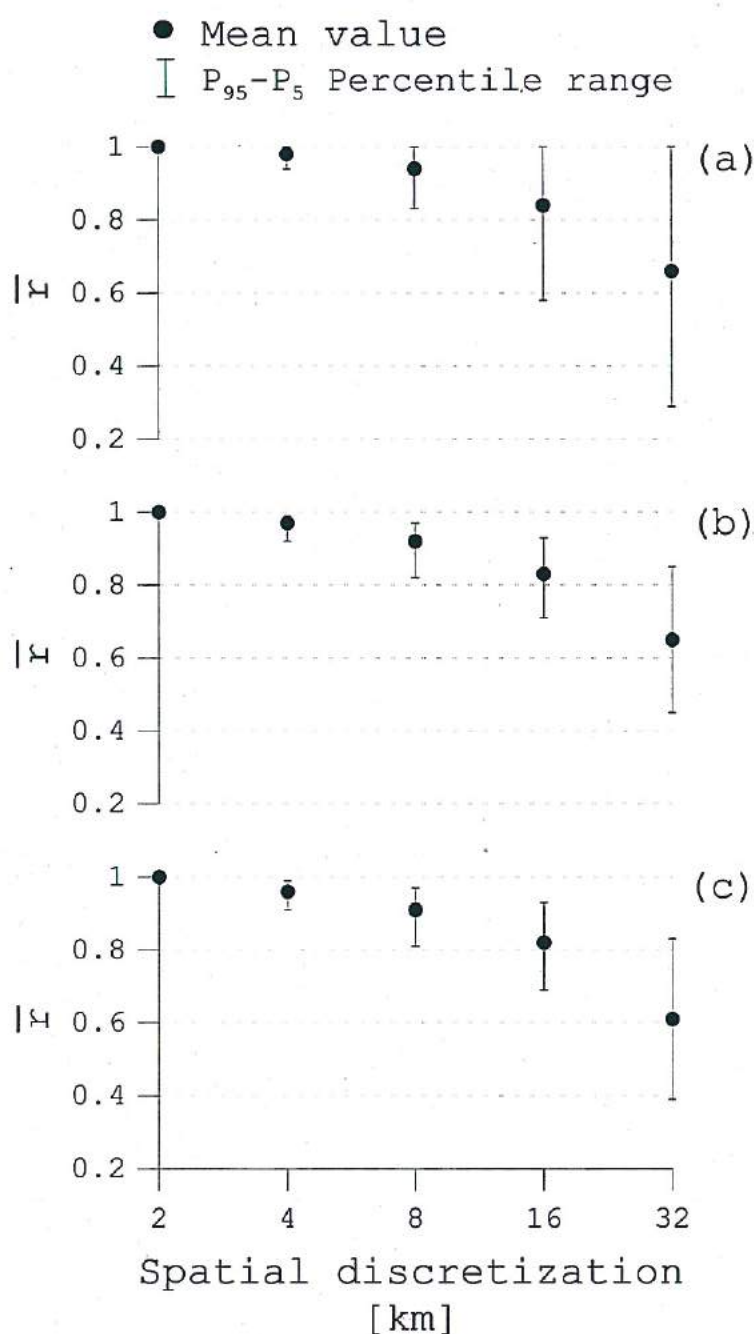


Figure 5.2: Mean and $P_{95} - P_5$ quantile range of the spatial correlation (\bar{r}) between 2 km resolution of (a) daily total precipitation, (b) daily average temperature, and (c) daily total potential evapotranspiration with their corresponding ones at coarser resolutions (shown on the horizontal axis) during the modeling period (1980-2001)

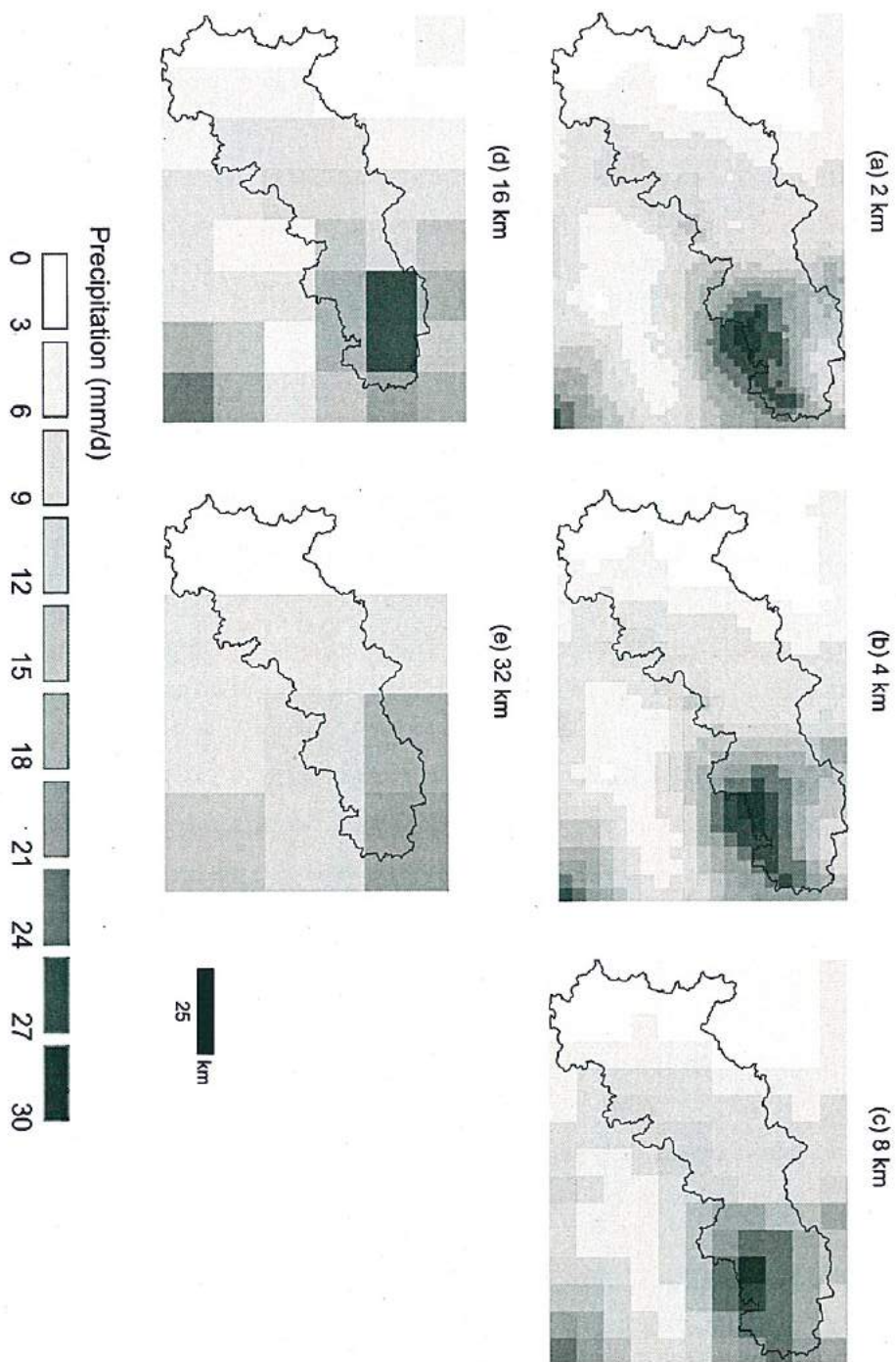


Figure 5.3: Spatial distribution of precipitation on day 21-09-2000 at the spatial resolutions of (a) 2 km, (b) 4 km, (c) 8 km, (d) 16 km, and (e) 32 km.

5.4 Analysis of Numerical Experiments

The following sections presents the results obtained from the numerical experiments for the MPR and the SR method. Since the model structure, input data and number of free parameters estimated through calibration process are kept same, any differences in performance may only arises from the parameterization method.

5.4.1 Sensitivity of Model Efficiency to the Sub-grid Variability

The results of the numerical experiment obtained with Algorithm 2 support the hypothesis that the sub-grid variability of the basin predictors played an important role both in the prediction of daily streamflow and the spatial distribution of water fluxes. For instance, the RMSE between observed and simulated streamflow increased by 12 %, if the ℓ_0 resolution varied from 100 m to 2000 m, with a fixed modeling scale of $\ell_1 = 2$ km (Table 5.1). Correspondingly, the NSE and the Pearson correlation coefficient r showed a decrement of 2 %.

Table 5.1: Effect of the sub-grid variability $\ell_0 = (100, 500, 1000, 2000)$ m on three model efficiency statistics (RMSE, NSE, and r) obtained for the daily discharge simulation for a given modeling scale ($\ell_1 = 2000$ m). These statistics were evaluated during themodeling period (1980-2001).

ℓ_0	ℓ_1	RMSE	NSE	r
m	m	mm/d	-	-
100	2000	0.38	0.88	0.94
500	2000	0.41	0.87	0.92
1000	2000	0.41	0.86	0.91
2000	2000	0.42	0.86	0.91

The variability of the spatial distribution of soil moisture in the top soil layer, as well as the actual evapotranspiration and runoff, exhibited a reduction up to 40 % of \bar{r} (Eq. (5.1)) with respect to their corresponding baseline simulation (Fig. 5.4). It is worth mentioning that MPR simulations in which $\ell_0 = \ell_1 = 2000$ m are equivalent to those determined with the SR method. As

a result, input data with a resolution $\ell_0 = 100$ m was used for the remaining numerical experiments employing the MPR technique.

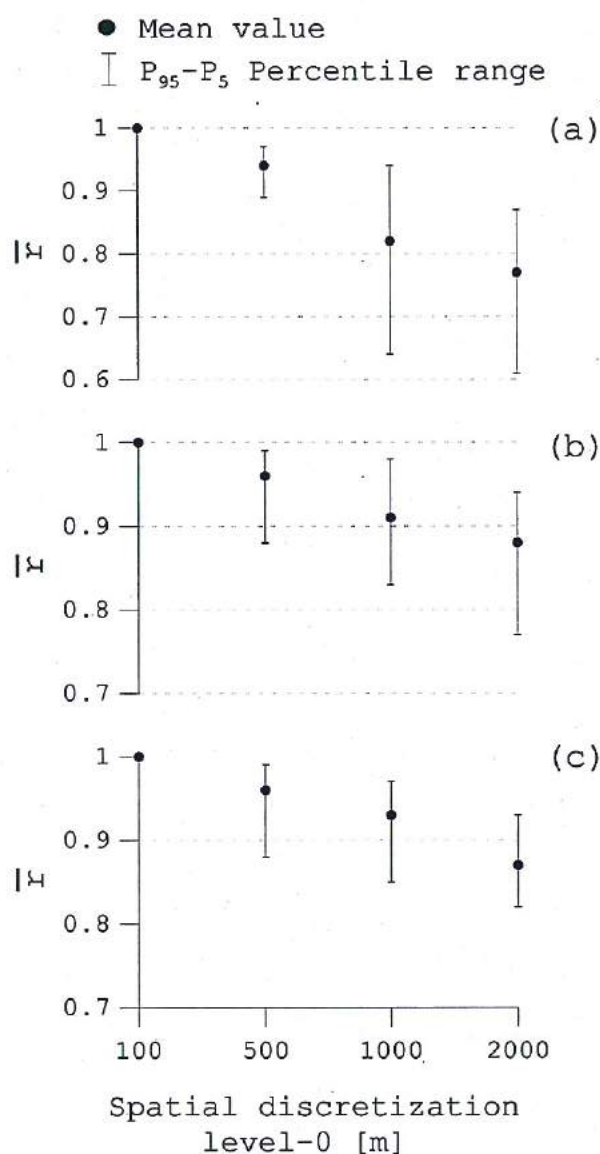


Figure 5.4: Mean and $P_{95}-P_5$ quantile range of the spatial correlation (\bar{r}) of (a) daily soil moisture, (b) daily total evapotranspiration, and (c) runoff between simulations obtained with a fixed modeling scale $\ell_1 = 2$ km but varying input data resolution $\ell_0 = (100, 500, 1000, 2000)$ m. The baseline values correspond to the simulations obtained with the smallest resolution. These statistics were estimated for the period for the modeling period (1980-2001).

5.4.2 Sensitivity of Streamflow Simulations to Global Parameters

Results obtained with Algorithm 3 are presented in Table 5.2. Both statistics, RMSE and NSE, shown in this table were estimated with the daily streamflow simulations at the outlet of the basin (i.e. Plochingen gauging station) for a given scale. Both parametrization methods were not significantly different from each other, with respect to the RMSE and the NSE, when the model was calibrated and evaluated at a given modeling scale as shown in Table 5.2 (values in boldface on the diagonal). In this case, MPR performed marginally better than SR (approximately 2 % for both statistics). This implies that there exist various levels of discretization and thus parameterizations that provide equally acceptable solutions for modeling streamflow. These results agreed with those obtained by the Distributed Model Intercomparison Project, phase 1 (DMIP-I) (Reed et al., 2004) with respect to the performance of lumped versus distributed hydrologic models. The performance regarding other state variables, however, may be unacceptable as will be shown afterwards.

Deficiencies of the regionalization methods, nevertheless, became apparent when global parameters were shifted across modeling scales as can be appreciated in the off-diagonal values in Table 5.2. The performance of SR, as compared to MPR, showed a significant deterioration when the global parameters were calibrated for a coarser modeling scale (say $\ell_1 = 8$ km) and subsequently applied in a finer one ($\ell_1 = 2$ km) as shown in the upper triangular matrices of Table 5.2. The RMSE obtained with MPR and SR was, on average, 0.46 mm/d and 0.62 mm/d, respectively. This means that the error of the daily streamflow simulations obtained with SR was, on average, 34 % higher than that estimated with MPR. The NSE, as expected, exhibited the opposite relationship. Mean NSE, in this case, was 0.80 and 0.64 for MPR and SR, respectively. Moreover, the average reduction of NSE with respect to the baseline simulations (i.e. no shift of global parameters) was 53 % for SR, whereas, this statistic only exhibited 12 % reduction for MPR.

Shifting global parameters calibrated for a given modeling scale to its immediate lower one (e.g. from 8 km to 4 km), however, does not induce a significant decrease in the performance of MPR as compared to that of SR. The increment of the RMSE was, on average, 1.1 % and 30.7 % for MPR and SR, respectively (Table 5.2). The decrement of NSE for MPR was at most 3%, whereas, SR

Table 5.2: RMSE and NSE obtained with both the multiscale (MPR) and the standard (SR) parameter regionalization techniques at various modeling scales obtained with daily streamflow values. Values on the diagonal (bold) refer to the statistics obtained for a model calibrated and evaluated at a given scale, whereas off-diagonal values denote statistics obtained with global parameters γ calibrated at other modeling scales. Results were obtained at Plochingen (basin outlet) during the modeling period (1980-2001).

Simulation Scale	Calibration Scale									
	2 km	4 km	8 km	16 km	32 km	2 km	4 km	8 km	16 km	32 km
RMSE [mm/d]										
	MPR					SR				
2 km	0.38	0.38	0.45	0.53	0.72	0.42	0.46	0.64	0.78	0.90
4 km	0.35	0.33	0.35	0.41	0.57	0.38	0.34	0.46	0.63	0.77
8 km	0.39	0.39	0.33	0.36	0.49	0.41	0.37	0.34	0.46	0.63
16 km	0.46	0.47	0.39	0.35	0.38	0.47	0.46	0.40	0.35	0.45
32 km	0.54	0.55	0.50	0.42	0.39	0.53	0.56	0.50	0.42	0.38
NSE [-]										
	MPR					SR				
2 km	0.88	0.87	0.82	0.76	0.56	0.86	0.81	0.64	0.46	0.29
4 km	0.89	0.90	0.89	0.85	0.73	0.87	0.90	0.81	0.65	0.48
8 km	0.86	0.87	0.90	0.89	0.80	0.85	0.88	0.90	0.81	0.66
16 km	0.82	0.82	0.87	0.89	0.87	0.81	0.81	0.86	0.89	0.82
32 km	0.75	0.75	0.78	0.84	0.88	0.75	0.72	0.78	0.84	0.88

exhibited reductions in NSE up to 11%.

Transferring global parameters calibrated for a finer modeling scale (say $\ell_1 = 2$ km) to a coarser one ($\ell_1 = 8$ km) was not so significant with both regionalization techniques as it was described above for the opposite case. In those cases, the RMSE obtained with MPR were only 1 % lower than those obtained by SR. NSE estimated with both methods was, on average, 0.83 and 0.82 for MPR and SR, respectively (based on the lower triangular matrices of Table 5.2). The same tendency for both methods was observed when global parameters were shifted to its immediately higher scale (e.g. from 4 km to 8 km).

The interpretation for this behavior of both methods is related with the amount of information used for regionalization. As a consequence, shifting global parameters from finer to coarse resolutions, for both methods, provide higher stability rather than the other way around. For the same reason, MPR performed significantly better than SR, when global parameters were shifted from coarser to finer modeling scales. Model parameters estimated with MPR, at any

modeling scale, are intrinsically linked with their sub-grid variability (Fig. 3.2). The average performance for both regionalization schemes at a given simulation scale obtained only with transferred global parameters is shown in Fig. 5.5. The average and the range of NSE depicted in this figure for a given scale were estimated based on their respective values of Table 5.2 (i.e. along rows). In general, model performance tends to increase as the simulation scale increases, regardless of the regionalization scheme (Fig. 5.5). However, there seems to be an upper limit, which for this study basin is around $\ell_1 = 8$ km. After this threshold scale is reached, further spatial discretization tends to decrease model performance.

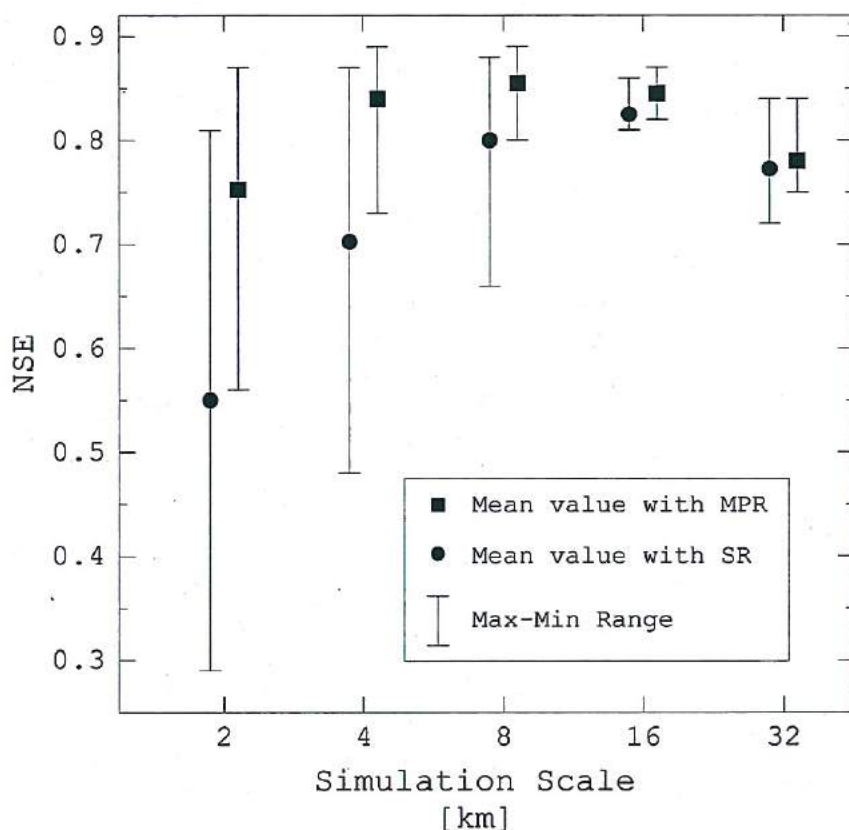


Figure 5.5: Mean and range of NSE obtained between observed and simulated daily streamflow simulations using MPR and SR at various modeling scales. Both statistics were determined with global parameters shifted from both coarser and finer scales to a given simulation scale. Simulations were carried out during the modeling period (1980-2001).

The range of NSE for both regionalization schemes tends to decrease towards the threshold scale. SR exhibited larger ranges than MPR for all simulation scales, though. Furthermore, the mean of NSE obtained with MPR was, on average, 12% higher than that of SR (Fig. 5.5).

The monthly water balance for both regionalization schemes exhibited similar behavior with respect to shifting global parameters as mentioned above (Fig. 5.6). The deterioration in performance, nevertheless, was not as higher as that estimated with daily streamflow simulations. The NSE between monthly observed and simulated streamflow during the period from 1979-11-01 to 2001-10-31 was at least 0.92 and 0.70 for MPR and SR, respectively. The specific long-term mean annual discharge at the outlet of the basin obtained with MPR and SR was quite close to the observed long-term mean of 407 mm/y for all spatial resolutions employed. The bias between the observed and simulated long-term annual discharge for both regionalization techniques, with or without shifting global parameters, was smaller than 7 mm/y. As an example, Table 5.3 presents the mean annual water balance over the whole basin obtained at different scales using global parameters transferred from a given modeling scale ($\ell_1 = 4$ km) with both the MPR and the SR methods.

Table 5.3: Mean annual water balance over the whole basin obtained at different scales using global parameters transferred from a given modeling scale ($\ell_1 = 4$ km) with the MPR and SR methods for the modeling period (1980-2001). Fluxes accounted: precipitation (P), runoff at the outlet (Q), actual evapotranspiration (E) [* \equiv estimated from raingauges, ** \equiv Estimated from streamflow gauge, *** \equiv Estimated from literature (Samaniego, 2003)]

Method	Flux [mm]	Mean Scale [km]					Standard Deviation Scale [km]				
		2	4	8	16	32	2	4	8	16	32
Estimated*	P	938	939	940	952	958	126	126	126	128	128
Estimated**	Q	407	407	407	407	407	93	93	93	93	93
Estimated***	E	560	560	560	560	560	-	-	-	-	-
MPR	Q	407	405	404	413	414	101	101	102	104	104
	E	564	566	567	569	570	24	24	24	23	23
SR	Q	409	405	400	409	408	100	100	100	102	102
	E	560	564	567	568	570	25	26	25	25	24

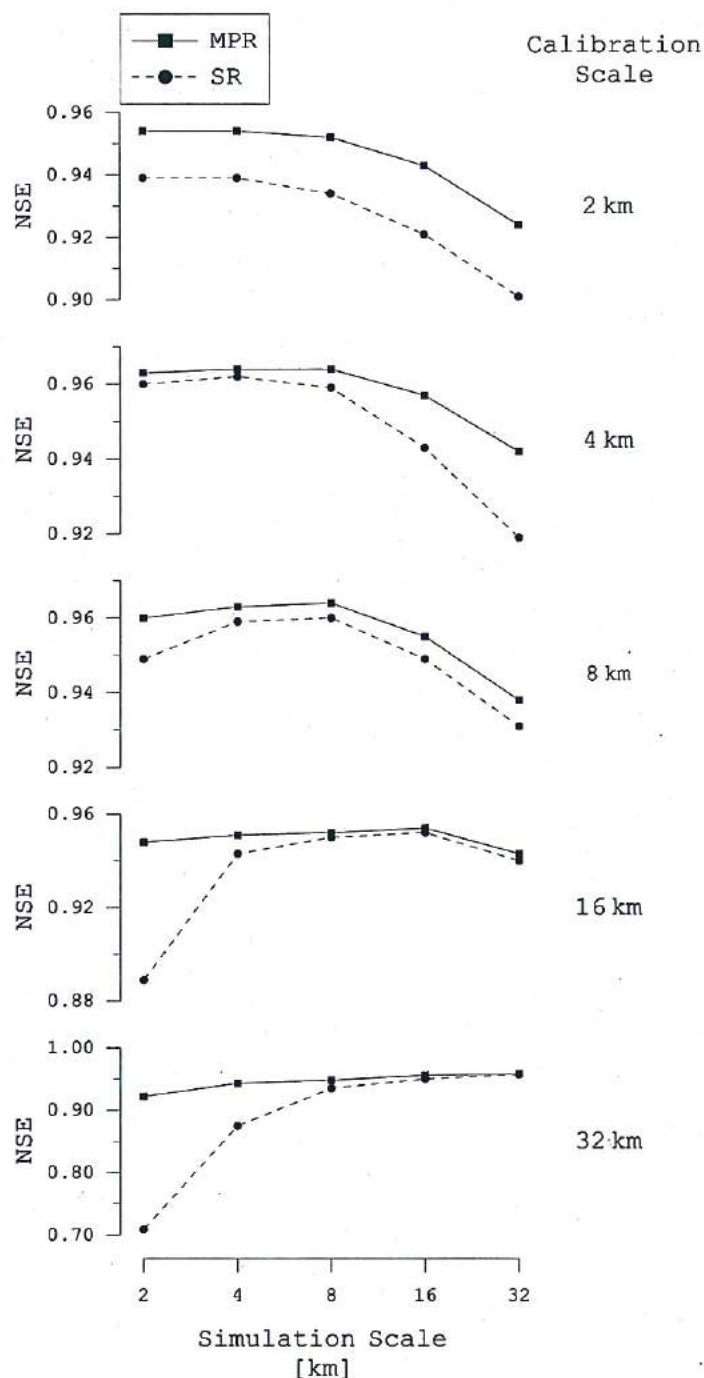


Figure 5.6: Sensitivity of the monthly water balance obtained by shifting global parameters from the calibration to the simulation scales for both regionalization schemes (MPR and SR). Baseline for the NSE are the monthly streamflow observations from the modeling period (1980-2001).

5.4.3 Effects of the Sub-grid Variability on Model Parameters

Model parameters (β^1) varied considerably depending on the regionalization method employed (Fig. 3.1), which denote the large degree of equifinality characterizing the model parameter space. A good example of this can be appreciated in Fig. 5.7, which depicts the spatial distribution of the porosity of the top ($k = 1$) soil layer β_6^1 , obtained at various modeling scales [i.e. $\ell_1 = (2, 4, 8)$ km] with both parametrization methods.

Comparison of the sub-grid distribution of β_6^0 ($\ell_0 = 100$ m) with the corresponding effective parameters β_6^1 obtained with MPR and SR respectively, showed that the MPR method preserved the spatial pattern significantly better than the SR method (Fig. 5.7). The spatial correlation coefficient r_s (Eq. (5.4)) between β_6 at level-0 and the corresponding field obtained with MPR at level-1 was, on average, 25 % greater than that obtained with SR.

The larger deviations observed in the SR technique can be mainly attributed to the upscaling mechanism (Fig. 3.1), in which input data are upscaled first to the modeling scale and then regionalization is performed. As a result, these, in turn, led to the emergence of significantly different spatial patterns at different scales. MPR, on the contrary, did not exhibit such large deviations because of the two step regionalization procedure which inherently accounts for sub-grid variability (Fig. 5.7).

5.4.4 Sensitivity of the Mass Balance to Global Parameters Calibrated at Various Modeling Scales

Two important water fluxes and one state variable were selected to carry out the continuity test: (a) actual evapotranspiration, (b) total discharge, and (c) the soil moisture of the top soil layer (depth 5 cm). Since no observations are available for any of these variables, simulated values obtained with global parameters calibrated at each control scale were used as a baseline for the estimation of NSE. Moreover, to ensure comparability, all simulations were driven by the same meteorological factors, which were estimated at the smallest modeling scale ($\ell_1 = 2$ km) and then aggregated to the required one. Deviations from the optimal value (i.e. no difference between fluxes or state variables) were quantified as indicated in Algorithm 3 with the statistic r_f (Eq. (5.3)) for every simulation and for both regionalization approaches independently.

The $P_{95} - P_5$ quantile range and the mean of NSE (r_f), between a simulated

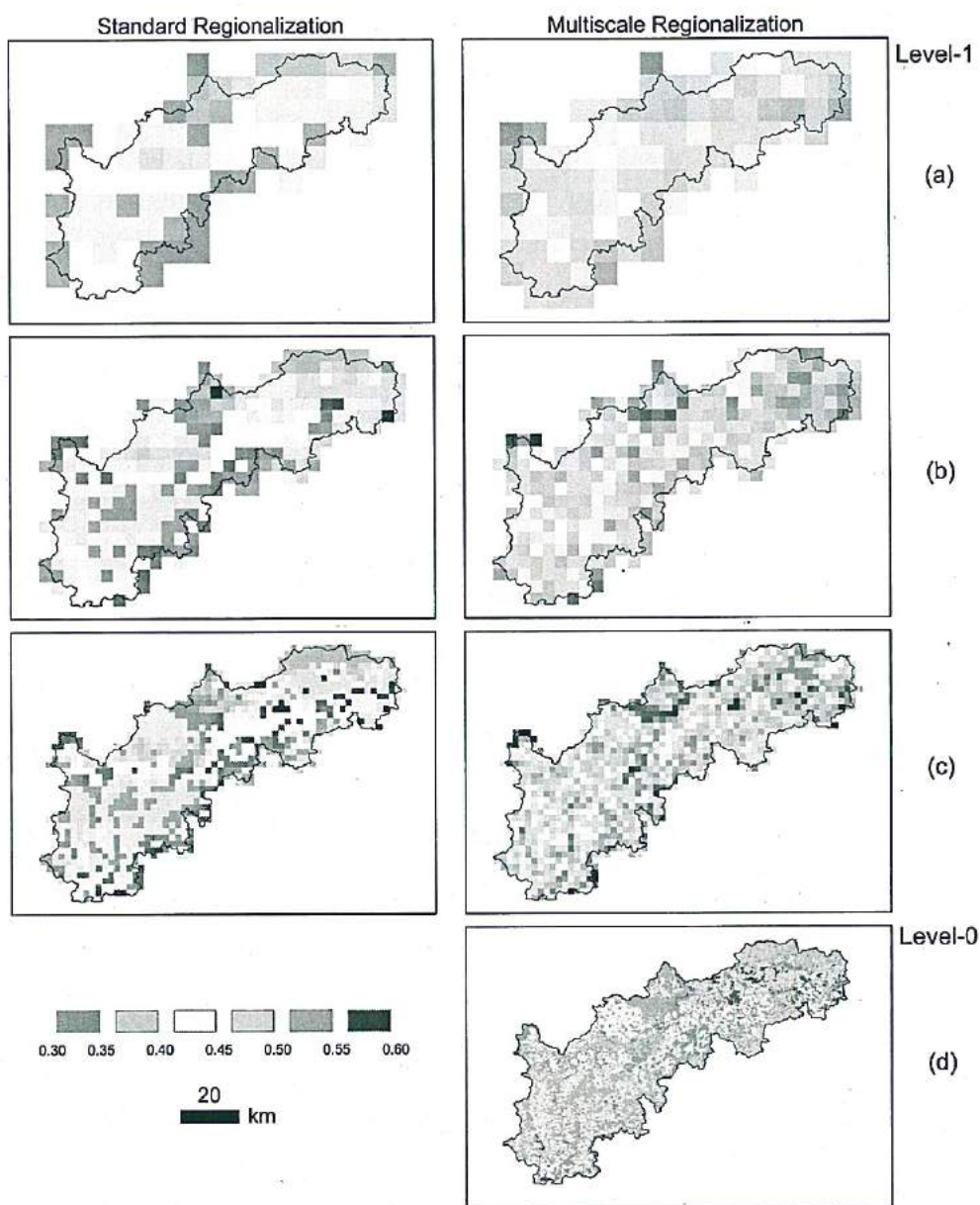


Figure 5.7: Spatial variability of the porosity (mm mm^{-1}) of the top-soil layer (i.e. $\beta_6^{(1)}$) estimated at three different modeling scales, $\ell_1 = (2, 4, 8)$ km, and for both regionalization techniques (SR and MPR) is depicted in panels (a), (b), and (c) respectively. The porosity of the top soil layer at $\ell_0 = 100$ m (i.e. $\beta_6^{(0)}$) is provided in panel (d) as a reference.

flux from a given control scale (ℓ_1) and the corresponding areal aggregated flux from a selected simulation scale (ℓ'_1) are shown in Figs. 5.8, 5.9 and 5.10, as an error bar with continuous line and solid circle, respectively. Each simulation, in this case, employed independently calibrated global parameters. For instance, if $\ell_1 = 4$ km and $\ell'_1 = 2$ km are selected as control and simulation scales, respectively, then global parameters $\gamma^{(4)}$ and $\gamma^{(2)}$ need to be determined via calibration. Based on them, r_f between fluxes $W_i(t)$ and $\langle w_{i'}(t) \rangle$ (Eq.5.3) was estimated taking the former as baseline (Fig. 5.1). In the same Figure, dashed lines and empty circles depict also the $P_{95} - P_5$ quantile range and the mean of NSE, but in this case, fluxes at the finer scale ($\langle w_{i'}(t) \rangle$) were estimated with global parameters obtained at the control scale. For the previous example, this would imply that both fluxes $W_i(t)$ and $\langle w_{i'}(t) \rangle$ have to be estimated with $\gamma^{(4)}$.

It was determined based on these three variables that the soil moisture of the top soil layer exhibited the highest sensitivity to the spatial resolution ℓ_1 , whereas the actual evapotranspiration (AET) was the less sensitive variable (Fig. 5.8). These results also corroborated a previous study of Liang et al. (2004), in which the AET obtained with VIC-3L model was found to be less sensitive as compared to soil moisture and runoff based on simulations with transferred parameters.

SR exhibited systematic deficiencies as compared with MPR (Figs. 5.8, 5.9 and 5.10). For instance, the NSE obtained with SR was, on average (r_f), not only much less than that obtained with MPR, but also exhibited a considerably larger range of variability as compared with MPR. Furthermore, MPR was less sensitive to the modeling scale than SR, specially when global parameters were calibrated at a given control scale (level-1) and then applied in other simulation scales (level-1').

It was also determined that r_f between soil moisture fields of the top soil layer obtained with the SR method was in most cases less than zero when the global parameters were calibrated at the control and simulation scales independently (Fig. 5.10). For the same simulations, however, r_f was greater than 0.85 (Fig. 5.9), which indicates that the total discharge flux $Q(t)$ was quite insensitive to both the scale and the regionalization method employed.

The spatial variability of the NSE [Eq. (5.3)] depicted in Fig. 5.11 based on a simulation performed at $\ell'_1 = 2$ km with global parameters obtained at the control scale $\ell_1 = 4$ km clearly shows the degree of influence that a regionalization

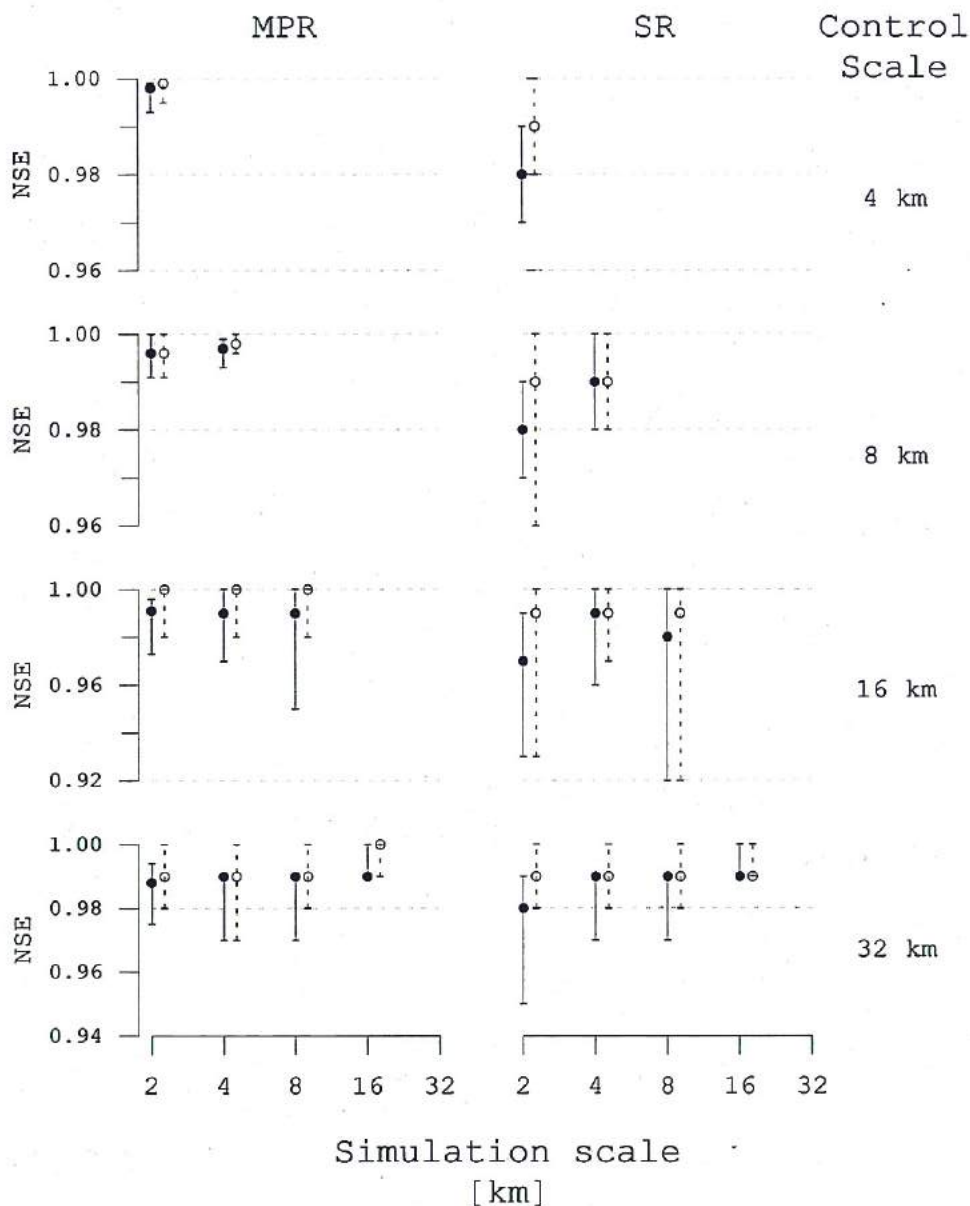


Figure 5.8: Evaluation of the conservation of mass for actual evapotranspiration at various control scales based on MPR and SR parameterizations. Filled circles and continuous lines denote the mean and $P_{95} - P_5$ quantile range of the NSE (Eq. (5.3)) between the fluxes obtained at a given simulation scale compared with those obtained at the respective control scale (assumed as baseline for NSE). Empty circles and dotted lines indicate the same statistics but using global parameters obtained at the given control scale (i.e. no shift).

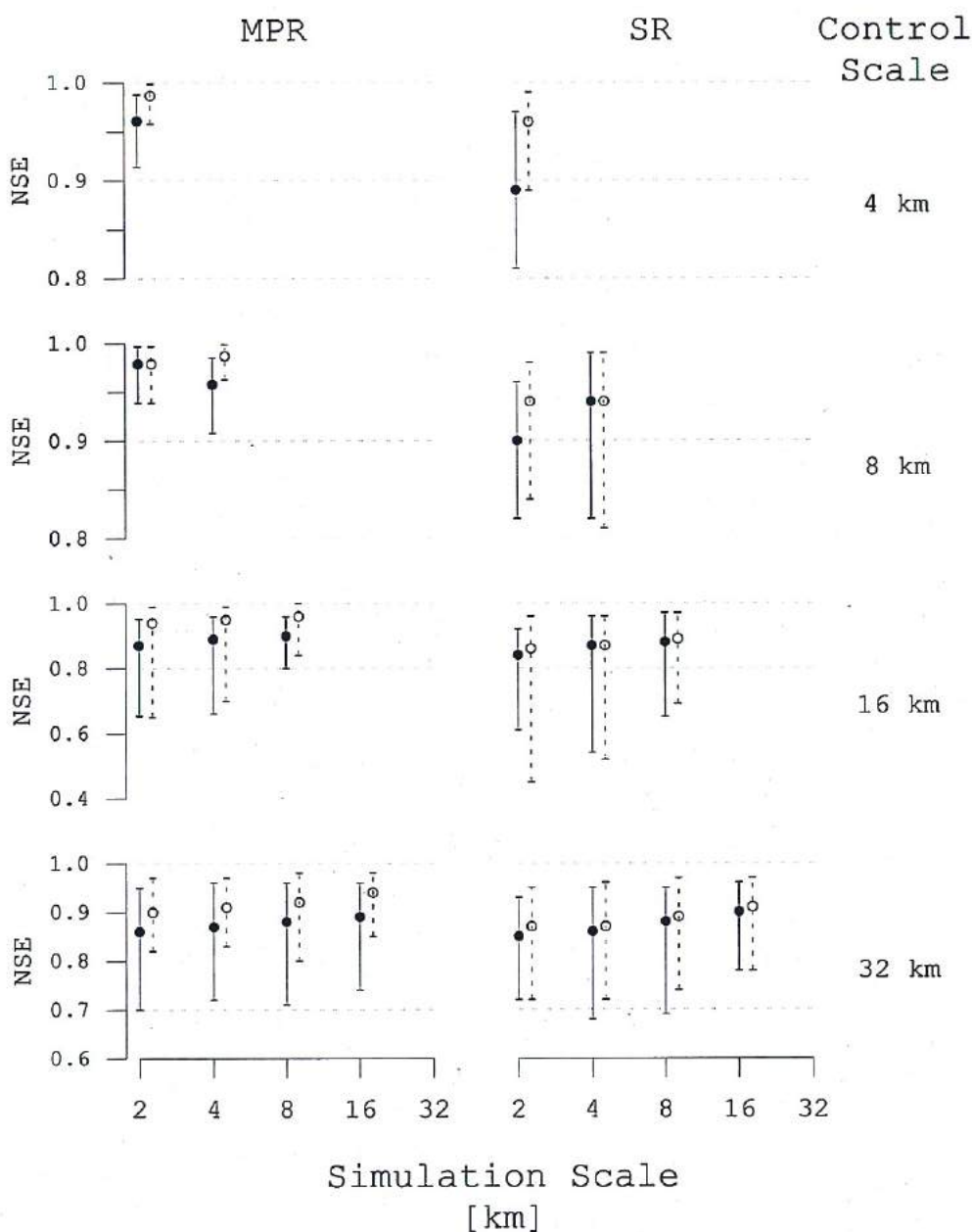


Figure 5.9: Evaluation of the conservation of mass for total discharge at various control scales based on MPR and SR parameterizations. Filled circles and continuous lines denote the mean and $P_{95} - P_5$ quantile range of the NSE (Eq. (5.3)) between the fluxes obtained at a given simulation scale compared with those obtained at the respective control scale (assumed as baseline for NSE). Empty circles and dotted lines indicate the same statistics but using global parameters obtained at the given control scale (i.e. no shift).

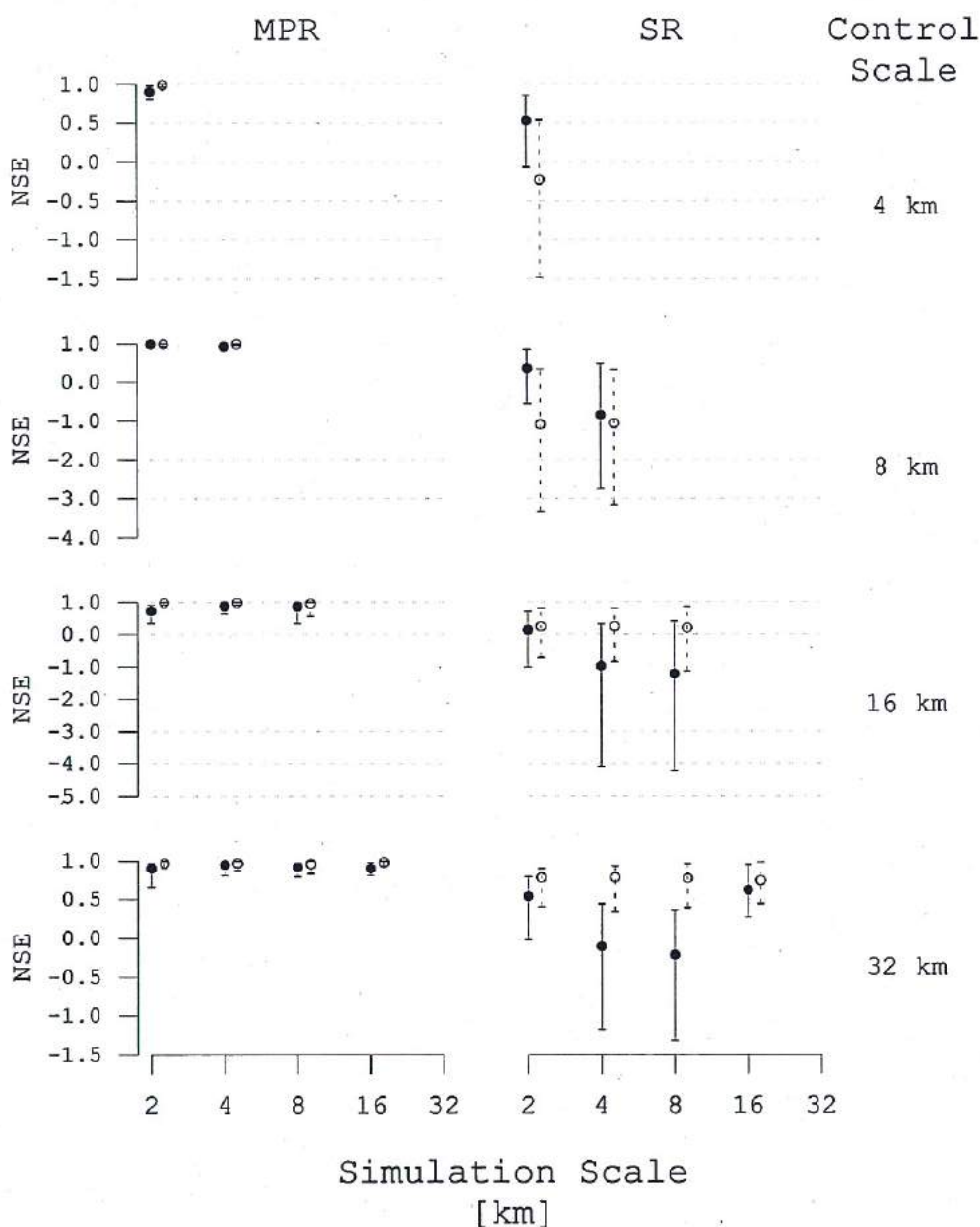


Figure 5.10: Evaluation of the conservation of mass top thin root zone soil moisture at various control scales based on MPR and SR parameterizations. Filled circles and continuous lines denote the mean and $P_{95} - P_5$ quantile range of the NSE (Eq. (5.3)) between the fluxes obtained at a given simulation scale compared with those obtained at the respective control scale (assumed as baseline for NSE). Empty circles and dotted lines indicate the same statistics but using global parameters obtained at the given control scale (i.e. no shift).

technique may have on the dynamics and the mass balance of relevant water fluxes and state variables. This simulation indicated that global parameters obtained with SR are scale specific, thus not transferable, since almost 53 % of the grid cells did not conserve the mass balance (say $NSE < 0.95$) as compared with the 2.5 % of the grid cells with MPR. The locations at which the NSE is less than this threshold are mostly karstic formations.

5.4.5 Preservation of Spatial Patterns

Daily time series of LST during the year 2000 were used as a proxy for the spatio-temporal variability of the top-layer soil moisture fields at the scale of $\ell_1 = 2$ km. A strong negative correlation between the volumetric water content of this layer and the LST (MODIS) is expected (Chauhan et al., 2003; Wang et al., 2007). As an example, a short sequence of LST and top layer soil moisture fields obtained with both regionalization methods is depicted in Fig. 5.12 to visualize the dynamics of these variables.

Based on these results, it was noticed that the soil moisture patterns calculated with MPR and the LST were closely related to each other. The dynamics of the moisture pattern obtained with SR, on the contrary, did not exhibit a strong dependence. As a result, the Spearman's rank correlation coefficient between the LST and the soil moisture of the top-layer obtained with the MPR and the SR technique varied between $[-0.82, -0.57]$ and $[-0.69, -0.07]$, respectively. The maximum difference observed between the Spearman's ρ estimated with MPR and SR was as high as 41 %.

5.4.6 Transferability of Global Parameters to Ungauged Locations

For this case study, nine gauging stations within the Upper Neckar basin were selected as cross-validation locations to test the efficiency of mHM to reproduce streamflow at interior locations. Fig. 5.13 shows the location of these stations within the study area and drainage area corresponding to these locations is provided in Table 5.4.

For these simulations, the modeling scale was set to $\ell_1 = 4$ km because this discretization covers all internal stations. Sets of global parameters for MPR and SR were obtained at this discretization as well as three coarser scales, namely: $\ell_1 = (8, 16, 32)$ km.

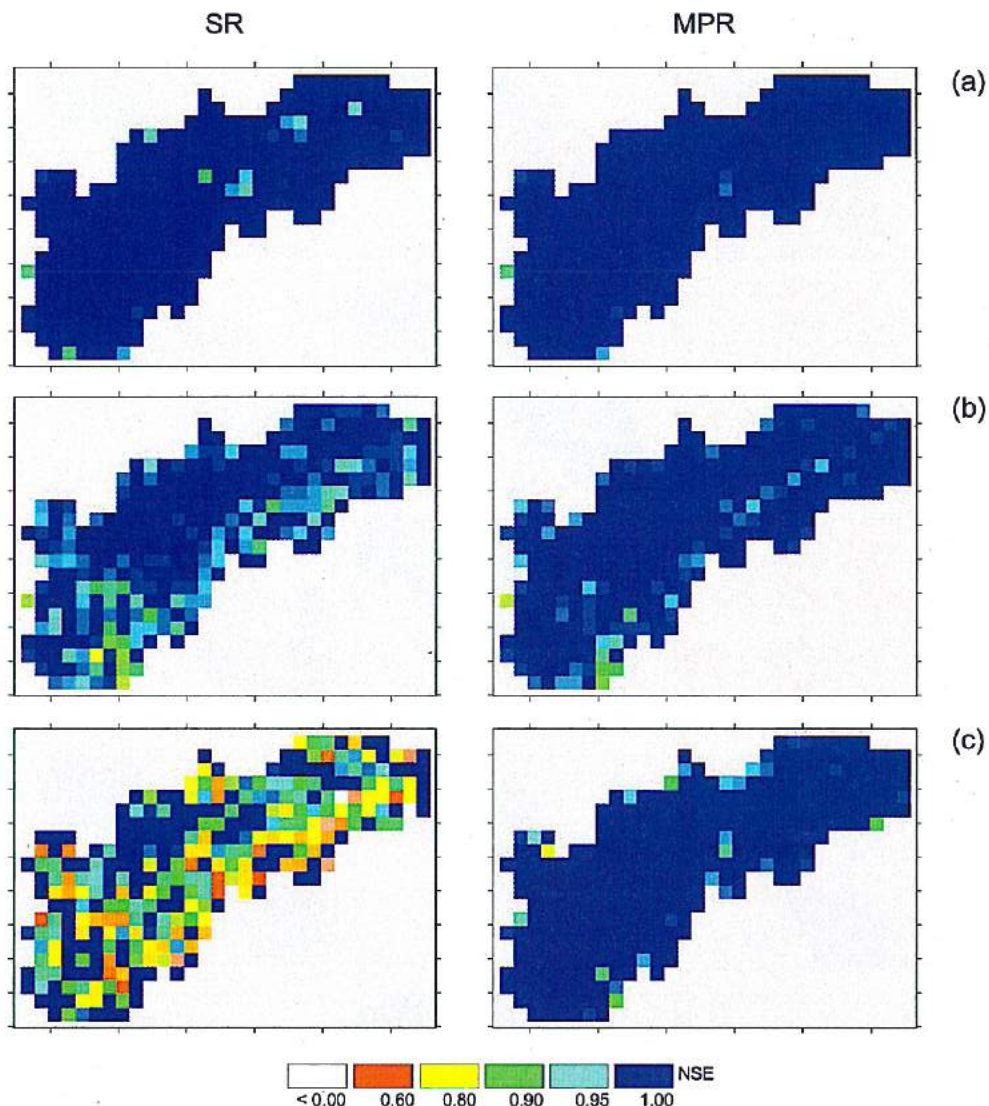


Figure 5.11: Discrepancy between fluxes simulated at two different modeling scales (the control scale $\ell_1 = 4$ km and the finer scale $\ell'_1 = 2$ km) during the modeling period (1980-2001). The NSE was used as a measure of correspondence between fluxes simulated at the control scale – assumed as baseline – and the areal aggregation of fluxes obtained from the finer scale, as depicted in Fig. 5.1. Global parameters were estimated at the control scale. The spatial distribution of the NSE for daily evapotranspiration, total discharge, and soil moisture of the top soil layer is depicted in panels (a), (b), and (c), respectively.

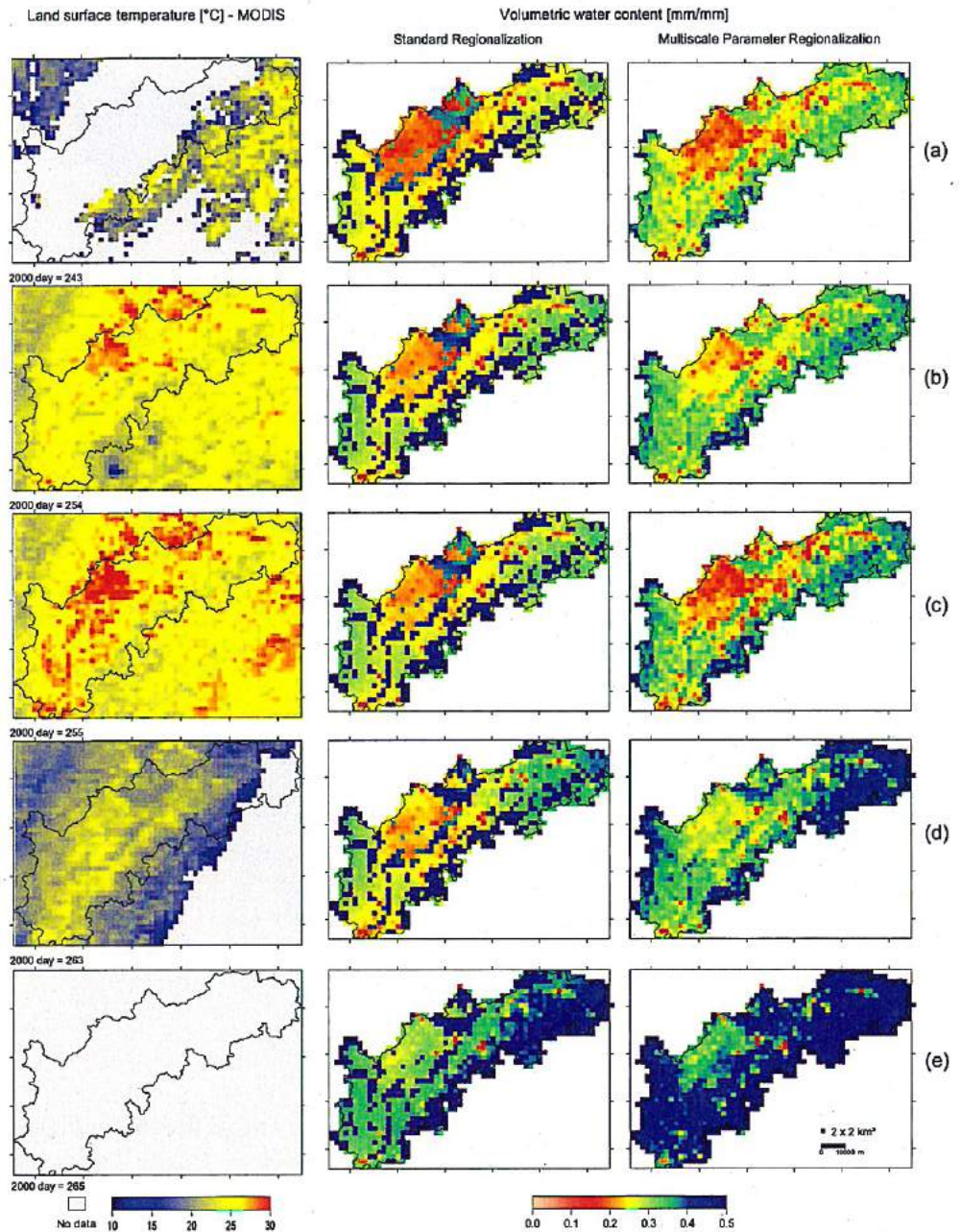


Figure 5.12: Land Surface Temperature ($^{\circ}\text{C}$) from MODIS and simulated volumetric water content (mm mm^{-1}) in the top-soil layer estimated with SR and MPR. Both variables are depicted for various days during year 2000 at the modeling scale $\ell_1 = 2 \text{ km}$.

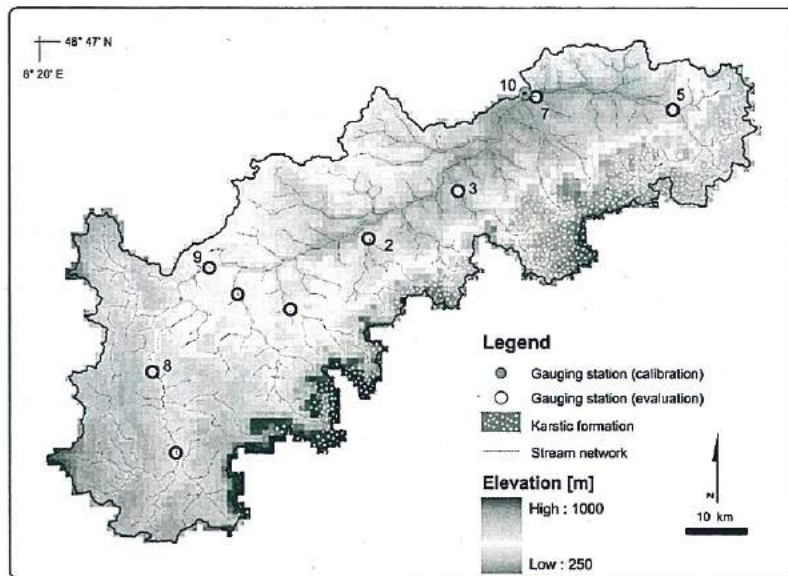


Figure 5.13: Location of interior locations within the Upper Neckar river basin. The basin's outlet corresponds to gauge Nr. 10. at Plochingen

The NSE obtained for daily streamflow simulations during the evaluation period using MPR was, on average, 6 % greater than those obtained with SR (Table 5.4). This result corresponds to simulations obtained with global parameters estimated at the modeling scale of $\ell_1 = 4$ km. The median reduction of NSE for internal gauging stations with respect to the performance obtained at the outlet (gauge Nr. 10) was 15 % and 20 % for MPR and SR, respectively. Simulations obtained with global parameters calibrated at $\ell_1 = 4$ km were used as reference. This was expected as both methods don't account for the discharge data of these internal stations in calibration process.

In the case that global parameters were estimated at the other modeling scales, then the NSE for SR was, on average, 18 % lower than that obtained with MPR (Fig. 5.14). Here, the median reduction was 16 % and 28 % for MPR and SR, respectively. This implies that MPR is more robust than SR for streamflow predictions at internal locations. Both methods, however, showed relatively poor performance for internal stations located within karstic formations (e.g. gauge Nr. 1 and 3, Fig. 5.13). For those locations, the NSE obtained with MPR was, on average, 62 % greater than that obtained with SR.

Table 5.4: Performance of MPR and SR for the daily streamflow predictions at the interior locations during the evaluation period (1989-2001). Global parameters were calibrated only with discharge information from the outlet gauging station (Nr. 10). Model runs were performed at modeling scale $\ell_1=4$ km.

Gauge Nr.	Area km ²	MPR				SR			
		Bias mm	RMSE mm	NSE -	r -	Bias mm	RMSE mm	NSE -	r -
1	134	0.36	0.64	0.44	0.81	0.41	0.73	0.41	0.79
2	152	0.09	0.56	0.72	0.83	0.09	0.63	0.71	0.84
3	168	0.09	0.93	0.34	0.78	0.07	0.98	0.21	0.76
4	346	0.16	0.71	0.67	0.79	0.15	0.73	0.67	0.81
5	350	0.33	0.70	0.77	0.91	0.38	0.77	0.71	0.89
6	467	0.09	0.58	0.78	0.87	0.17	0.63	0.75	0.87
7	698	0.16	0.58	0.83	0.91	0.19	0.63	0.79	0.90
8	716	0.11	0.50	0.76	0.88	0.16	0.58	0.73	0.89
9	1132	0.05	0.46	0.88	0.94	0.08	0.51	0.86	0.92
10	3969	-0.01	0.29	0.90	0.95	-0.01	0.36	0.88	0.94

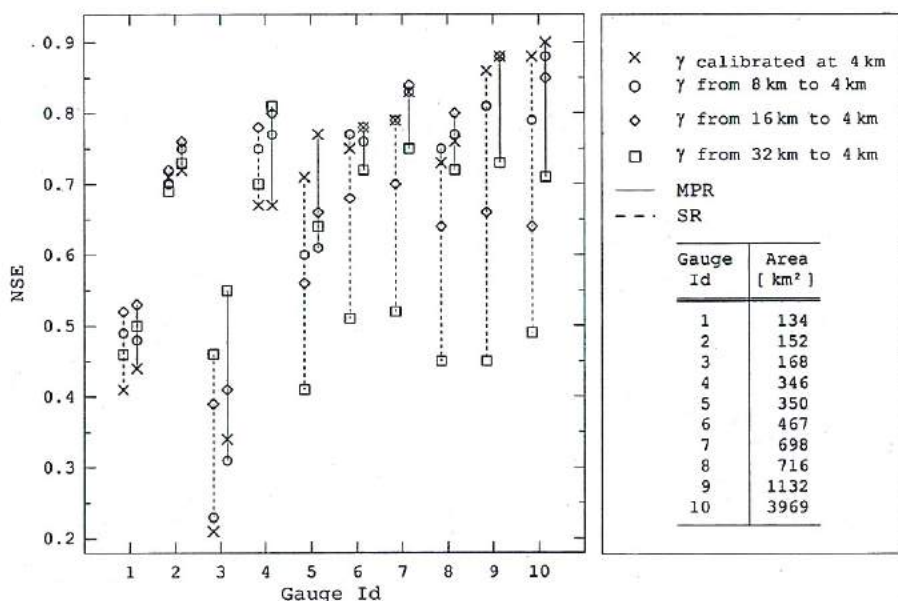


Figure 5.14: Performance of MPR and SR for daily discharge simulations at internal locations of the study area during the evaluation period. Simulations were carried out at $\ell_1 = 4$ km using global parameters γ obtained from different scales: $\ell_1 = (4, 8, 16, 32)$ km.

Chapter 6

Predictions of Streamflow Characteristics: High and Low flows ¹

"Water is a good friend but also a bad enemy"

Anonymous

6.1 Introduction

The accurate and the reliable prediction of streamflow as well as their related extreme characteristics, such as magnitude and frequency of high- and low-flows, in a mesoscale river basin has always been a major objectives of the hydrological studies mainly because of their implication in various water resources planing and management purposes including the design and operation of hydraulic structures, municipal or industrial water supply systems. This need for opportune and reliable estimates of hydrological extremes has further intensified during the last decades with compelling evidence [see e.g. Parry et al. (2007)] that climate change, induced either due to natural causes or anthropogenic activities such as afforestation, deforestation, may significantly modify the likelihood of the occurrences of the high- and low-flows events. Evidently, both hydrological extreme events entail substantial socioeconomic and

¹This chapter is a modified version of the manuscript: Kumar, R., Samaniego, L. and S. Attinger (2010). The effects of spatial discretization and model parameterization on the prediction of extreme runoff characteristics. J. Hydrol. 392 (1-2), pp. 54-69

environmental consequences and, in the worst case, bears an enormous risk for life.

Water balance models are increasingly used for these prediction purposes. The performance of these models, however, depends on various factors. The aim of this case study was to explore some of these factors, in particular, the effects of objective function formulated for the calibration purpose, spatial discretization (e.g. lumped, distributed) used to model different hydrological processes, and the parameterization techniques. These effects were studied here to assess the model performance for the predictions of daily streamflow and their related high and low flow characteristics. For these purposes mHM was applied in the study area at two spatial resolutions: lumped and distributed. The distributed version of mHM was in-turn parameterized based on hydrological response unit (HRU) and multiscale parameter regionalization (MPR). The calibration of free parameters in each case (i.e. for lumped and distributed and within distributed for the HRU and the MPR parameterization methods) were carried out with a dynamically dimensioned search (DDS) algorithm (Tolson and Shoemaker, 2007) instead of the simulated annealing (SA) algorithm. It is worthwhile pointing out here that the DDS algorithm was available at the latter stage of the present research work and therefore no attempts were made to compare its efficiency with those of the SA algorithm. It had been left for the future study. The sensitivity of model performances to the calibration objective functions was assessed by formulating three objective functions: an error statistic focusing only on high flows, only on low flows, and a combination of above. Subsequently, different high and low flow characteristics, such as frequency of high flows, total drought duration, amongst others, were derived from the daily discharge data on a seasonal time scale (winter and summer). Model performances were accordingly assessed for the prediction of these characteristics.

6.2 Implementation of mHM in Upper Neckar River Basin

The mHM model being a process based conceptual hydrologic model offers a flexibility to run not only at different grid resolutions but also in a spatially lumped mode. To utilize this property and to study the effect of spatial dis-

cretization on model performance, mHM was set up in a spatially lumped and distributed version. The lumped version of the model represents a catchment as a single and homogeneous unit and thus ignoring the spatial variability of both the meteorological forcings and the basin physical characteristics. The lumped model simulates daily streamflow at the basin outlet using the basin averaged meteorological variables as input data. It may be noted that the cell to cell routing process of the distributed model version was not included in the lumped model. Instead the runoff routing process in the streams was modeled as a triangular unit hydrograph. The formulation of this process is similar to a parameter MAXBAS of the HBV model (Lindström et al., 1997).

For the distributed mHM version, the spatial resolutions of level-2 and level-1 were both kept at $4 \text{ km} \times 4 \text{ km}$. Whereas, level-0 resolution was set at $100 \text{ m} \times 100 \text{ m}$. The MPR parameterization method was implemented in the same way as described in previous chapters. The implementation of the HRU method within the distributed mHM model is described below.

6.2.1 HRU Parameterization

A HRU is a distributed, heterogeneously structured identity having a common pedo-topo-geological basin characteristic controlling its hydrological dynamics (Flügel, 1995). While HRU is one of the most common methods for parameterizing the spatially distributed models (Leavesley et al., 1983; Flügel, 1995; Blöschl et al., 2008; Das et al., 2008), there are no hard and fast rules as to the delineation of HRUs. A *k-means* clustering algorithm (Lloyd, 1982) was used to group all modeling cells at level-1 into fifteen HRUs. Catchment characteristics used for the delineation of HRU were: elevation, slope, aspect, soil textural data, land cover classes (fraction of forest, impervious and impermeable cover), and geological information (fraction of karstic and non-karstic area). Mean values of these characteristics for each grid at level-1 were estimated from their corresponding input data at level-0. Each HRU was assigned to one of the three land cover classes (i.e. forest, impervious and permeable cover) based on the dominant land cover class. Table 6.1 shows the catchment characteristics of the HRUs delineated for the study area, and Fig. 6.1 shows the locations of delineated HRUs within the study area. It can be noticed from this figure that the geographic locations of modeling cells are not explicit because of the categorical classification scheme used in the delineation of HRU.

Table 6.1: Physiographical characteristics used for the delineation of HRUs in the study area.

HRU Id	x_1^a (m)	x_2^b (°)	x_3^c (°)	x_4^d (-)	x_5^e (-)	x_6^f (-)	x_7^g (mm)	x_8^h (-)
1	439.9	5.6	160.2	0.18	0.09	0.73	155.2	0.00
2	412.7	11.1	159.2	0.65	0.04	0.31	132.0	0.58
3	695.9	11.4	158.9	0.29	0.03	0.67	100.1	0.80
4	784.9	6.4	115.6	0.70	0.02	0.28	71.4	0.02
5	846.0	8.4	255.1	0.81	0.03	0.16	112.9	0.00
6	516.8	9.6	166.4	0.71	0.04	0.25	100.3	0.00
7	419.3	6.4	184.2	0.17	0.13	0.70	109.1	0.00
8	870.5	3.1	199.5	0.00	0.05	0.95	64.5	0.94
9	735.7	6.0	221.9	0.20	0.01	0.79	119.1	0.87
10	626.5	16.9	193.4	0.42	0.06	0.52	81.3	0.06
11	468.9	6.6	183.3	0.19	0.37	0.48	57.4	0.00
12	667.5	6.0	143.8	0.29	0.03	0.67	102.1	0.01
13	727.4	19.8	184.4	0.52	0.04	0.44	76.4	0.65
14	787.8	9.7	204.3	0.54	0.02	0.44	93.6	0.95
15	507.1	9.7	190.2	0.40	0.06	0.54	109.2	0.00

^a Elevation

^b Mean slope

^c Aspect

^d Fraction of the forest cover

^e Fraction of the impervious cover

^f Fraction of the permeable cover

^g Maximum water holding capacity of the soil profile

^h Fraction of karstic aquifers

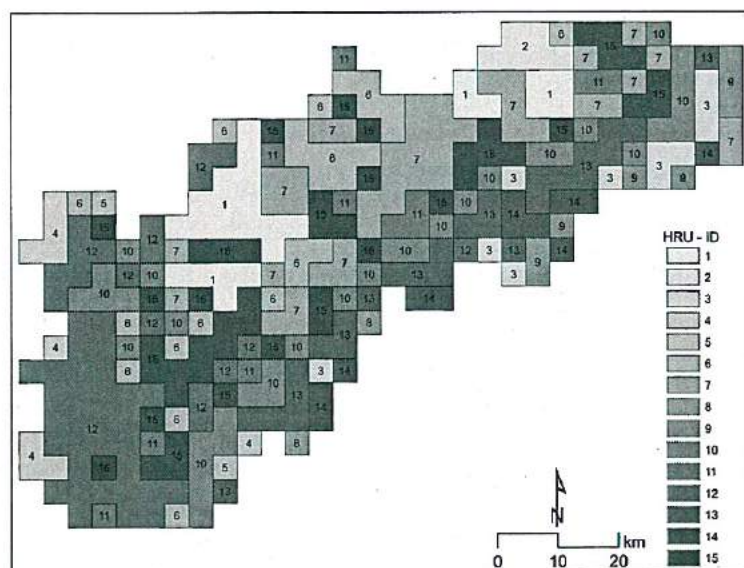


Figure 6.1: Location of modeling cells at level-1 ($\ell_1 = 4$ km) within a particular HRU for the study area.

Three parameter allocation methods were used in the HRU parameterization method to obtain the parameter fields of the distributed mHM model. First allocation method consisted of assignment of those model parameters (e.g. threshold temperature for conversion of precipitation into snow or liquid rain) which were assumed to be spatially invariant. These set of parameters were equally assigned to all modeling cells at level-1, irrespective of the HRUs location. The second allocation was related to those parameters which were assumed to be dependent on a particular catchment characteristic (e.g. snow accumulation and melting parameters depends only on the land cover class). These parameters were first weighted according to their respective catchment characteristics (e.g. land cover fraction) of particular HRU and then assigned equally to all modeling cells belonging to that HRU. And, finally the third allocation method was related to those parameters which were assumed to be dependent on more than one catchment characteristics (e.g. soil related and runoff response parameters). These groups of parameters were first allotted independently to each HRU through calibration, and then assigned to all those modeling cells having similar HRU irrespective of their geographic location. The detail description of these allocations for all 28 mHM model parameters with their appropriate maximum and minimum ranges, used during the calibration process, is shown in Table 6.2. These allocation schemes were mainly to reduce the model over-parameterization problem, and also to being consistent with the MPR parameterization method as far as possible to make a fair comparison between them. Moreover, the HRU allocation method used in this study is consistent with the previous study of Das et al. (2008) conducted in the same region.

6.3 Parameter Identification

Good sets of free parameters for both the lumped version and the distributed version of mHM, and for the HRU and the MPR parameterization methods were identified using a DDS algorithm Tolson and Shoemaker (2007). DDS is a robust and parsimonious downhill global optimization algorithm that mimics the manual calibration by dynamically and probabilistically reducing the number of parameters during the search procedure. The search algorithm requires only one parameter i.e. the maximum number of model evaluations. During

Table 6.2: Range of mHM model parameters for the HRU parameterization method during the calibration process. Three allocation schemes to obtain spatial fields of model parameters are abbreviated as: E \equiv assigned to all cells irrespective of the HRU class, W \equiv weighted according to fraction of landcover class or aspect, and S \equiv HRU specific parameters assigned to each modeling cells independently. Landcover is grouped in three different classes: Forest (F), Impermeable (I) and Permeable (P) cover.

Param. Id	Min.	Max.	Alloc. Method	Param. Id	Min.	Max.	Alloc. Method
β_1	0.1	0.5	W	β_{15}	0.05	0.3	S
β_2	-1.0	1.0	E	β_{16}	0.8	1.0	S
β_3	1.0	4.0	W	β_{17}^F	0.1	0.3	W
				β_{17}^I	0.8	1.0	W
β_4	0.1	0.8	E	β_{17}^P	0.6	0.8	W
β_5	4.0	8.0	W	β_{18}	1.0	40.0	S
β_6^I	10.0	100.0	S	β_{19}	1.0	10.0	S
β_6^P	100.0	500.0	S				
β_7	1.0	5.0	S	β_{20}	5.0	100.0	S
β_8	30.0	70.0	S	β_{21}	0.0	1.0	S
β_9	1.0	5.0	S	β_{22}	1.0	100.0	S
β_{10}	270.0	274.0	S	β_{23}	10.0	10000.0	S
β_{11}	270.0	273.0	S	β_{24}	0.5	1.5	S
β_{12}	0.2	0.5	S	β_{25}	1.0	3.0	S
β_{13}	0.1	1.0	S	β_{26}	0.1	10.0	E
β_{14}	0.1	1.0	W	β_{27}	0.0	0.5	E
				β_{28}	0.9	1.2	W

the course of search, a new set of model parameters is generated by perturbing some of randomly selected parameters from their best values identified so far. In a case of a minimization problem this newly generated set is selected only if an objective function (or an aggregated error statistic) associated with this set is less than that of the so far found best solution. Recently the study conducted by Tolson and Shoemaker (2007) had shown the effectiveness of the DDS algorithm over other existing optimization algorithms for searching a good parameter set of a computationally expensive hydrological model in relatively less model runs. Readers interested in more details about the DDS algorithm may please refer to Tolson and Shoemaker (2007).

6.3.1 Formulation of Calibration Objective Function

The DDS algorithm was implemented in this study as a single objective optimization algorithm. It requires the formulation of an objective function (or error statistic or cost function) that is either maximized or minimized depending on the problem. The formulation of a proper objective function is quite

crucial for the successful calibration process. The usage of different objective function may finally lead to a different set of model parameters and thus a different model simulation (Oudin et al., 2006). For instance, a parameter sets obtained with an objective function that have emphasis on the high flow simulations may produce a bias result for the low flow simulations, and vice versa (Boyle et al., 2000; Oudin et al., 2006).

Three different variations of an objective function were tested to better understand the sensitivity of a model performance to the different formulation of objective functions. These variants were derived from the daily time series of observed and simulated discharge, emphasizing separately either the high flows or the low flows or a combination of above two. Additionally, the seasonal extreme runoff characteristics (described in detail in the next sections) were used as a penalty term to improve the model predictions for the runoff characteristics at the seasonal scale. The overall objective function Φ to be minimized can be given as:

$$\Phi = \left(\prod_{c=1}^C (2 - \Theta_c) \right) (1 - E) \quad (6.1)$$

where, C denotes the total number of penalty terms and Θ_c is the pearson correlation coefficient between the observed and the simulated seasonal runoff characteristic c . The seasonal specific volume of high flows and the seasonal cumulative specific deficit were used as penalty terms for the high flow and low flow calibrations, respectively. Both penalty terms were used in the combined calibration case. E is the Nash Sutcliffe efficiency (NSE) which for different objective functions can be formulated as:

$$E = \begin{cases} E_Q & = 1 - \frac{\sum_t (Q_t - \widehat{Q}_t)^2}{\sum_t (Q_t - \overline{Q})^2} & \text{for high flow} \\ E_{\log Q} & = 1 - \frac{\sum_t (\log Q_t - \widehat{\log Q}_t)^2}{\sum_t (\log Q_t - \overline{\log Q})^2} & \text{for low flow} \\ E_{Q \log Q} & = 0.5(E_Q + E_{\log Q}) & \text{for combined high and low flow} \end{cases} \quad (6.2)$$

where, E_Q is NSE between the daily observed (Q) and simulated (\widehat{Q}) discharge time series. This error statistic puts more emphasis matching the high flow simulation (Oudin et al., 2006). $E_{\log Q}$, on the contrary, is the NSE value between the logarithmic transformed time series of observed and simulated discharge

time series. This error statistic puts relatively higher emphasis on matching of recessions and low flow spells (Oudin et al., 2006). The third calibration case consists of an objective function $E_{Q\log Q}$ that equally weight the previous two error statistics (i.e. E_Q and $E_{\log Q}$) to obtain a balanced simulation (Oudin et al., 2006). \overline{Q} and $\overline{\log Q}$ are the mean values of the daily observed and its logarithmic transformed discharge time series over the calibration period, respectively.

6.3.2 Parametric Uncertainty Analysis

The “*equifinality*” of parameters sets has been long recognized as one of the common problems in hydrological modeling (Beven and Binley, 1992). This, in turn, induces some degree of uncertainty in model outputs. Equally good model simulations can be obtained from different sets of model parameter. A DDS-approximation of uncertainty (DDS-AU) method (Tolson and Shoemaker, 2008) was used in this case study to quantify the variability of model outputs due to different equally good parameter sets. In this method, several independent trials of the DDS algorithm are performed for searching several equally good sets of model parameter. A total 200 DDS trials were performed for both lumped and distributed models with their respective parameterization schemes, independently for all three objective functions. The best parameter set obtained at the end of each trail were termed as a behavioral or acceptable parameter set. Each trial was initialized with a different random initial solution and a different random seed so that the each DDS trail can follow a different search path. The maximum number of model evaluations per DDS optimization trail was set in advance. This number for the distributed model with the HRU parameterization method was set to 500 due to the large number of free parameters, and for the MPR method and for the lumped model were set to 300 and 200, respectively. Note that the maximum model runs per DDS optimization trial conducted in this study are two to five times higher than those of the previous study by (Tolson and Shoemaker, 2008) for quantifying uncertainty in model outputs using the DDS-AU algorithm.

Based on the 200 different good parameter set, the deterministic model prediction was estimated as the median of the ensemble. The variability of model outputs were given by the 5% and 95% percentile ranges or ($P_5 - P_{95}$) variability bounds. It may be noted that the so-derived variability bounds are note

confidence bounds in a statistical sense that is they are not expected to include in all cases a given percentage of observations.

6.4 Seasonal High and Low Flow Characteristics

River flows in many river basins around the world and particularly in the study area exhibits a seasonal behavior mainly because these hydrological responses are governed by the climatic conditions such as precipitation and temperature, which shows a strong seasonality. High and low flows in a river can occur in both summer and winter season but extreme runoff characteristics, such as magnitude or frequency of high and low flows, may have different behavior in different seasons. Consequently, to gain more understanding on the seasonal behavior of model simulations several high and low flow characteristics were estimated separately for the winter and summer seasons².

Three seasonal high flow characteristics namely, specific volume (Q_1), total duration (Q_2), and frequency (Q_3) of high flows were estimated from the daily discharge time series using a peak over threshold (POT) method (Stedinger et al., 1993; Robson and Reed, 1999). The POT method uses all peak discharges that exceed some threshold value such as maximum within-bank discharge. This threshold value in this study was set to the 95th percentile ($F_{0.95}$) of the observed daily discharge ($Q(t)$). The threshold limit $F_{0.95}$ was kept fixed for deriving all seasonal high flow characteristics during both winter and summer. Fig. 6.2 shows the schematic representation of high flows characteristics used in this study. Table 6.3 presents the mathematical formulation of these characteristics, based on the previous study of Samaniego (2003).

Similarly, three seasonal low flow characteristic namely, cumulative specific deficit (Q_4), total drought duration (Q_5) and maximum drought intensity (Q_6) were estimated from the daily discharge time series using a truncation level method (Smakhtin, 2001; Tallaksen et al., 1997). This method defines all flows as low flows that are below a certain threshold limit. The threshold level in this study was set to the 10th percentile ($F_{0.10}$) of the daily observed discharge ($Q(t)$) values. $F_{0.10}$ kept same for deriving all low flow characteristics during both seasons. Fig. 6.3 shows the schematic representation of low flows

²In study area, hydrological water year is divided into summer and winter water seasons. Summer from hydrological point of view, starts on the 1st of May and ends on the 31st of October, whereas winter spans from the 1st of November to the 30th of April.

characteristics, and Table 6.3 presents their mathematical formulations. Readers may refer to Samaniego (2003) for more in-sight into the estimation details on extreme runoff characteristics.

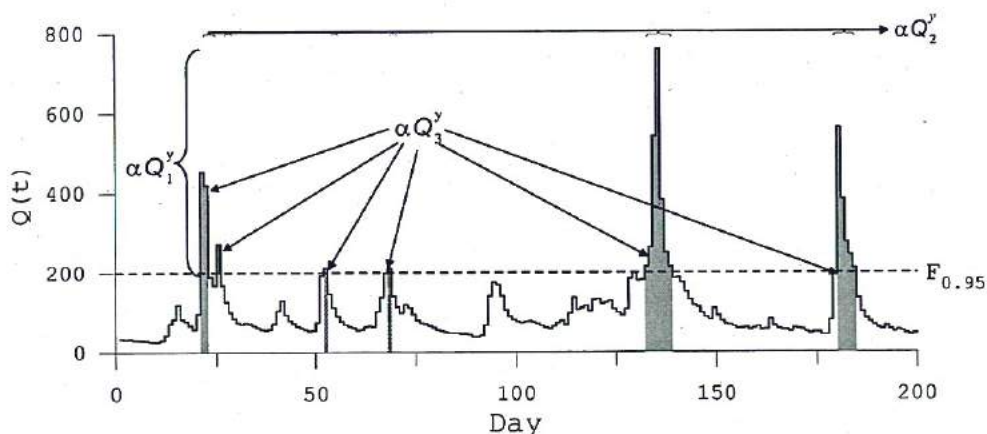


Figure 6.2: Schematic representation of high flow characteristics: specific volume (Q_1^y), total duration (Q_2^y), and frequency (Q_3^y) of high flows during the water year y .

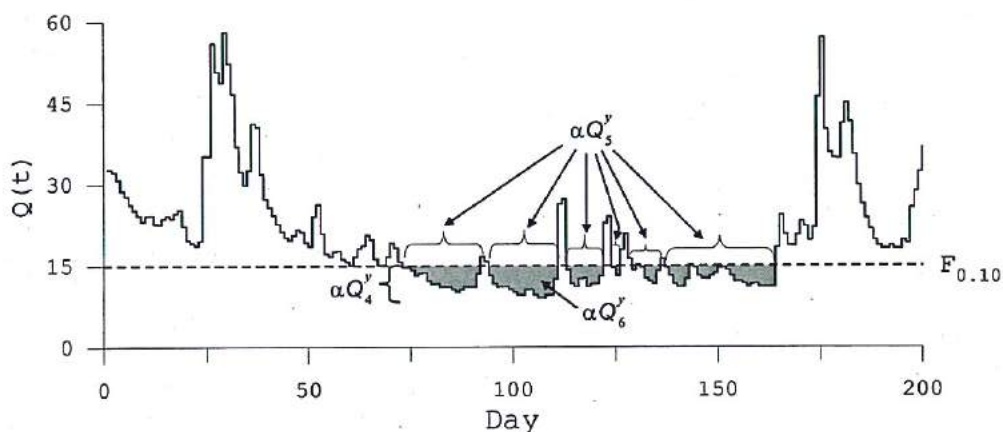


Figure 6.3: Schematic representation of low flow characteristics: specific cumulative deficit (Q_4^y), total drought duration (Q_5^y), and maximum drought intensity (Q_6^y) during the water year y .

Table 6.3: Mathematical formulation of seasonal high and low flow characteristics.

Runoff characteristics	Mathematical expression
High flows	
1. Specific volume of high flows (mm)	$Q_1^y = \frac{86.4}{A} \sum_{d=d_s^y}^{d_e^y} \mu_{0.95}^d Q(d)$, where $\mu_{0.95}^d = \begin{cases} 1 & \text{if } Q(d) \geq F_{0.95} \\ 0 & \text{otherwise} \end{cases}$
2. Total duration of high flows (d)	$Q_2^y = \sum_{d=d_s^y}^{d_e^y} \mu_{0.95}^d$
3. Frequency of high flows (y^{-1})	$Q_3^y = \mathcal{H}_i^y \forall i \in \{d_s^y \leq d \leq d_e^y\}$, where $\mathcal{H}_i^y = \{Q(d) \mid \forall Q(d) \geq F_{0.95} \wedge d_0^y \leq d \in [d_0^y(i), \dots, d_1^y(i)]\}$
Low flows	
4. Cumulative specific deficit (mm)	$Q_4^y = \frac{86.4}{A} \sum_{d=d_s^y}^{d_e^y} \mu_{0.10}^d (F_{0.10} - Q(d))$, where $\mu_{0.10}^d = \begin{cases} 1 & \text{if } Q(d) \leq F_{0.10} \\ 0 & \text{otherwise} \end{cases}$
5. Total drought duration (d)	$Q_5^y = \sum_{d=d_s^y}^{d_e^y} \mu_{0.10}^d$
6. Maximum drought intensity (mm y^{-1})	$Q_6^y = \sup(\mathcal{E}_k^y) \forall k = 1, \dots, K_y$, where $\mathcal{E}_k^y = \frac{(Q_5^y)_k}{(Q_5^y)_k}$

1. $Q(d)$ is daily mean discharge on day d in $m^3 s^{-1}$.
2. d_s^y and d_e^y denotes the beginning and the end day of a particular water year y , respectively.
3. A is catchment area in km^2 .
4. $F_{0.95}$ is the threshold value for deriving high flow characteristics.
5. $d_0^y(i)$ and $d_1^y(i)$ denotes the beginning and the end of the high flow event i during the water year y , respectively.
6. $|\bullet|$ denotes the cardinality of sets of high flow events \mathcal{H}_i^y for a particular water year y .
7. $F_{0.10}$ is the threshold value for deriving low flow characteristics.
8. K_y is the total number of drought events occurring in a particular water year y .
9. \mathcal{E}_k^y denotes the intensity of a drought event k .

6.5 Results and Discussion

Both mHM model versions with their respective parameterization methods were set up in study area to simulate the observed streamflow at the Plochingen gauging station during the period from 1980 to 2001. This period was split into two parts, 1980-1988 for the calibration, and 1989-2001 for the validation purposes. Six months of data prior to the calibration period were used as the spin up time to establish reliable initial conditions of modeled state variables. The interior Horb gauging station was selected as a cross-validation site mainly to explore the effects of two distributed model parametrization methods (i.e. HRU and MPR method) on the discharge simulations. It may be noted that discharge data of this station were not used for the model calibration, and therefore it constitutes a cross-validation location.

The threshold values of high flows ($F_{0.95}$) and low flows ($F_{0.10}$) at the Plochingen gauging station were estimated as $130 \text{ m}^3\text{s}^{-1}$ and $13 \text{ m}^3\text{s}^{-1}$, respectively. For the interior Horb gauging station these values were $42 \text{ m}^3\text{s}^{-1}$ and $4 \text{ m}^3\text{s}^{-1}$, respectively. These estimates were derived from the daily observed discharge time series of the whole modeling period.

6.5.1 Daily Discharge Simulations

This section presents the results of model performances for the daily discharge simulation which provides the base for deriving simulated seasonal runoff characteristics. Furthermore, in this section the results for the sensitivity of the different objective functions on the daily discharge simulations of the lumped and the distributed mHM versions parameterized with different methods (i.e. HRU and MPR).

The performance of lumped and distributed mHM for daily discharge simulation at the Plochingen gauging station in the calibration and the validation periods based on the 200 best parameter sets found for three different objective functions (Eq. 6.1) are graphically summarized in Fig. 6.4. As a complementary to this figure, the median statistics corresponding to these simulations are presented in Table 6.4. These results clearly indicated that the dependency of model simulations on the objective functions. A clear trade-off between high and low flow simulations can be clearly observed in both calibration and validation periods, irrespective of the model structure and the parameterization

scheme. For example, when models were calibrated using E_Q as an objective function statistic, their performances were, on average, higher for the same efficiency measure than those obtained with the cross-validation efficiency measure E_{logQ} (i.e. one which was not used for the calibration purpose), and vice-versa. This was expected as models were tuned to minimize errors computed with the same objective function in their calibration phase. Same behaviors have been also observed using other models in previous studies [e.g. Boyle et al. (2000), Oudin et al. (2006), Yilmaz et al. (2008)].

Table 6.4: Ensemble median statistics of daily discharge simulations at Plochingen (outlet) during calibration and validation periods for lumped and distributed versions of the mHM. The distributed mHM was parameterized with the HRU and the MPR methods. For both models, three different variants of objective function were used that includes E_Q focusing on only high flows, E_{logQ} focusing on only low flows and E_{QlogQ} combination of them. Additionally RMSE statistic for all three cases is also presented.

Model	Objective function	Calibration			Validation		
		E_Q (-)	E_{logQ} (-)	RMSE (m^3s^{-1})	E_Q (-)	E_{logQ} (-)	RMSE (m^3s^{-1})
Lump	E_Q	0.83	0.73	23.67	0.80	0.71	18.53
Dist.-HRU		0.89	0.85	19.78	0.86	0.83	15.11
Dist.-MPR		0.90	0.87	18.17	0.89	0.86	14.20
Lump	E_{logQ}	0.74	0.79	29.07	0.73	0.75	21.26
Dist.-HRU		0.84	0.87	22.73	0.81	0.84	17.40
Dist.-MPR		0.88	0.89	19.03	0.87	0.89	14.47
Lump	E_{QlogQ}	0.84	0.83	22.45	0.84	0.82	16.60
Dist.-HRU		0.89	0.90	19.74	0.86	0.88	15.06
Dist.-MPR		0.90	0.91	18.04	0.90	0.90	13.73

However, the percentage decrease in the cross-validation efficiency were different for different model versions. The lumped model showed the higher sensitivity to the objective function as compared to the distributed model, irrespective of the parameterization methods used. The average decrease in cross-validation median statistics (either E_{logQ} or E_Q) for the distributed model with the HRU and the MPR parameterization methods were 4.1% and 2.2% in the calibration, and 3.0% and 3.1% in validation periods, respectively. Whereas, the lumped model for such results showed the decrease of 11% and 8% in the calibration and the validation periods, respectively (Table 6.4).

Moreover, the distributed model with both parametrization methods showed

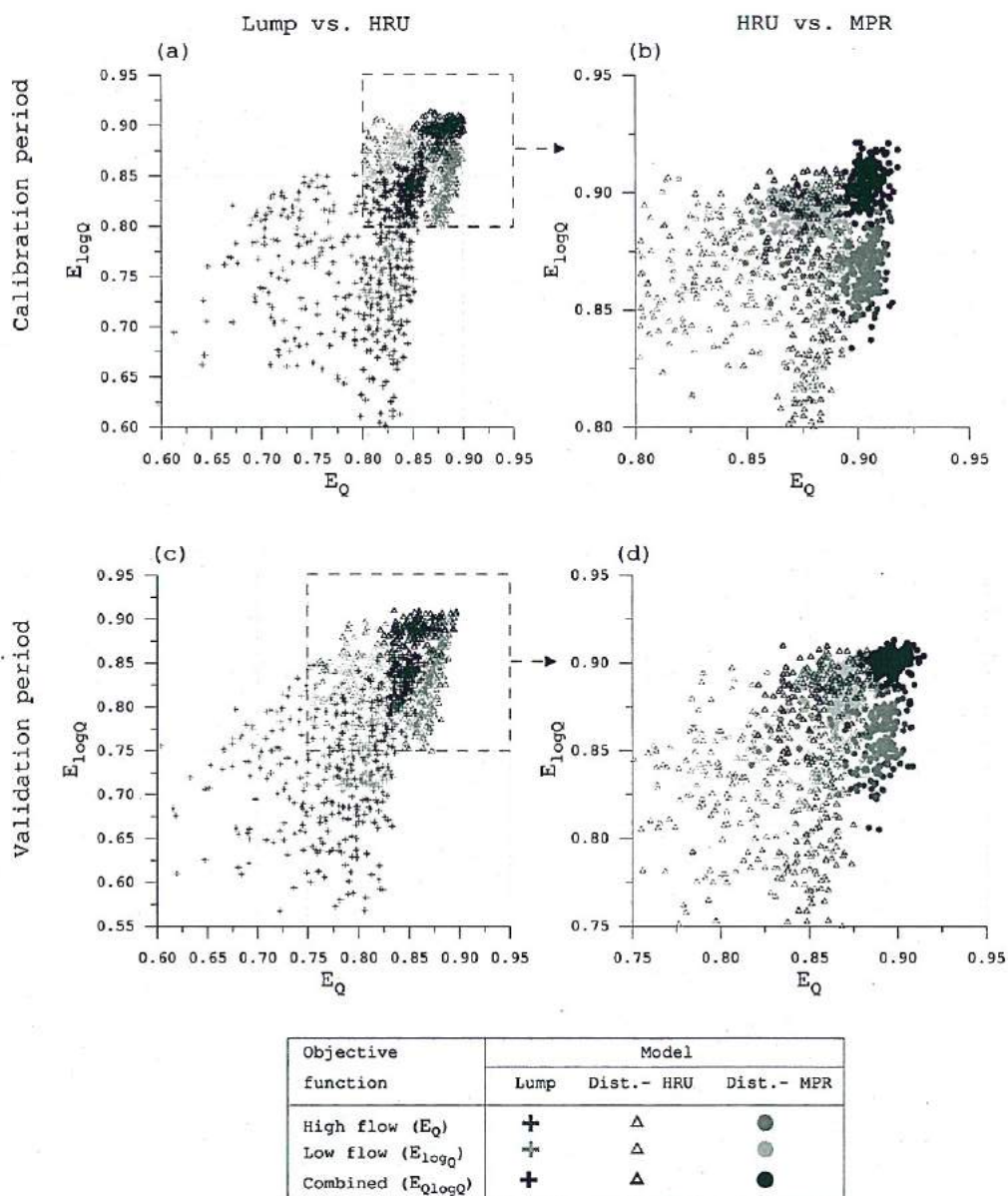


Figure 6.4: Performance of the lumped and the distributed models for daily discharge simulations at Plochingen for different objective functions. Left panels [(a-I) and (b-I)] shows the performance of the lumped model and the distributed model with the HRU parameterization method, whereas right panels [(a-II) and (b-II)] shows the performance of the HRU and the MPR parameterization methods employed in the distributed model. For both models, simulations were conducted with the 200 best parameter sets found separately for different objective functions.

better performances than that of the lumped model for both high and low flow calibration cases (Table 6.4). For instance, the ensemble median $E_{\log Q}$ values of the distributed model with the HRU and the MPR parameterization methods were 12.0% and 18.7%, respectively, higher than those obtained with the lumped model for the low flow calibration case during the validation period.

The distributed model performance for the above results also varied depending on the parameterization method employed. The MPR method was not only less sensitive to the changes in the objective function, but also it provided better performance for daily discharge simulations than the HRU method (Table 6.4). Furthermore, the variability within good solutions for the HRU method was also higher than those obtained for the MPR method (Fig. 6.4; right panels).

Another significant observations drawn from Fig. 6.4 and Table 6.4 was that the performance of both models, for both high and low flows error statistic, using the combined objective function was on average superior than those obtained with the separate objective function (i.e. focusing on either high or low flows). This result was quite surprising as one would expect that a given model would perform better for high flows, if the emphasis during calibration was given only to match high flows, as compared to those obtained with an emphasis to both high and low flows together. We believe that this improvement in the model performance for the combined objective function is related to the fact that the daily discharge hydrograph is a sequence of high and low flows, thus focusing on only one of them may produce biased results for the other one and this bias can significantly effects the model simulation for next events. The variability within the final solutions obtained with both models for the combined objective function was also, on average, lower than those obtained for the separate objective function (Fig. 6.4).

On average, the highest improvement for the combined calibration case was found for the lumped model and the least for the distributed model with the MPR parameterization method. This result further supports the claim regarding the higher sensitivity of the lumped model performance to the objective function. However, in spite of this gain, the lumped model performance for daily discharge simulations was again lower than those obtained with the distributed model with both parameterization methods. For example, the ensemble median value of $RMSE$ for the distributed model with the HRU and the MPR parameterization method were 10.2% and 20.8% lower than those

obtained with the lumped model, respectively, in the validation period. Other statistics also supported the above findings (Table 6.4).

Nevertheless, the ensemble median values of E_Q and $E_{Q \log Q}$ obtained with both model versions for the combined calibration were greater than 0.80. This result commonly indicates a good agreement between observed and simulated streamflow. It may be noted that these results obtained in this study are quite consistent with previous findings of Das et al. (2008) using different spatial representation of HBV model for the same study area.

The visual inspection of daily discharge hydrograph (Fig. 6.5) revealed that the lumped model had difficulties in simulating the observed hydrograph recession as well as the low flow spells during summer season. A plausible explanation for this behavior is the fact that the recessions are mainly controlled by basin physical characteristics (e.g. soil properties, land covers, geological formations), which are not considered in formulation of the lumped model. This results clearly shows an advantage of distributed model over their lumped counterparts, since the recession parts simulated by the distributed model with both parameterization scheme are fitting much better than those simulated by the lumped model (Fig. 6.5).

The distributed model parameterization based on the MPR method exhibited higher predictive performance as compared to the HRU method. The ($P_5 - P_{95}$) variability bounds of the daily discharge simulations obtained with the MPR method were narrower than that obtained with the HRU method, in particular for the recession part of hydrographs (Fig. 6.5). The deviation in the distributed model performance can only be attributed only to the parameterization method since that is only the difference between these simulation results. The larger variability of model outputs in case of the HRU method might be related to either an ignorance of the sub-grid variability or due to the higher variability of the good parameter sets found (Fig. 6.4). Another reason may be related to the larger number of free calibration parameters in case of the HRU parameterization method as compared to the MPR method, since the higher the dimensionality of parameter search space is, the harder it becomes for the optimization algorithm to find consistently good solutions. It may be also noted that these results were obtained with the DDS optimization algorithm which is one of the most efficient algorithm available, in particular for the computationally expensive models (Tolson and Shoemaker, 2007).

However, all results presents above are based on model runs using the DDS algorithm.

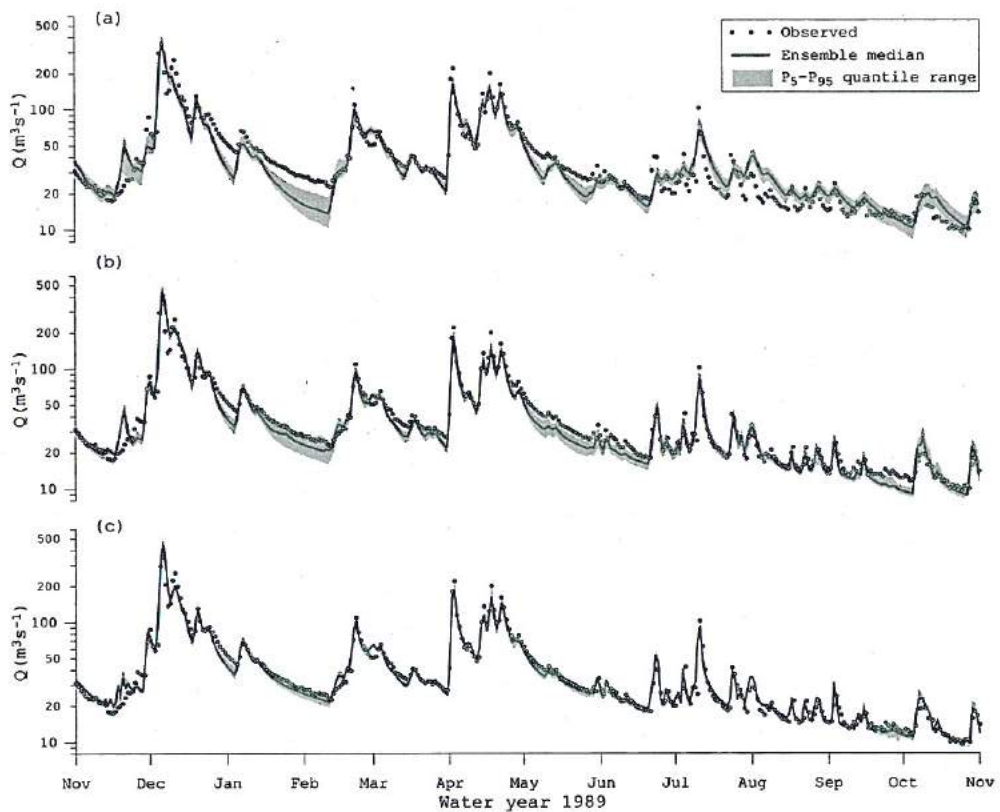


Figure 6.5: Ensemble of daily streamflow simulations at Plochingen during the evaluation water year 1989 using the lumped model (a) and the distributed model with the HRU (b) and the MPR (c) parameterization methods. The ensemble median and variability range (5% - 95% percentile range) of the modeled streamflow were estimated with the best 200 parameter sets. These sets were obtained with the combined objective function (i.e. high and low flows together).

The cross-validation results of the distributed model with both parameterization methods at Horb showed similar trade-offs between high and low flow simulations, and also for the sensitivity of the calibration objective function on the model performance (Table 6.5). The best model simulations for both high and low flows during the entire modeling period (1980-2001) were again obtained with the use of combined objective function amongst all three variants of objective functions. Comparing the performance of both distributed model

parameterization schemes revealed that the MPR method is superior in its performance than the HRU method for daily discharge simulations at this internal location (Table 6.5). For instance, the median E_Q and E_{logQ} values obtained with the MPR method were, on average, 5.5% higher than those obtained with the HRU method. Other statistics shown in Table 6.5 also corroborated the above result.

Table 6.5: Ensemble median statistics of daily discharge simulations at Horb during the modeling period (1980-2001). Simulations were carried out with the distributed mHM model with HRU and MPR parameterization methods. For both methods, three different objective functions: E_Q focusing on only high flows, E_{logQ} focusing on only low flows and E_{QlogQ} a combination of them, using the discharge data of Plochingen (outlet) were used.

Parameteriz. method	Objective function	RMSE (m^3s^{-1})	τ (-)	E_Q (-)	E_{logQ} (-)
HRU MPR	E_Q	8.83	0.88	0.81	0.75
		7.09	0.93	0.86	0.84
HRU MPR	E_{logQ}	9.08	0.89	0.79	0.82
		7.14	0.93	0.85	0.87
HRU MPR	E_{QlogQ}	8.51	0.90	0.82	0.83
		6.85	0.94	0.87	0.87

Both parameterization methods showed a deterioration in their performances when cross-validated at Horb (Table 6.4 and 6.5) as compared to those obtained at the calibration station (i.e. Plochingen gauging station). This was expected as the data of this station were not used during calibration. However, this decrement in efficiency measures for the HRU method was, on average, higher than those for the MPR method. For instance, the median E_Q obtained during the modeling period for the HRU method decreased by 8.7% while the MPR method exhibited a decrease of only 2.8%. This relatively poor cross-validation performance of the HRU method compared to that obtained with the MPR method may also be attributed to the over-fitting problem. This effect becomes more evident by visual inspection of the daily streamflow simulations as shown in Fig. 6.6. The ($P_5 - P_{95}$) variability bounds of daily discharge simulations with the HRU method were at least 10% wider than those obtained with the MPR method. These results clearly demonstrated the robustness and the reliability of the MPR method over the HRU method for daily discharge predictions at the interior location.

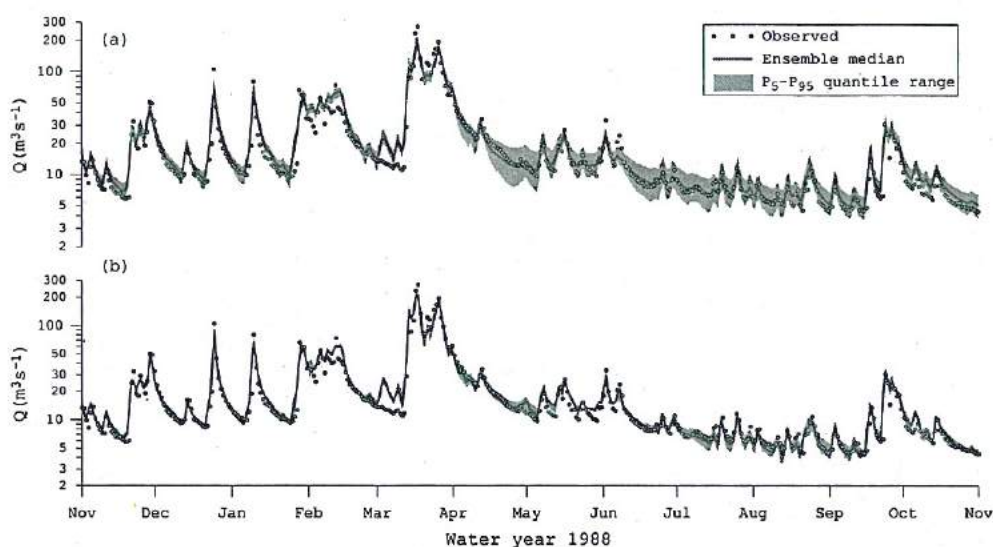


Figure 6.6: Ensemble of daily streamflow simulations at Horb gauging station (internal) during the water year 1988 using the HRU (a) and the MPR (b) parameterization methods. The ensemble median and variability range (5% - 95% percentile range) of the modeled streamflow were estimated with the best 200 parameter sets. These sets were obtained with the combined objective function and the discharge data of Plochingen (outlet).

6.5.2 Prediction of the Seasonal High and Low Flow Characteristics

In this section, simulation results for the prediction of seasonal runoff characteristics and their sensitivity to the calibration objective functions are presented. Fig. 6.7 illustrates the sensitivity of the lumped and distributed models for the prediction of seasonal specific volume of high flows (Q_1) and cumulative specific deficit (Q_4) during the modeling period at the Plochingen gauging station. It should be noted that the seasonal characteristics Q_1 and the Q_4 were used as penalty terms for the high and the low flow objective functions, respectively, while both of these characteristics were used as a penalty term in the combined calibration case. Both model versions showed the sensitivity to the chosen objective function on the predictions of extremes runoff characteristics. The lumped model showed the highest sensitivity, whereas the distributed model with the MPR parameterization method the least (Fig. 6.7). Furthermore, the performance of both model versions for the combined objective function were consistently better than that obtained from the separate

objective function used during calibration (either high flows or low flows). In particular, the performances of both models for the low flow characteristic with the combined objective function showed a significant improvement over those obtained with an objective function that focus only on low flows during the calibration process. The in-depth analysis of model simulation results for different seasonal runoff characteristics are presented below. Note that all results presented, hereafter, are obtained from model runs which use combined objective function in their calibration process.

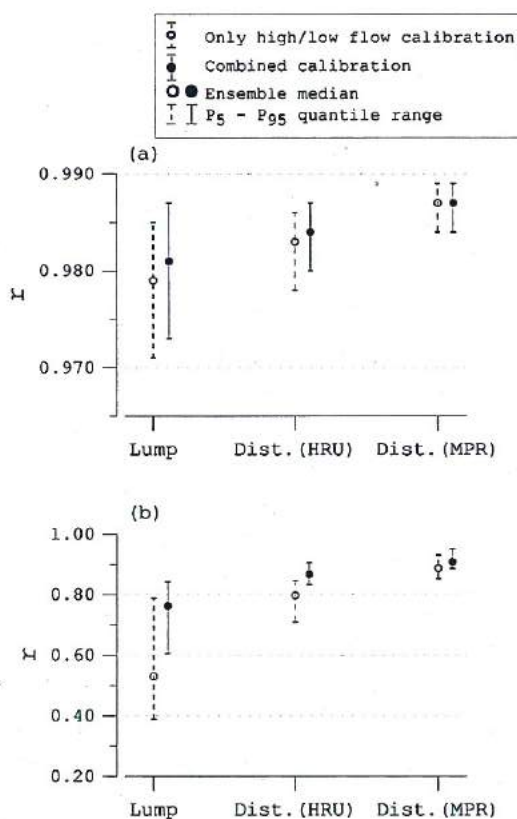


Figure 6.7: Sensitivity of the lumped and the distributed models performance for the prediction of seasonal specific volume of high flows (a) and cumulative specific deficit (b) to the objective functions. The distributed model was parameterized with the HRU and the MPR methods. Simulations were carried at Plochingen during the modeling period (1980-2001) with 200 best parameter sets found separately for different objective function.

6.5.2.1 High Flow Characteristics

The results obtained for seasonal high flow characteristics at the Plochingen gauging station for both lumped and distributed mHM and for the MPR and the HRU parameterization methods are summarized in Table 6.6. It can be noticed from this table that the distributed model, regardless of the parameterization scheme, during the winter season performed better than the lumped model. For instance, the median *RMSE* values for the distributed model with both HRU and MPR regionalization methods in this season were, on average, 10% and 32% lower than those obtained with the lumped model, respectively, considering all high flow characteristics. However, the other two efficiency measures [i.e. Pearson correlation coefficient (r) and Spearman rank correlation coefficient (ρ)] do not showed big difference between the lumped and the distributed model simulations for the high flow characteristics. These efficiency measures (r and ρ) obtained for the distributed model were, on average, less than 5% higher than those obtained for the lumped model.

Table 6.6: Ensemble median statistics between observed and simulated seasonal high flow characteristics at Plochingen during the modeling period from 1980 to 2001. Simulations were conducted with the lumped and the distributed mHM model. The distributed model was parameterized with two methods: Hydrological Response Unit (HRU) and Multiscale Parameter Regionalization (MPR).

Season/ Character.	RMSE			r			ρ		
	Lump	Dist. HRU	Dist. MPR	Lump	Dist. HRU	Dist. MPR	Lump	Dist. HRU	Dist. MPR
Winter									
Q_1 (mm)	13.34	12.11	9.93	0.97	0.98	0.99	0.96	0.96	0.98
Q_2 (d)	3.49	3.04	2.61	0.95	0.96	0.98	0.93	0.94	0.97
Q_3 (y^{-1})	1.37	1.21	1.07	0.85	0.89	0.91	0.84	0.87	0.92
Summer									
Q_1 (mm)	9.01	8.05	7.96	0.90	0.90	0.91	0.89	0.90	0.93
Q_2 (d)	2.01	1.93	1.87	0.89	0.89	0.90	0.90	0.90	0.91
Q_3 (y^{-1})	1.05	0.96	0.86	0.86	0.88	0.89	0.89	0.90	0.92

Both lumped and distributed models showed relatively poor performances for the predictions of frequency of high flows (Q_3) during winter season as compared to the other two characteristics (i.e. specific volume (Q_1) and total duration (Q_2) of high flows). For example, the Pearson correlation coefficient (r) obtained with both models for Q_3 , were at least 10% lower than those obtained for the other two characteristics (Table 6.6). This behavior was observed regardless of the parameterization method employed in the distributed model.

The visual inspection of both models simulation for high flow characteristics also corroborated the above findings (Fig. 6.8).

The efficiency of distributed model simulations regarding high flow characteristics during summer was as good as that obtained by the lumped model, since both models were able to explain between 86% to 91% of the observed variance (r). Other efficiency measures for both models also showed minor differences in accordance with the previous result (Table 6.6). The performance of both models for the frequency of high flows (Q_3) during this season were also relatively lower than those obtained for the other two characteristics (Table 6.6).

The predictive efficiency of both models, irrespective of the parameterizations method, for high flow characteristics in summer was lower than that obtained in winter (Table 6.6). This lack of predictability of high flows in summer is mainly related with the occurrence of convective precipitation events, whose short time of occurrence and limited spatial extent is often not captured by the coarser network climatological stations available in the area.

The performance of the distributed model for the simulations of high flow characteristics was dependent on the parameterization method employed. Results indicated that the MPR method performed, on average, better than the HRU method (Table 6.6). For example, the ensemble median *RMSE* value obtained with the latter method were, on average, 24% and 5% greater than those obtained with the former method during winter and summer, respectively.

Cross-validation test conducted at Horb (Table 6.7) further corroborated the robustness and reliability of the MPR method over the HRU method. For instance, the median *RMSE* values between observed and simulated high flow characteristics obtained with the MPR method were, on average, 45% and 18% lesser than those obtained with the HRU method during winter and summer, respectively. Additionally, the median values of both correlation coefficients r and ρ obtained with the MPR method were also higher than those obtained from the model runs of the HRU method (Table 6.7).

6.5.2.2 Low Flow Characteristics

The efficiency of the distributed model with respect to the low flow characteristics was significantly better than those obtained by the lumped model (Table 6.8). This results were obtained irrespective of parameterization method

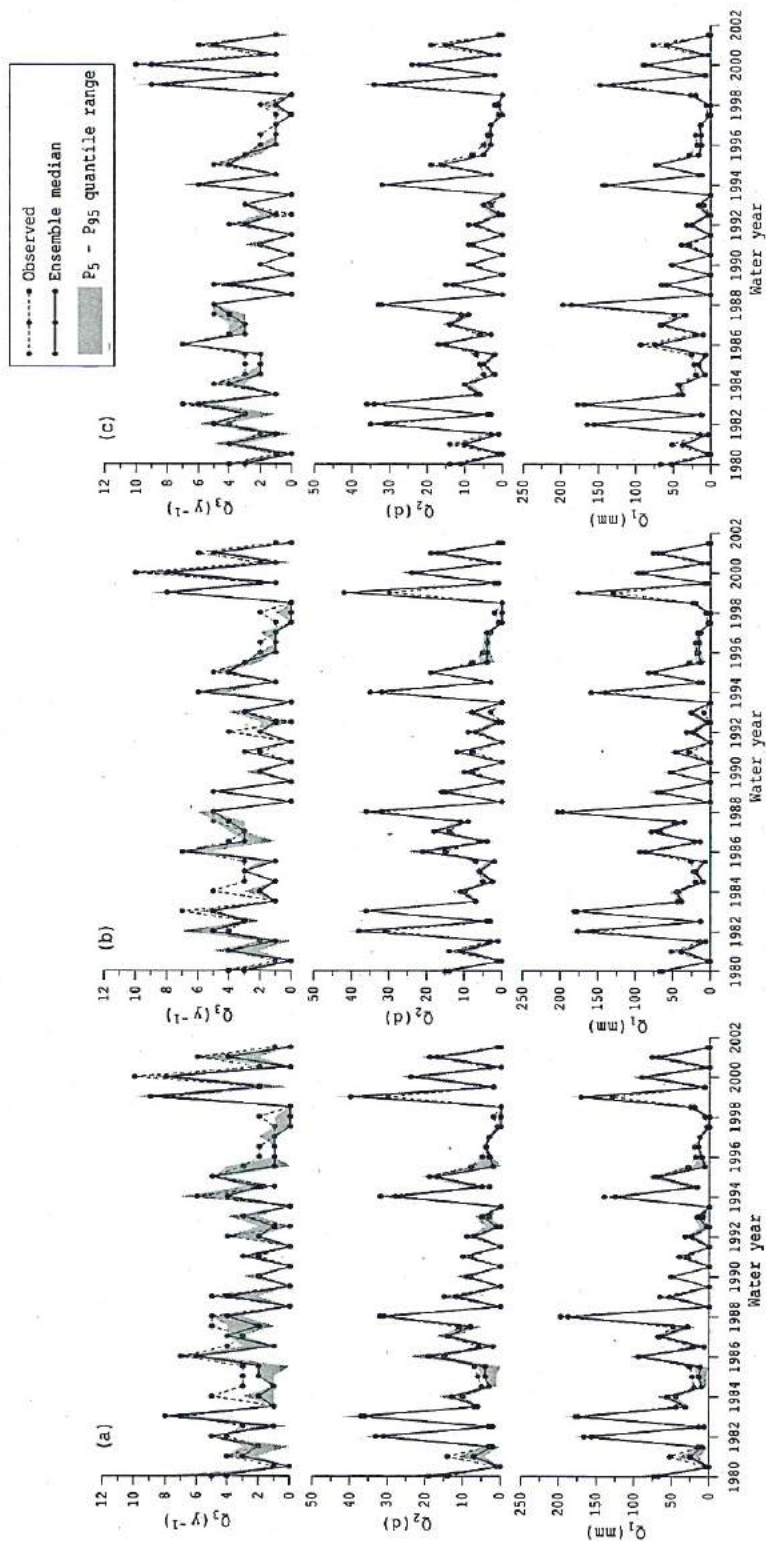


Figure 6.8: Performance of the lumped (a) and the distributed model with the HRU (b) and the MPR (c) parameterization methods for the prediction of seasonal high flow characteristics at Plochingen during the modeling period (1980-2001).

Table 6.7: Ensemble median statistics between observed and simulated seasonal high flow characteristics at Horb during the modeling period from 1980 to 2001. Simulations were conducted with the distributed mHM model with two parameterization methods: Hydrological Response Unit (HRU) and Multiscale Parameter Regionalization (MPR).

Season/ Character.	RMSE		r		ρ	
	HRU	MPR	HRU	MPR	HRU	MPR
Winter						
Q_1 (mm)	29.73	20.94	0.95	0.97	0.96	0.97
Q_2 (d)	6.69	4.65	0.94	0.96	0.95	0.96
Q_3 (y^{-1})	1.65	1.07	0.83	0.87	0.84	0.89
Summer						
Q_1 (mm)	7.80	7.03	0.85	0.88	0.92	0.97
Q_2 (d)	1.38	1.11	0.84	0.90	0.88	0.92
Q_3 (y^{-1})	0.83	0.69	0.82	0.90	0.84	0.91

employed in the distributed model. For example, the median *RMSE* values obtained with the distributed model for the MPR method were, on average, at least 50% lower than those obtained with the lumped model in both winter and summer. The values of ensemble median correlation coefficients (r and ρ) obtained with the latter model were also significantly lower than those obtained with the former model version. The same results were observed when the distributed model was parameterized with the HRU method. The main reasons behind the poor performance of the lumped model is due to significant mismatch between the season time series of observed and simulated low flow characteristics (Fig. 6.9). Moreover, the ($P_5 - P_{95}$) variability bounds of the simulated low flow characteristics obtained with the lumped model were also significantly wider than those obtained from the runs of the distributed model. The relatively poor performance of the lumped model compared to spatially distributed model clearly shows the effects of spatial discretization to model various components of hydrological process. This in-turn also shows an importance of accounting the spatial heterogeneity of the catchment characteristics which have a large impact on the simulation of low flow characteristics.

The performance of the distributed model were also different depending on the parameterization method employed. For instance, the median value of Pearson correlation coefficient (r) obtained with the MPR method were, on average, 6% and 4% higher than those obtained by the HRU method during winter and summer, respectively. Other statistics also corroborated the above result. It was also observed that the simulations of low flow characteristics obtained

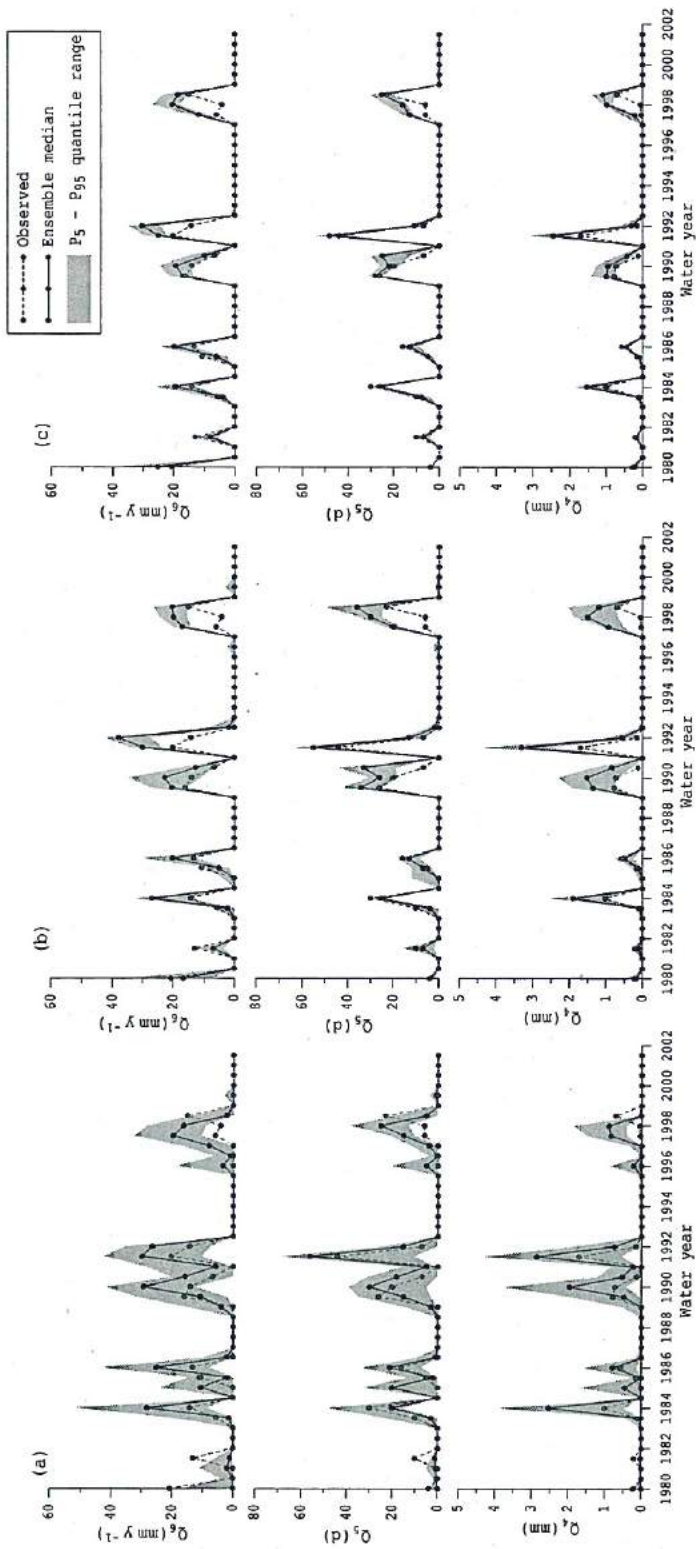


Figure 6.9: Performance of the lumped (a) and the distributed model with the HRU (b) and MPR (c) parameterization methods for the prediction of seasonal low flow characteristics at Plochingen in the modeling period (1980-2001).

Table 6.8: Ensemble median statistics between observed and simulated seasonal low flow characteristics at Plochingen during the modeling period from 1980 to 2001. Simulations were conducted with the lumped and the distributed mHM model. The distributed model was parameterized with two methods: Hydrological Response Unit (HRU) and Multiscale Parameter Regionalization (MPR).

Season/ Character.	RMSE			r			ρ		
	Lump	Dist. HRU	Dist. MPR	Lump	Dist. HRU	Dist. MPR	Lump	Dist. HRU	Dist. MPR
Winter									
Q_4 (mm)	0.58	0.41	0.32	0.80	0.82	0.86	0.83	0.98	0.99
Q_5 (d)	8.14	5.57	5.03	0.76	0.85	0.90	0.82	0.97	0.98
Q_6 (mm y ⁻¹)	9.69	7.16	6.51	0.78	0.87	0.93	0.80	0.98	0.99
Summer									
Q_4 (mm)	0.56	0.45	0.37	0.82	0.93	0.96	0.81	0.95	0.98
Q_5 (d)	8.51	7.62	4.64	0.81	0.92	0.94	0.83	0.95	0.99
Q_6 (mm y ⁻¹)	7.03	4.21	3.87	0.69	0.88	0.92	0.82	0.96	0.99

with the HRU method exhibited a larger variability as compared to the MPR method. For example, the ($P_5 - P_{95}$) variability bounds of the median r values obtained for the simulation of the maximum drought intensity (Q_5) in summer was (0.73–0.91) and (0.86–0.94) for the HRU and MPR methods, respectively.

Cross validation tests conducted at Horb gauging station (Table 6.9) further corroborated the robustness of the MPR method over the HRU method. For instance, the median *RMSE* value obtained with the MPR were at least 50% lesser than that obtained with the HRU method. Both correlation coefficients obtained with the latter method were also significantly lower than those obtained with the former method. The HRU method also exhibited a significantly larger variability for the simulations of low flow characteristics than those obtained with the MPR method (Fig. 6.10). The variability bounds of simulated low flow characteristics for the HRU method were, on average, at least 30% higher than those obtained with the MPR method. However, the coverage of observed values within variability bounds for both methods were approximately similar.

In general, it can be stated that both model versions (i.e. lumped and distributed) exhibited a larger uncertainty in the simulation of low flows characteristics as compared to the simulation of high flow characteristics (Fig. 6.8, and Fig. 6.9). This results for the distributed model were also obtained regardless of the parameterization method employed. The lack of predictability for low flows are due to various reasons which include, for instance, a non-inclusion

of human induced discharge fluctuations (e.g. outlets of treatment plants or water supply intake facilities) in the modeling framework , structural errors of the model (e.g. exclusion of regulation structures in the model conceptualization), measurement errors (e.g. discharge measurement during the extreme low flow conditions), amongst other error sources.

Table 6.9: Ensemble median statistics between observed and simulated seasonal low flow characteristics at Horb during the modeling period (1980-2001). Simulations were conducted with the distributed mHM model with two parameterization methods: Hydrological Response Unit (HRU) and Multiscale Parameter Regionalization (MPR).

Season/ Character.	RMSE		r		ρ	
	HRU	MPR	HRU	MPR	HRU	MPR
Winter						
Q_4 (mm)	0.41	0.23	0.84	0.96	0.95	0.99
Q_5 (d)	9.06	5.21	0.88	0.95	0.94	0.99
Q_6 (mm y ⁻¹)	6.23	5.70	0.92	0.97	0.96	0.98
Summer						
Q_4 (mm)	0.92	0.63	0.89	0.93	0.88	0.95
Q_5 (d)	11.49	6.58	0.86	0.92	0.90	0.96
Q_6 (mm y ⁻¹)	8.27	4.13	0.83	0.95	0.87	0.96

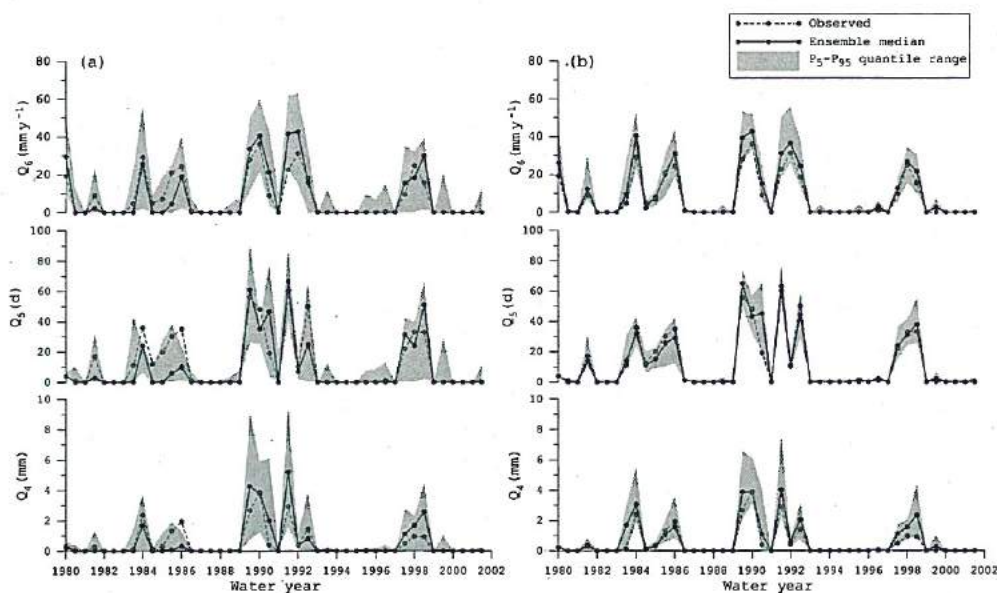


Figure 6.10: Performance of the HRU (a) and the MPR (b) parameterization methods employed in the distributed model for the prediction of seasonal low flow characteristics at Horb in the modeling period (1980-2001).

Chapter 7

Summary and Outlook

7.1 Summary

Water resources planning and management under changing environmental conditions require, amongst other things, a robust and efficient hydrologic model that can not only provide a reliable estimate on streamflow at a gauged and ungauged location within a river basin, but also can provide a reliable estimate on spatio-temporal dynamics of different state variables and water fluxes. Distributed hydrologic models which are developed for these purposes exhibits deficiencies in their implementation on a mesoscale such as overparametrization, the lack of an effective technique to integrate the spatial heterogeneity of basin physical characteristics, the non-transferability of parameters across scales and locations, amongst others. The aim of this study was to address these issues simultaneously. The research questions that have motivated and guided this work, as posed in Chapter 1, are reiterated below:

1. *How to formulate a robust and computationally efficient spatially distributed hydrologic model for a mesoscale river basin, which can not only reproduce the discharge hydrograph at any point within a basin but also able to provide a reasonable estimate of the spatio-temporal dynamics of soil moisture, snow cover, amongst other state variables?*
2. *How to obtain spatial fields of model parameters robust enough to reduce the overparameterization problem but still adequate enough to incorporate the sub-grid basin heterogeneity, while ensuring the transferability of model parameters to scales other than that used during model calibration?*

To address these questions, the present study was aimed at developing a spatially distributed hydrologic model and its parameterization technique which can be suitable for both scientific and operation purposes at a mesoscale river basin. A summary of research works performed for this study is detailed below.

In Chapter 2, a detail formulation of spatially distributed mesoscale hydrologic model (mHM) was presented. In summary, mHM is a fully distributed process based water balance model that uses grid cells as a primary hydrologic unit and simulates the following dominant hydrologic processes: canopy interception, snow accumulation and melting, soil moisture dynamics, infiltration and surface runoff, evapotranspiration, surface and subsurface storage and discharge generation, deep percolation and baseflow, and discharge attenuation and flood routing. mHM is based on numerical approximations of dominant hydrological processes that have been tested in the well known HBV model (Bergström, 1995). The mHM model, however, includes also a number of new features such as soil freezing and thawing process, near surface root zone soil moisture process, canopy interception processes, cell to cell routing process, module for automatic upscaling and delineation of flow routing network, as well as the new parameterization technique. Moreover, since in mHM the discharge generation process is modeled at each grid cell, as apposed to the HBV model in which this process is modeled at a predefined sub-basin level, mHM can be effectively used to estimate discharge hydrograph at any point along the river network within a basin. It can also efficiently incorporate remote sensing data sets. One of the significant features of mHM is that it uses different levels of spatial information to better incorporate and represent the spatial variability of hydrological processes and input data.

The theme of Chapter 3 was dedicated to present a detail review on the state-of-art regionalization approaches used for the parameterization of a distributed hydrologic model. After pointing out certain deficiencies in current approaches, a Multiscale Parameter Regionalization (MPR) was proposed to reduce the overparameterization problem while incorporating the sub-grid variability of basin physical characteristics within the parameterization framework. In summary, the proposed MPR method follows two step procedure. In first step, the regionalization is performed at a finer resolution (i.e. at the data input level) to account for the sub-grid variability of basin characteristics. Subsequently in the second step, effective parameter fields required

to describe spatial variability of hydrological processes at a coarser grid are obtained with appropriate upscaling operators. MPR differs with the currently used standard regionalization approach in the way that it does not focus on estimating "*aggregated basin characteristics*" having little or no information regarding the spatial variability of the natural factors that regulate the hydrological process at the sub-grid scale, but rather in estimating "*effective fields of model parameters*" that capture the emergent properties of these processes. One significant advantage of using the two step MPR technique is that it always have the information of parameter fields at finer sub-grid scale that can efficiently used to generate effective parameters fields at any modeling scale using upscaling operators, but without further calibration. MPR, when implemented within mHM reduced significantly the number of free parameters over which calibration is made, while retaining model capability to represent the sub-grid variability of basin characteristics.

In Chapter 4, a detailed application of mHM with the MPR parameterization method was presented for the study area. Modifications of the standard conceptual model structure such as the frozen soil algorithm, the inclusion of two-top soil layers, incorporation of satellite data such as weekly leaf area index, and the usage of distributed driving forcings obtained via external drift krigging interpolation scheme, as well as the new multiscale parameterization method, were fundamental to improve the model performance. The low time complexity of the resulting model did, in turn, speed up the convergence of the optimization algorithm.

The proposed multiscale parameter regionalization (MPR) technique not only reduced the complexity of the model, but also led to a fast and robust hydrologic model which was able to reproduced quite well the discharge hydrograph not only at outlet of the basin but also at the interior locations discharge data of which were not used for model calibration. Furthermore, the plausibility test carried out to compare the spatial patterns of snow cover and near surface soil moisture also matched quite well with the direct and proxies data obtained from MODIS (i.e. snow cover and land surface temperature (LST), respectively).

The inclusion of new soil freezing module and canopy interception module showed improvements in the discharge simulations. The mHM implementation in the study are has significantly improved streamflow predictions (e.g.

NSE \approx 0.85 to 0.90) as compared with those obtained with the HBV model (NSE \approx 0.79 to 0.84). Moreover, the spatial patterns of soil moisture obtained from the mHM model simulation with the MPR parameterization were much more realistic than those obtained through the HRU method, when compared with LST data of MODIS imageries. These results suggested that commonly used HRU based parameterization method is not efficient for providing the realistic patterns of spatio-temporal dynamics of state variables, mainly due to their static categorical method to classify HRUs that not necessarily preserves the local relationships between basin characteristics and model parameters. However, further research is still required in this aspect to compare model simulated soil moisture patterns with real data sets instead of proxy data (i.e. LST).

In Chapter 5, several numerical experiments were designed to study the impact of incorporating sub-grid variability of basin characteristics in regionalization framework. MPR was compared with the standard regionalization (SR) technique. Both methods were implemented within mHM with similar regionalization functions. The mHM model runs with both methods were performed at various modeling scales (2 km to 32 km). Results of this study indicated that both regionalization techniques do not exhibit significant differences in global efficiency measures (e.g. NSE) for daily discharge simulations as long as the model is calibrated and evaluated at a given modeling scale. These results pointed out the extent of the equifinality of global parameter sets and a substantial shortcoming of the calibration procedure when the objective function does not consider components other than observed and simulated streamflow.

Substantial differences, however, became apparent when the global parameters were calibrated at a coarser modeling scale and then transferred to a finer one. In such a case, MPR exhibited a clear superiority with respect to SR. Running the model at coarser scale, as compared to the finer scale, in given modeling domain have many advantages such as significant reduction in computational time required for tedious task of calibration, which requires several thousands of search iteration. In such cases MPR is quite advantageous as global parameters obtained at coarser scale with MPR can be transferred to finer scale with reasonable performance.

The dynamics of state variables such as soil moisture and water fluxes varied significantly depending on the regionalization method employed as well as

the modeling scale used for the calibration of global parameters. Therefore, it is crucial for the evaluation of any regionalization technique to assess the error induced into the mass balance, at a given control volume when global parameters are shifted across modeling scales.

Compelling evidence have been presented in this study with respect to the effect of accounting for the sub-grid variability in the regionalization method, as well as the importance of the upscaling sequence (i.e. either predictors in SR or parameters in MPR) to satisfy the continuity principle. MPR consistently performed better than SR. Cross-scale experiment results bring us to the conclusion that upscaling regionalized model parameters (i.e. MPR), instead of performing parameter regionalization with upscaled basin predictors (i.e. SR), lead to significantly different spatio-temporal distributions for both state variables and water fluxes due to the nonlinearity of the system. Transferring the parameter across scales for conserving spatial mass balance of water fluxes and state variables with MPR was much more feasible than SR mainly because of its two step regionalization procedure.

Another advantage of MPR over SR, as shown in this study, was its capability to produce better streamflow simulations in cross-validated interior locations, discharge data of which were held out from the calibration process. This property of the distributed model with robust parameterization method is of great importance for the prediction in ungauged basins (PUB).

Finally, in Chapter 6, a case study was performed to assess the mHM capability to reproduce seasonal runoff characteristics. The specific objectives, in this case were to assess the effects of spatial discretization, model parameterization and calibration objective function on the prediction of daily streamflow as well as seasonal high and low flow characteristics. Here, mHM was run at two different spatial resolutions: lumped and spatially distributed versions. The distributed mHM version was, in turn, parameterized with the HRU and the MPR methods. For both model versions with their respective parameterizations, calibration were performed with three objective functions with an emphasis on high flows, low flows, and a combination of them.

The results of this case study indicated that performances of the lumped and the distributed models for the simulations of daily discharge as well as seasonal high and low flow characteristics were sensitive to the choice objective function used for calibration. The lumped model showed the highest sensitivity and the

distributed model with the MPR parameterization the least. For both models, the objective function that accounts for both high and low flows together consistently performed better than other individual objective functions. Based on these results it can be said that the formulation of objective function in the calibration process is one of the crucial aspect for the successful implementation of hydrologic model, but degree of sensitivity can vary depending on the spatial discretization and model parameterizations.

Regarding the seasonal high flow characteristics no significant differences in the performance of lumped and distributed model were found in this study. Winter high flow characteristics predicted by the distributed model were, however, slightly better than those obtained by the lumped model. Consequently it can be stated that the spatial discretization may not play a significant role on the prediction of high flow characteristics at seasonal time scale. It is worthwhile emphasizing here that the spatial discretization may have the impact on peak flow characteristics such as volume and timing, on daily or hourly time scale. Further research is needed in this aspect.

On the contrary, for the simulation of low flow characteristics, distributed model with both parameterization methods performed significantly better than those obtained from the lumped model simulation. It was also observed that the lumped model has a difficulties in simulating the recession part of the observed daily hydrograph. Distributed model with both parameterization methods for simulating such parts of daily hydrograph showed relatively better fit. These result supported the hypothesis that the spatial discretization and thereby accounting for the spatial heterogeneity of basin physical characteristics (e.g. soil and land cover properties, geological formations) plays a significant role on the prediction of seasonal low flow characteristics as well as recession part of the daily hydrograph. In this case, a clear gain was observed for the usage of a distributed model over its lumped counterpart.

Results of the same case study also highlighted the importance of robust parameterization technique in case of a distributed hydrologic modeling in a mesoscale river basin. The MPR method not only reduced the complexity of mHM, but also exhibited better efficiency for the simulations of both the daily discharge and the seasonal runoff characteristics as compared to those obtained with the HRU parameterization method. Moreover, the results of cross-validation tests conducted for the predictions at internal site, revealed that the MPR method

was more robust and reliable than the HRU method. These results again indicated the effect of sub-grid variability of basin characteristics on model performance since the HRU method does not account for these variability.

In summary, this thesis has presented an efficient spatially distributed hydrologic model (mHM) with a robust multiscale parameter regionalization (MPR) technique that can be applicable for solving problems related to water resources at a mesoscale. The two-step MPR parameterization method introduced in this work not only reduced the model overparameterization problem, but also provided a way to explicitly incorporate the sub-grid variability within the parameter regionalization framework. As a result it ease the transferability of global parameters to other scales and locations other than that used during calibration, without inducing statistical significant bias in either streamflow predictions and/or simulated water fluxes. The distributed model parameterization based on the MPR method proved to be more robust and reliable in various aspects in comparison to the currently used standard regionalization method and the commonly hydrological response units method. Finally, it must be mentioned that the model and the parameterization technique developed in this study is general and can be applied elsewhere, if required data are available.

7.2 Outlook

All applications of the developed model (mHM) and the parameterization (MPR) scheme presented in this work was applied for the case study area which is the Upper Neckar river basin. For proving its further robustness and reliability, mHM need to be applied in several other river basins. In this regard the author of this thesis is currently applying mHM in several mesoscale river basins in and outside of Germany. Moreover, in this study the performance of the mHM model was only compared with the HBV model. It would be interesting to test the mHM performance with other existing spatially distributed models.

Regarding regionalization technique, experiences of working with upscaling techniques have shown that there are no explicit simple averaging rules for various model parameters. In this direction further investigation regarding upscaling operators and their fundamental properties, required to describe dominant processes in a mesoscale control volume, is still needed.

The MPR method, as shown in this study, reduced considerably the parameter search space over which existing optimization algorithms can efficiently search for good sets of global parameter. However, it had not led to find to an optimum global parameter set. This implies that there is still a considerable amount of uncertainty that arises from various sources of error. In this study, attempts were made only to quantify variability in model outputs due to the good sets of global parameter. The future study should carry out detailed uncertainty analysis associated with model outputs due to various sources of error, which include, for instance, model structural uncertainty, uncertainty due to errors in input data, amongst others.

One key area where regionalization techniques can be effectively explored is for the predictions in ungauged basins. Although not presented in this thesis the MPR technique had been effectively used for the predictions in ungauged basins (Samaniego et al., 2010a). However, still much research efforts have to be devoted in this respect to test both mHM and MPR at several ungauged sites.

Finally, as shown in this thesis adding some new processes in existing model have improved model performance. It is worthwhile to extend the model structure so to incorporate other relevant processes. In this regard investigations can be conducted towards the inclusion of a vegetation growth model which may be able to simulate not only leaf area index but also ensuring that the soil-plant-atmosphere interactions are accounted explicitly in the hydrologic model. Second possibility would be to include an explicit low-complexity energy balance model coupled to mHM so to improve further the spatio-temporal dynamics of soil moisture, evapotranspiration, radiation fluxes, amongst other key state variables and water and energy fluxes. These inclusion of new modules could make the mHM model favorable for coupling it with a regional climate model.

Bibliography

- Aarts, E., Korst, J., 1990. Simulated annealing and Boltzmann machines: A stochastic approach to combinatorial optimization and neural computing. Wiley, Chichester.
- Abdulla, F., Lettenmaier, D., 1997. Development of regional parameter estimation equations for a macroscale hydrologic model. *J. Hydrol.* 197, 230–257.
- AG Boden, 1994. Bodenkundliche Kartieranleitung - 4. Aufl., 392 S., 33 Abb., 91 Tab.; Hannover.
- Ahmed, S., Marsily, G. d., 1987. Comparison of geostatistical methods for estimating transmissivity using data on transmissivity and specific capacity. *Water Resour. Res.* 23 (9), 1717–1737.
- Allen, R., Pereira, L., Raes, D., Smith, M., 1998. Crop Evapotranspiration- Guidelines for computing Crop Water Requirements. FAO Irrigation and Drainage Paper 56.
- Arnold, J. G., Fohrer, N., 2005. SWAT 2000: Current capabilities and research opportunities in applied watershed modeling. *Hydrol. Process.* 19 (3), 536–572.
- Bárdossy, A., Hartmann, G., Giese, H., 1999. Impact of climate change on river basin hydrology under different climatic conditions. Final report. CC-HYDROENV4-CT95-0133. P. Nachtnebel (Editor).
- Bárdossy, A., Samaniego, L., 2002. Fuzzy Rule-Based Classification of Remotely Sensed Imagery. *IEEE Trans. Geosci. Remote Sens.* 40 (2), 362–374.
- Barling, R., Moore, I., Grayson, R., 1994. A quasi-dynamic wetness index for

- characterizing the spatial distribution of zones of surface saturation and soil water content. *Water Resour. Res.* 30, 1029–1044.
- Bastidas, L., Bonell, M., Kabat, P., Schuttleworth, J., 2005. The Nature of the Land-Biosphere-Atmosphere Feedbacks in the Hydrological Cycle. In: Bronstert, A., Carrera, J., Kabat, P., Lütkeimeier, S. (Eds.), *Coupled Models for the Hydrological Cycle: Integrating Atmosphere, Biosphere and Pedosphere*. Springer, pp. 8–21.
- Bastola, S., Ishidaira, H., Takeuchi, K., 2008. Regionalisation of hydrological model parameters under parameter uncertainty: A case study involving topmodel and basins across the globe. *J. Hydrol.* 357, 188–206.
- Becker, A., McDonnell, J. J., 1998. Topographical and ecological controls of runoff generation and lateral flows in mountain catchments. *International Association of Hydrological Sciences, IAHS Publication 248*, 199–206.
- Beighley, R. E., Dunne, T., Melack, J. M., 2005. Understanding and modeling basin hydrology: interpreting the hydrogeological signature. *Hydrol. Process.* 19, 1333 – 1353.
- Beldring, S., Engeland, K., Roald, L. A., Saelthun, N. R., Vokso, A., 2003. Estimation of parameters in a distributed precipitation-runoff model for Norway. *Hydrol. Earth Syst. Sci.* 7 (3), 304–316.
- Bergström, S., 1976. Development and application of a conceptual runoff model for Scandinavian catchments. *Tech. Rep. 7, SMHI Reports RHO*.
- Bergström, S., 1995. The HBV Model. In: Singh, V. (Ed.), *Computer Models of Watershed Hydrology*. Water Resour. Publ., Colorado, USA, pp. 443–476.
- Bergström, S., Carlsson, B., Grahn, G., Johansson, B., 1997. A more consistent approach to catchment response in the HBV model. *Vannet i Norden* 4, 1–7.
- Beven, K. J., 2001a. How far can we go in distributed hydrological modelling? *Hydrol. Earth Syst. Sci.* 5 (1), 1–12.
- Beven, K. J., 2001b. *Rainfall Runoff Modelling. The Primer*. John Wiley and Sons, Chichester, UK.

- Beven, K. J., Binley, A. M., 1992. The future of distributed models: Model calibration and predictive uncertainty. *Hydrol. Process.* 6, 279–298.
- Beven, K. J., Lamb, R., Quinn, P., Romanowicz, R., Freer, J., 1995. TOP-MODEL. In: Singh, V. (Ed.), *Computer Models of Watershed Hydrology*. Water Resour. Publ., Colorado, USA, pp. 627–668.
- Blaney, H., Criddle, W., 1950. Determining water requirements in irrigation areas from climatological and irrigation data. Tech. Rep. 96, USDA, SCS-TP.
- Blöschl, G., 2001. Scaling in hydrology. *Hydrol. Process.* 15 (4), 709–711.
- Blöschl, G., Reszler, C., Komma, J., 2008. A spatially distributed flash flood forecasting model. *Environ. Model. Softw.* 23 (4), 464–478.
- Blöschl, G., Sivapalan, M., 1995. Scale issues in hydrological modelling: A review. *Hydrol. Process.* 9 (3–4), 251–290.
- Booij, M. J., 2005. Impact of climate change on river flooding assessed with different spatial model resolutions. *J. Hydrol.* 303, 176–198.
- Boughton, W., Chiew, F., 2007. Estimating runoff in ungauged catchments from rainfall, PET and the AWBM model. *Environ. Model. Softw.* 22, 476–487.
- Boyle, D. P., Gupta, H. V., Sorooshian, S., 2000. Toward Improved Calibration of Hydrologic Models: Combining the Strengths of Manual and Automatic Methods. *Water Resour. Res.* 36 (12), 3663–3674.
- Bronstert, A., 2004. Rainfall-runoff modelling for assessing impacts of climate and land-use change. *Hydrol. Process.* 18, 567–570.
- Brooks, R. H., Corey, A. T., 1964. Hydraulic properties of porous media. Tech. Rep. 3, 786, Colorado State University, Fort Collins.
- Burnash, R., 1995. The NWS River Forecast System - Catchment Modeling. In: Singh, V. (Ed.), *Computer Models of Watershed Hydrology*. Water Resources Publications, Colorado, USA, pp. 311–366.

- Carlson, T., 2007. An Overview of the "Triangle Method" for Estimating Surface Evapotranspiration and Soil Moisture from Satellite Imagery. *Sensors* 7, 1612–1629.
- Chauhan, N. S., Miller, S., Ardanuy, P., 2003. Spaceborne soil moisture estimation at high resolution: a microwave-optical/ir synergistic approach. *Inter. J. Remote Sens.* 24 (22), 4599–4622.
- Chow, V. (Ed.), 1964. *Handbook of Applied Hydrology: A compendium of water resources technology*. McGraw-Hill, New York.
- Crawford, N. H., Linsley, R. K., 1966. Digital simulation in hydrology: Stanford Watershed Model IV. Tech. Rep. 39, Stanford Univ. Dept. of Civil Engineering.
- Cunge, J. A., 1969. On the subject of a flood propagation computation method (muskingum method). *J. Hydraulic Res.* 7, 205–230.
- Das, T., 2006. The Impact of Spatial Variability of Precipitation on the Predictive Uncertainty of Hydrological Models. Institute of Hydraulic Engineering, University of Stuttgart, Faculty of Civil Engineering, Stuttgart, Ph.D. dissertation No. 154, ISBN 3-9337 61-57-3.
- Das, T., Bárdossy, A., Zehe, E., He, Y., 2008. Comparison of conceptual model performance using different representations of spatial variability. *J. Hydrol.* 356, 106–118.
- Deardorff, J. W., 1978. Efficient prediction of ground surface temperature and moisture with inclusion of a layer of vegetation. *J. Geophys. Res.* 83, 1889–1903.
- Denmead, O. T., Shaw, R. H., 1962. Availability of soil water to plants as affected by soil moisture content and meteorological conditions. *Agron. J.* 54, 385–390.
- Dickinson, R., 1984. Modelling evapotranspiration for three-dimensional global climate models. In: Hansen, J. E., Takahashi, T. (Eds.), *Climate Processes and Climate Sensitivity*. Vol. 29 of Geophysical Monograph Series. AGU, pp. 58–72.

- Doherty, J., 2003. Groundwater model calibration using pilot points and regularization. *Groundwater* 41 (2), 170–177.
- Donigian, A. S. D., Bicknell, B. R., Imhoff, J. C., 1995. Hydrologic simulation program - Fortran. In: Singh, V. (Ed.), *Computer Models of Watershed Hydrology*. Water Resour. Publ., Colorado, USA, pp. 395–442.
- Dooge, J., 1986. Looking for hydrologic laws. *Water Resour. Res.* 22, 46S–58S.
- Duan, Q., Sorooshian, S., Gupta, V., 1992. Effective and Efficient Global Optimization for Conceptual Rainfall-Runoff Models. *Water Resour. Res.* 28 (4), 1015–1031.
- Duckstein, L., 1984. Multiobjective optimization in structural design: The model choice problem. In: Atrek, E., Gallagher, R. H., Ragsdell, K. M., Zienkiewicz, O. C. (Eds.), *New Directions in Optimum Structural Design*. Eds. John Wiley and Sons Inc., New York, pp. 459–481.
- Fenicia, F., Savenije, H. H. G., Matgen, P., Pfister, L., 2008. Understanding catchment behavior through stepwise model concept improvement. *Water Resour. Res.* 44, W01402.
- Fennessy, M. J., Shukla, J., 1999. Impact of Initial Soil Wetness on Seasonal Atmospheric Prediction. *J. Climate* 12, 3167–3180.
- Fernandez, W., Vogel, R., Sankarasubramanian, A., 2000. Regional calibration of a watershed model. *Hydrol. Sci. J.* 45 (5), 689–707.
- Flügel, W. A., 1995. Delineating hydrological response units by geographical information system analyses for regional hydrological modelling using PRMS/MMS in the drainage basin of the river Bröl, Germany. *Hydrol. Process.* 9, 423–436.
- Freeze, R. A., Harlan, R. L., 1969. Blueprint for a physically-based, digitally-simulated hydrologic response model. *J. Hydrol.* 9 (3), 237–258.
- Geman, S., Geman, D., 1984. Stochastic relaxation Gibbs distributions and the Bayesian restoration of images. *IEEE-Trans. Pattern Analysis and Machine Intelligence* 6 (6), 721–741.

- Götzinger, J., Bárdossy, A., 2007. Comparison of four regionalisation methods for a distributed hydrological model. *J. Hydrol.* 333, 374–384.
- Grayson, R., Blöschl, G., 2000. *Spatial Patterns in Catchment Hydrology: Observations and Modelling*. Cambridge University Press, The Edinburgh Building, Cambridge, UK, ISBN 0-521-63316-8.
- Grayson, R. B., Moore, I. D., McHahon, T. A., 1992. Physically based hydrologic modeling, 2. Is the concept realistic? *Water Resour. Res.*, 28 (10), 2659–2666.
- Guo, J., Liang, X., Leung, L., 2004. A new multi-scale flow network generation scheme for land surface models. *Geophys. Res. Letters* 31, L23502.
- Gupta, H. V., Sorooshian, S., Hogue, T. S., Boyle, D. P., 2002. Advances in Automatic Calibration of Watershed Models. In: Duan, Q., Gupta, H., Sorooshian, S., Rousseau, A., Turcotte, R. (Eds.), *Calibration of Watershed Models*. Vol. 6 of Water Science and Application. AGU, pp. 9–28.
- Haddeland, I., Matheussen, B., Lettenmaier, D., 2002. Influence of spatial resolution on simulated streamflow in a macroscale hydrologic model. *Water Resour. Res.* 38 (7), 593–605.
- Hargreaves, G. H., Samani, Z. A., 1985. Reference crop evapotranspiration from temperature. *Appl. Engrg. in Agri.* 1, 96–99.
- Hargreaves, G., H., 1994. Defining and using reference evapotranspiration. *J. Irrig. and Drain. Engineer.* 120 (6), 1132–1139.
- Hartmann, G. M., 2003. *Investigation of Evapotranspiration Concepts in Hydrological Modelling for Climate Change Impact Assessment*. Institute of Hydraulic Engineering, University of Stuttgart, Faculty of Civil Engineering, Stuttgart, Ph.D. dissertation No. 161, ISBN 3-9337 61-65-4.
- Heuvelmans, G., Muys, B., Feyen, J., 2006. Regionalization of the parameters of a hydrologic model: comparison of linear regression models with artificial neural nets. *J. Hydrol.* 319, 245–265.
- Hopmans, J. W., Simunek, J., Romano, N., Durner, W., 2002. Inverse methods. In: Dane, J. H., Topp, C. (Eds.), *Methods of Soil Analysis*. Part 4: Physical

- Methods. Vol. 5 of Soil Science Society of America Book Series. Soil Science Society of America, Inc., Madison, WI., pp. 963–1008.
- Hundecha, Y., Bárdossy, A., 2004. Modeling effect of land use changes on runoff generation of a river basin through parameter regionalization of a watershed model. *J. Hydrol.* 292, 281–295.
- Hundecha, Y., Ouarda, T. B. M. J., Bárdossy, A., 2008. Regional estimation of parameters of a rainfall-runoff model at ungauged watersheds using the “spatial” structures of the parameters within a canonical physiographic-climatic space. *Water Resour. Res.* 44.
- Jakeman, A., Hornberger, G., Littlewood, I., Whitehead, P., Harvey, J., Ben-cala, K., 1992. A systematic approach to modelling the dynamic linkage of climate, physical catchment descriptors and hydrological response components. *Math. Comp. Sim.* 33, 359–366.
- James, L., 1972. Hydrologic modeling, parameter estimation and watershed characteristics. *J. Hydrol.* 17, 283–307.
- Kavetski, D., Kuczera, G., Franks, S. W., 2006. Bayesian analysis of input uncertainty in hydrological modeling: 1. Theory. *Water Resour. Res.* 42, W03407.
- Kim, U., Kaluarachchi, J., 2008. Application of parameter estimation and regionalization methodologies to ungauged basins of the Upper Blue Nile River Basin, Ethiopia. *J. Hydrol.* 362, 39–56.
- Kirchner, J. W., 2006. Getting the right answers for the right reasons: Linking measurements, analyses, and models to advance the science of hydrology. *Water Resour. Res.* 42.
- Kirkpatrick, S., Gelatt, C., Vecchi, M., 1983. Optimization by simulated Annealing. *Science* 220 (9), 671–680.
- Kling, H., Gupta, H., 2009. On the development of regionalization relationships for lumped watershed models: The impact of ignoring sub-basin scale variability. *J. Hydrol.* 373 (3–4), 337–351.
- Köppen, W. P., Geiger, R., 1939. *Handbuch der Klimatologie*. Vol. 6. Gebrüder Borntraeger, Berlin.

- Koren, V., Schaake, J., Mitchell, K., Duan, Q. Y., Chen, F., Baker, J. M., 1999. A parameterization of snowpack and frozen ground intended for NCEP weather and climate models. *J. Geophys. Res.* 104, 19569–19585.
- Koren, V. I., Smith, M., Wang, D., Zhang, Z., 2000. Use of soil property data in the derivation of conceptual rainfall-runoff model parameters. 15th Conference on Hydrology, American Meteorological Society, Long Beach, CA, pp. 103–106.
- Kutilek, M., Nielsen, D., 1994. Soil hydrology. Catena Verlag, Cremlingen-Destedt.
- Le Moine, N., Andréassian, V., Perrin, C., C., M., 2007. How can rainfall-runoff models handle intercatchment groundwater flows? theoretical study based on 1040 french catchments. *Water Resour. Res.* 43, W06428.
- Leavesley, G. H., Lichty, R. W., Troutman, B. M., Saindon, L. G., 1983. Precipitation - Runoff Modeling System: Users Manual, U.S. Geological Survey Water-Resources Investigations. Denver - Colorado, 83rd Edition.
- Liang, X., Guo, J., Leung, L. R., 2004. Assessment of the effects of spatial resolutions on daily water flux simulations. *J. Hydrol.* 298, 287–310.
- Liang, X., Lettenmaier, D. P., Wood, E. F., Burges, S. J., 1994. A Simple Hydrologically Based Model Of Land-Surface Water And Energy Fluxes For General-Circulation Models. *J. Geophys. Res.* 99 (D7), 14415–14428.
- Liang, X., Wood, E., Lettenmaier, D., 1996. Surface soil moisture parameterization of the VIC-2L model: Evaluation and modification. *Global and Planetary Change* 13, 195–206.
- Liang, X., Xie, Z., 2001. A new surface runoff parameterization with subgrid-scale soil heterogeneity for land surface models. *Adv. Water Resour.* 24 (9–10), 1173–1193.
- Lindström, G., Johansson, B., Persson, M., Gardelin, M., Bergström, S., 1997. Development and test of the distributed HBV-96 hydrological model. *J. Hydrol.* 201, 272–288.
- Linsley, R. K., 1943. A Simple Procedure for Day-to-Day Forecast of Runoff from Snow Melt. *Trans. Am. Geophys. Union* 24, 62–67.

- Lloyd, S. P., 1982. Least squares quantization in PCM. *IEEE Trans. on Inform. Theory* 28 (2), 129–137.
- Magette, W. L., Shanholtz, V. O., Carr, J. C., 1976. Estimating selected parameters for the Kentucky watershed model from watershed characteristics. *Water Resour. Res.* 12 (3), 472–476.
- Mahrt, L., Pan, H., 1984. A two-layer model of soil hydrology. *Boundary-Layer Meteorol.* 29, 1–20.
- McDonnell, J. J., Tanaka, T., Mitchell, M. J., Ohte, N., 2001. Hydrology and biogeochemistry of forested catchments: Foreword. *Hydrol. Processes* 15, 1673–1674.
- Merz, R., Blöschl, G., 2004. Regionalisation of catchment model parameters. *J. Hydrol.* 287, 95–123.
- Monteith, J., 1965. *Evaporation and environment*. In: Foggy, G. T. (Ed.), *The state and movement of water in living organisms*. Cambridge University Press, London.
- Monteith, J. L., Unsworth, M. H., 2007. *Principles of Environmental Physics*, 3rd Edition. Academic Press, New York.
- Mosley, M., 1981. Delimitation of new zealand hydrologic regions. *J. Hydrol.* 49, 173–192.
- Niu, G., Yang, Z., 2006. Effects of Frozen Soil on Snowmelt Runoff and Soil Water Storage at a Continental Scale. *J. Hydrometeorol.* 7 (5), 937–952.
- Nykanen, D. K., Foufoula-Georgiou, E., Lapenta, W. M., 2001. Impact of Small - Scale Rainfall Variability on Larger - scale Spatial Organization of Land - Atmosphere Fluxes. *J. Hydrometeor.* 2, 105–120.
- O'Donnell, G., Nijssen, B., Lettenmaier, D. P., 1999. A simple algorithm for generating streamflow networks for grid-based, macroscale hydrological models. *Hydrol. Process.* 13, 1269–1275.
- Olivera, F., Lear, M. S., Famiglietti, J. S., Asante, K., 2002. Extracting low-resolution river networks from high-resolution digital elevation models. *Water Resour. Res.* 38 (11), 1231.

- Oudin, L., Andréassian, V., Perrin, C., C., M., 2006. Dynamic averaging of rainfall-runoff model simulations from complementary model parameterizations. *Water Resour. Res.* 42, W07410.
- Oudin, L., Andreassian, V., Perrin, C., Michel, C., Le Moine, N., 2008. Spatial proximity, physical similarity, regression and ungaged catchments: A comparison of regionalization approaches based on 913 French catchments. *Water Resour. Res.* 44, W03413.
- Pachepsky, Y., Rawls, W., Lin, H., 2006. Hydropedology and pedotransfer functions. *Geoderma* 131, 308–316.
- Parajka, J., Blöschl, G., 2008. The value of MODIS snow cover data in validating and calibrating conceptual hydrologic models. *J. Hydrol.* 358, 240–258.
- Parajka, J., Blöschl, G., Merz, R., 2007. Regional calibration of catchment models: Potential for ungauged catchments. *Water Resour. Res.*, W06406.
- Parajka, J., Merz, R., Blöschl, G., 2005. A comparison of regionalisation methods for catchment model parameters. *Hydrol. Earth Sys. Sci.* 9 (3), 157–171.
- Parry, M. L., Conziani, O. F., Palutikof, J. P., Van der Linden, P. J., Hanson, C. E. (Eds.), 2007. Freshwater resources and their management, In: *Climate Change 2007: Impacts, Adaptation and vulnerability, contribution of working group II to the fourth assessment report of the Intergovernmental Panel on climate Change*. Cambridge University Press, Cambridge, UK,.
- Patterson, D. E., Smith, M. W., 1981. The measurement of unfrozen water content by time domain reflectometry: results from laboratory tests. *Canadian Geotech. J.* 18, 131–144.
- Pokhrel, P., Gupta, H. V., 2009. On the Use of Spatial-Regularization Strategies to Improve Calibration of Distributed Watershed Models. *Water Resour. Res.* (In Press).
- Pokhrel, P., Gupta, H. V., Wagener, T., 2008. A spatial regularization approach to parameter estimation for a distributed watershed model. *Water Resour. Res.* 44, W12419.

- Pokhrel, P., Yilmaz, K. K., Gupta, H. V., 2009. Multiple-criteria calibration of a distributed watershed model using spatial regularization and response signatures. *J. Hydrol.* (In Press).
- Porporato, A., Ridolfi, L., 2003. Detecting determinism and nonlinearity in river-flow time series. *Hydrol. Sci. J.* 48 (5), 763–780.
- Post, D., Jakeman, A., 1996. Relationships between physical attributes and hydrologic response characteristics in small Australian mountain ash catchments. *Hydrol. Process.* 10, 877–892.
- Rawl, W., 1983. Estimating soil bulk density from particle size analysis and organic matter content. *Soil Sci.* 135, 123–125.
- Reed, S., Koren, V., Smith, M., Zhang, Z., Moreda, F., Seo, D. J., DMIP Participants, 2004. Overall distributed model intercomparison project results. *J. Hydrol.* 298 (1-4), 27–60.
- Reed, S. M., 2003. Deriving flow directions for coarse-resolution (1 - 4 km) gridded hydrologic modeling. *Water Resour. Res.* 39 (9), 1238.
- Refsgaard, J., Storm, B., 1995. MIKE SHE. In: Singh, V. (Ed.), *Computer Models of Watershed Hydrology*. Water Resour. Publ., Colorado, USA, pp. 809–846.
- Refsgaard, J. C., 1997. Parameterisation, calibration and validation of distributed hydrological models. *J. Hydrol.* 198, 69–97.
- Refsgaard, J. C., Knudsen, J., 1996. Operational validation and intercomparison of different types of hydrological models. *Water Resour. Res.* 32 (7), 2189–2202.
- Richards, L. A., 1931. Capillary conduction of liquids through porous media. *Physics* 1, 318–333.
- Robson, A., Reed, D., 1999. *Flood Estimation Handbook*, vol. 3: Statistical procedures for flood frequency estimation. Institute of Hydrology, Wallingford, UK.
- Russo, R., A., P., Becchi, I., Bemporad, G. A. (Eds.), 1994. *Advances in Distributed Hydrology*. Water Resour. Publ., Chelsea, MI, USA.

- Samaniego, L., 2003. Hydrological Consequences of Land Use/Land Cover Change in Mesoscale Catchments. Institute of Hydraulic Engineering, University of Stuttgart, Faculty of Civil Engineering, Stuttgart, Ph.D. dissertation No. 118, ISBN 3-9337 61-21-2.
- Samaniego, L., Bárdossy, A., 2007. Exploratory Modelling applied to Integrated Water Resources Management. In: Schumann, A., Pahlow, M. (Eds.), Reducing the Vulnerability of Societies to Water Related Risks at the Basin Scale (Proceedings of the third International Symposium on Integrated Water Resources Management, Bochum, Germany, September 2006). Vol. 317 of IAHS Red Books. IAHS, pp. 197–203.
- Samaniego, L., Bárdossy, A., Kumar, R., 2010a. Streamflow prediction in ungauged catchments using copula-based dissimilarity measures. *Water Resour. Res.* 46, W0250.
- Samaniego, L., Kumar, R., Attinger, S., 2010b. Multiscale parameter regionalization of a grid-based hydrologic model at the mesoscale. *Water Resour. Res.* 46, W05523.
- Schulla, J., Jasper, K., 2007. Model Description WaSiM-ETH (Water balance Simulation Model ETH). Tech. rep., ETH, Zürich.
- Sefton, C., Howarth, S., 1998. Relationships between dynamic response characteristics and physical descriptors of catchments in England and Wales. *J. Hydrol.* 211, 1–16.
- Seibert, J., 1999. Regionalisation of parameters for a conceptual rainfall-runoff model. *Agric. Fores. Meteorol.* 98–99, 279–293.
- Seibert, J., 2003. Reliability of model predictions outside calibration conditions. *Nord. Hydrol.* 34, 477–492.
- Seneviratne, S., Stöckli, R., 2008. The Role of Land-Atmosphere Interactions for Climate Variability in Europe. In: Brönnimann, S., Luterbacher, J., Ewen, T., Diaz, H., Stolarski, R., Neu, U. (Eds.), *Climate Variability and Extremes during the Past 100 years*. Vol. 33 of *Advances in Global Change Research*. Springer Verlag, xvi.

- Shevenell, L., 1999. Regional potential evapotranspiration in arid climates based on temperature, topography and calculated solar radiation. *Hydrol. Process.* 13 (13), 577–596.
- Singh, V., 1995. *Computer Models of Watershed Hydrology*. Water Resour. Publ., Highlands Ranch, CO, USA.
- Singh, V., Frevert, D., 2002. *Mathematical Models of Large Watershed Hydrology*. Water Resour. Publ., LLC: Colorado, USA.
- Singh, V. P., Frevert, D. K., 2006. *Watershed Models*. Taylor and Francis, Philadelphia, Pa.
- Sivapalan, M., 2005. Chapter 13: Pattern, Process and Function: Elements of a Unified Theory of Hydrology at a Catchment Scale. In: Anderson, M. (Ed.), *Encyclopedia of Hydrological Sciences*. John Wile & Sons, Ltd, pp. 193–219.
- Smakhtin, V. U., 2001. Low flow hydrology: a review. *J. Hydrol.* 240, 147–186.
- Stedinger, J. R., Vogel, R. M., Foufoula-Georgiou, E., 1993. Frequency analysis of extreme events. In: *Handbook of Hydrology*. McGraw-Hill, New York, USA.
- Tallaksen, L. M., Madsen, H., Clausen, B., 1997. On the definition and modelling of streamflow drought duration and deficit volume. *Hydrol. Sci. J.* 42 (1), 15–33.
- Tewolde, M. H., Smithers, J. C., 2006. Flood routing in ungauged catchments using Muskingum methods. *Water SA* 32 (3), 379–388.
- Todini, E., 1996. The ARNO rainfall-runoff model. *J. Hydrol.* 175 (1-4), 339–382.
- Tolson, B. A., Shoemaker, C. A., 2007. Dynamically dimensioned search algorithm for computationally efficient watershed model calibration. *Water Resour. Res.* 43, WR004723.
- Tolson, B. A., Shoemaker, C. A., 2008. Efficient prediction uncertainty approximation in the calibration of environmental simulation models. *Water Resour. Res.* 44, WR005869.

- Troy, T., Eric F. Wood, E. F., Sheffield, J., 2008. An efficient calibration method for continental-scale land surface modeling. *Water Resour. Res.* 44, W09411.
- Uhlenbrook, S., Roser, S., Tilch, N., 2004. Hydrological process representation at the meso-scale: the potential of a distributed, conceptual catchment model. *J. Hydrol.* 291 (3-4), 278-296.
- UNDP, 2003. Human Development Report 2003: Millennium Development Goals: A Compact Among Nations to End Human Poverty. Oxford University Press, New York.
- Vieux, B., 2001. Distributed Hydrologic Modeling Using GIS. Kluwer Academic Publishers, Dordrecht, The Netherlands.
- Vinnikov, K. Y., Robock, A., Speranskaya, N. A., Schlosser, C. A., 1996. Scales of temporal and spatial variability of midlatitude soil moisture. *J. Geophys. Res.* 101, 7163-7174.
- Viviroli, D., Zappa, M., Gurtz, J., Weingartner, R., 2009. An introduction to the hydrological modelling system PREVAH and its pre- and post-processing-tools. *Environ. Model. Softw.* 24, 1209-1222.
- Vogel, R. M., 2005. Chapter 3: Regional Calibration of Watershed Models. In: Singh, V. P., Frevert, D. (Eds.), *Watershed Models*. CRC Press, Colorado, USA.
- Vrugt, J., Diks, C., Gupta, H., Bouten, W., Verstraten, J., 2005. Improved treatment of uncertainty in hydrologic modeling: Combining the strengths of global optimization and data assimilation. *Water Resour. Res.* 41, W01017.
- Wagener, T., Sivapalan, M., McDonnell, J., Hooper, R., Lakshmi, V., Liang, X., Kumar, P., 2004. Predictions in Ungauged Basins (PUB)- A catalyst for multi-disciplinary hydrology. *EOS, Newsletter of American Geophysical Union* 85 (44), 451-457.
- Wagener, T., Wheater, H. S., 2006. Parameter estimation and regionalization for continuous rainfall-runoff models including uncertainty. *J. Hydrol.* 320 (1-2), 132-154.

- Wang, L., Qu, J. J., Zhang, S., Hao, X., Dasgupta, S., 2007. Soil moisture estimation using MODIS and ground measurements in eastern China. *International Journal of Remote Sensing* 28 (6), 1413–1418.
- Williams, P. J., Smith, M. W., 1989. *The Frozen Earth: Fundamentals of Geocryology*. Cambridge. University Press, Cambridge.
- Wood, E. F., Lettenmaier, D., Liang, X., Nijssen, B., Wetzel, S. W., 1997. Hydrological modeling of continental-scale basins. *Annual Review Of Earth And Planetary Sciences* 25, 279–300.
- Yilmaz, K. K., Gupta, H. V., Wagener, T., 2008. A process-based diagnostic approach to model evaluation: Application to the NWS distributed hydrologic model. *Water Resour. Res.* 44, WR006716.
- Young, A. R., 2006. Stream flow simulation within UK ungauged catchments using a daily rainfall-runoff model. *J. Hydrol.* 320, 95155–172.
- Young, P. C., Parkinson, S., 2002. Simplicity out of Complexity. In: Beck, M. B. (Ed.), *Environmental foresight and models: a manifesto*, 1st Edition. Vol. 22. Elsevier Science, Ltd, Amsterdam, pp. 251–301.
- Zacharias, S., Wessolek, G., 2007. Excluding Organic Matter Content from Pedotransfer Predictors of Soil Water Retention. *Soil. Sci. Soc. Am. J.* 71 (1), 43–50.
- Zehe, E., Blöschl, G., 2004. Predictability of hydrologic response at the plot and catchment scales: Role of initial conditions. *Water Resour. Res.* 40, W10202.
- Zehe, E., Lee, H., Sivapalan, M., 2006. Dynamical process upscaling for deriving catchment scale state variables and constitutive relations for mesoscale process models. *Hydrol. Earth Sys. Sci.* 10, 981–996.
- Zhao, R. J., Zhang, Y. L., Fang, L. R., Liu, X. R., Zhang, Q. S., 1980. The Xinnanjiang model. *Hydrological Forecasting Proceedings Oxford Symposium*, IAHS 129, 351–356.
- Zhu, J., Mohanty, B., 2002. Spatial Averaging of van Genuchten Hydraulic Parameters for Steady-State Flow in Heterogeneous Soils: A Numerical Study. *Vadose Zone J.* 1 (2), 261–272.

Selbständigkeitserklärung

Ich erkläre, dass ich die vorliegende Arbeit selbständig und unter Verwendung der angegebenen Hilfsmittel, persönlichen Mitteilungen und Quellen angefertigt habe.

Rohini Kumar

This thesis is based on the following published and unpublished articles, in which contributions of the author of this thesis are mentioned below.

- Samaniego, L., Kumar, R., and S. Attinger. A parsimonious spatially distributed hydrologic model for water resources management at the mesoscale.(manuscript unpublished).

In this paper, I was involved in partly writing phase, making all necessary mHM simulation runs, preparing graphs and tables, and analyzing the result parts. I have written the maximum part of the Chapter 3, which is a part of this paper.

- Samaniego, L., Kumar, R., and S. Attinger (2010). Multiscale parameter regionalization of a grid-based hydrologic model at the mesoscale. *Water Resour. Res.*, 46, W05523.

In this paper, I was involved partly in the writing phase, making all necessary mHM simulation runs, preparing graphs and tables, and analyzing results.

- Kumar, R., Samaniego, L. and S. Attinger (2010). The effects of spatial discretization and model parameterization on the prediction of extreme runoff characteristics. *J. Hydrol.* 392 (1-2), pp. 54-69

In this paper, I was involved fully in the writing phase, making all necessary mHM simulation runs, preparing graphs and tables, and analyzing result and discussion parts.

Curriculum Vitae

Rohini Kumar was born on the 20th of December, 1982 in Darbhanga, India. He attended Sarvodaya High School, Darbhanga, India until 1997, for his primary education, before pursuing further education at the C. M. Science College, Darbhanga, India until 1999. After that in year 2000, he started his further study in Bachelor of Technology in Agricultural Engineering at the College of Agricultural Engineering, Bapatla, India under the Acharya N. G. Ranga Agricultural University, Hyderabad, India and successfully completed his studies in the year 2004. In the same year he started his advanced study in Master of Technology in Water Resource Development and Management at the Indian Institute of Technology, Kharagpur, India and completed his study in August 2006. From mid of September 2006, he started his doctoral research at the Helmholtz Center for Environmental Research UFZ Leipzig, Germany at the Department of Computational Hydrosystems under the supervision of Prof. Dr. Sabine Attinger and Dr. Luis E. Samaniego. He submitted his dissertation to the School of Chemical and Earth Sciences at the Friedrich Schiller University of Jena, Germany in December 2009.

